AD-A079 562 WOODS HOLE OCEANOGRAPHIC INSTITUTION MASS F/G 17/1
ATTENUATION OF LOW ORDER MODES IN LOSSY ACOUSTIC WAVE GUIDES.(U)
DEC 79 H D LESLIE N00014-75-C-0852
UNCLASSIFIED WHOI-79-91 NL

1 OF 3
ADA 079 562

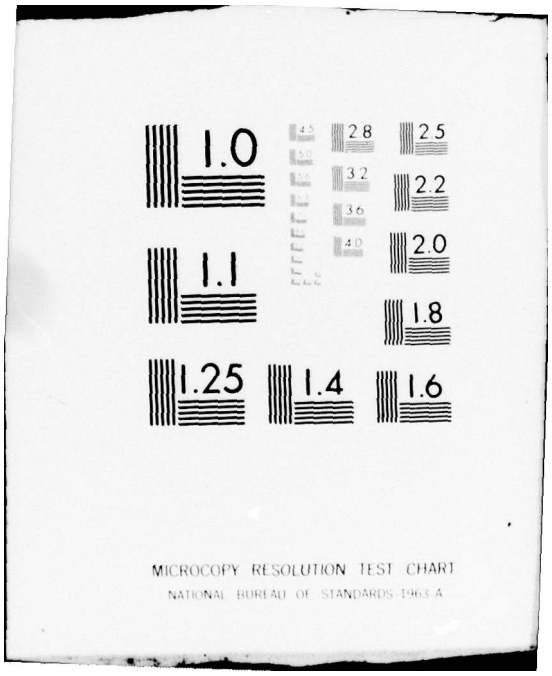
1.0
1.1
1.25
1.4
1.6
1.8
2.0
2.2
2.5
2.8
3.2
3.6
4.0
4.5
5.0
MICROCOPY RESOLUTION TEST CHART
NATIONAL BUREAU OF STANDARDS-1963-A

LEVEL

Institution

DDC

[illegible]

by

[illegible]

[illegible] 1979

[illegible]

[illegible]

UNCLASSIFIED 12/79

SECURITY CLASSIFICATION OF THIS PAGE (When Data Entered)

REPORT DOCUMENTATION PAGE

READ INSTRUCTIONS BEFORE COMPLETING FORM

1. REPORT NUMBER: WHOI-79-91
2. GOVT ACCESSION NO.
3. RECIPIENT'S CATALOG NUMBER
4. TITLE (and Subtitle): ATTENUATION OF LOW ORDER MODES IN LOSSY ACOUSTIC WAVE GUIDES.
5. TYPE OF REPORT & PERIOD COVERED: Technical rept.,
6. PERFORMING ORG. REPORT NUMBER
7. AUTHOR(s): Harold David Leslie
8. CONTRACT OR GRANT NUMBER(s): N00014-75-C-0852
9. PERFORMING ORGANIZATION NAME AND ADDRESS: Woods Hole Oceanographic Institution, Woods Hole, MA 02543
10. PROGRAM ELEMENT, PROJECT, TASK AREA & WORK UNIT NUMBERS
11. CONTROLLING OFFICE NAME AND ADDRESS: NORDA, National Space Technology Laboratory, Bay St. Louis, MS 39529
12. REPORT DATE: Dec [redacted]79
13. NUMBER OF PAGES: 258
14. MONITORING AGENCY NAME & ADDRESS (if different from Controlling Office): 263
15. SECURITY CLASS. (of this report): Unclassified
15a. DECLASSIFICATION/DOWNGRADING SCHEDULE

16. DISTRIBUTION STATEMENT (of this Report)

Approved for public release; distribution unlimited.

17. DISTRIBUTION STATEMENT (of the abstract entered in Block 20, if different from Report)

18. SUPPLEMENTARY NOTES

19. KEY WORDS (Continue on reverse side if necessary and identify by block number)

1. Acoustic wave guides
2. Low order modes
3. Attenuation coefficients

20. ABSTRACT (Continue on reverse side if necessary and identify by block number)

Acoustic propagation is treated for sound sources in an ocean bounded from below by stratified layering. The bounding layers of the waveguide may be homogeneous-isovelocity or inhomogeneous with vertical sound speed gradients The layers may be dissipative or nondissipative. The acoustic field is described with a normal mode expansion and modal attenuation coefficients are calculated for low order modes as a function of mode number and either frequency or phase velocity. The theoretical basis of the calculations is pre-

(Cont. on back)

DD FORM 1 JAN 73 1473 EDITION OF 1 NOV 65 IS OBSOLETE S/N 0102-014-6601 | 381 000

UNCLASSIFIED 12/79

SECURITY CLASSIFICATION OF THIS PAGE (When Data Entered)

sented for multilayer isovelocity guides and for multilayer guides with index of refraction squared varying linearly with depth. Numerical results are presented for the Pekeris model of a fluid layer over a dissipative fluid halfspace. A comparison is made between various attenuation coefficients proposed in the literature.

WHOI-79-91

ATTENUATION OF LOW ORDER MODES IN LOSSY ACOUSTIC WAVE GUIDES

by

Harold David Leslie

WOODS HOLE OCEANOGRAPHIC INSTITUTION
Woods Hole, Massachusetts 02543

December 1979

DISSERTATION

Prepared for the Office of Naval Research under Contract N00014-75-C-0852.

Approved for Distribution:

Robert C. Spindel, Acting Chairman
Department of Ocean Engineering

Charles D. Hollister
Dean of Graduate Studies

ATTENUATION OF LOW ORDER MODES

IN

LOSSY ACOUSTIC WAVEGUIDES

by

H. David Leslie

B.S.E.E., Princeton University
(1969)

Submitted in Partial Fulfillment of the
Requirements for the Degree of

Ocean Engineer

at the

Woods Hole Oceanographic Institution

and at the

Massachusetts Institute of Technology

and

Master of Science in Ocean Engineering

at the

Massachusetts Institute of Technology

September 1, 1978

Signature of Author..... H. David Leslie .....
Joint Program in Oceanographic Engineering, Woods Hole Oceanographic Institution - Massachusetts Institute of Technology, and the Department of Ocean Engineering, Massachusetts Institute of Technology, September, 1978

Certified by..... Arthur B. Baggeroer .....
Thesis Supervisor

..... Robert R. Rose .....
Thesis Supervisor

Accepted by... Earl E. Hays .....
Chairman, Joint Committee for Oceanographic Engineering, Woods Hole Oceanographic Institution - Massachusetts Institute of Technology

ATTENUATION OF LOW ORDER MODES IN LOSSY ACOUSTIC WAVEGUIDES

by

H. David Leslie

Submitted to the Department of Ocean Engineering on September 1, 1978 in partial fulfillment of the requirements for the degree of Ocean Engineer and Master of Science in Ocean Engineering.

Abstract

Accustic propagation is treated for sound sources in an ocean bounded from below by stratified layering. The bounding layers of the waveguide may be homogeneous-isovelocity or inhomogeneous with vertical sound speed gradients. The layers may be dissipative or nondissipative. The acoustic field is described with a normal mode expansion and modal attenuation coefficients are calculated for low order modes as a function of mode number and either frequency or phase velocity. The theoretical basis of the calculations is presented for multilayer isovelocity guides and for multilayer guides with index of refraction squared varying linearly with depth. Numerical results are presented for the Pekeris model of a fluid layer over a dissipative fluid halfspace.

A comparison is made between various attenuation coefficients proposed in the literature.

Thesis Supervisor: Arthur B. Baggeroer

Title: Associate Professor of Ocean Engineering

Associate Professor of Electrical Engineering

ACKNOWLEDGEMENTS

The original direction of this work, as an attempt to account for transmission loss anomalies in oceanic waveguides bounded by lossy sediments with velocity structure, was suggested by Dr. Ira Dyer. Initial floundering with perturbation approaches to the inhomogeneous problem led to the suggestion by Prof. A.B.Baggeroer that the computational analysis be developed first in the context of the Pekeris model. I am grateful to Prof. Baggeroer for insightful suggestions along the way and for the patience and persistence required to insure that the work evolved to the point that it has. Dr. George Frisk and Dr. Robert Porter have read and commented on much of what is written here and frequently have offered suggestions and criticizms. Dr. Porter has also graciously allowed me the time and provided resources with which to complete the work during my stay at Schlumberger. Completion of the manuscript is due largely to the typing, interpreting skills and good spirits of Patty Martinich.

TABLE OF CONTENTS

	Page
Title Page	1
Abstract	2
Acknowledgements	3
Table of Contents	5
Chapter 1-Introduction	7
1.1 Problem context	8
1.2 Overview of the work	10
1.3 Organization of the chapters	11
Chapter 2-Normal Modes in Waveguides with Nondissipative Boundaries	21
2.1 Wave equation	22
2.2 Helmholtz equation solution	23
2.3 Reflection coefficient	24
2.4 Characteristic equation	29
2.5 Mode shapes	40
Appendices	41
Chapter 3-Normal Modes in Waveguides with Dissipative Boundaries	60
3.1 Introduction	61
3.2 Phenomenological approach to dissipation and relaxation mechanisms	64
3.3 Introduction os dissipation into the wave equation	68
3.4 Isovelocity layers with dissipation	71
3.5 General statement of the problem	82
3.6 Method of solution	84
Appendices	92

Chapter 4- Modal Attenuation 118
4.1 Introduction 119
4.2 Rigorous formulation 119
4.3 Intuitive formulation 120
4.4 The relation between the intuitive attenuation coefficient and the attenuation coefficient calculated with the accepted period equation 133
4.5 Literature attenuation coefficient summary, implementation details 140
Appendix 157

Chapter 5-Observations and Computational Results 160
5.1 Introduction 161
5.2 Reflection coefficient for real incidence angle 164
5.3 Reflection coefficient for complex incidence angle 164
5.4 Snell equations: details and observations 168
5.5 Summary of observed behaviour of the reflection coefficient and of the Snell algorithm 178
5.6 Analysis of R, refracted angle discontinuity 180
5.7 Comments on angle trajectories 183
5.8 Reflection coefficient phase behaviour 189
5.9 Dispersion results 193
5.10 Attenuation coefficient results 194
5.11 Sensitivity 202
5.12 Numerical difficulties 203

Table of Notation 209
Figures 213
Tables 238
References 254

Chapter 1- Introduction

1.1 Problem context

1.2 Overview of the work

1.3 Organization of the chapters

Chapter 1- Introduction

1.1 Problem context

Acousticians involved with long range sound propagation in the ocean have classically neglected energy contributions from that portion of the trapped acoustic field which interacts with waveguide boundaries. The relative contribution is frequently insignificant and difficult to account for accurately, due to heterogeneities in the bottom layering and unknown attenuation mechanisms. In the near field and at medium ranges the problem is compounded by contributions from leaky modes of untrapped waves. Sound speed gradients and attenuation in the bottom tend to obscure the distinction between normal and evanescent contributors to the acoustic field. Recently, however, interest has renewed in these portions of the field in connection with transmission loss anomalies and with the possible use of horizontal coherence and attenuation functions as tools for inferring bottom properties. It is our purpose here to investigate theoretically modal propagation in deep ocean waveguides to medium ranges, giving attention to sound speed gradients and leaking energy in the problem formulation. We are particularly interested in those portions of the field which interact with the bottom and the changing energy distribution of the field with range. We will calculate and compare modal attenuation coefficients derived by several authors, under varying assumptions and examine their suitability for accurately characterizing the field. We indicate regions of the modal dispersion curves within which these formulae are useful for parameter estimation.

Normal mode analysis is well established in underwater acoustics. Analytically it provides a framework for decomposition of the acoustic field into additive components whose characteristic dispersive and attenuative properties may be investigated independently. Empirically it provides a basis for associating measurable acoustical behaviour to parametrically related geological properties. The normal modes are physically separable as spatial intensity distributions and for transient sources are temporally separable on the basis of their dispersion. An effect of accounting for energy not confined

entirely within the water column is to alter the bandwidth of modal dispersion curves. Inclusion of waves with deeper penetration and higher horizontal phase velocities affects the relative energy distribution among modes by allowing lower frequencies in the low order modes. Attenuation in the broader waveguide physically leads to "mode stripping" and causes relative energy distribution to be range dependent. The effects of attenuation on dispersion curves needs to be examined systematically.

Modal analysis leads to several measurable quantities with varying degrees of sensitivity to multilayer structure. That these measurements are realizable is ultimately the motivation and justification for studying attenuation in a normal mode context. CW sources with variable frequency may be used to probe mode excitation functions. A vertical array designed to match mode shape should be capable of isolating low order modes when the source depth and frequency are variable. Absolute sound pressure levels then can be used to determine mode attenuation coefficients. Impulsive excitation can be used advantageously to study the details of dispersive propagation. In particular, the group velocity characteristics of low order modes may be examined for Airy frequencies, resonances and antiresonances, where the relative minima and maxima are functions of guide layering. Bucker (ref. 14) has demonstrated the effect of significant attenuation of Airy phase, for the layer over an attenuating halfspace and a pronounced resonance may be completely damped. This effect should be observable in multilayer channels with gradients as well.

Previous analysis of normal mode wave fields in ocean acoustics is extensive (ref. 9 , 10 , 17 , 18). Several authors have included energy aborption factors in their expression for the modal fields. We examine some of these in detail in chapter 4, where modal attenuation coefficients from the literature are presented for comparison. Kornhauser and Raney (ref. 19) obtain an imaginary part to horizontal wavenumber K_x for the isovelocity layer over a fluid halfspace when K_2 the wavenumber in the halfspace is made complex. Bucker develops an attenuation coefficient raising the reflec-

tion coefficient to a power equal to the number of bounces per unit distance for a fluid layer over an absorbing halfspace. Rays and modes are related through phase velocity. Bucker later develops a more rigorous coefficient in his sum of residues solution where the ray-mode analogy is used to establish starting values of Re(K) and Im(K) in a dispersion equation he developed in terms of generalized solutions U and V to the Helmholtz equation. Ingenito writes a solution in terms of power ratios for water column and bottom and later another as a perturbation solution in terms of the reflection coefficient at a fluid solid boundary. Morris (ref. 22) determines the solution for complex N^2-linear layers where dissipation varies linearly with depth in the same proportion as sound speed squared does. Her solutions are Airy functions. In the geophysical literature we have noted differences in approach when restrictions are made to either real frequency ω, real wavenumber k, or real group velocity while satisfying the modal characteristic equation. By requiring real ω in what follows we are consistent with the acoustical literature.

1.2 Overview of the work

In our own computational effort we have principally accompanied the work of Brekhovskikh and Tolstoy in developing an algorithm for the solution of several multilayer waveguide problems. A normal mode decomposition is used. We are concerned with underwater acoustic propagation for ranges long enough that lateral wave portions of the acoustic field are either subdominant with harmonic excitation, or temporally separable for pulsed excitation. We are interested in ranges short enough that attenuating modes still make a significant contribution to the field. For closer ranges additional analysis must be included and we have examined briefly the characteristics of leaky modes observable at close range.

We indicate below analytical results for a series of waveguides of interest. We have chosen several layering models which cover a wide range of expected physical environments. (see figure 1.1)

Model 1 has isovelocity liquid layering with constant density within each layer. It has been our principal concern in this study. We have analyzed the dissipative Pekeris model extensively (model 1 with layer 2 an absorbing halfspace), preliminary, and as a basis for the more complicated models. Dispersion solutions using real frequency and complex wavenumber are presented for a variety of layer thickness, impedance contrasts and halfspace absorption. These solutions are based on existing theory (Brekhovskikh), explicitly expressed here in terms of complex sound speed and complex incidence angle. Analytic results for other models are also developed in the appendices. Model 2A has an isovelocity ocean overlaying a liquid bottom halfspace with index of refraction N varying as the square root of depth in the halfspace ("N^2-linear layering"). Model 2B allows a sound speed discontinuity at the interface in Model 2A. Model 3 has multi N^2-linear layering throughout the waveguide, with sound speed discontinuities permitted at all interfaces. Density is constant in each layer. Model 4 has arbitrary continuous sound speed variation permitted within each layer. Velocity and density discontinuities are permitted at the interfaces. The field in Model 4 is described using the WKB approximation within each layer, thus the model is a "piecewise WKB approximation". Model 4 is expected to be of the greatest utility. Analytic forms of Helmholtz equation solution, normal impedance, reflection coefficient and mode shape may be used to determine modal attenuation characteristics for these models. These forms are developed in the nondissipative and dissipative cases in Chapters 2, 3, and 4. Computational results are presented in Chapter 5 for model 1 only.

1.3 Organization of the chapters

In chapter 2 we review basic theory and make explicit the extension to inhomogeneous (c=c(z)) layering of layer normal impedances, and reflection coefficients, which are usually left to the reader or sketched in the classic texts. (eq. ref. 2 , 8). These quantities are later used to develop modal characteristics in the form

of algorithms for dispersion curves, and mode shapes. We review briefly the theoretical basis of modal analysis, separating the undamped scalar wave equation into horizontal x, vertical z and temporal t dependencies. Classical solutions of the Helmholtz equation for the velocity potential vertical dependence $\Phi(z)$ are given.

1. isovelocity layers:

$$\phi(z) = A \sin k_z \cdot z + B \cos k_z \cdot z \qquad 1.1$$

or

$$\phi(z) = A \exp(i k_z \cdot z) + B \exp(-i k_z \cdot z)$$

k=horizontal propagation constant

$k_z = \left(\frac{\omega^2}{c^2} - k^2\right)^{1/2}$ is the vertical component of wavenumber.

In appendix 2.1 we find the forms

2. N^2-linear layers:

$$\phi(z) = \omega^{1/3} \left[A H^{(1)}_{1/3}(u) + B H^{(2)}_{1/3}(u) \right] \qquad 1.2$$

$$u = \frac{2}{3} \left(\frac{k_0}{g} \right) \zeta^{3/2} \qquad \zeta = N^2(z) - \sin^2 \varphi_0$$

$N^2(z) = \rho - g z$ $\qquad k_0 = \omega / c_1(z=0)$

g is the gradient of N^2 in the layer.

ρ is the index of refraction at the top of the layer.

φ_0 is the incidence angle at $z = 0$

3. In the WKB approximation

$$\phi(z) = \frac{1}{\sqrt{k_z z}} \left\{ C_1 \exp\left[i \int_{z_0}^{z'} k_z(z)\, dz \right] + C_2 \exp\left[-i \int_{z_0}^{z'} k_z(z)\, dz \right] \right\} \qquad 1.3$$

Solutions to the Helmholtz equation are seen to be waves traveling up or down (-z or +z direction), when account is taken of the time dependence exp(-iwt).

We next pose the boundary conditions for fluid layers, the continuity of pressure and the vertical component of particle velocity $V_3(3)$, and define a directed normal impedance $Z(3)\downarrow$ of a particular layer, at depth 3, as the ratio of $P(3)/V_3(3)$ for the upward or downward traveling solution to the Helmholtz equation, $\phi\uparrow$ or $\phi\downarrow$. We review the concept of plane wave coefficient R in continuously stratified media, and note the forms of the characteristic equation

$$R\uparrow \cdot R\downarrow = 1 \quad \text{or} \quad \chi\uparrow + \chi\downarrow = m\pi \qquad 1.4$$

usually used in solving for modal eigenvalues of lossless model. $R\uparrow$ and $R\downarrow$ are the upward and downward reflection coefficients with reflection coefficient phase $\chi\uparrow$, $\chi\downarrow$ i.e. $R = \exp(2i\chi)$

Formulae for calculating $R\uparrow$ and $R\downarrow$ are presented for single and multilayer isovelocity systems in terms of normal impedance. In appendix 2.2 they are developed for inhomogeneous layering systems. These formulae are recursive. For a particular incidence angle within a turning point layer* they propagate the reflection coefficient upward or downward to the source layer. The approach taken is to relate the normal and input impedances on either side of two interfaces to the 3 layer system input impedance and to the thickness of the middle layer, for isovelocity layers. The recursive formula for the reflection coefficient for isovelocity layers was derived by Abeles (ref. 23) and used extensively by Tolstoy. Using the concept of directed normal impedance and the relation $Z\uparrow = -Z\downarrow^*$ which we find to be true for the particular nondissipative models chosen here, we are able to derive recursive reflection coefficient formulae for inhomogeneous layerings analagous to Schelkunoff's. These formulae explicitly include the satisfaction of boundary conditions at interfaces required to match intralayer solutions to the

* A turning point layer is an inhomogeneous layer in which the vertical generalized wavenumber goes to zero, or a layer on whose boundary the wave critically reflects.

Helmholtz equation. Brekhovskikh used $Z\uparrow = -Z\downarrow$ to derive the relation for the special case of isovelocity layering. $Z\uparrow = -Z\downarrow^{*}$ also holds for incidence angles less than critical angle in nondissipative isovelocity layers. These recursive reflection coefficients have the forms shown below. In the isovelocity case with layer thickness h

$$R_{12} = \frac{R_{12} + R_{23}\exp(2i k_3 . h)}{1 + R_{12}\cdot R_{23}\exp(2i k_3 . h)} \qquad 1.5$$

where R_{12}, R_{23} are reflection coefficients at the interface between layers 1, 2 and 2, 3 respectively, treating the layers as halfspaces. In its recursive form R_{23} is replaced by $\mathcal{R}_{23}$ the reflection coefficient of the next lower system. Normal impedance for the isovelocity case is $Z = \frac{\rho c}{\cos\varphi}$ and the halfspace reflection coefficient is

$$R_{23} = \frac{Z_3 - Z_2}{Z_3 + Z_2} \qquad 1.6$$

In the N^2-linear case

$$\mathcal{R}_{12} = (R_{12} + \mathcal{R}_{23} F_N)/(1 + \mathcal{R}_{23} F_d) \qquad 1.7$$

and F_n and F_d, the generalizations of $e^{j2k.h}$ in the isovelocity case, are here combinations of Bessel functions. Normal impedance will be

$$Z = \frac{-i\omega\rho}{k} \cdot \frac{H^{(1)}_{1/3}(\xi) \cdot 1}{H^{(1)}_{-2/3}(\xi)\ \rho - 1 + \cos^2\varphi_0 \pm g_3} \qquad 1.8$$

Halfspace reflection coefficient is

$$R_{23} = \frac{H^{(1)}_{1/3}}{H^{(2)}_{1/3}} \cdot \frac{Z_2^{*}}{Z_2}\left[\frac{Z_3 - Z_2}{Z_3 + Z_2^{*}}\right] \qquad 1.9$$

For WKB solutions appendix 2 shows

$$\mathcal{R}_{12} = (R_{12} + \mathcal{R}_{23} . F_n)/(1 + \mathcal{R}_{23} \cdot F_d) \qquad 1.10$$

and Fn and Fd are complicated expressions involving impedances and phase integrals.

Here

$$Z = \frac{\omega k_3 \rho}{\left[k_3^4 + \frac{1}{4}\left(\frac{d k_3}{d_3}\right)^2\right]^{1/2}} \cdot \exp\left[-i\frac{\pi}{2} + i\tan^{-1}\left(\frac{k_3^2(3)}{-\frac{1}{2}\frac{d k_3(3)}{d_3}}\right)\right] \qquad 1.11$$

$$R_{23} = e^{i2S_2(3)} \frac{Z_2^*}{Z_2}\left[\frac{Z_3 - Z_2}{Z_3 + Z_2}\right] \qquad S \equiv \pm \int_{30}^{3} k_{z_3}(3)\, d_3 + S_0 \qquad 1.12$$

We note the similarity in general form of the quantities Q, R, Z above.

Normal modes of propagation are introduced in chapter 2 when the characteristic equation is developed, both on physical and rigorous mathematical grounds. In the intuitive approach we follow Buckers analysis of the modal field as the superposition of constructively interfering plane waves. This leads to the relation

$$2 \cdot k \cos\varphi \cdot h + \epsilon_s + \epsilon_b = n 2\pi \qquad 1.13$$

where

$k \cos\varphi$ is the vertical wavenumber in the waveguide layer

ϵ_s is phase change from reflection at the surface

ϵ_b is phase change from reflection at the bottom

Brekhovskikh's rigorous development of the acoustic field expression is the basis for the accepted period equation. Writing the field for a spherical wave source in terms of an infinite set of image sources satisfying the boundary conditions and using the integral representation of a spherical wave for each image, he transforms the ray series into a sum of normal modes. The denominator of the expression contains the quantity

$$1 - \tilde{R}\uparrow \cdot \tilde{R}\downarrow \exp(i k_3 \cdot h) \qquad 1.14$$

which determines pole locations in the sum of residues solution.

$1-\tilde{R}\downarrow\cdot\tilde{R}\uparrow\exp(ik_3\cdot h)=0$ is presented as the "accepted" period equation even when dissipation is present. That is,

$$\exp\left[i\left(2\cdot k\cdot h\cdot\cos\tilde{\varphi}+\tilde{\phi}\uparrow+\tilde{\phi}\downarrow\right)\right]=1 \Rightarrow 2kh\cos\tilde{\varphi}+\tilde{\phi}\downarrow+\tilde{\phi}\uparrow=2\pi l \qquad 1.15$$

where $\sim \equiv$ complex quantity. Equation 1.16 requires more than just constructive interference of component waves. It determines the imaginary part of source angle as well.

Using the reflection coefficients derived above and an iteration routine we will solve the characteristic equation 1.15 for eigenvalues $\omega(n, Cp)$ with Cp the horizontal phase velocity, a function of angle of incidence φ, and n the mode number. These eigenvalues in combination with layer eigenfunction coefficients may be used to generate mode shapes as a function of frequency. In chapter 2 we give the mode shape for model 2a and 2b. For model 3 we indicate in appendix 2.3.b the matrix equation whose solution is required to determine layer eigenfunction coefficients. For WKB analysis we present in appendix 2.3.c a set of simultaneous equations to be solved for layer eigenfunction coefficients $\tilde{C}_i = C_i\, e^{i\Theta_i}$, and the mode shape in terms of these coefficients. None of the models in chapter 2 includes dissipation.

In chapter 3 we introduce dissipation into models 1 and 2; examine its effect on wave representation, impedance, and reflection coefficients; and trace its inclusion in the mathematical algorithm for dispersion curves and attenuation coefficients. Theories of frequency dependence of body wave attenuation in sediments are noted and it is indicated that various models exist for attenuation-dispersion pairs. Tolstoy's derivation of the effect of attenuation in a relaxation process is presented to show how the exponential damping term arises. We have developed a program capable of generating solutions to the modal eigenvalue problem for models 1, 2A and 2B, with accompanying dispersion curves and attenuation coefficients. We indicate in chapter 3 the theoretical basis and organization of the calculations for models both with and without dissipation. Attenuation in the dissipative modal formalism is obtained first by expressing Brekhovskikh's

treatment for the isovelocity multilayer reflection coefficient in terms of complex angles of incidence and then by developing an algorithm (Newtons method) for solving simultaneously the complex Snell's law equations. This allows us to start with a complex incidence angle and determine modal component wave incidence angles in each layer and a reflection coefficient for the system of layers. Trial solutions are propagated through the layering, matching stress-motion vectors at the interfaces implicitly with the recursive reflection coefficient. A convergence routine seeks solutions which satisfy the characteristic equation. We introduce dissipation in the layering through complex sound speed. Modal eigenfunctions and eigenvalues must now satisfy complex Helmholtz equations. For all but the simple isovelocity case these equations are unwieldy and require solution by numerical or approximation techniques. In the case of N^2-linear isodissipative layers, we are lead in the appendix of chapter 3 to a complex Helmholtz equation.

$$\frac{d^2\phi(\xi)}{d\xi^2} + \left(\frac{k_0}{g}\right)^2 \left[\xi + A + iB\xi^{1/2}\right]\phi(\xi) = 0 \qquad 1.16$$

where

$$A \equiv -\left(\sin^2\theta_0 + \frac{k''c_0^2}{\omega^2}\right) \qquad c_0 \equiv c(z=0)$$

$$B \equiv \frac{2k''c_0}{\omega} \qquad \xi \equiv 1 \pm gz$$

Without attenuation recall that the equation was

$$\frac{d^2\phi(\xi)}{d\xi^2} + \left(\frac{k_0}{g}\right)^2 \xi\,\phi(\xi) = 0 \qquad 1.17$$

with Hankel function solutions. With the approximation

$$\sqrt{1 \pm gz} \approx 1$$

in one term of equation 1.16 the complex Helmholtz equation is also shown to have Hankel function solutions, and the argument becomes complex. The reflection coefficient is then derived in terms of the Hankel waveform in the N^2-linear region and incorporated in the modal iterative solution procedure as a function of complex angle.

Brekhovskikh's development of the accepted period equation is the basis for the rigorous attenuation coefficient presented in chapter 4. The period equation is justified through its derivation in the sum of residues expression for the field integral given in chapter 2, combined with the use of complex angle shown in chapter 3. Since the refraction law preserves the horizontal phase velocity and attenuation, the first intuitive obstacle is introduced in chapter 4, namely that of getting any horizontal attenuation at all from a wave whose angle of incidence would be expected on physical grounds to be real at the source. This motivates an examination of the effect on wave amplitude of plane wave propagation from a nondissipative halfspace into a dissipative halfspace. We see how inhomogeneous plane waves naturally arise and how complex angles are required to describe them. Then equating modal attenuation to the attenuation of component waves we develop an intuitive modal attenuation coefficient as a simple phase integral (imaginary part) along component wave paths normalized by horizontal cycle length. We do this in terms of complex wavenumbers. For the multilayered media this intuitive attenuation coefficient (exponential damping factor $e^{-\delta x}$) becomes

$$\delta = \left[2 \int_{z_{LS}}^{z_{LS+1}} \xi_x'' \, dx(z) + \xi_z'' \, dz + 1 - |R\uparrow| \cdot |R\downarrow| \right] \Big/ \left[2 \int_{z_{LS}}^{z_{LS+1}} \frac{\sin \varphi_0}{(N^2(z) - \sin^2 \varphi_0)^{1/2}} \, dz \right] \qquad 1.18$$

Here the source layer is $z_{LS} < z < z_{LS+1}$

ξ_x'' , ξ_z'' are the imaginary parts of wavenumber within the source layer. $|R\uparrow|$, $|R\downarrow|$ are upward and downward reflection coefficient magnitudes at the source layer boundaries. The denominator is the cycle length. The integral is along a ray in the source layer.

To make the theory explicit we need to find particular forms of ξ_x'' and ξ_3'' for the inhomogeneous layering. In the case of homogeneous isovelocity layers we verify the validity of the complex solution to the wave equation . ξ_x' and ξ_3'' are then simply kx'' and kz'', the complex parts of wavenumber. The required reflection coefficients are determined from Brekhovskikh's recursive formulation. By taking the log of both the rigorous and intuitive attenuation coefficients for the isovelocity case, and expanding the exponential form of the reflection coefficient in an infinite series, we are able to show that to first order the coefficients are equal. For N^2-linear layers we are lead in appendix 3.1 to a complex Helmholtz equation for $\Phi(3)$, and to reflection coefficients from this type of complex inhomogeneous layering. Solutions of the complex Helmholtz equations are required both for the intuitive formulation and for determining reflection coefficients used in the accepted period equation. We discuss the intuitive solution because it provides insight that the formal solution in terms of contour integration and residues fails to do. At this point in chapter 4 we return to the literature and examine previous solutions for modal attenuation coefficients. These coefficients are presented in the context of our model parameters so that comparison may be made from numerical results in chapter 5.

Chapter 5 presents details essential to implementation of the theory discussed in chapters 3 and 4. In particular, close attention is paid to complex angle domains permissible for solution of the characteristic equation and of the layer refraction laws. Observations are made from the numerical results related to reflection coefficient magnitude and phase and to the refracted angle in layer 2. A nonintuitive discontinuity in the reflection coefficient magnitude is examined and found to result from the constraints placed upon the refracted angle as the incident angle is varied along a particular complex locus. Numerical results are presented for several models of general interest. Interest is focused on the deep ocean eg 1000 m depth, low frequency 1 - 50 Hz and velocity gradients in the sediments of 1 m/sec/m. Dispersion and attenuation coefficient results are

presented for the rigorous formulation, the intuitive formulation, Ingenito's method, Brekhovskikh's asymptotic approximation, and the Kornhauser and Raney method when the model is the classical Pekeris guide. Sensitivity of modal characteristics to dissipation is determined and numerical difficulties in the algorithm are discussed.

In chapter 6 conclusions are drawn as to suitability of the various attenuation coefficient formulae for matching of empirical curves and for parameter estimation.

Chapter 2- Normal Modes in Waveguides with Nondissipative Boundaries

2.1 Wave equation
2.2 Helmholtz equation solution-isovelocity layers
2.3 Reflection coefficient
2.4 Characteristic equation
    a.Physical formulation of the characteristic equation
    b.Rigorous formulation of the characteristic equation
2.5 Mode shapes

Appendix 2.1 Helmholtz equation solutions
    a.N2-linear case
    b.WKB approximation
Appendix 2.2 Reflection coefficient formulae
    a.Reflection coefficient and derivation for model 2a.
    b.Recursive reflection coefficient and derivation for N^2-linear case
    c.Reflection coefficient for multilayer guide with WKB approximation
Appendix 2.3 Mode shapes
      a.Model 2a,b
      b.Model 3
      c.Model 4

2.1 The wave equation

The undamped scalar wave equation is

$$\nabla^2 \Phi - 1/c^2 \frac{\partial^2 \Phi}{\partial t^2} = 0 \qquad 2.1$$

where Φ may represent pressure, velocity potential, or displacement potential, and c the sound speed in a liquid is related to the bulk modulus and density, $c^2 = B/\rho$. For harmonic time dependence $e^{-i\omega t}$ the wave equation becomes

$$\nabla^2 \Phi + k^2 \Phi = 0 \qquad \text{with} \quad k = \omega/c \qquad 2.2$$

In stratified layering with cylindrical symmetry the harmonic wave equation is

$$\frac{\partial^2 \Phi}{\partial r^2} + \frac{1}{r}\frac{\partial \Phi}{\partial r} + \frac{\partial^2 \Phi}{\partial z^2} + k^2(z)\,\Phi = 0 \qquad 2.3$$

Separation is achieved by substituting

$$\Phi(r,z) = \phi(z) \cdot L(r) \qquad 2.4$$

yielding the two equations

$$\frac{\partial^2 L(r)}{\partial r^2} + \frac{1}{r}\frac{\partial L(r)}{\partial r} + K^2 L(r) = 0 \qquad 2.5$$

and

$$\frac{\partial^2 \phi(z)}{\partial z^2} + \left[k^2(z) - K^2\right]\phi(z) = 0 \qquad 2.6$$

The first equation has solutions

$$L(r) = A\,H_0^1(Kr) + B\,H_0^2(Kr) \qquad 2.7$$

Asymptotically

$$H_0^{1,2}(Kr) \cong \sqrt{\frac{2}{\pi Kr}}\; e^{\pm i\left(Kr - \frac{\pi}{4}\right)} \qquad 2.8$$

for $Kr \gg 1$. H_0^1 represents an outward propagating wave . H_0^2 represents a wave converging to r=0. Equation 2.6 is the *Helmholtz equation* whose solution is dependent on parameter $\gamma(z)$

where

$$\gamma^2(z) \equiv k_z(z)^2 = \frac{\omega^2}{c(z)^2} - k^2 = k^2\left(\frac{v^2}{c(z)^2} - 1\right) \qquad 2.9$$

with $v = c_p = \frac{\omega}{k}$, the radial phase velocity. If $\Phi(r,z,t)$ is chosen to represent the velocity potential, the pressure and z component of particle velocity are given by

$$P = -\rho \frac{\partial \Phi}{\partial t} \qquad 2.10$$

$$; \qquad v_z = \frac{\partial \Phi}{\partial z} \qquad 2.11$$

2.2 Helmholtz equation solution-

For isovelocity layers Kz(z) is a constant for any particular value of K. Then in layer i

$$\phi_i(z) = A_i \sin k_{z_i} \cdot z + B_i \cos k_{z_i} \cdot z \qquad 2.12$$

with

$$k_{z_i} = \left(\frac{\omega^2}{c_i^2} - k^2\right)^{1/2} = k\left(\frac{c_r^2}{c_i^2} - 1\right)^{1/2} \quad \text{for } k < \frac{\omega}{c_i} \text{ i.e. } c_r > c_i$$

$$k_{z_i} = i\left(k^2 - \frac{\omega^2}{c_i^2}\right)^{1/2} = i k\left(1 - \frac{c_r^2}{c_i^2}\right)^{1/2} \quad \text{for } k > \frac{\omega}{c_i} \text{ i.e. } c_r < c_i$$

Ai and Bi are determined by the 2(n+1) boundary conditions

$$P_i = P_{i+1} \qquad v_{z_i} = v_{z_{i+1}} \qquad 2.13$$

$$\text{at } z = \sum_{j=1}^{i} h_j \triangleq z_i$$

where

n is the number of layers in the system
c_r is the horizontal phase velocity
c_i is the sound speed in layer i
ρ_i is the density in layer i
h_i is the layer thickness
k_{zi} is the vertical component of wavenumber
K is the horizontal propagation constant

Helmholtz equation solutions $\phi(z)$ for the N^2-linear case and in the WKB approximation are given in the appendix 2.1.

2.3 Reflection coefficient

For multilayer wave guides each of the forms for $\phi(z)$ will hold within a layer with the appropriate sound speed depth dependence. For fluid layers the boundary conditions to be met at the interface are continuity of pressure and the vertical component of particle velocity. Particle velocity is given by $V = -\nabla \Phi$ and the pressure by $P = -i\omega\rho\Phi$ when Φ is the velocity potential. At the interface between layers i and i+1

$$P_i = -i\omega\rho_i \Phi_i = -i\omega\rho_{i+1} \Phi_{i+1} = P_{i+1} \qquad 2.14$$

$$V_{z_i} = \frac{\partial \Phi_i}{\partial z} = \frac{\partial \Phi_{i+1}}{\partial z} = V_{z+1} \qquad 2.15$$

For isovelocity layers the incident, reflected, and transmitted waves at interface 1, 2 will be

$$\Phi_{inc} = A \exp\left[i k_1 (x \sin\varphi_1 + z \cos\varphi_1)\right] \qquad 2.16$$

$$\Phi_{refl} = RA \exp\left[i k_1 (x \sin\varphi_1 - z \cos\varphi_1)\right] \qquad 2.17$$

$$\Phi_{trans} = TA \exp\left[i k_2 (x \sin\varphi_2 + z \cos\varphi_2)\right] \qquad 2.18$$

The boundary conditions 2.14 and 2.15 then lead to the refraction law

$$k_1 \sin \varphi_1 = k_2 \sin \varphi_2 \qquad 2.19$$

and the reflection and transmission coefficients

$$R = \frac{Z_2 - Z_1}{Z_2 + Z_1} \quad ; \quad T = \frac{\rho_1}{\rho_2}(1+R) = \frac{2\rho_1}{\rho_2}\frac{Z_2}{Z_2+Z_1} \qquad 2.20 \; ; \; 2.21$$

where for layer i

$$Z_i = \frac{\rho_i c_i}{\cos \varphi_i} \qquad 2.22$$

Defining the normal impedance

$$Z_i \triangleq \frac{P_i}{V_{j_i}} \qquad 2.23$$

allows one to form the single boundary condition

$$Z_i = Z_{i+1} \qquad 2.24$$

at interface i, i+1. We also define the directed normal impedance $Z_i \downarrow(z)$ of a particular layer at depth z to be the ratio $\frac{P_i \downarrow}{V_{j_i} \downarrow}$ for the Helmholtz solution representing the wave traveling downward in the positive z direction. The suffix $\downarrow$ is appended to distinguish $Z\downarrow$ from $Z\uparrow$ the pressure/normal velocity ratio for the upward traveling Helmholtz solution component.

For multilayer waveguides continuity of mechanical impedance (stress motion vector) at an interface allows recursive equations to be written for R. At an interface between isovelocity layers j and j+1 in a system of n layers

$$R_{j,j+1}^{(n-j)} = \frac{R_{j,j+1} + R_{j+1,j+2}\, e^{2i\gamma_{j+1} h_{j+1}}}{1 + R_{j+1,j}\, R_{j+1,j+2}\, e^{2i\gamma_{j+1} h_{j+1}}} \qquad 2.25$$

$$R_{n,n+1}^{(o)} = R_{n,n+1}$$

with the reflection coefficient written in terms of rotations so that

$$R = \exp(i2\chi)$$

$$\chi_{j,j+1}^{(n-j)} = \arctan\left[\frac{\gamma_j \rho_{j+1}}{\gamma_{j+1} \rho_j} \tan\left(\gamma_{j+1} h_{j+1} + \chi_{j+1,j+2}^{(n-j-2)}\right)\right]$$

Here the superscript (n-j) designates the number of underlying reflecting layers.

$R_{j,j+1}$ is the reflection coefficient at an interface between two halfspaces with the same properties as layers j and j+1.

$R_{j,j+1}$ is the reflection coefficient when partial reflections from underlying layers are included.

When the isovelocity halfspace is treated as a liquid the bottom boundary condition gives

$$R_{n,n+1}^{(o)} = R_{n,n+1} = \frac{\gamma_n(H)\rho_{n+1}(H) - \rho_n(H)\gamma_{n+1}(H)}{\gamma_n(H)\rho_{n+1}(H) + \rho_n(H)\gamma_{n+1}(H)} \qquad 2.26$$

$$\chi_{n,n+1}^{(o)} = \arctan\left[\gamma_n \rho_{n+1} / \gamma_{n+1} \rho_n\right] \qquad 2.27$$

The classical equation 2.25 for the reflection coefficient in an isovelocity layer system has been derived by Abeles (ref. 23) and others. Brekhovskih offers two derivations which are important to us in our extension of these results to inhomogeneous layering. In his approach using normal and input impedances the ratio ρ/ν_j on either side of two interfaces is related to the 3 layer system input impedance Z_{inp} and the thickness of the middle layer for isovelocity layers. i.e. for the system depicted in figure 2.7. Three equations may be written:

$$Z_1(y=0) = \left.\frac{A\exp(-i\gamma_2 y) + B\exp(+i\gamma_2 y)}{A\exp(-i\gamma_2 y) - B\exp(+i\gamma_2 y)}\right|_{y=0} \cdot Z_2 \qquad 2.28$$

$$Z_{inp}(y=d) = \left.\frac{A\exp(-i\gamma_2 y) + B\exp(+i\gamma_2 y)}{A\exp(-i\gamma_2 y) - B\exp(+i\gamma_2 y)}\right|_{y=d} \cdot Z_2 \qquad 2.29$$

$$Z_3(y=d) = \frac{C\exp(-i\gamma_3(y-d)) + D\exp(i\gamma_3(y-d))}{C\exp(-i\gamma_3(y-d)) - D\exp(i\gamma_3(y-d))} \cdot Z_{inp} \qquad 2.30$$

The right hand sides of these equations are by definition simply the ratios p/v_y in layer 2 with z=0, 2 with z=d and 3 with z=d, respectively. A, B, C and D are plane wave amplitudes.
Equation 2.28 yields

$$\frac{B}{A} \equiv R_{21} = \frac{Z_1 - Z_2}{Z_1 + Z_2} \qquad 2.31$$

After substituting for $\frac{B}{A}$ from equation 2.31, equation 2.29 yields

$$Z_{inp} = \frac{Z_1 - i Z_2 \tan\gamma_2 d}{Z_2 - i Z_1 \tan\gamma_2 d} \cdot Z_2 \qquad 2.32 \text{ (Brek. 5.7)}$$

Equation 2.30 yields

$$\frac{D}{C} \equiv R = \frac{Z_{inp} - Z_3}{Z_{inp} + Z_3} \qquad 2.33 \text{ (Brek. 5.9)}$$

Manipulation gives

$$R = \frac{R_{23} + R_{12}\exp(2i\gamma_2 d)}{1 + R_{23}\cdot R_{12}\cdot\exp(2i\gamma_2 d)} \qquad 2.34$$

For systems of layers the equation becomes recursive with R_{12} replaced by R of the previous layer system.

In order to write equations 2.28, 2.29 and 2.30, it is necessary to take account of the fact that the ratio p/v_j has different signs in the incident and the reflected waves. Note also that for these isovelocity layers the field at the lower interface can be related to the field at the upper interface in layer 2 through the simple phase change $\exp(\gamma_{zj})$. The relation $Z\downarrow = -Z\uparrow$ used by Brekhovskih is a special case of the relation

$$Z\downarrow = -Z\uparrow^{*} \qquad 2.35$$

Actually, $Z\downarrow = -Z\uparrow$ is always true for isovelocity layers. $Z\downarrow = -Z\uparrow^{*}$ is trivially true for incidence angles less than critical in nondissipative layers (where $Z\downarrow$ is real). It does not hold for angles beyond critical or for dissipation in isovelocity layers as is demonstrated in Chapter 3. Extension of these results to inhomogeneous layers using equation 2.35 and the input impedance approach is given in the appendix.

In the limit of a large number of thin layers the multilayer isovelocity system approximates an inhomogeneous waveguide continuously variable with depth. Similarly, the multilayer guide comprised of small inhomogenous layers approaches the physical continuum as the number of layers increases. Computational noise is expected to be proportional to the number of layers required in the layering approximation and should be reduced with the use of higher order inhomogeneous models of the continuum.

Tolstoy and Clay (ref. 2, p. 28-33) develop the concept of plane wave reflection coefficients R for continuously stratified, constant density media and derive a complex Ricatti equation for R.

$$\frac{dR}{dz} - \frac{1}{2}(1-R^2)\frac{d}{dz}\log K_z + 2iK_z R = 0 \qquad 2.36$$

Solution is given by the ray approximation reflection coefficient

$$R = R(z_0)\exp\left(-2i\int_{z_0}^{z} K_z\, dz\right) \qquad 2.37$$

when their criterion $\frac{1}{k_j}\frac{d}{dj}\log k_j << 1$ is satisfied. 2.38

This solution form holds exactly within homogeneous layers. For inhomogeneous layers, its validity depends on satisfaction of the criterion 2.38

In the appendix we present exact reflection coefficient formulae valid in inhomogeneous layering systems.

The concept of plane wave reflection coefficient in continuously stratified media is well illustrated in figure 2.4 of Tolstoy and Clay (ref. 2, p. 28), sketched here in figure 2.1 $R(z_0)$ is defined as the ratio of upgoing wave amplitude to incident wave amplitude assumed =1 at level z_0 and R(z) is defined at arbitrary point z in either section. The effect of smoothly varying c(z) within a layer is simply to bend rays. The reflection coefficient is defined at depth z independent of the presence of an interface between discontinuities in sound speed or density. In fact the normal mode solution is frequently formulated in terms of $R\downarrow$ and $R\uparrow$, the plane wave reflection coefficients looking up and looking down at the source depth.

2.4 Characteristic equation:

Normal modes of propagation may be shown to be represented by upward and downward traveling wavetrains which reflect at boundaries, or refract through turning points in a waveguide, and interfere with each other constructively. In order to determine the incidence angles at a given frequency for which interference will be constructive, we require the reflection coefficient in the source isovelocity layer looking up and down. These will be denoted $R\uparrow$ and $R\downarrow$ respectively. We follow Tolstoy in writing the characteristic equation at an arbitrary level z as $R\uparrow \cdot R\downarrow = 1$ 2.40

for total reflection. Writing the coefficient in terms of rotations has $R = \exp(i2\chi)$ and the characteristic equation becomes

$$\chi\uparrow + \chi\downarrow = m\pi \qquad 2.41$$

Writing the equation at one depth as in equation 2.40 makes clear the constancy of the modal field at any depth. Physically these equations are interpreted as specifying conditions for standing waves in z. The mode system will propagate horizontally, but there will be no change in amplitude at depth z due to the combined effect of reflections from underlying media (aside from attenuation and $e^{-i\omega t}$ which are both independent of depth). That is, the upward and downward traveling wave components combine to give the vertical standing wave which is called the mode shape. This wave is a traveling wave in the direction of the waveguide axis. In the next sections we summarize derivations of the characteristic equation, applicable to waveguides with both dissipative and nondissipative boundaries. These equations require $\mathcal{R}\uparrow$ and $\mathcal{R}\downarrow$ now defined at bottom and top of the source layer (ocean or layer in which c and ρ are continuous). We must formulate the characteristic equation for the case of damped and undamped normal modes. Intuitively it would seem $\mathcal{R}\uparrow \cdot \mathcal{R}\downarrow \neq 1$ in the case of absorption, but that $\chi\uparrow + \chi\downarrow = m\pi$ might still be used to represent constructive interference. We will find from the rigorous formulation that $\mathcal{R}\downarrow \cdot \exp(2ik_z \cdot h) \cdot \mathcal{R}\uparrow = 1$ will be used even in the presence of absorption to select waves for constructive interference.

2.4.a. Physical formulation of the characteristic equation:

Bucker (ref. 14) has analyzed the problem of normal mode propagation with lossy boundaries and explains the characteristic equation in the following terms. Considering the normal mode to be an interfering set of plane waves, (the downgoing set shown in figure 2.2a) the condition that must be satisfied is that points A and D be in phase, so that

$$2\pi \int_{ABCD} \frac{dl}{\lambda} - \epsilon_b - \epsilon_s = (n-1)\,2\pi \qquad n = 1, 2, 3 \qquad 2.42$$

where ϵ_b and ϵ_s are the phase shifts suffered on bottom and surface reflection. In our case $\epsilon_s = -\pi$ and $\epsilon_b = \phi'$

because the field at B+ is represented by $|R| e^{i\phi'}$ due to partial reflections of the whole wavefront from the system of layers extending infinitely in x. Bucker rewrites this as

$$2\pi \int_{ABCD} \frac{dl}{\lambda} = 2\pi \int_{ABCDE} \frac{dl}{\lambda} - 2\pi \int_{DE} \frac{dl}{\lambda} = \epsilon_b + \epsilon_s + (n-1)2\pi \qquad 2.43$$

The second integral is interpreted as

$$2\pi \int_{ABCDE} \frac{dl}{\lambda} = \omega \int_{\text{complete cycle}} \frac{dl}{c(y)} = \omega T \qquad 2.44$$

where T, the ray cycle time is the period in which a ray completes a full cycle through any particular depth. Also, with phase velocity Cp

$$2\pi \int_{DE} \frac{dl}{\lambda} = 2\pi \int_{DE} \sin\theta_A \frac{dx}{\lambda_A} = \frac{2\pi \sin\theta}{\lambda} \int_{AE} dx = \frac{\omega X}{c_p} \qquad 2.45$$

where X is the ray cycle length, because

$$\frac{dl}{\lambda} = \frac{dl_a}{\lambda_a} = \frac{dx \sin\theta_A}{\lambda_a} \qquad 2.46$$

with $\frac{\sin\theta}{\lambda}$, the ray parameter, constant along any ray. dl_a and λ_a are arc length and wavelength along a ray at level A. Bucker then observes that with dx and dz now the projections of increment dl,

$$\omega \int_{\text{cycle length}} \frac{dl}{c(y)} - \omega \int_{\text{cycle length}} \frac{dx}{c_p} = \omega \int \frac{dy}{c(y)\cos\theta} - \omega \int \frac{dy}{c(y)} \frac{\sin^2\theta}{\cos\theta}$$

$$= \omega \int \frac{dy \cos\theta}{c(y)} = \int k_y \cdot dy \qquad 2.47$$

But this is just the vertical phase integral in the water column. So the characteristic equation becomes

$$\int_{cycle} k_j \cdot d_j + \epsilon_b + \epsilon_s = (n-1)\, 2\pi \qquad 2.48$$

For the isovelocity ocean or source layer of thickness d

$$\int_{cycle} k_j \cdot d_j = 2 \cdot k_j \cdot d \qquad 2.49$$

and the characteristic equation is

$$2 k_j \cdot d + \epsilon_b + \epsilon_s = (n-1)\, 2\pi \qquad 2.50$$

We will later use complex incidence angle $\tilde{\varphi} = \varphi' + i\,\varphi''$ 2.51

Then

$$e^{i k_0 (\cos(\varphi' + i\varphi'')\, d)} = e^{(i\, k' \cos\varphi' \cdot \cosh\varphi'' \cdot d)} \cdot e^{(-\sin\varphi' \cdot \sinh\varphi'' \cdot d)}$$

Since we physically expect the attenuation $1 - e^{-\sin\varphi' \cdot \sinh\varphi'' \cdot d}$ 2.52 in the water column to be negligible relative to reflection loss $1 - |R|$ we will assume real incidence angle by setting $\varphi'' = 0$ and attenuation in the water column =0. At the free surface we set $\epsilon_s = -\pi$ (Tolstoy uses χ=0 here because his definition is $R = -e^{-2\chi}$). Then the characteristic equation with an isovelocity source layer is,

$$2 k' \cos\varphi' \cdot d + \epsilon_b - \pi = (n-1)\, 2\pi \qquad 2.53$$

a phase equation.

2.4.b. Rigorous formulation of the characteristic equation:

Brekhovskih has developed normal mode theory for an isovelocity waveguide bounded by media with arbitrary velocity variation. We use his method as the rigorous method for determining normal mode dispersion and attenuation in both the dissipative and nondissipative boundary models. Our problem then becomes one of evaluating the complex reflection coefficient for the chosen model of the bounding media, and implementing a numerical routine to solve the characteristic equation. In this section we briefly present the equations

leading to the rigorous characteristic equation. The wave radiated by a point source at frequency ω has a velocity potential

$$\varphi_0 = \frac{V_0}{4\pi} \frac{e^{i(k\cdot R - \omega t)}}{R}, \quad R = \sqrt{x^2+y^2+z^2} \qquad 2.54$$

where V_0 is the source volume velocity in units $length^3/sec.$. In the plane z=0 the field of the source has a double Fourier integral representation

$$\frac{e^{ikr}}{r} = \iint_{-\infty}^{\infty} A(k_x, k_y) \exp\left[i(k_x\cdot x + k_y\cdot y)\right] dk_x\, dk_y \qquad 2.55$$

Brek. 18.11

$A(k_x, k_y)$ is given by the inverse transform

$$A(k_x, k_y) = \frac{1}{(2\pi)^2} \iint_{-\infty}^{\infty} \frac{e^{ikr}}{r} \exp\left[-i(k_x\cdot x + k_y\cdot y)\right] dx\, dy \qquad 2.56$$

Brek. 18.12

Transforming to polar notation with

$$k_x = q\cos\psi \qquad k_y = q\sin\psi \qquad q = \sqrt{k_x^2+k_y^2}$$

$$x = r\cos\phi \qquad y = r\sin\phi \qquad dx\,dy = r\,dr\,d\phi$$

$$A(k_x, k_y) = \frac{1}{(2\pi)^2} \int_0^{2\pi} d\phi \int_0^{\infty} \exp\left\{ir\left[k - q\cos(\psi-\phi)\right]\right\} dr \qquad 2.57$$

leads to

$$A(k_x, k_y) = \frac{i}{2\pi\sqrt{k^2-k_x^2-k_y^2}} \qquad 2.58$$

$$\frac{e^{ikr}}{r} = \frac{i}{2\pi} \iint_{-\infty}^{\infty} \frac{\exp\left[i(k_x \cdot x + k_y \cdot y)\right]}{\sqrt{k^2 - k_x^2 - k_y^2}} \, dk_x \cdot dk_y \qquad \begin{matrix} 2.59 \\ \text{Brek. } 18.15 \end{matrix}$$

This is the expression for the field in the x,y plane in a homogeneous medium. It is "continued" into space by adding the term $\pm i k_z \cdot z$ where $k_z = \sqrt{k^2 - k_x^2 - k_y^2}$

\+ is used for points in the halfspace $z > 0$

\- is used for points in the halfspace $z < 0$

Then for $z \gtrless 0$

$$\frac{e^{ikR}}{R} = \frac{i}{2\pi} \iint_{-\infty}^{\infty} \exp\left[i(k_x \cdot x + k_y \cdot y \pm k_z \cdot z)\right] \frac{dk_x \, dk_y}{k_z} \qquad \begin{matrix} 2.60 \, * \\ \text{Brek } 18.17 \end{matrix}$$

The integration over wave vector may be replaced by an integration over angles φ and ϕ using $k_x = k \sin\varphi \cos\phi$

$k_y = k \sin\varphi \sin\phi$, $k_z = k \cos\varphi$

Integration with respect to ϕ is performed between $(0, 2\pi)$.

Integration with respect to φ can not be restricted to real values since k_z varies from $k_z = k$ when $k_x = k_y = 0$ to $k_z = i\infty$ when $k_x \longrightarrow \pm\infty$ or $k_y \longrightarrow \pm\infty$. Equation Brek. 18.17 is transformed to equation Brek. 18.19

for $z > 0$

$$\frac{e^{ikR}}{R} = \frac{ik}{2\pi} \int_0^{\frac{\pi}{2} - i\infty} \int_0^{2\pi} \exp\left[i\left(k\cos\phi \sin\varphi \cdot x + k \sin\phi \sin\varphi \cdot y + k\cos\varphi\right)\right] \sin\varphi \, d\varphi \, d\phi$$

$$\begin{matrix} 2.61 \\ \text{Brek } 18.19 \end{matrix}$$

* An interesting derivation of the unbounded medium Greens function represented by equation 2.60 which uses a triple Fourier integral representation and does not appeal to analytic continuation is given in reference 30.

for $z < 0$

2.61
Brek. 18.19

$$\frac{e^{ikR}}{R} = \frac{ik}{2\pi} \int_0^{\frac{\pi}{2}-i\infty} \int_0^{2\pi} \exp\left[i\left(k\cos\phi \sin\varphi \cdot x + k\sin\phi \cdot \sin\varphi \cdot y + k\cos\varphi\right)\right] \sin\varphi \, d\varphi \, d\phi$$

Brekhovskih remarks that the inhomogeneous waves at $\varphi = \frac{\pi}{2} - ia$ with "a" real and positive are propagated at shortened wavelength along some direction in the x-y plane (depending on ϕ) with exponentially decreasing amplitude in the z direction. The plane does not necessarily correspond to any physical interface in the z direction. This condition is necessary in order to get a field with an impulse at the source and bounded elsewhere. The contour goes to $-i\infty$ rather than $+i\infty$ so that the inhomogeneous waves have reduced amplitude with depth.

The inner integral is performed by noting that

$$\int_0^{2\pi} \exp\left[ikx\cos\phi + y\sin\phi)\sin\varphi\right] d\phi =$$

$$\int_0^{2\pi} \exp\left[ikr\sin\varphi \cdot \cos(\phi - \phi_1)\right] d\phi = 2\pi J_0(u)$$

2.62
Brek 19.4

where $u = kr\sin\varphi$

Then since $J_0(u) = \frac{1}{2}\left[H_0^{(1)}(u) + H_0^{(2)}(u)\right]$

$H_0^{(1)}$ and $H_0^{(2)}$ are Hankel functions of the first and second kinds and so is the zero order Bessel function. Since

$$H_0^{(2)}\left(e^{-i\pi}u\right) = -H_0^{(1)}(u)$$

the outer integral may be written as

$$\frac{ik}{2}\int_{-\frac{\pi}{2}+i\infty}^{\frac{\pi}{2}-i\infty} H_0^{(1)}(u)\ \exp\left[\pm i k_3 \cdot 3\right] \sin\varphi\, d\varphi \qquad \begin{matrix} 2.63 \\ \text{Brek 26.1} \end{matrix}$$

The contour of integration is now as depicted in figure 2.5.

For the waveguide problem Brekhovskih starts with the field of a spherical wave over an interface represented as a superposition of plane waves of type

$$\exp\left\{i\left[k_x \cdot x + k_y \cdot y + k_3 (z - z_0)\right]\right\}$$

and reflected waves of type

$$R(\varphi)\exp\left\{i\left[k_x \cdot x + k_y \cdot y + k_3 (3 + 3_0)\right]\right\}$$

In the layer with upper and lower boundaries the field is due to an infinite series of waves reflected at the boundaries. Brekhovskih sums over all plane waves of a given direction cosine but different number of reflections, and then integrates the sum over all values of direction cosine. He gives the expression

$$\psi = \frac{ik}{2\pi}\int_0^{\frac{\pi}{2}-i\infty}\int_0^{2\pi} \exp\left[i(k_x \cdot x + k_y \cdot y)\right] \sum_{l=0}^{\infty} \left\{\exp\left[ik_3(3-3_0)\right] + \right.$$

$$R_1 \exp\left[ik_3(3+3_0)\right] + R_2 \exp\left[ik_3(2h-3-3_0)\right] +$$

$$\left. R_1 \cdot R_2 \cdot \exp\left[ik_3(2h-3+3_0)\right]\right\} (R_1 \cdot R_2)^l \cdot \exp(2ik_3 \cdot l \cdot h) \cdot$$

$$\cdot \sin\varphi\, d\varphi \cdot d\phi \qquad \begin{matrix} 2.64 \\ \text{Brek 27.1} \end{matrix}$$

where R_1 and R_2 are reflection coefficients at lower and upper boundaries respectively.

The sum of images representation of the field is discussed at length by Brekhovskih (ref. 1 , p. 325-333). For the layer assumed

initially to have perfectly reflecting boundaries, image sources may be positioned at equal distance vertically from each boundary so that by symmetry the boundary condition $d\psi/dz$ is maintained. As each

new image source is introduced another is required to achieve the boundary condition at the other interface. It can be shown that the direct path from each image corresponds to a ray path emanating from the original source and undergoing a definite number of reflections from the boundaries. The source and its image in either boundary, as well as the image in the upper boundary of the first source image in the lower boundary are illustrated in figure 2.3. In figure 2.4 the corresponding intralayer ray paths are indicated. Additional sets of four image ray paths are distinguished from this first set by having interacted with both boundaries and traveled an additional distance $2 \cdot h \cdot l$ with l the set index.

Brekhovskih uses the expressions

$$\sum_{l=0}^{\infty} (R_1 \cdot R_2)^l \exp(2lbh) = \frac{1}{1 - R_1 \cdot R_2 \exp(2bh)} \qquad 2.65$$

$b = ib_z$ Brek 26.6

and

$$\exp[b(z-z_0)] + R_1 \exp[b(z+z_0)] + R_2 \exp[b(2h-z-z_0)] +$$

$$R_1 \cdot R_2 \cdot \exp[b(2h-z+z_0)] = [\exp(-bz_0) + R_1 \exp(bz_0)] \cdot$$

$$[\exp(bz) + R_2 \exp(b \cdot (2h-z))] \qquad 2.66$$

Brek. 26.5

to get

$$\psi = \frac{ik}{2} \int_{\Gamma} \frac{[\exp(-bz) + R_1 \exp(bz)] \cdot [\exp(-b(h-z_0)) + R_2 \exp(b(h-z_0))]}{\exp(-bh) \cdot [1 - R_1 \cdot R_2 \exp(2bh)]} \cdot$$

$$H_0^{(1)}(kr \sin\varphi) \cdot \sin\varphi \, d\varphi \qquad 2.67$$

Brek 26.7

This is the essential equation. Brekhovskih equations 27.1 and 26.7 come from expressing the field in a layer bounded by arbitrary media as a contribution from a direct wave and from an infinite series of waves which have been reflected at the boundaries of the layer various numbers of times. He has generalized the picture of image sources invoked when the boundaries are perfectly reflecting by starting from the spherical wave representation and for each value of wavenumber (direction cosine) summing over all combinations of reflections. He includes wavefront portions of a particular wavenumber which arrive directly, after reflection from the upper boundary, after reflection from the lower boundary, or after reflection from both (assuming ℓ previous interactions with both boundaries). This is expressed in equation Brek. 27.1. Brekhovskih notes that the generalization of the image source representation to layers with arbitrary boundaries is valid in layers thick compared with a wavelength, but that in thin layers the number of reflections must be great or an additional series of correction terms must be included.

To evaluate equation 26.7 Brekhovskih transforms the path of integration. The integral over path Γ_1 is written as the sum of integrals over contours Γ_2 and Γ_3 shown in figure 2.5b He shows that the overlapping integrals in Γ_2 and Γ_3 cancel and that the total integral over Γ_2 is zero. When the path deformation is made, and with contribution along Γ_4 at infinity equal to zero, the total field is evaluated by taking residue contributions at poles of the integrand and integrals along branch lines corresponding to

$$\mathrm{Im}\sqrt{n_1^2-\sin^2\varphi}=0 \qquad \text{and} \qquad \mathrm{Im}\sqrt{n_2^2-\sin^2\varphi}=0$$

The field is now given by Brek. 27.21

$$\psi = \int_{\Gamma_1} \Phi(\varphi)\, H_0^{(1)}(kr\sin\varphi)\cdot\sin\varphi\cdot d\varphi = 2\pi i \sum \mathrm{Res}\left[\Phi(\varphi_\ell)\right]\cdot H_0^{(1)}(kr\sin\varphi_\ell)\cdot\sin\varphi_\ell +$$

$$\int_{i\infty}^{A_1+} \Phi(\varphi)\, H_0^{(1)}(kr\sin\varphi)\sin\varphi\cdot d\varphi + \int_{\infty}^{A_2+} \Phi(\varphi)\, H_0^{(1)}(kr\sin\varphi)\sin\varphi\, d\varphi \qquad \begin{matrix}2.68\\ \text{Brek 27.21}\end{matrix}$$

The first term in 2.68 is the contribution from poles at the roots of the equation

$$1 - R_1(\varphi) \cdot R_2(\varphi) \cdot \exp(2ikh\cos\varphi) = 0 \qquad \text{Brek 27.22}$$

This is the characteristic equation for both real and complex c and real or complex φ. Poles will be found at complex values of $\varphi = \tilde{\varphi}$ provided that $R(\tilde{\varphi})$ can be evaluated. The branch line integrals appear because $R_1(\varphi)$ and $R_2(\varphi)$ are not single valued, depending on which of $\pm\sqrt{n_{1,2}^2 - \sin^2\varphi}$ are taken, where n_1 and n_2 are the indices of refraction re layer velocity for upper and lower media. Brekhovskih defines four Riemann sheets (++, +-, -+, --) depending on the sign chosen and keeps Γ_1, Γ_2, Γ_3 and Γ_4 on the ++ sheet. The continuous spectrum corresponds to the branch line integral (see Brek. p. 350), but may be evaluated partially from contributions of discrete leaky modes in the manner of Rosenbaum (after uncovering another sheet). We will find that these contributions correspond to taking solutions with - or + part of imaginary angle in layer 2 of the Pekeris guide. In figure 2.6.a. we indicate positions of poles and the branch line for the case of a lossless bounding halfspace. Poles are located on the real φ axis in the range $\varphi_{critical} < \varphi' < \frac{\pi}{2}$ with pole density and location dependent on frequency. The branch line lies along the real axis for $0 < \varphi' < \varphi_{critical}$ and coincides with the imaginary axis for $\varphi' = 0$, $0 < \varphi'' < \infty$. Along the branch line, $\mathrm{Im}\sqrt{n_1^2 - \sin^2\varphi} = 0$ and in the lossless case n_1 is real.

For the case of an absorbing halfspace pole and branch line positions are indicated in figure 2.6.b. Pole positions are shown in more detail for particular model parameter values in figure 5.5. Both poles and the branch line came into the first quadrant as sound speed is made complex. Brekhovskih's equation 27.19 may be used to evaluate the acoustic field or Brek. 27.22 may be used by itself to determine properties of the eigenvalues. In either case the reflect-

ion coefficient for the waveguide boundaries must be evaluated either as an estimate from field data or as a property of the selected model. In the latter case multilayer models are usually required to adequately represent realized coefficients over large frequency and wavenumber domains.

2.5 Mode shapes:

The formulae for R when combined with the characteristic equation allow solution for eigenvalues $k_n(\omega)$. We have implemented a program to search for eigenvalues $\omega_n(c_p)$ as a function of phase velocity c_p and mode number n . These eigenvalues in combination with layer eigenfunction coefficients are then used to generate mode shapes as a function of frequency.

For multilayer systems calculation of the interface reflection coefficients recursively using equation 2.34 during the eigenvalue search yields the ratio of upward to downward eigenfunction coefficient Bi/Ai in each layer i. This is equivalent to having a downward traveling wave with unit coefficient in each layer and an upward traveling wave whose coefficient is Ri. To calculate absolute mode shape within each layer we must adjust each downward coefficient so that the boundary conditions are again met, but with the downward traveling wave of unit amplitude in the source layer only.

For the upper isovelocity medium in model 2a the field is described by

$$\phi(y) = \exp(i k_0 y \cos\varphi_0) + R(\varphi_0) \exp(-i k_0 y \cos\varphi_0)$$

$$R(\varphi_0) = \exp(i 2\theta) \quad \text{and} \quad -d < y < 0 \qquad 2.69$$

$k_0 = \frac{\omega}{c_0}$ is the wavenumber in the ocean

$k_{0x} = \frac{\omega}{v_0}$ is the eigenvalue in ocean layer 0

φ_0 is the incidence angle = $\sin^{-1}\left(\frac{c_0}{v}\right)$

$$\phi(z) = 2 \cos N (\cos M + i \sin M) \qquad 2.70$$

where $M = \frac{1}{2}(a+b)$

$N = \frac{1}{2}(a-b)$

$a \equiv k_0 z \cos\varphi_0 \qquad b \equiv 2\Theta - k_0 z \cos\varphi_0$

$$\Theta = \tan^{-1}\left[\frac{J_{\frac{1}{3}}(V_0) + J_{-\frac{2}{3}}(V_0)}{J_{\frac{1}{3}}(V_0) - J_{-\frac{1}{3}}(V_0)}\right] \qquad 2.71$$

$$V_0 = \frac{2}{3}\left(\frac{k_0}{g}\right) f_0^{3/2} \qquad f_0 = \cos^2\varphi_0 \qquad 2.72$$

g is N^2- linear slope

and the characteristic equation is

$$2 k_0 d \cos\varphi_0 - 2\Theta - \pi = n\, 2\pi \qquad 2.73$$

We define the mode shape to be

$$S(z) \equiv |\phi(z)| = 2 \cos N \left[\cos^2 M + \sin^2 M\right]^{\frac{1}{2}}$$

$$= 2 \cos (k_0 z \cos\varphi_0 - \Theta)$$

If the underlying medium were isovelocity Θ would be the phase of the recursive reflection coefficient. Mode shape for the underlying N^2-linear layer itself is given in the appendix.

Appendix 2.1 Helmholtz equation solutions.

2.1.a. N^2-linear layers.

For N^2-linear layers, with N the index of refraction, the wavenumber squared varies linearly within the layer. The vertical component of velocity potential $\phi_j(z)$ in layer j is given by

$$\phi_j(z) = A_j f_j(z) + B_j g_j(z)$$

Here

$$\left[\frac{\omega}{c(z)}\right] = \left[\frac{\omega}{c(z_{j,j-})}\right]^2 (1 \pm g_j z)$$

where $c(z_{j,j-})$ is the sound speed at the top of the jth layer.

Solutions for f_j , g_j are well known to be Airy functions (Morris) or 1/3 order Hankel functions (Brek.). We follow Brekhovskih in using

$$\phi(z) = \sqrt{}^{1/3} \left[A H^{(1)}_{1/3}(v) + B H^{(2)}_{1/3}(v)\right]$$

where

$$v \equiv \frac{2}{3}\left(\frac{k_0}{g}\right) J^{3/2} \qquad k_0 \equiv \frac{\omega}{c_j(z=0)}$$

$$J \equiv \cos^2\varphi_0 - g z = N^2(z) - \sin^2\varphi_0$$

$$\text{and} \quad N^2 = 1 - g z$$

φ_0 is the incidence angle for a plane wave at the source

2.1.b. WKB approximation.

In a layer with arbitrary velocity variation, the WKB solution for $\phi(z)$ is obtained by substituting

$$\phi(z) = \Psi(z)\, e^{i\Theta(z)}$$

into the Helmholtz equation to obtain

$$\Psi'' + 2i\Theta'\Psi' + i\Theta''\Psi + \left[\gamma^2(z) - (\Theta')^2\right]\Psi = 0 \qquad ' \equiv \frac{d}{dz}$$

Neglecting Ψ'' leads to two equations

$$(\Theta')^2 = \gamma^2(z) \qquad \text{and} \qquad 2\Theta'\Psi' + \Theta''\Psi = 0$$

Solutions are

$$\Theta' = \pm\gamma_z \implies \Theta = \pm\int_{z_0}^{z} \gamma(z)\, dz \quad \text{and}$$

$$\Psi = \frac{c}{\sqrt{\gamma(z)}}$$

so that

$$\phi(z) = \frac{1}{\sqrt{\gamma(z)}}\left\{C_1 \exp\left[i\int_{z_0}^{z}\gamma(z)\,dz\right] + C_2 \exp\left[-i\int_{z_0}^{z}\gamma(z)\,dz\right]\right\}$$

Then with

$$s \equiv \pm \int_{z_0}^{z} \gamma(z)\, dz + s_0 \quad , \quad \Phi(z) = A\, \gamma^{-1/2} e^{-s}$$

Appendix 2.2 Reflection coefficient formulae.

2.2.a. Reflection coefficient and derivation in model 2a.

For model 2a where the system of layers reduces to an isovelocity layer over an N^2-linear halfspace the reflection coefficient will be shown to be

$$R = -\left[\frac{\rho_1 \left(J_{\frac{2}{3}} - J_{-\frac{2}{3}} \right) + i \rho_2 \left(J_{1/3} + J_{-1/3} \right)}{\rho_1 \left(J_{\frac{2}{3}} - J_{-\frac{2}{3}} \right) - i \rho_2 \left(J_{1/3} + J_{-1/3} \right)}\right]$$

where u the argument of J is evaluated at the interface $z = 0$

$$u \equiv \frac{2}{3} \left(k / g \right) \cos^3 \varphi_0$$

$$k = \omega / c_1(z=0) \qquad g \text{ is the } N^2\text{-linear gradient}$$

Then $R = \exp[-i 2\Theta]$ with $\Theta = \tan^{-1}\left[\dfrac{J_{1/3} + J_{-1/3}}{J_{1/3} - J_{-2/3}}\right]$

This result except for the minus sign is given by Brekhovskih. (see Brek 15.15)

For the case of a velocity discontinuity at the interface we have modified this to

$$R = \exp(i 2\Theta) \quad \text{with} \quad \Theta = \tan^{-1}\left[\frac{(J_{1/3} + J_{-1/3})}{K_\rho(\varphi_0)\left(J_{\frac{2}{3}} + J_{-\frac{2}{3}}\right)}\right]$$

$$K_\rho(\varphi_0) \equiv \frac{k_2(0)}{k_1(0)} \frac{[\rho - 1 + \cos^2 \varphi_0]}{\cos \varphi_0}$$

$$k_1(0) \equiv \frac{\omega}{c_1(z=0)} \qquad k_2(0) \equiv \frac{\omega}{c_2(z=0)}$$

p is the index of refraction squared at z=0, the top of the N^2-linear halfspace.

Derivation:

Writing the field in the upper medium as

$$\phi_1(z) = \exp(i k_{1z} \cos\varphi_0) + R(\varphi_0) \exp(-i k_{1z} \cos\varphi_0)$$

and in the lower medium as

$$\phi_2(z) = u^{1/3} \left[A H^{(1)}_{1/3}(u) + B H^{(2)}_{1/3}(u) \right]$$

We have to satisfy the boundary conditions

$$u \equiv \frac{2}{3} \frac{k_1}{g} \zeta^{3/2}$$

$$\zeta \equiv \cos^2\varphi_0 \pm g z$$

$$k_1 \equiv \frac{\omega}{c_1(z=0)} = \frac{\omega}{c_2(z=0)}$$

$$-i\omega\rho_1 \phi_1(z) = -i\omega\rho_2 \phi_2(z)$$

$$-\frac{\partial \phi_1(z)}{\partial z} = -\frac{\partial \phi_2(z)}{\partial z}$$

Then

$$-i\omega\rho_1 (1+\tilde{R}) = \tilde{B}(-i\omega\rho_2)\left[e^{i\frac{\pi}{3}} u_0^{1/3} H^{(1)}_{1/3}(u_0) + u_0^{1/3} H^{(2)}_{1/3}(u_0) \right]$$

$$i k_1 \cos\varphi_0 (1-\tilde{R}) = \pm k_1 \cos\varphi_0 \left[e^{i\pi/3} u_0^{1/3} H^{(1)}_{-\frac{2}{3}}(u_0) + u_0^{1/3} H^{(2)}_{-\frac{2}{3}}(u_0) \right] \tilde{B}$$

and index of refraction is increasing so we use the - sign.

Then since

$$\frac{du}{dz} = -k_1 \cos\varphi_0 \quad \text{dividing}$$

$$\frac{1}{\rho_1}\left(\frac{R-1}{R+1}\right) = \frac{1}{\rho_2} \left[\frac{-i u^{1/3} \left[e^{i\pi/3} H^{(1)}_{-\frac{2}{3}}(u_0) + H^{(2)}_{-\frac{2}{3}}(u_0) \right] \tilde{B}}{u^{1/3} \left[e^{i\pi/3} H^{(1)}_{1/3} + H^{(2)}_{1/3} \right] \tilde{B}} \right]$$

and $\quad R = \dfrac{1 + \{\quad\}}{1 - \{\quad\}}$ $\quad$ where $\{\quad\} \equiv \dfrac{\rho_1}{\rho_2} \cdot [\text{above}]$

$$R = \frac{\rho_2 \left[e^{i\pi/3} H^{(1)}_{1/3} + H^{(2)}_{1/3} \right] - i\rho_1 \left[e^{i\pi/3} H^{(1)}_{-2/3} + H^{(2)}_{-2/3} \right]}{\rho_2 \left[e^{i\pi/3} H^{(1)}_{1/3} + H^{(2)}_{1/3} \right] + i\rho_1 \left[e^{i\pi/3} H^{(1)}_{-2/3} + H^{(2)}_{-2/3} \right]}$$

$$R = \frac{\rho_2 \left[e^{i\pi/3} \left\{ \frac{i}{\sin \frac{\pi}{3}} \left[e^{i\pi/3} J_{1/3} - J_{-1/3} \right] \right\} + \left\{ \frac{-i}{\sin \frac{\pi}{3}} \left[e^{i\frac{\pi}{3}} J_{1/3} - J_{-1/3} \right] \right\} \right]}{\rho_2 \left[e^{i\pi/3} \left\{ \frac{i}{\sin \pi/3} \left[e^{-i\pi/3} J_{1/3} - J_{-1/3} \right] \right\} + \left\{ \frac{-i}{\sin \frac{\pi}{3}} \left[e^{i\pi/3} J_{1/3} - J_{-1/3} \right] \right\} \right]} \cdots$$

$$\cdots \frac{-i\rho_1 \left[e^{i\pi/3} \left\{ \frac{i}{\sin -\frac{2\pi}{3}} \left[e^{i\frac{\pi}{3}} J_{-\frac{1}{3}} - J_{\frac{1}{3}} \right] \right\} + \left\{ \frac{-i}{\sin -\frac{2\pi}{3}} \left[e^{-i\frac{2\pi}{3}} J_{-\frac{1}{3}} - J_{\frac{1}{3}} \right] \right\} \right]}{i\rho_1 \left[e^{i\pi/3} \left\{ \frac{i}{\sin -\frac{2\pi}{3}} \left[e^{i\frac{\pi}{3}} J_{-\frac{2}{3}} - J_{\frac{2}{3}} \right] \right\} + \left\{ \frac{-i}{\sin -\frac{2\pi}{3}} \left[e^{-i\frac{2\pi}{3}} J_{-\frac{2}{3}} - J_{\frac{2}{3}} \right] \right\} \right]}$$

$$R = \frac{\rho_2 \left\{ J_{1/3} \left[\frac{i\left(1 - e^{i\pi/3}\right)}{\sin \frac{\pi}{3}} \right] + J_{-\frac{1}{3}} \left[\frac{i\left(1 - e^{i\pi/3}\right)}{\sin \frac{\pi}{3}} \right] \right\}}{\rho_2 \left\{ J_{1/3} \left[\frac{i\left(1 - e^{i\pi/3}\right)}{\sin \frac{\pi}{3}} \right] + J_{-\frac{1}{3}} \left[\frac{i\left(1 - e^{i\pi/3}\right)}{\sin \frac{\pi}{3}} \right] \right\}} \cdots$$

$$\cdots \frac{-i\rho_1 \left\{ J_{-\frac{2}{3}} \left[i\left(e^{i\frac{2\pi}{3}} - e^{-i2\frac{\pi}{3}} \right) \right] / \sin\left(\frac{2\pi}{3}\right) + J_{\frac{2}{3}} \frac{i\left(1 - e^{i\frac{\pi}{3}}\right)}{\sin\left(-\frac{2\pi}{3}\right)} \right\}}{i\rho_1 \left\{ J_{-\frac{2}{3}} \left[\frac{i\left(e^{i0} - e^{-i2\pi/3}\right)}{\sin\left(-\frac{2}{3}\pi\right)} \right] + J_{\frac{2}{3}} \, i \left(\frac{1 - e^{i\pi/3}}{\sin\left(-\frac{2}{3}\pi\right)} \right) \right\}}$$

$$R = \frac{-\left[\rho_1 \left(J_{-\frac{2}{3}} - J_{\frac{2}{3}} \right) + i\rho_2 \left(J_{\frac{1}{3}} + J_{-\frac{1}{3}} \right) \right]}{\left[\rho_1 \left(J_{-\frac{2}{3}} - J_{\frac{2}{3}} \right) - i\rho_2 \left(J_{\frac{1}{3}} + J_{-\frac{1}{3}} \right) \right]}$$

2.2.b. Recursive reflection coefficient and derivation for N^2-linear case:

For inhomogeneous layers it may not be sufficient to simply replace the exponential phase change in equation 2.34 by the phase integral *from* layer bottom to top. Conditions leading to the plane wave reflection coefficient which satisfies equation 2.37 may be violated. When condition equation 2.38 holds the phase integral should be a good approximation and is equivalent to continuing the reflection coefficient upward as in equation 2.37. However, there will also be an amplitude change due to varying index of refraction. We require an equation for calculating the reflection coefficient at interfaces recursively in the manner of equation 2.34. This equation will explicitly include matching at the boundaries required to continue solutions beyond the layer where phase integral approximations are valid. Additionally it will be more accurate than a solution like equation 2.37 within any layer, when approximations are not made in calculating the functions involved.

For N^2-linear layer systems we use Helmholtz solutions given at the beginning of this chapter. The relation $Z\downarrow = -Z\uparrow^*$ holds as long as J_{mag} (below) is real and Θ_N and Θ_D are real. This will be true for argument ν real so that the Bessel functions are real. Thus it holds at levels z above the turning point in nondissipative N^2-linear layers. We have

$$Z_j\downarrow = \left[-i\omega\left(\rho_j A H^{(2)}_{1/3}(\nu(3))\right]\right] \Big/ \left[-\frac{d}{d3}\left(A H^{(1)}_{1/3}(\nu(3))\right)\right]$$

where

$$\nu = \frac{2}{3}\frac{k_0}{g} J^{3/2} \qquad J = \cos^2\varphi_0 \pm g\,3^4(\rho - 1)$$

with the variation of index of refraction $N^2 = \rho \pm g3$. The - sign is chosen for sound speed increasing with depth and z axis pointing downward. ω is the frequency. Performing the differentiation we find

$$Z_j\downarrow = \frac{+i\omega\rho_j \; H^{(1)}_{1/3}(\nu(j))}{(\pm 1)\, k_j(0) \; H^{(1)}_{-2/3}(\nu(j))} \cdot \frac{1}{(\rho - 1 + \cos^2\varphi_0 \pm gj)}$$

For the upward going wave

$$Z_j\uparrow = \frac{+i\omega\rho_j \; H^{(2)}_{1/3}(\nu(j))}{(\pm 1)\, k_j(0) \; H^{(2)}_{-2/3}(\nu(j))} \cdot \frac{1}{(\rho - 1 + \cos^2\varphi_0 \pm gj)}$$

Expansion of the Hankel functions exactly using

$$H^{(1)}_\rho(x) = \frac{i}{\sin\pi\rho}\left[e^{-i\pi\rho} J_\rho(x) - J_{-\rho}(x)\right]$$

$$H^{(2)}_\rho(x) = \frac{-i}{\sin\pi\rho}\left[e^{i\pi\rho} J_\rho(x) - J_{-\rho}(x)\right]$$

yields with $j = 2$

$$Z_2\downarrow = \frac{\omega\rho_2}{k_2(0)\,\varphi} J_{mag}\, e^{-i(\Theta_N + \Theta_0)_2}\, e^{\mp i\frac{\pi}{2}}$$

$$Z_2\uparrow = \frac{\omega\rho_2}{k_2(0)\,\varphi} J_{mag}\, e^{+i(\Theta_N + \Theta_0)_2}\, e^{\mp i\frac{\pi}{2}}$$

where $\varphi \equiv \rho - 1 + \cos^2\varphi_0 \pm gj$

$$J_{mag} \equiv \left[\frac{\left[\cos\frac{\pi}{3} J_{\frac{1}{3}}(\nu) - J_{-\frac{1}{3}}(\nu)\right]^2 + \left[\sin\frac{\pi}{3} J_{\frac{1}{3}}(\nu)\right]^2}{\left[\cos\frac{\pi}{3} J_{-\frac{2}{3}}(\nu) - J_{\frac{2}{3}}(\nu)\right]^2 + \left[\sin\frac{\pi}{3} J_{-\frac{1}{3}}(\nu)\right]^2}\right]$$

$$\Theta_N \equiv \tan^{-1}\left[\frac{\sin\frac{\pi}{3}\ J_{\frac{1}{3}}(v)}{\cos\frac{\pi}{3}\ J_{\frac{1}{3}}(v) - J_{-\frac{1}{3}}(v)}\right] \; ; \; \Theta_D \equiv \tan^{-1}\left[\frac{\sin\frac{2\pi}{3}\ J_{\frac{2}{3}}(v)}{\cos\frac{2\pi}{3}\ J_{-\frac{2}{3}}(v) - J_{\frac{2}{3}}(v)}\right]$$

Note that $Z_2 \downarrow = - Z_2 \uparrow^*$

Using equation (Appendix 2.2.20) we can derive a recursive form of the reflection coefficient for N^2-linear layer systems similar to the Schelkunoff equation. We follow the input impedance approach and find that

$$R_{32} = \frac{R_{32} + R_{21}\ F_N}{1 + R_{21}\ F_D}$$

where

$$R_{32} \equiv \frac{H^{(1)}_{1/3}(u_3(0))}{H^{(2)}_{1/3}(u_3(0))} \cdot \frac{Z_3^*(0)}{Z_3(0)} \left[\frac{Z_2(-d) - Z_3(0)}{Z_2(-d) + Z_3^*(0)}\right]$$

We drop the suffix after deriving all quantities in terms of $Z_i \downarrow$

$$u_i = \frac{2}{3}\left(\frac{k_i(0)}{g_i}\right)\xi_i^{3/2} \qquad \xi_i = \left(\cos^2\theta_0 \pm g_i y_i + \rho_i - 1\right)$$

Similarly

$$R_{21} = \frac{H^{(1)}_{1/3}(u_2(0))}{H^{(2)}_{1/3}(u_2(0))} \cdot \frac{Z_2^*(0)}{Z_2(0)} \left[\frac{Z_1(-d) - Z_2(0)}{Z_1(-d) + Z_2^*(0)}\right]$$

R_{32} or R_{21} can be put in the form R_{ij}

$$R_{ij} = e^{2i\Theta_{Di}}\ B_m\ e^{iB_p}$$

$$F_N = \frac{-\left[e^{i\frac{\pi}{3}} J_{\frac{1}{3}}(u_2(-d)) - J_{-\frac{1}{3}}(u_2(-d))\right]\cdot\left[e^{-i\frac{\pi}{3}} J_{\frac{1}{3}}(u_3(0)) - J_{-\frac{1}{3}}(u_3(0))\right]}{\left[e^{-i\frac{\pi}{3}} J_{\frac{1}{3}}(u_2(-d)) - J_{-\frac{1}{3}}(u_2(-d))\right]\cdot\left[e^{i\frac{\pi}{3}} J_{\frac{1}{3}}(u_3(0)) - J_{-\frac{1}{3}}(u_3(0))\right]}$$

$$\left[\frac{|Z_3|\, e^{-i(\Theta_N+\Theta_D)_3 - i\frac{\pi}{2}}\Big|_{z=0} + |Z_2|\, e^{+i(\Theta_N+\Theta_D)_2 + i\frac{\pi}{2}}\Big|_{z=d}}{-|Z_2|\, e^{-i(\Theta_N+\Theta_D)_2 - i\frac{\pi}{2}}\Big|_{z=-d} - |Z_3|\, e^{+i(\Theta_N+\Theta_D)_3 + i\frac{\pi}{2}}\Big|_{z=0}}\right] \cdot$$

$$2i\left[(\Theta_N+\Theta_D)_3 - (\Theta_N+\Theta_D)_2\right]$$
$$\cdot\ e$$

$$F_D = \left[\frac{e^{i\frac{\pi}{3}} J_{\frac{1}{3}}(u_2(-d)) - J_{-\frac{1}{3}}(u_2(-d))}{e^{-i\frac{\pi}{3}} J_{\frac{1}{3}}(u_2(-d)) - J_{-\frac{1}{3}}(u_2(-d))}\right] e^{-2i(\Theta_N+\Theta_D)_2 - i\pi} \cdot$$

$$\left[\frac{|Z_2|\, e^{i(\Theta_N+\Theta_D)_2 + i\frac{\pi}{2}}\Big|_{z=-d} - |Z_3|\, e^{+i(\Theta_N+\Theta_D)_3 + i\frac{\pi}{2}}\Big|_{z=0}}{|Z_2|\, e^{-i(\Theta_N+\Theta_D)_2 - i\frac{\pi}{2}}\Big|_{z=-d} - |Z_3|\, e^{+i(\Theta_N+\Theta_D)_3 + i\frac{\pi}{2}}\Big|_{z=0}}\right]$$

$$Z_2(z=z') \equiv \left[\frac{(\pm)(-1)\rho_2\omega}{k_2(0)\,P}\right] \exp\left(-i\left[\Theta_1 + \Theta_2 - \frac{\pi}{2}\right]\right) \cdot$$

$$\left[\frac{\left[\cos\frac{\pi}{3}\, J_{\frac{1}{3}}(u_2(z')) - J_{-\frac{1}{3}}(u_2(z'))\right]^2 + \left[\sin\frac{\pi}{3}\, J_{\frac{1}{3}}(u_2(z'))\right]^2}{\left[\cos\frac{2\pi}{3}\, J_{-\frac{2}{3}}(u_2(z')) - J_{-\frac{2}{3}}(u_2(z'))\right] + \left[\sin\frac{2\pi}{3}\, J_{-\frac{2}{3}}(u_2(z'))\right]}\right]^{1/2}$$

- sign for c(z) increasing with depth.

$$\Theta_N \equiv \tan^{-1}\left(\frac{\sin\frac{\pi}{3}\, J_{\frac{1}{3}}(u_2(j'))}{\cos\frac{\pi}{3}\, J_{\frac{1}{3}}(u_2(j')) - J_{-\frac{1}{3}}(u_2(j'))} \right)$$

$$\Theta_D \equiv \tan^{-1}\left(\frac{\sin\frac{2\pi}{3}\, J_{-\frac{2}{3}}(u_2(j'))}{\cos\frac{\pi}{3}\, J_{\frac{1}{3}}(u_-(j')) - J_{-\frac{1}{3}}(u_2(j'))} \right)$$

$$P \equiv \left(p_i - 1 + \cos^2\varphi_{0_i} \pm g_i g_j \right)$$

We can express R_{32} above as the complex number

$$R_{32} = \frac{\left\{ -e^{2i(\Theta_D)_3} B_m e^{iB_p} + |R_{21}||F_N| e^{i(\quad + F_{Np})} - e^{2i(\Theta_N)_3} B_m e^{iB_p} |R_{21}||F_D| e^{-i(\quad + F_{Dp})} + |R_{21}|^2 \cdot |F_N| \cdot |F_D| \cdot e^{i(F_{Np} - F_{Dp})} \right\}}{\left\{ 1 + 2\cos(R_{21p} + F_{Dp}) + |R_{21}|^2 |F_D|^2 \right\}}$$

where $$B_m = \frac{\left\{ \left[-|Z_i||Z_j|\cos(\Theta_j - \Theta_i) - |Z_i||Z_j|\cos(\Theta_i + \Theta_j) + |Z_i|^2\cos 2\Theta_i + |Z_j|^2 \right]^2 + \left[-|Z_i||Z_j|\sin(\Theta_j - \Theta_i) - |Z_i||Z_j|\sin(\Theta_i + \Theta_j) - |Z_i|^2 \sin 2\Theta_i \right]^2 \right\}^{1/2}}{\left\{ |Z_j|^2 + |Z_i|^2 - 2|Z_j|\cdot|Z_i|\cos(\Theta_j + \Theta_i) \right\}}$$

$$B_p = \tan^{-1}\left(\frac{-|Z_i|\cdot|Z_j|\sin(\Theta_j - \Theta_i) + |Z_i||Z_j|\sin(\Theta_i + \Theta_j) - |Z_i|^2 \sin 2\Theta_i}{\left(|Z_i|\cdot|Z_j|\cos(\Theta_j - \Theta_i) - |Z_i||Z_j|\cos(\Theta_i + \Theta_j) + |Z_i|^2\cos 2\Theta_i + |Z_j|^2 \right)} \right)$$

with $i = 3$ and $j = 2$

$\Theta_i = \Theta_3 \equiv (\Theta_N + \Theta_D)_3$, $\Theta_j = \Theta_2 \equiv (\Theta_N + \Theta_D)_2$

These equations are certainly lengthy and unappealing. However, for any particular initial source exit angle they do allow layerwise recursion from the lower turning point layer to the upper turning point. By grouping all information about the current layer in R_{32}, F_N, F_D and that for previous layer in R_{21} we retain the recursive property when $Q \rightarrow R_{21}$.

Derivation:

Using $Z\downarrow = -Z\uparrow^*$ we write pressure at a level z as $p = p^{(1)} + p^{(2)}$ and vertical component of particle velocity as $v_3 = v_3^{(1)} + v_3^{(2)}$

Here the superscript (1) or (2) denotes functions associated with incident ((1), downgoing) or reflected ((2), upcoming) wave.

Then $$v_3 = \frac{p^{(1)}}{Z} - \frac{p^{(2)}}{-Z^*}$$

Where $\downarrow$ has been dropped in $Z\downarrow$, but z refers to the downward traveling wave. At interface 1,2 we can write

$$Z_1 = \frac{(p^{(1)} + p^{(2)})\,|Z_2|^2}{p^{(1)} Z_2^* - p^{(2)} Z_2}$$

or

$$Z_1 = \frac{\left[A\,H^{(1)}_{1/3}(u_0) + B\,H^{(2)}_{1/3}(u_0)\right]\,|Z_2(0)|^2}{\left[A\,H^{(1)}_{1/3}(u_0)\,Z_2^*(0) - B\,H^{(2)}_{1/3}(u_0)\,Z_2(0)\right]}$$

This is analagous to the form used to start the recursive reflection coefficient for the isovelocity case. There is a major difference here however. The boundary condition is not on $Z\downarrow$ but on the total field. The RHS of equation (Appendix 2.2.38) involves the total field. The LHS involves only $Z\downarrow$ because no energy sources are assumed below the lowest interface, nor reflecting horizons. In the N^2-linear case we can write only $Z\downarrow$ if we assume the downgoing wave dissipates before reaching the turning point, or that the gradient is small enough so that the lowest layer is essentially iso-

velocity. If this condition does not hold we must use both $\phi\uparrow$ and $\phi\downarrow$ for the turning point layer. That is, we must start the recursion with reflection coefficient R_{TP} at some level z within a turning point layer (see model 2a.)

Solving for the ratio B/A we get with $u_0 \equiv u(z=0)$, $u_d \equiv u(z=-d)$

$$R_{21} = \frac{B}{A} = \frac{H^{(1)}_{1/3}(u_0)}{H^{(2)}_{1/3}(u_0)} \left[\frac{Z_2(0) - Z_1(0)}{-Z_1(0) - Z_2^*(0)}\right] \cdot \left[\frac{Z_2^*(0)}{Z_2(0)}\right]$$

Then since

$$Z_{inp}\Big|_{z=-d} = \frac{\left[A\, H^{(1)}_{1/3}(u_d) + B\, H^{(2)}_{1/3}(u_d)\right] \left|Z_2(-d)\right|^2}{\left[A\, H^{(1)}_{1/3}(u_d)\, Z_2^*(-d) - B\, H^{(2)}_{1/3}(u_d)\, Z_2(-d)\right]}$$

we can substitute for B/A and write

$$Z_{inp}\Big|_{z=-d} = \frac{\left[H^{(1)}_{1/3}(u_d) + Z_0 \dfrac{H^{(1)}_{1/3}(u_0) \cdot H^{(2)}_{1/3}(u_d)}{H^{(2)}_{1/3}(u_0)}\right] \cdot \left|Z_2(-d)\right|^2}{\left[H^{(1)}_{1/3}(u_d) \cdot Z_2^*(-d) - Z_0 \dfrac{H^{(1)}_{1/3}(u_0) \cdot H^{(2)}_{1/3}(u_d) \cdot Z_2(-d)}{H^{(2)}_{1/3}(u_0)}\right]}$$

where

$$Z_0 \equiv \left[\frac{Z_2(0) - Z_1(0)}{-Z_1(0) - Z_2^*(0)}\right] \cdot \frac{Z_2^*(0)}{Z_2(0)}$$

Similarly Z_{inp} may be related to the normal impedance in layer 3

$$Z_{inp} = \frac{\rho^{(1)} + \rho^{(2)}}{\rho^{(1)} Z_3^* - \rho^{(2)} Z_3} \cdot |Z_3|^2$$

$$Z_{inp} = \frac{\left[C\, H^{(1)}_{1/3}(J_0) + D\, H^{(2)}_{1/3}(J_0)\right] |Z_3(0)|^2}{\left[C\, H^{(1)}_{1/3}(J_0)\, Z_3^*(0) - D\, H^{(2)}_{1/3}(J_0)\cdot Z_3(0)\right]}$$

Then

$$R \equiv \frac{D}{C} = \frac{H^{(1)}_{1/3}(J_0)}{H^{(2)}_{1/3}(J_0)} \left[\frac{Z_3(0) - Z_{inp}(-d)}{-Z_{inp}(-d) - Z_3^*(0)}\right] \left[\frac{Z_3^*(0)}{Z_3(0)}\right]$$

Note that we are using z axes with a zero in each layer. We substitute now for Z_{inp}. After considerable manipulation and using the Bessel function representation of Hankel functions we arrive at the forms given in section A 2.2.b. above). To assess fairly the convenience of these forms they should be compared to the computations required to evaluate matrices in the Thomson-Haskell, Dunkin-Thrower, or Knopoff methods (although these methods do not treat inhomogeneous media).

Appendix 2.2.c. Reflection coefficient for multilayer guide with "Piecewise WKB layering".

For "WKB layers" we can perform a similar analysis

$$\phi(3) = \frac{1}{\gamma(3)^{1/2}} \left\{ C_1 \underbrace{\exp\left(i \int_{30}^{3} \gamma(3)\, d3\right)}_{\Phi\downarrow} + C_2 \underbrace{\exp\left(-i \int_{30}^{3} \gamma(3)\, d3\right)}_{\Phi\uparrow} \right\}$$

$$Z\downarrow = \frac{-i\omega\rho_1 \phi\downarrow}{-\frac{d}{d3}\phi\downarrow} = \frac{-i\omega\rho_1 \gamma(3)}{-\gamma^2(3) - \frac{1}{2}\gamma'(3)} \qquad \gamma' \equiv \frac{d\gamma}{d3}$$

$$= \frac{\omega\gamma\rho}{\left[\gamma^4 + \frac{1}{4}(\gamma')^2\right]^{1/2}} \; e^{i\frac{\pi}{2} - i\tan^{-1}\left(\frac{\gamma^2(3)}{-\frac{1}{2}\gamma'(3)}\right)}$$

$$Z\uparrow = \frac{-i\omega\phi\uparrow}{-\frac{1}{2\gamma}\phi\uparrow} = \frac{-i\omega\gamma(\gamma)}{(-1)(-i\gamma^2(\gamma) - \frac{1}{2}\gamma'(\gamma))}$$

$$= \frac{\omega\gamma_1\rho_1}{\left[\gamma^4 + \frac{1}{4}(\gamma')^2\right]^{1/2}} e^{+i\frac{\pi}{2} + i\tan^{-1}\left(\frac{\gamma^2(\gamma)}{-\frac{1}{2}\gamma'(\gamma)}\right)}$$

Again $Z_1\uparrow = -Z_1\downarrow^*$ and following the input impedance approach we find

$$R_{32} = \frac{R_{32} + R_{21}F_N}{1 + R_{21}F_D} \quad \text{or recursively} \quad R_{32} = \frac{R_{32} + R_{21}F_N}{1 + R_{21}F_D}$$

$$R_{32} = e^{i2S_3(\gamma)}Z_3(\gamma) = e^{i2S_3(\gamma)}\frac{Z_3^*(\gamma)}{Z_3(\gamma)}\left[\frac{Z_2(\gamma) - Z_3(\gamma)}{Z_2(\gamma) + Z_3^*(\gamma)}\right]$$

$$R_{21} = e^{i2S_2(\gamma)}Z_2(\gamma) = e^{i2S_2(\gamma)}\frac{Z_2^*(\gamma)}{Z_2(\gamma)}\left[\frac{Z_1(\gamma) - Z_2(\gamma)}{Z_1(\gamma) + Z_2^*(\gamma)}\right]$$

Here the z's are different for the media and Z always refers to $Z\downarrow$ for a coordinate system with z increasing downward.

These formulae can be combined to give

$$R_{32} = \left\{e^{i2\phi_3(0)}\left[\frac{Z_2(-d) - Z_3(0)}{Z_2(-d) + Z_3^*(0)}\right] + e^{i2\phi_2}\left[\frac{Z_1(-d) - Z_2(0)}{Z_1(-d) + Z_2^*(0)}\right] e^{i2(\phi_3(0) - \phi_2(-d)}\left[\frac{Z_3(0) + Z_2^*(-d)}{Z_2(-d) + Z_3^*(0)}\right]\right\}$$

$$\left\{1 + e^{i2\phi_2(0)}\left[\frac{Z_1(-d) - Z_2(0)}{Z_1(-d) + Z_2^*(0)}\right] e^{-2i\phi_2(-d)}\left[\frac{Z_2^*(-d) - Z_3^*(0)}{Z_2(-d) + Z_3^*(0)}\right]\right\}$$

$$\phi_2 \equiv S_2(z) + \tan^{-1}\left(\frac{-2\gamma_2^2(z)}{\gamma_2'(z)}\right) - \frac{\pi}{2}$$

$$\phi_3 \equiv S_3(z) + \tan^{-1}\left(\frac{-2\gamma_3^2(z)}{\gamma_2'(z)}\right) - \frac{\pi}{2}$$

$$S_1 \equiv \pm \int_{z_0}^{z} \gamma_1(z)\, dz + S_0 \quad .$$

The complex constant e^{iS_0} drops out of Q_{32} altogether.

In solving for modal eigenvalues k_n in an N^2-linear "WKB layering" we need only calculate the phase integral within the layers and the vertical component of wavenumber at the layer boundaries. Thus we require

$$\Theta = \frac{\omega}{c_0} \int_{z_{j-1}}^{z_j} \left[N^2(z) - \cos^2\phi \right] dz$$

with $\dfrac{\cos\phi_0}{\cos\phi} = \dfrac{c_0}{c(z)}$ ϕ_0 is source exit angle, ϕ is a grazing angle

Using the gradient

$$q_j = \frac{2\Delta c(z)}{c_0 \Delta z} \approx \frac{c(z_j) - c(z_{j-1})}{z_j - z_{j-1}}$$

gives

$$\Theta = \left\{ \sum_{i=M}^{L} \frac{\left[N^2(z_{i-1}) - \cos^2\phi\right]^{3/2} - \left[N^2(z_i) - \cos^2(\phi)\right]^{3/2}}{N^3(z_{i-1})\, q_i} \right\} \frac{2\omega}{3}$$

For turning points within the N^2-linear layer there will be an additional contribution

$$\frac{2\omega}{3} \left\{ \left[N^2(z_{j-1}) - \cos^2\phi\right]^{3/2} \Big/ N^3(z_{j-1})\, q_j \right\}$$

and the characteristic equation will require $m\pi + \frac{\pi}{2}$ to account for phase shift at the turning point.

Appendix 2.3 Mode shapes.

Model 2.a.

In the N^2-linear ocean bottom above the turning point

$$0 < \zeta < \zeta_m = \frac{\cos^2 \varphi_a}{g}$$

we find that

$$\phi(\zeta) = \nu^{1/3} \left[B e^{i\pi/3} H^{(1)}_{1/3}(\nu) + B H^{(2)}_{1/3}(\nu) \right]$$

$$\rightarrow \quad \phi(\zeta) = \nu^{1/3} B' \left[J_{\frac{1}{3}} + J_{-\frac{1}{3}} \right] \left\{ \cos\left(b + \tfrac{\pi}{2}\right) - \cos\left(b + \tfrac{5\pi}{6}\right) + i \sin\left(b + \tfrac{\pi}{2}\right) \right\}$$

$$\Rightarrow \quad S(\zeta) = 2\nu^{1/3} B' \left[J_{\frac{1}{3}} + J_{-\frac{1}{3}} \right] \left[\left\{ \cos\left(b + \tfrac{\pi}{2}\right) - \cos\left(b + \tfrac{5\pi}{6}\right) \right\}^2 + \sin^2\left(b + \tfrac{\pi}{2}\right) \right]^{1/2}$$

with

$$B' = \frac{\sin \frac{\pi}{3}}{\nu_0^{1/3} \left[J_{\frac{1}{3}}(\nu_0) + J_{-\frac{1}{3}}(\nu_0) \right]} \cdot \frac{\left[(1 - \cos 2\theta)^2 + \sin^2 2\theta \right]^{1/2}}{\left[\left(1 - \cos \frac{\pi}{3}\right)^2 + \sin^2 \frac{\pi}{3} \right]^{1/2}}$$

$$b = \tan^{-1}\left(\frac{\sin 2\theta}{1 - \cos 2\theta} \right) - \tan^{-1}\left(\frac{-\sin \frac{\pi}{3}}{1 - \cos \frac{\pi}{3}} \right)$$

Below the turning point in the N^2-linear layer, $\zeta > \zeta_m$, we find that

$$S(\zeta) = (-1)\, \nu_1^{1/3} B' \left\{ \left[J_+(\nu) \cdot \cos\left(\gamma_+(\nu) + b\right) - J_-(\nu) \cdot \cos\left(\gamma_-(\nu) + b + \tfrac{\pi}{3}\right) \right] + \left[J_+(\nu) \cdot \sin\left(\gamma_+(\nu) + b\right) - J_-(\nu) \cdot \sin\left(\gamma_-(\nu) + b + \tfrac{\pi}{3}\right) \right]^2 \right\}^{1/2}$$

where $\nu_1 = \frac{2}{3} \left(\frac{k_0}{g} \right) \left(-\xi \right)^{3/2} \Big|_{\zeta = 0}$, $\xi = \cos^2 \varphi_0 - g\zeta$

$$J_{\pm} \equiv \left[\left(\sum_{m=0}^{\infty} N_{m\pm} \cos \Theta_{m\pm} \right)^2 + \left(\sum_{m=0}^{\infty} N_{m\pm} \cdot \sin \Theta_{m\pm} \right)^2 \right]^{1/2}$$

$$J_{\pm} \equiv \tan^{-1} \left\{ \frac{\left[\sum_{m=0}^{\infty} N_{m\pm} \cdot \sin \Theta_{m\pm} \right]}{\left[\sum_{m=0}^{\infty} N_{m\pm} \cdot \cos \Theta_{m\pm} \right]} \right\}$$

$$N_{m\pm} = \frac{(-1)^m \quad \nu^{2m \pm \frac{1}{3}}}{m! \; \Gamma(m+1\pm\tfrac{1}{3}) (2)^{2m\pm\frac{1}{3}}}$$

$$\Theta_{m\pm} = \frac{\pi}{4m \pm \frac{2}{3}}$$

We have programmed $S(\zeta)$ for $\zeta < \zeta_m$ only, at the present.

Model 2.b.

When the velocity discontinuity exists at the interface the mode shape formulae remain the same as for model 2.a. with the substitution

$$J = \cos^2 \varphi_0 - g\zeta + \rho - 1$$

$$\Theta = \tan^{-1} \left[\frac{J_{1/3}(\nu_0) + J_{-1/3}(\nu_0)}{K_\rho(\varphi_0) \left(J_{-\frac{2}{3}}(\nu_0) - J_{\frac{2}{3}}(\nu_0) \right)} \right]$$

$$K_\rho(\varphi_0) = \frac{k_1(0)}{k_0} \frac{\left[\rho - 1 + \cos^2 \varphi_0 \right]^{1/2}}{\cos \varphi_0}$$

Model 3.

For multilayer systems Tolstoy and Clay suggest matching through the matrix equation.

$$M_n \begin{pmatrix} A_n \\ B_n \end{pmatrix} = M_{n+1} \begin{pmatrix} A_{n+1} \\ B_{n+1} \end{pmatrix} \qquad \text{with} \qquad M_n = \begin{bmatrix} J_{\frac{1}{3}}(\xi_n) & J_{-\frac{1}{3}}(\xi_i) \\ J_{-\frac{2}{3}}(\xi_n) & -J_{\frac{2}{3}}(\xi_i) \end{bmatrix}$$

for the case of N^2-linear layers. In our formulation A_i , B_i , A_{i+1} , B_{i+1} are complex. In the lowest layer (the turning point layer) we may write $A = 1 e^{i\theta}$ and the matrix equation will be

$$M_i \begin{pmatrix} 1 + i\,0 \\ B_R + i\,B_I \end{pmatrix}_i = M_{i+1} \begin{pmatrix} A_R + i\,A_I \\ B_R + i\,B_I \end{pmatrix}_{i+1}$$

Additionally, however, we know that $\tilde{B} = \tilde{R}\tilde{A} = (R_R + i R_I) \cdot (A_R + i A_I)$

$$B_R = R_R \cdot A_R - R_I \cdot A_I$$

$$\Rightarrow$$

$$B_I = R \cdot A_R + R_R \cdot A_I$$

and we need to solve the matrix equation for $(A_R, A_I)_{i+1}$ given $(A_R, A_I)_i$, $\tilde{R}_i$, $\tilde{R}_{i+1}$

Model 4.

For WKB layering

$$\phi_i(y) = \gamma_i(y)^{-1/2} \left\{ C_i \exp\left(i \int_{y_0}^{y} \gamma_i(y)\, dy\right) + C_i R_i \exp\left(-i \int_{y_0}^{y} \gamma_i(y)\, dy\right) \right\}$$

and we get four equations, two of which should be dependent.

From pressure continuity

$$C_{R_i}(a_i) + C_{I_i}(-b_i) = W \left\{ C_{R_{i-1}} \cdot a_{i-1} - C_{I_{i-1}} \cdot b_{i-1} \right\}$$

$$C_{R_i}(-b_i) + C_{I_i}(a_i) = W \left\{ C_{I_{i-1}} \cdot a_{i-1} - C_{I_{i-1}} \cdot b_{i-1} \right\}$$

with

$$a_{i-1} \equiv \cos(s_{i-1}) + |R_{i-1}| \cdot \cos(2\theta_{i-1} - s_{i-1})$$

$$b_{i-1} \equiv \sin(s_{i-1}) + |R_{i-1}| \cdot \sin(2\theta_{i-1} - s_{i-1})$$

$$a_i \equiv \cos(s_i) + |R_i| \cdot \cos(2\theta_i - s_i)$$

$$b_i \equiv \sin(s_i) + |R_i| \cdot \sin(2\theta_i - s_i)$$

$$s_i \equiv \int_{y_0}^{y} \gamma_i(y)\, dy + s_0 \qquad s_0 = 0 \text{ except in a turning point layer}$$

$$W \equiv \frac{\rho_{i-1}}{\rho_i} \frac{\gamma_i(y_i)^{1/2}}{\gamma_{i-1}(y_{i-1})^{1/2}} \qquad R_i = |R|_i\, e^{i 2\theta_i}$$

From particle velocity continuity

$$C_{R_{i-1}} \cdot e_{i-1} + C_{I_{i-1}} \cdot f_{i-1} = C_{R_i} \cdot e_i + C_{I_i} \cdot f_i$$

$$C_{R_{i-1}} \cdot f_{i-1} - C_{I_{i-1}} \cdot e_{i-1} = C_{R_i} \cdot f_i - \quad \cdot e_i$$

$$e_{i-1} \equiv -U_{i-1} \cdot \sin(S_{i-1}) - T_{i-1} \cdot \cos(S_{i-1}) + |R_{i-1}| \cdot \{U_{i-1} \cdot \sin(2\Theta_{i-1} - S_{i-1}) - T_{i-1} \cdot \cos(2\Theta_{i-1} - S_{i-1})\}$$

$$f_{i-1} \equiv -U_{i-1} \cdot \cos(S_{i-1}) + T_{i-1} \sin(S_{i-1}) + |R_{i-1}| \cdot \{U_{i-1} \cdot \cos(2\Theta_{i-1} - S_{i-1}) + T_{i-1} \cdot \sin(2\Theta_{i-1} - S_{i-1})\}$$

$$e_i \equiv -U_i \cdot \sin(S_i) - T_i \cdot \cos(S_i) + |R_i| \cdot \{U_i \cdot \sin(2\Theta_i - S_i) - T_i \cdot \cos(2\Theta_i - S_i)\}$$

$$f_i \equiv -U_i \cdot \cos(S_i) + T_i \cdot \sin(S_i) + |R_i| \cdot \{U_i \cdot \cos(2\Theta_i - S_i) + T_i \cdot \sin(2\Theta_i - S_i)\}$$

$$U_{i-1} \equiv \gamma_{i-1}^{1/2}(\zeta_{i-1}) \qquad U_i \equiv \gamma_i^{1/2}(\zeta_i)$$

$$T_{i-1} \equiv [\tfrac{1}{2}\gamma'_{i-1}(\zeta_{i-1})] / [\gamma_{i-1}^{3/2}(\zeta_{i-1})] \qquad T_i \equiv \tfrac{1}{2}\gamma'_i(\zeta_i) / \gamma^{3/2}(\zeta_i)$$

where $\gamma' \equiv \frac{d}{d\zeta}\gamma$. and depends on the particular velocity profile used with the WKB approximation.

When these equations are solved for C_{R_i}, C_{I_i} we have

$$|C|_i = [C_{R_i}^2 + C_{I_i}^2]^{1/2} \qquad \Theta_{C_i} = \tan^{-1}\left(\frac{C_{I_i}}{C_{R_i}}\right)$$

and the mode shape for the WKB layer i

$$S(\zeta) = Re[\phi(\zeta)] = \frac{|C|_i}{\gamma^{1/2}(\zeta)} \{\cos(\Theta_{C_i} + S(\zeta)) + |R|_{i=1} \cos(\Theta_{C_i} + 2\Theta_R - S(\zeta))\}$$

For the case $|R| = 1$ with total reflection

$$S(\zeta) = \frac{|C|}{\gamma^{1/2}(\zeta)} \cdot \{[\cos(\Theta_{C_i} + S(\zeta)) + |R| \cos(\Theta_{C_i} + \Theta_R - S(\zeta)]^2 + [\sin(\Theta_{C_i} + S(\zeta)) + |R| \cdot \sin(\Theta_C + \Theta_R - S(\zeta))]^2\}^{1/2}$$

Chapter 3- Normal Modes in Waveguides with Dissipative Boundaries

3.1 Introduction
3.2 Phenomenological approach to dissipation and relaxation mechanisms
3.3 Introduction of dissipation in the wave equation
3.4 Isovelocity layers with dissipation:
    3.4.1 Wave representation
    3.4.2 Refraction law
    3.4.3 Phase velocity
    3.4.4 Impedances
    3.4.5 Reflection coefficients
          Two halfspaces, multilayer isovelocity
3.5 General statement of the problem
    3.5.1 Characteristic equation
    3.5.2 Attenuation coefficient
3.6 Method of solution
    3.6.1 Characteristic equation
    3.6.2 Snell equation
    3.6.3 Regarding Riemann sheets

Appendix 3.1 N^2-linear layers with dissipation
         3.2 Reflection coefficient for dissipative model 2A

3.1 Introduction

In the present chapter the wave attenuation encountered in real waveguides will be accounted for as absorption is included in the mathematical description of our layered models. Attenuation is described first in terms of the measures we make of it: loss per cycle of energy in an incremental volume, amplitude decay of a progressing wave, and decay with time of the peak energy at a point in space. Mention is made of various mechanistic approaches to attenuation, which we avoid here by modeling the observed attenuation, from whatever cause, through the use of complex sound speed. This is the phenomenological approach to the description of decay. We strengthen the argument by showing that if stress and strain are related to each other through relaxation functions, the same exponential decay factor ultimately arises. Next we indicate the effect of complex sound speed on wave representation, acoustic impedance, and reflection coefficients, and trace its inclusion in the mathematical algorithms for dispersion curves and attenuation coefficients. We present the theoretical basis and organization of the calculations for models both with and without dissipation. In the case of isovelocity layering we have explicitly developed Brekhovskikh's treatment of the recursive reflection coefficient for absorbing layers in terms of complex incidence angle and sound speed. We have formulated an algorithm for solution of the simultaneous complex refraction law equations and the complex characteristic equation. In the case of N^2-linear layering we develop the complex Helmholtz equation and its solution, required to determine reflection coefficients from that type of layering.

Much precedent exists for dealing with both modal attenuation and body wave attenuation. The original shallow water modal work dates back to Pekeris (ref. 24) who treated 1, 2, 3 layer nonabsorbing fluid waveguides. Kornhauser and Raney (ref. 19) introduced attenuation into the lower halfspace of the Pekeris guide and determined mode attenuation coefficients. Eby et al (ref. 25) validated the general K+R expression in a model study and improved it by including

the effect of shear in the lower medium. For multilayer guides empirical coefficients rather than closed form analytic expressions have generally been used to adjust the field data (ref.). This conveniently avoids the mechanism of attenuation problem.

Attenuation of body waves is typically assumed to be proportional to the first power of frequency in ocean bottom sediments. However the validity of this statistical law has not been firmly established in the VLF $0.1 - 10$ Hz band. Ingenito (ref. 20) for example shows evidence for $f^{1.75}$ law at 400 Hz. Saclant has implemented f^1 in its programs. Hamilton (ref. 26) reports confirmation by Zemztov, Tullos, and Reid of f^1 laws in coastal clay and land surveys in the $5 - 50$ Hz band. Knopoff (ref. 61) has made measurements of specific attenuation factor $1/Q$ in homogeneous materials in the lab and in the field and shows that $1/Q$ is independent of frequency in solids, but varies as the first power of frequency in liquids, suggesting that the mechanism of attenuation in solids is substantially different from that in liquids. The working definition of Q^{-1} , the specific attenuation factor, is related to the expression from electrical circuit theory

$$\frac{2\pi}{Q} = \frac{\Delta E}{E} \qquad 3.1$$

where ΔE is the amount of energy dissipated per cycle of a harmonic excitation in a certain volume and E is the peak elastic energy in the system in the same volume. The spatial attenuation for a wave function observed throughout space at a fixed time is of the form $\exp(-\alpha x)$ where $\alpha = \frac{\omega}{2cQ}$ and c is the phase velocity. Observation of this wave function as a function of time at a fixed point in space yields the damping factor $\exp(-\gamma t)$ where $\gamma = \omega/2Q$. Only in homogeneous systems without dispersion are the definitions equivalent. Knopoff claims that lab experiments indicate an attenuation factor α , proportional to f^2 in liquids and f^1 in solids.

Various attenuation-dispersion pairs have been proposed corresponding to models of dissipative media. There has been some discussion of their behaviour at low frequencies where little experimental data exists, and of the constraints upon form imposed by causality. In particular, Strick's minimum phase power law model (ref. 62) has been criticized by White and Walsh (ref. 63) who propose a lumped element transmission line model. They state that attenuation very nearly proportional to frequency over a wide frequency range does not require substantial velocity variation at low frequency, but qualify their analysis restricting it to competent rock such as sandstone, shales and limestones, conceding that other conclusions may be reached for oozes, muds and loose soil.

The properties of any composite material are statistical in nature. Measurements must be made over large samples and average properties taken to correspond to features of the homogeneous mathematical model. In the case of low frequencies samples of relativity constant properites are difficult to encounter in dimensions comparable to the wavelengths involved. The measurement of absorption is then tied to tracing the flow of seismic energy. When correction can be made for partition of energy at boundaries and geometrical spreading then the recording of a quantity that is proportional to the log of the peak absolute value of the square of the particle velocity (the log of the energy density) may be used to determine absorption. Hermont (ref. 64) has emphasized the utility of this measure when correlated with conventional reflection data.

The approach taken to absorption in this study accounts mathematically for observational changes in the acoustic field with range. No attempt is made to relate these changes to possible underlying attenuation mechanisms. Frequency dependence will be a parameter of the computational algorithm, but the algorithm has not been applied to matching real data and we will offer no support of any one mechanism over another. Application of the methods developed here to specific acoustic environments will, however, require selection of specific values for frequency dependence and attenuation coefficient. For this reason we briefly review existing theory and

data.

3.2 Phenomenological approach to dissipation and relaxation mechanisms:

In the phenomenological approach to volumetric absorption for spherically spreading waves the decrease in intensity associated with volumetric absorption is proportional to the magnitude of the vector intensity and to the spherical shell thickness through which the wave is passing. $dI = -\alpha I dr$ 3.2

This assumes that the shell is far from the source so the variation of I as r^{-2} is neglected. The integral is $I = I_0 \exp(-\alpha r)$

I and p^2 are closely related and this is equivalent to

$$p = \frac{A}{r} \exp\left[i\left(k + \frac{i\alpha}{2}\right) r - i\omega t\right] \qquad 3.3$$

Absorption is represented as a complex part of wavenumber.

Dyer (ref. 7) has related volumetric absorption in seawater to relaxation mechanisms. The physical basis of the relaxation mechanism in water relates to transfer of acoustic energy to some internal process of the liquid. e.g. kinetic (viscosity), structural (molecular rearrangement), or chemical (reaction between constituents). He shows that the reciprocal absorption length α for a relaxation process can be put in the form

$$\alpha \left(\frac{c}{\omega}\right) \cdot \left(\frac{c_0}{c}\right)^2 = \frac{D\,\omega\tau}{1 + \omega^2\tau^2} \qquad 3.4 \text{ (Dyer 3.7)}$$

D and τ are parameters pertaining to properties of the liquid. Sound speed, c, is such that

$$\left(\frac{c_0}{c}\right)^2 = 1 - D\,\frac{\omega^2\tau^2}{1 + \omega^2\tau^2} \qquad 3.5 \text{ (Dyer 3.8)}$$

Equation (Dyer 3.8) comes from modifying Hookes law to include a time derivative

$$p = -B\left(1 + \tau\frac{\partial}{\partial t}\right) \nabla \cdot \underline{\ell} \qquad 3.6$$

(p is pressure, ℓ is displacement), and then using the momentum equation

$$\rho_o \frac{\partial v}{\partial t} = -\nabla p \qquad 3.7$$

and the Helmholtz equation modified to include absorption

$$\nabla^2 p + \left(k + \frac{i a}{2}\right)^2 p = 0 \qquad 3.8$$

For small $\omega\tau$ he gets

$$a = D\tau\omega^2/c_o \qquad 3.9$$

i.e. there is a frequency squared dependence for absorption and unchanged sound speed. For large $\omega\tau$

$$a = \frac{D}{(1-D)^{1/2}} \cdot \frac{1}{c_o \tau} \quad \text{and} \quad c = \frac{c_o}{(1-D)^{1/2}} \qquad 3.10$$

i.e. constant absorption and increased sound speed. Here τ is the relaxation time.

In seawater the inverse absorption length associated with shear viscosity has the form

$$a = \frac{D\tau\omega^2}{c_o} \quad \text{and} \quad c \approx c_o$$

The classical absorption equation is

$$a = \frac{4\nu\omega^2}{3c_o^3} \qquad \omega\tau << 1$$

ν is the kinematic shear viscosity of seawater. Dyer notes that the relaxation time applicable to heat conduction is about three orders of magnitude less than this. Experiments show that the absorption due to structural relaxation (polymeric fluid) are of the order

$$\alpha \approx 3.2 \frac{4 \nu \omega^2}{3 c_0^3}$$

$$\tau \approx O(10^{-12} \text{sec}) \text{ for } f \leq 2 \times 10^6 \text{ Hz}$$

Additionally in seawater chemical processes associated with magnesium sulfate and boron dominate at low frequencies. The boric acid, borate acid base equilibrium reaction is influential for frequencies < 3.5 KHz.

Here

$$\tau = 5.15 \times 10^{-7} \exp\left(\frac{1590}{T+273}\right) \text{ sec}$$

$$\alpha \approx \left(4.03 \times 10^{-9} \frac{\text{sec}}{m}\right) \cdot \left[\frac{\omega^2 \tau}{1+\omega^2 \tau^2}\right]$$

In the intermediate depth models studied in this report frequencies of low order modes are in the range for which the chemical relaxation mechanism will dominate in seawater.

White (ref. 4) has summarized current views of seismic wave attenuation in solids in terms of both measurable parameters, and analytic means of expressing attenuation in the equations of motion. He observes that current experimental results point out that (1) progressive wave attenuation is directly proportional to frequency (2) sharpness of resonance Q for driven samples is independent of frequency, and (3) the fractional energy loss per cycle for slow cyclic stresses is independent of frequency. Any theory invoked to explain attenuation should account for these observations and the additional facts that attenuation is reduced by high confining pressures and increased by addition of moisture to solid samples. White reviews the description of lossy material in terms of (1) complex elastic moduli, (2) inclusion of time derivatives in the relation between stress and

strain, (3) use of more general relaxation functions to relate stress and strain and (4) nonlinear stress strain relations such as sliding friction. Of these only (4) can produce first power frequency dependence of attenuation and no dispersion over large bandwidths. The others may approximate f^1 in local regions of frequency.

Finally, Hamilton (ref. 26) presents exhaustive studies and summaries of compressional wave attenuation in marine sediments. Two phase media such as sediments might be expected to display characteristics of both their constituents, seawater and solid matrix. Hamilton concludes however that (1) attenuation in water saturated sediments, in dB/unit length, is also approximately dependent on the first power of frequency, that (2) velocity dispersion is negligible or absent, and (3) that intergrain friction appears to be the dominant cause of wave energy damping. Viscous losses due to relative movement of pore water and mineral structure are probably negligible at seismic frequencies.

In modeling losses in sediments, a critical factor is the extent of relative movement of pore water and mineral particles. If there is significant motion then viscous damping and velocity dispersion should be present. If there is little fluid motion with respect to the solid then we expect no velocity dispersion, and energy damping is not dependent on the fluid viscosity or permeability of the mineral structure. Hamilton presents evidence that little velocity dispersion occurs even in sands where grain size is large, and permeability high, with interconnecting pores.

The important factors in attenuation will be sediment structure, porosity, grain size and shape, interparticle contacts, surface areas in sands and coarse silts, and physicochemical forces (cohesion) in fine silts and clays. Hamilton presents empirical evidence that at seismic wavelengths the attenuation coefficient $\alpha = k f^n$ varies as $k f^1$ and that k increases with decreasing grain size from coarse to fine sands. It is highest for silty sand or sandy silt. Attenuation then decreases with decreasing grain size into fine silts and clays. Similarly, porosity varies with k in the same way as

mean grain size. The highest values of k are in very fine sands and sandy silts. In silt clays k decreases with increasing porosity.

An average value of the attenuation α in seawater from Dyer is $\alpha \approx 10^{-6}$ dB/m at 100 Hz. From Hamilton, an average value of α in sediments is $\alpha \approx 10^{-2}$ dB/m at 100 Hz. Thus we see that water column losses should be unimportant for energy traveling through both water and sediment. In latter sections we will treat ocean bottom layers as absorbing acoustic (liquid) media. Our computer algorithms will, however set dissipation in the source layer (the ocean) =0 under the assumption that it is very much smaller than any other layer.

3.3 Introduction of absorption into the wave equation

Tolstoy (ref. 3) analytically introduces attenuation for a relaxation process into the wave equation. For a one dimensional conservative medium the acoustic wave equation is

$$\ddot{\xi} = c^2 \frac{\partial^2 \xi}{\partial x^2} \qquad 3.11 \quad \text{(Tolstoy 9.71)}$$

where

ξ is the perturbation displacement.

c is the adiabatic sound speed.

This equation assumes that the response to a pressure increment p_1 is an instantaneous increment in density ρ_1 . When the response is allowed to include a delay, the relation between pressure increment and density increment could realistically involve the first derivative of ρ with respect to time. One description might be

$$p_1 = c^2 \rho_1 + f \cdot \dot{\rho}_1 \qquad 3.12 \quad \text{(Tolstoy 9.72)}$$

a dynamic equation of state. The factor f determines the importance of the time derivative. The solution of this differential equation for a step pressure increment p_{10} is

$$\rho_1 = \frac{\rho_{10}}{c^2}\left(1 - e^{-(c^2/f)t}\right) \qquad \begin{matrix}3.13\\(\text{Tolstoy } 9.73)\end{matrix}$$

The relaxation time is $\tau = f/c^2$. The new damped 1-D wave equation is

$$\ddot{\xi} = c^2 \frac{\partial^2 \xi}{\partial x^2} + f \frac{\partial^2 \dot{\xi}}{\partial x^2} \qquad \begin{matrix}3.14\\(\text{Tolstoy } 9.75)\end{matrix}$$

satisfied by the damped harmonic wave

$$\xi = \xi_0 e^{-\delta x} \cdot e^{i(\omega t - \alpha x)} \qquad \begin{matrix}3.15\\(\text{Tolstoy } 9.76)\end{matrix}$$

where

$$\alpha^2 - \delta^2 = \frac{\omega^2}{c^2(1+\omega^2\tau^2)} \qquad \begin{matrix}3.16\\(\text{Tolstoy } 9.77)\end{matrix}$$

$$2\alpha\delta = \frac{\omega^3 \tau}{c^2(1+\omega^2\tau^2)} \qquad \begin{matrix}3.17\\(\text{Tolstoy } 9.78)\end{matrix}$$

The complex wavenumber will be $\tilde{K}_x = \alpha - i\delta$ with propagation $\exp\left[i\omega t - i\,\tilde{K}_x \cdot x\right]$

The effect of the relaxation process is to introduce dissipation and make the propagation dispersive. Body wave attenuation in nepers/m is given by

$$\delta = \frac{\omega^2 \tau v}{2c^2(1+\omega^2\tau^2)} \qquad \begin{matrix}3.18\\(\text{Tolstoy } 9.79)\end{matrix}$$

Phase velocity is

$$c_p = \frac{\omega}{\alpha} = \frac{2^{1/2} c}{\omega \tau} \left\{ (1+\omega^2\tau^2) \left[(1+\omega^2\tau^2)^{1/2} - 1 \right] \right\}^{1/2} \qquad 3.19$$

(Tolstoy 9.80)

c_p shows a second order dependence on $\omega\tau$ and is approximately constant in the low frequency limit. The specific attenuation factor will be peaked at a period of the order 2π times the relaxation time. The important point is that for a relaxation process we may modify solutions to the undamped wave equation by an exponential decay with respect to distance. These relations will describe well the chemical disassociation absorption noted in seawater.

From the previous section we see that frictional and other nonlinear attenuation mechanisms may be more appropriate than relaxation mechanisms in describing attenuation in sediments over wide bandwidths. White (ref. 4 , p. 115-117) shows, however, that for small strains nonlinear stress strain relations may be approximated to give displacement wave propagation

$$u_x = U_0 \, e^{-(\omega \Theta_p / 2c_p)x} \, e^{-i\omega x / c_p} \, e^{i\omega t} \qquad 3.20$$

Here Θ_p , the phase shift between stress and strain, is a constant related to stress strain hysterisis. Attenuation is exponential with respect to distance and directly proportional to frequency. Sound speed, c_p , is independent of frequency. Linear theory is then preserved and superposition still applies. Observations of exponential decay at fixed frequencies similar to that represented in equation 3.15 for a relaxation process, and the utility of frequency domain synthesis for a linear process, lead us to adopt the model with exponential decay over limited bandwidths.

3.4 Isovelocity layers with dissipation

Attenuation in the acoustic media we are treating is represented by letting sound speed become complex

$$\tilde{c} = \frac{\omega c'}{\omega + \imath k'' c'} \qquad 3.21$$

So wavenumber is complex,

$$\tilde{k} = \frac{\omega}{\tilde{c}} = \frac{\omega}{c'} + i k'' \equiv k' + i k'' \qquad 3.22$$

with k'' the attenuation in nepers/length. We show below that the refraction law then requires the angles of propagation in each layer to become complex,

$$\tilde{\varphi} = \varphi' + i \varphi'' \qquad 3.23$$

even with real incidence angle at the source.

3.4.1 *Wave representation* for isovelocity layers

In solving equation 2.3 separation of variables was employed and the velocity potential written as in equation 2.4. The assumption was made that $k(z)$ was independent of r . It could be real or complex. The separation constant K , identified as the radial wavenumber, was independent of r or z , but could also be complex. Solution 2.8 for the radial dependence of Φ still holds for complex K since the Hankel function is defined for complex argument Kr . For arbitrary variation of $c(z)$ with depth we must insure that $\phi(z)$ satisfies the Helmholtz equation 2.6. For isovelocity layers solution equation 2.12 will still hold and may be written in the form

$$\phi(z) = A \exp(i \tilde{\gamma} \cdot z) + B \exp(-i \tilde{\gamma} \cdot z) \; ; \tilde{\gamma} \equiv \tilde{k}_z \qquad 3.24$$

Solution of the complex Helmholtz equation for N^2-linear layers is treated in appendix 3.1.

Equation 2.9 is still the defining relation for $\tilde{k}_z$. When substitutions

$$\tilde{k}(z) = \frac{\omega}{c(z)} + i k'' \qquad 3.25$$

and

$$\tilde{K} = K' + i K'' \qquad 3.26$$

are made it is easily shown that

$$\gamma'^2 = \left(\frac{\omega}{c'}\right)^2 - k'^2 \quad ; \quad \gamma''^2 = k''^2 - K''^2 \quad ; \quad \gamma'\gamma'' = \frac{\omega}{c'}k'' - K'K'' \qquad 3.27$$

Equation 2.9 is identically satisfied for arbitrary real or complex angle $\tilde{\varphi}$ if we make the associations

$$\tilde{\gamma}^2 = \tilde{k}^2 \sin^2\tilde{\varphi} \qquad 3.28$$

and

$$\tilde{K}^2 = \tilde{k}^2 \cos^2\tilde{\varphi} \qquad 3.29$$

For then

$$\tilde{\gamma}^2 = \tilde{k}^2 - \tilde{K}^2 \Rightarrow \tilde{k}^2 = \tilde{\gamma}^2 + \tilde{K}^2 = \tilde{k}^2\left(\sin^2\tilde{\varphi} + \cos^2\tilde{\varphi}\right) = \tilde{k}^2 \qquad 3.30$$

The inverse relations are

$$\tilde{k}^2 = \tilde{\gamma}^2 + \tilde{K}^2 \qquad 3.31$$

$$\tilde{\varphi} = \tan^{-1}\left(\frac{\tilde{K}}{\tilde{\gamma}}\right) \qquad 3.32$$

If we pick angle $\tilde{\varphi}$ to be the real incidence angle between the normal to the wavefront and the cartesian axis 3, equations 3.28 and 3.29 give the cartesian components of wavenumber K and γ. Equations 3.27 are easily shown to hold. The polar representation in terms of angle $\tilde{\varphi}$ will be unique to mod 2π. In chapter 5 detailed consideration will be given to the inverse relations mapping from wavenumber to incidence angle. For a given locus of $\tilde{K}$ care must be taken to preserve continuity in K_3 and $\tilde{\varphi}$.

The propagation variables are now ω', ω'', k', k'', φ', φ''. c and $\delta(\omega) \equiv k''$ are specified for each layer so that for real frequency $(\omega'' = 0)$ the layer wavenumbers are given by $\tilde{k} = k' + i\,k'' = \frac{\omega}{c'} + \delta(\omega)$

With complex $\tilde{k}$ and $\tilde{\varphi}$ we have

$$\tilde{K_x} \equiv \tilde{\kappa} = \tilde{k} \sin\tilde{\varphi} \equiv k_x' + i k_x'' \qquad 3.33$$

$$\tilde{K_y} \equiv \tilde{\gamma} = \tilde{k} \cos\tilde{\varphi} \equiv k_y' + i k_y'' \qquad 3.34$$

Within an isovelocity layer we will define

$$\kappa' \equiv k_x' = \mathrm{Re}\left[\tilde{k}_x \sin\tilde{\varphi}\right] = \mathrm{Re}\left[(k'+ik'')\sin(\varphi'+i\varphi'')\right]$$
$$\kappa'' \equiv k_x'' = \mathrm{Im}\left[\tilde{k} \sin\tilde{\varphi}\right] = \mathrm{Im}\left[(k'+ik'')\sin(\varphi'+i\varphi'')\right]$$
$$\gamma' \equiv k_y' = \mathrm{Re}\left[\tilde{k} \cos\tilde{\varphi}\right] = \mathrm{Re}\left[(k'+ik'')\cos(\varphi'+i\varphi'')\right]$$
$$\gamma'' \equiv k_y'' = \mathrm{Im}\left[\tilde{k} \cos\tilde{\varphi}\right] = \mathrm{Im}\left[(k'+ik'')\cos(\varphi'+i\varphi'')\right]$$

3.35 – 3.38

Since

$$i\tilde{k}\sin\tilde{\varphi} = i(k'\sin\varphi'\cosh\varphi'' - k''\cos\varphi'\sinh\varphi'') - (k'\cos\varphi'\sinh\varphi'' + k''\sin\varphi'\cosh\varphi'')$$

3.39

and

$$i\tilde{k}\cos\tilde{\varphi} = i(k'\cos\varphi'\cosh\varphi'' + k''\sin\varphi'\sinh\varphi'') + (k'\sin\varphi'\sinh\varphi'' - k''\cos\varphi'\cosh\varphi'')$$

3.40

we have

$$i k_x' \equiv i(k'\sin\varphi'\cosh\varphi'' - k''\cos\varphi'\sinh\varphi'') \qquad 3.41$$
$$k_x'' \equiv -(k'\cos\varphi'\sinh\varphi'' + k''\sin\varphi'\cosh\varphi'') \qquad 3.42$$
$$i k_y' \equiv i(k'\cos\varphi'\cosh\varphi'' + k''\sin\varphi'\sinh\varphi'') \qquad 3.43$$
$$k_y'' \equiv +(k'\sin\varphi'\sinh\varphi'' - k''\cos\varphi'\cosh\varphi'') \qquad 3.44$$

Propagation is represented by $e^{(ik_x'+k_x'')x} \cdot e^{(ik_y'+k_y'')\cdot y}$

in the +x, +z direction and time dependence $e^{-i\omega t}$.

3.4.2 Refraction law

The refraction law itself is now complex,

$$\tilde{k}_i \sin \tilde{\varphi}_i = \tilde{k}_{i+1} \cdot \sin \tilde{\varphi}_{i+1} \qquad 3.45$$

To see that this law still holds for the complex wave representation Brekhovskikh has taken the incident, reflected and transmitted waves at the interface between two halfspaces *

$$\psi_{inc} = A \exp\left[i \tilde{k}_1 (x \sin \tilde{\varphi}_1 - z \cos \tilde{\varphi}_1)\right] \qquad 3.46$$

$$\psi_{refl} = RA \exp\left[i \tilde{k}_1 (x \sin \tilde{\varphi}_1 + z \cos \tilde{\varphi}_1)\right] \qquad 3.47$$

$$\psi_{trans} = TA \exp\left[i \tilde{k}_2 (x \sin \tilde{\varphi}_2 - z \cos \tilde{\varphi}_2)\right] \qquad 3.48$$

In the upper medium 1, $\psi_1 = \psi_{inc} + \psi_{refl}$. In the lower medium 2, $\psi_2 = \psi_{trans}$. Continuity of acoustic pressure and the normal component of particle velocity at the interface, z=0, with

$$p = -i\omega\rho\psi \quad ; \quad v = -\nabla\psi \qquad 3.49 \quad 3.50$$

requires

$$\rho_1 \psi_1 = \rho_2 \psi_2 \quad ; \quad \frac{d\psi_1}{dz} = \frac{d\psi_2}{dz} \qquad 3.51 \quad 3.52$$

Then

$$\frac{A_1}{\rho_2}(1 + R) = T \exp\left[i(\tilde{k}_2 \sin \tilde{\varphi}_2 - \tilde{k}_1 \sin \tilde{\varphi}) x\right] \qquad 3.53$$

* Note that Brekhovskikh uses here the same angle for incident and reflected waves as shown in his figure 6 (ref. 1, p. 15), drawn here as figure 3.1.a. This leads to a different representation of incident and reflected wave, thus minus sign in equation 3.46. If the definition of incidence angle as the angle between the normal to the wavefront in its direction of propagation and the +z axis is maintained a consistent representation using equation 3.47 results for both incident and reflected waves. The angle $\tilde{\varphi}$ will give the correct sign for k_z in both incident and reflected waves.

Since both sides must be independent of x he gets

$$\tilde{k}_1 \sin \tilde{\varphi}_1 = \tilde{k}_2 \sin \tilde{\varphi}_2 \qquad 3.54$$

the refraction law. This complex equation may then be written for arbitrary interface i, i+1 as the two real equations

$$k'_i \sin \varphi'_i \cosh \varphi''_i - k''_i \cos \varphi'_i \sinh \varphi''_i = k'_{i+1} \sin \varphi'_{i+1} \cosh \varphi''_{i+1} - k''_{i+1} \cos \varphi'_{i+1} \sinh \varphi''_{i+1} \qquad 3.55$$

$$k'_i \cos \varphi'_i \sinh \varphi''_i + k''_i \sin \varphi''_i \cosh \varphi''_i = k'_{i+1} \cos \varphi'_{i+1} \sinh \varphi''_{i+1} + k''_{i+1} \sin \varphi'_{i+1} \cosh \varphi''_{i+1} \qquad 3.56$$

These transcendental equations have multiple roots φ'_{i+1}, φ''_{i+1}. At any particular frequency ω, the quantities k' and $k''(\omega)$ are fixed for each layer. When $\tilde{\varphi}_i$ is known, two solutions for $\tilde{\varphi}_{i+1}$ may be found within the range $-\pi < \varphi_{i+1} < \pi$ with different signs in φ''_{i+1}. Additionally there is the modulus 2π ambiguity in φ'_{i+1}. Our method of solution for $\tilde{\varphi}_{i+1}$ is discussed in section 3.6.2.

3.4.3. Phase velocity

With propagation

$$\exp\left[(ik'_x + k''_x)x + (ik'_y + k''_y) - i\omega t\right]$$

we get phase velocity by setting the phase in the exponent equal to a constant, say zero, and projecting the velocity onto the x axis

$$ik'_x \cdot x - i\omega t = 0 \quad \Rightarrow \quad \frac{x}{t} = \frac{\omega}{k'_x} \qquad 3.57$$

In the ocean

$$k'_x = k' \sin\varphi' \cosh\varphi'' - k'' \cos\varphi' \sinh\varphi'' \qquad 3.58$$

with $k'' \cong 0$

$$c_p = \frac{\omega}{k'_x} = \frac{\omega}{k' \sin\varphi' \cosh\varphi''} = \frac{c_1}{\sin\varphi' \cosh\varphi''} \qquad 3.59$$

In other layers the phase velocity will be

$$c_p = \frac{\omega}{k' \sin\varphi' \cosh\varphi'' - k'' \cos\varphi' \sinh\varphi''} \qquad 3.60$$

and if attenuation is proportional to frequency

$$k'' = k''(\omega_o) \cdot \left(\frac{\omega}{\omega_o}\right)^{1.0}$$

we will have

$$c_p = \frac{\omega}{\frac{\omega}{c_o} \sin\varphi' \cosh\varphi'' - \frac{k''(\omega_o)}{\omega_o} \cdot \omega \cdot \cos\varphi' \sinh\varphi''} \qquad 3.61$$

$$= \frac{c_o \cdot \omega}{\omega_o \sin\varphi' \cosh\varphi'' - c_o \cdot k''(\omega_o) \cos\varphi' \sinh\varphi''}$$

In searching for modal eigenvalues ω , $\tilde{\varphi}$ as a function of phase velocity c_p we use equation 3.59 . Note that by constraining φ' and φ'' in the source layer to the locus on which

$$c_p = \frac{c_1}{\sin\varphi' \cosh\varphi_1''}$$

we are setting the refraction law equation 3.55 equal to a constant (a function of c_p and c_1).

3.4.4 Impedances

With sound speed and incidence angle complex the defining relations for the normal impedances are still valid,

$$Z = \frac{p}{v_3} \qquad \text{for waves traveling downward in the +z} \qquad 3.62$$

direction, and $\frac{P}{V_j} = -Z$ for waves traveling in the -z direction. That is, with $V = -\nabla \Phi$ and $P = -i\omega\rho\Phi$ we have 3.63

$$Z \equiv Z\downarrow = \frac{-i\omega\rho\,\Phi\downarrow}{-\frac{i\omega\cos\tilde{\varphi}}{\tilde{c}}\,\Phi\downarrow} = \frac{\rho\tilde{c}}{\cos\tilde{\varphi}} \qquad 3.64$$

and

$$Z\uparrow = \frac{-i\omega\rho\,\Phi\uparrow}{\frac{i\omega\cos\tilde{\varphi}}{\tilde{c}}\,\Phi\uparrow} = \frac{-\rho\tilde{c}}{\cos\tilde{\varphi}} \qquad 3.65$$

We have used

$$\phi\downarrow = \exp(i k_j^{\sim} \cdot j) \;;\; \phi\uparrow = \exp(-i k_j^{\sim} \cdot j)$$

and $k_j^{\sim} = \tilde{k}\cos\tilde{\varphi}$ with the same $\tilde{\varphi}$ used for $\phi\uparrow$ or $\phi\downarrow$. $Z_c \equiv \rho\tilde{c}$ is the complex characteristic impedance. Z gives both the amplitude and phase relation between local pressure and particle velocity normal to the boundary throughout the isovelocity layer. The minus sign arises with the upward propagating wave because of the sense of the particle velocity.

Defining Z in terms of its real and imaginary components, as Brekhovskikh does, we can explicitly relate Z to the complex polar wavenumber coordinates $\tilde{k}$ and $\tilde{\varphi}$. Using Brekhovskikh's notation for

$$\tilde{Z} \equiv \gamma + i\delta \qquad 3.66$$

we obtain

$$\gamma = \rho\omega c_0 \frac{A_z}{A_z^2 + B_z^2} \qquad \delta = -\rho\omega c_0 \frac{B_z}{A_z^2 + B_z^2} \qquad 3.67 \quad 3.68$$

where

$$A_{\tilde{z}} = \omega \cos\varphi' \cosh\varphi'' + k'' c_o \sin\varphi' \sinh\varphi'' \qquad 3.69$$

$$B_{\tilde{z}} = k'' c_o \cos\varphi' \cosh\varphi'' - \omega \sin\varphi' \sinh\varphi'' \qquad 3.70$$

In the nondissipative case we saw that the relation $\tilde{Z}\downarrow = -\tilde{Z}\uparrow^*$ held for incidence angles $<$ critical in isovelocity layers, and above the turning point in N^2-linear layers. The relation $\tilde{Z}\downarrow = -\tilde{Z}\uparrow$ is used to derive reflection coefficients, and for isovelocity layers is correct as shown above in equation 3.65. $\tilde{Z}\downarrow = -\tilde{Z}\uparrow^*$ is also formally correct for isovelocity layers if $\tilde{Z}\uparrow$ and $\tilde{Z}\downarrow$ are real. Starting with definition eq 3.64 for $\tilde{Z} = \tilde{Z}\downarrow$, and substituting $\varphi_{refl} = \pi - \varphi_{inc}$ into the expressions for $A_{\tilde{z}}$, $B_{\tilde{z}}$, γ, δ above we alternately may show that $A_{refl_{\tilde{z}}} = -A_{inc_{\tilde{z}}}$, and $B_{refl_{\tilde{z}}} = -B_{inc_{\tilde{z}}}$. Then if $B_{inc_{\tilde{z}}} \neq 0$ we must have $\tilde{Z}\downarrow = -\tilde{Z}\uparrow$, not $\tilde{Z}\downarrow = -\tilde{Z}\uparrow^*$. This latter form does not hold in isovelocity layers for complex angles of incidence.

3.4.5 Reflection and transmission coefficients

a. Reflection coefficient over a dissipative halfspace.

Both reflection and transmission coefficients at an interface between two halfspaces are now found to be complex. Pressure is $P = -i\omega\rho\psi$ and the vertical component of particle velocity may be written

$$V_z = \frac{P}{\tilde{Z}} = \frac{-i\omega\rho}{\tilde{Z}}\left(A \exp[ik(x\sin\varphi - z\cos\varphi)] - RA \exp[ik(x\sin\varphi + z\cos\varphi)]\right) \qquad 3.71$$

The $-RA$ term comes from the difference in impedance definition for incident and reflected waves. Then since the ratio P/V_z must be equal to the impedance in the lower medium as well

$$\tilde{Z}_2 = \tilde{Z}_1\left(\frac{A+B}{A-B}\right) \Rightarrow \tilde{R} = \frac{B}{A} = \frac{\tilde{Z}_2 - \tilde{Z}_1}{\tilde{Z}_2 + \tilde{Z}_1} \qquad 3.72$$

Then for interface i , j

$$R_{ij} = \rho_{ij}\, e^{i\Phi_{ij}} \quad \text{with} \quad \rho = \frac{(\gamma_i - \gamma_j)^2 + (\delta_i - \delta_j)^2}{(\gamma_i + \gamma_j)^2 + (\delta_i + \delta_j)^2} \qquad 3.73$$

$$\text{and} \quad \tan \Phi_{ij} = \frac{2(\delta_i \gamma_j - \delta_j \gamma_i)}{(\gamma_i^2 - \gamma_j^2 + \delta_i^2 - \delta_j^2)} \qquad 3.74$$

Since the reflection coefficient will have magnitude $\neq 1$ even for incidence angles beyond the critical we write

$$R = e^{i\tilde{\Phi}} = e^{i(\Phi' + \Phi'')} = e^{-\Phi''} \cdot e^{i\Phi'} \qquad 3.75$$

$$-\Phi'' = \ln|R| \qquad 3.76$$

We later use the transmission coefficient T for critical reflection. There with

$$\tilde{\varphi}_1 = \left[(\varphi_1' > \varphi_{1\,crit}'), (\varphi_1'' = 0)\right] \; ; \; \tilde{\varphi}_2 = \left[(\varphi_2' = \tfrac{\pi}{2}), \varphi_2''\right]$$

and with medium 2 nondissipative

$$T = \frac{2\rho_1 c_2 \cos\varphi_1}{\rho_2 c_2 \cos\varphi_1 - i\rho_1 c_1 \sinh\varphi_2''} \qquad 3.77$$

These representations correspond to those of Tolstoy and Clay, for example, who with

$$\underline{\Phi} = e^{i(k_x \cdot x + k_{1z} \cdot z - \omega t)} + R_{12}\, e^{i(k_x \cdot x - k_{1z} \cdot z - \omega t)} \qquad 3.78$$

and

$$\underline{\Phi}_2 = \tau\, e^{i(k_x \cdot x + k_{2z} \cdot z - \omega t)} \qquad 3.79$$

using v = phase velocity

$$K_{2j} = \left(\frac{\omega^2}{c_2^2} - K_x^2 \right)^{1/2} = K_x \left(\frac{v^2}{c_2^2} - 1 \right)^{1/2} \qquad 3.80$$

find

$$R_{12} = \frac{\rho_2 K_{1j} - \rho_1 K_{2j}}{\rho_2 K_{1j} + \rho_1 K_{2j}} \quad \text{and} \quad \tau_{12} = \frac{2\rho_1 K_{1j}}{\rho_2 K_{1j} + \rho_1 K_{2j}} \qquad 3.81 \quad 3.82$$

For critical reflection $K_{2j} = i r_2$ in the Tolstoy formula where

$$r_2 = \frac{\omega}{v} \left(1 - \frac{v^2}{c_2^2} \right)^{1/2} \quad \text{and with} \quad R = e^{\pm 2\chi}$$

$$\chi = \tan^{-1} \left(\frac{\rho_1 r_2}{\rho_2 K_{1j}} \right) \quad \text{equivalent to Tolstoy 2.90} \qquad 3.83$$

The Brekhovskikh representation emphasises the role of complex angle and explicitly includes absorption.

3.4.5.b. Multilayer reflection coefficient for dissipative isovelocity *media:*

Brekhovskikh has indicated a direction that might be taken for the case of absorption in multilayer systems. He has given the reflection coefficient including partial reflections for absorbing media. Briefly with isovelocity media, and after modifying his notation

$$R = \frac{R_{23} + R_{12} \exp(2i\alpha_2 d)}{1 + R_{23} R_{12} \exp(2i\alpha_2 d)} \qquad 3.84$$

R_{ij} are interface reflection coefficients such that

$$R_{12} = \frac{Z_2 - Z_1}{Z_2 + Z_1} \qquad R_{23} = \frac{Z_3 - Z_2}{Z_3 + Z_2} \qquad 3.85 \quad 3.86$$

with Z_i the normal impedance. For the multilayer guides Z_2 will become the input impedance to the lower layer system. The equation is recursive.

Brekhovskikh defines

$$\alpha_2 \equiv K_{2z} = k_2 \cos\varphi_2 \qquad 3.87$$

$$\sigma_2 \equiv K_{2x} = k_2 \sin\varphi_2 \qquad 3.88$$

and $$2\alpha_2 d = 2 k_2 \cos\varphi_2 \cdot d \equiv \alpha + i\beta \qquad 3.89$$

so that with $$Z_j \equiv \gamma_j + i\delta_j \qquad 3.90$$

and with the R_{12} and R_{23} given above he finds

$$R_{23} = \rho_{23} e^{i\phi_{23}} \quad ; \quad R_{12} = \rho_{12} e^{i\phi_{12}} \qquad 3.91,\ 3.92$$

$$\rho_{23}^2 = \frac{(\gamma_3-\gamma_2)^2 + (\delta_3-\delta_2)^2}{(\gamma_3+\gamma_2)^2 + (\delta_3+\delta_2)^2} \qquad \tan\phi_{23} = \frac{2(\delta_3\gamma_2 - \delta_2\gamma_3)}{\gamma_3^2 - \gamma_2^2 + \delta_3^2 - \delta_2^2} \qquad 3.93,\ 3.94$$

He then gets the modulus and phase of the three layer (or recursive) reflection coefficient $$R = \rho e^{i\phi} \qquad 3.95$$

$$\rho^2 = |R|^2 = \frac{\rho_{12} + 2\rho_{23}\rho_{12} e^{-\beta}\cos(\phi_{23} - \phi_{12} + \alpha) + \rho_{23}^2 e^{-2\beta}}{1 + \rho_{23}^2\rho_{12}^2 e^{-2\beta} + 2\rho_{23}\rho_{12} e^{-\beta}\cos(\phi_{23} + \phi_{12} + \alpha)} \qquad 3.96$$

$$\phi = \phi_a + \phi_b + \phi_{12} \qquad 3.97$$

$$\phi_a = \arctan\left[\frac{\rho_{23} e^{-\beta}\sin(\phi_{23} - \phi_{12} + \alpha)}{\rho_{12} + \rho_{23} e^{-\beta}\cos(\phi_{23} - \phi_{12} + \alpha)}\right] \qquad 3.98$$

$$\phi_b = \arctan\left[\frac{\rho_{23}\rho_{12} e^{-\beta}\sin(\phi_{23} + \phi_{12} + \alpha)}{1 + \rho_{23}\rho_{12} e^{-\beta}\cos(\phi_{23} + \phi_{12} + \alpha)}\right] \qquad 3.99$$

We see that he has $R = R(\rho_{23}, \rho_{12}, \phi_{23}, \phi_{12}, \alpha, \beta) = R(\gamma_2, \gamma_3, \delta_2, \delta_3, \gamma_1, \delta_1, \alpha, \beta)$

Substituting for c_j and φ_j in his definition of Z_j and $2\alpha_j d$ we determine

$$\alpha = \frac{2 \cdot d}{c_{j0}} \cdot A \qquad \beta = \frac{2 \cdot d}{c_{j0}} \cdot B \qquad 3.100 \quad 3.101$$

$$\gamma_j = \rho_j \omega c_{j0} \frac{A_2}{A_2^2 + B_2^2} \qquad \delta_j = -\rho_j \omega c_{j0} \frac{B_2}{A_2^2 + B_2^2} \qquad 3.102 \quad 3.103$$

where

$$A_2 = \omega \cos \varphi_j' \cosh \varphi_j'' + k_j'' c_{j0} \sin \varphi_j' \sinh \varphi_j'' \qquad 3.104$$

$$B_2 = k_j'' c_{j0} \cos \varphi_j' \cosh \varphi_j'' - \omega \sin \varphi_j' \sinh \varphi_j'' \qquad 3.105$$

We see then that $R = |R| e^{i\phi}$ can be determined solving the refraction law for a particular frequency ω at each interface and recursively calculating R to the ocean bottom.

3.5 General statement of the problem:

3.5.1. Characteristic equation:

From the above we see that the refraction law lets us determine complex angle $\tilde{\varphi}_2$ in the lower medium given $\tilde{\varphi}_1$ in the upper medium. Then we can compute $\tilde{R}\downarrow(3)$ at the ocean bottom. $\tilde{R}\uparrow(3)$ at the ocean surface is assumed = -1 for the pressure release surface. If we choose phase velocity c_p as the independent parameter (we could just as well choose frequency ω) we may solve the characteristic equation for eigenfrequency ω , constrained to be real, and complex eigenincidence angle $\tilde{\varphi}_1$, in the source layer. The c_p relation, equation 3.59, lets us solve for φ_1'' given φ_1' and the assumed value of c_p .

The complex characteristic equation can now be split into its

real and imaginary parts

$$1 - \tilde{R}\uparrow \cdot \tilde{R}\downarrow \exp(2i\tilde{k}_z \cdot h) = 0 \qquad 3.106$$

it becomes

$$2 k_i' h \cos\varphi_i' \cosh\varphi_i'' + \phi'\uparrow + \phi'\downarrow = 2\pi l \qquad 3.107$$

$$-2 k_i' h \sin\varphi_i' \sinh\varphi_i'' + \phi''\uparrow + \phi''\downarrow = 0 \qquad 3.108$$

These two real equations must be satisfied. Given the Cp relation we have two equations and two unknowns ω and φ_i'. In summary the equations at hand are:

1. Phase velocity in the source layer

$$C_p = C_i' / \sin\varphi_i' \cosh\varphi_i'' \qquad 3.109$$

2. Refraction law at each interface

$$k_i' \sin\varphi_i' \cosh\varphi_i'' - k_i' \cos\varphi_i' \sinh\varphi_i'' = k_{i+1}' \sin\varphi_{i+1}' \cosh\varphi_{i+1}'' - k_{i+1}'' \cos\varphi_{i+1}' \sinh\varphi_{i+1}'' \qquad 3.110$$

$$k_i' \cos\varphi_i' \sinh\varphi_i'' + k_i'' \sin\varphi_i' \cosh\varphi_i'' = k_{i+1}' \cos\varphi_{i+1}' \sinh\varphi_{i+1}' + k_{i+1}'' \sin\varphi_{i+1}' \cosh\varphi_{i+1}'' \qquad 3.111$$

3. Characteristic equation

$$2 k_i' h \cos\varphi_i' \cosh\varphi_i'' + \phi'\uparrow + \phi'\downarrow = 2\pi l \qquad 3.112$$

$$-2 k_i' h \sin\varphi_i' \sinh\varphi_i'' + \phi''\uparrow + \phi''\downarrow = 0 \qquad 3.113$$

Also we have a formula for the reflection coefficient

$$R = \tilde{R}\left(\underbrace{\rho_1, \rho_2, c_1, c_2, k_1'', k_2''}_{\text{model}}, \underbrace{\omega, \varphi_1', \varphi_1'', \varphi_2', \varphi_2''}_{\text{variable}}\right) \qquad 3.114$$

for the Pekeris guide with

$$\tilde{R}\downarrow = e^{-\phi''\downarrow} e^{i\phi'\downarrow} \quad ; \quad \tilde{R}\uparrow = -1 \Rightarrow \phi''\uparrow = 0 \,, \; \phi'\uparrow = \pm\pi$$

Thus we see that for the layer over a halfspace N=2 we have five equations and five unknowns. In the multilayer case of N-1 layers over a halfspace we have 2N+1 equations in 2N+1 unknowns. For each additional layer we add two unknown angle components, $\tilde{\varphi}_i = (\varphi_i', \varphi_i'')$, and two additional refraction law equations. Reflection coefficients calculated with the recursive formulation must be used as well.

$$R\downarrow = \tilde{R}\downarrow(\rho_i, c_i, k_i'', \omega, \varphi_i', \varphi_i'') \qquad i = 1, 2, \ldots N$$

Of these equations the refraction law equations are solved as N-1 simultaneous transcendental pairs. The characteristic equation is also treated as a transcendental pair. Trigonometric ambiguities occur in all these equations, and constraints must be placed on angle domains. The c_ρ equation is also ambiguous with roots whose imaginary part of angle φ_1'' may be $\gtrless 0$. When angle constraints are established and roots chosen for the refraction and c_ρ equations the reflection coefficient follows simply by substitution. In section 3.6 we discuss the interative procedure for solving the refraction and characteristic equations.

3.5.2 Attenuation coefficient

Our goal is to determine the modal attenuation of each mode as a function of frequency or wavenumber. The rigorous attenuation coefficient is shown in chapter 4 to be

$$\zeta = -k_1 \cos\varphi_1' \left[\frac{\phi''\uparrow + \phi''\downarrow}{2k_1 h \sin\varphi_1'}\right] = -\left[\frac{\phi''\uparrow + \phi''\downarrow}{2h \tan\varphi_1'}\right] \qquad 3.115$$

This may be solved for as a function of φ_1' and $\phi''\uparrow(\varphi_1', \varphi_1'', \ldots)$

3.6 Method of solution

3.6.1. Characteristic equation

Newton-Raphson convergence schemes are used to solve both the Snell equations and the characteristic equations. For the characteristic equation iteration is performed over the eigenvalues ω, φ_1'. φ_1'' is related to φ_1' through independent parameter c_p and independent of ω in the ocean where $k'' \approx 0$.

For iteration $i+1$

$$\omega_{i+1} = \omega_i - \frac{f \cdot g_{\varphi_i'} - g \cdot f_{\varphi_i'}}{J(f,g)} \qquad 3.116$$

$$\varphi_{i+1} = \varphi_i - \frac{g \cdot f_\omega - f \cdot g_\omega}{J(f,g)} \qquad 3.117$$

Here

$$f_{\varphi_1'} \equiv \frac{\partial f(\varphi_1', \varphi_1'', \omega)}{\partial \varphi_1'} \qquad f_\omega \equiv \frac{\partial f(\varphi_1', \varphi_1'', \omega)}{\partial \omega} \qquad 3.118,\ 3.119$$

$$g_{\varphi_1'} \equiv \frac{\partial g(\varphi_1', \varphi_1'', \omega)}{\partial \varphi_1'} \qquad g_\omega \equiv \frac{\partial g(\varphi_1', \varphi_1'', \omega)}{\partial \omega} \qquad 3.120,\ 3.121$$

$$J(f,g) = f_\omega \cdot g_{\varphi_1'} - g_\omega \cdot f_{\varphi_1'} \qquad 3.122$$

$$f(\varphi_1', \varphi_1'', \omega) = 2\pi l - 2kh \cos\varphi_1' \cosh\varphi_1'' - \phi'\uparrow - \phi'\downarrow \qquad 3.123$$

$$g(\varphi_1', \varphi_1'', \omega) = -2kh \sin\varphi_1' \sinh\varphi_1'' + \phi''\uparrow + \phi''\downarrow \qquad 3.124$$

Analytic forms of the derivative defined above are largely intractable (even for the two layer case). This is because the phase and amplitude of the reflection coefficient are dependent on ω and φ_1' in complicated ways. Each of the angles φ_i' entering into the reflection coefficient are also dependent on ω and φ_1' and the number of partial derivative evaluations is excessive. We have attempted, however, to initially implement the Newton-Raphson method for the charac-

teristic equation using analytic forms for the partial derivatives. Since solutions for the layer angles themselves come from an iterative procedure. (Closed form solutions have not been determined for the refraction law equations), partial derivation of the required angles must be estimated during the refraction law iterations. We have had little success in getting this method to converge however. After some effort we have settled on a finite difference approximation to the required derivatives. Functional values for the characteristic equation are calculated along lines of constant φ_i' and ω and the finite differences combined with $\Delta\varphi_i'$ and $\Delta\omega$ step size to give approximations to the derivatives. Later when the program continued to be plagued by faulty derivatives, "extrapolation to the limit" was used to further improve the estimates of derivatives. First order extrapolation is shown by Conte (ref. 6) to give derivative estimate

$$f'(x_0) = \left[4\,D(h/2) - D(h)\right]/3 \qquad 3.125$$

where

$$D(h, f(x_0)) = \left[f(x_0+h) - f(x_0-h)\right]/2h \qquad 3.126$$

$h > 0$ is the step size. At each point x_0 we continue to halve the interval h until $D(h/2)$ and $D(h)$ agree to within a prescribed amount.

3.6.2. Refraction law equation

In the implementation of the refraction law at each layer solutions for $\tilde{\varphi}_{i+1} = (\varphi'_{i+1}, \varphi''_{i+1})$ are obtained iteratively in the following manner. Using $\tilde{\varphi}_i$ from the previous layer, an initial estimate of φ'_{i+1} is made from the real "Snell equation" for this interface assuming no dissipation and the same incident angle with its imaginary part set to zero. A solution for φ''_{i+1} may be obtained from one Snell equation and used to generate a correction to φ'_{i+1} from the other. In the Newton-Raphson form actually used here, correction factors for both φ'_{i+1} and φ''_{i+1} are generated sim-

ultaneously after the initial guess. Specifically equation 3.56 becomes

$$BLHS = B_{1_{\lambda+1}} \cdot \sinh \varphi''_{\lambda+1} + B_{2_{\lambda+1}} \cdot \cosh \varphi''_{\lambda+1} \qquad 3.127$$

with

$$BLHS \equiv B_{1_\lambda} \cdot \sinh \varphi_\lambda'' + B_{2_\lambda} \cdot \cosh \varphi_\lambda'' \qquad 3.128$$

$$B_{1_\lambda} \equiv k'_\lambda \cdot \cos \varphi'_\lambda \qquad B_{2_\lambda} \equiv k''_\lambda \cdot \sin \varphi'_\lambda \qquad 3.129,\ 3.130$$

$$B_{1_{\lambda+1}} \equiv k'_{\lambda+1} \cdot \cos \varphi'_{\lambda+1} \qquad B_{2_{\lambda+1}} \equiv k''_{\lambda+1} \cdot \sin \varphi'_{\lambda+1} \qquad 3.131,\ 3.132$$

Manipulation gives $\varphi''_{\lambda+1}$ as solution to

$$\frac{B3_{\lambda+1}}{B4_{\lambda+1}} e^{2\varphi''_{\lambda+1}} - \frac{BLHS}{B4_{\lambda+1}} e^{\varphi''_{\lambda+1}} + 1 = 0 \qquad 3.133$$

with

$$B3 \equiv (B2_{\lambda+1} + B1_{\lambda+1})/2. \qquad 3.134$$

$$B4 \equiv (B2_{\lambda+1} - B1_{\lambda+1})/2. \qquad 3.135$$

and an additional root has been introduced by expanding sinh and cosh and multiplying by $e^{\varphi''_{\lambda+1}}$. A solution for $\varphi''_{\lambda+1}$ is then

$$\varphi''_{\lambda+1} = \ln\left[\frac{B4}{2\,B3} \cdot \left(\frac{BLHS}{B4} \pm \left(\left(\frac{BLHS}{B4}\right)^2 - 4\,\frac{B3}{B4}\right)^{1/2}\right]\right] \equiv f(\varphi'_{\lambda+1}\ \text{real})$$

Equation 3.55 is written

$$ALHS = A'_{\lambda+1} \cosh \varphi''_{\lambda+1} - A2_{\lambda+1} \sinh \varphi''_{\lambda+1} \qquad 3.136$$

where

$$ALHS \equiv k_i' \sin \varphi_i' \cosh \varphi_i'' - k_i'' \cos \varphi_i' \sinh \varphi_i'' \qquad 3.137$$

$$A_{i+1}^1 \equiv k_{i+1}' \sin \varphi_{i+1}' \qquad A_{i+1}^2 \equiv k_{i+1}'' \cdot \cos \varphi_{i+1}' \qquad 3.138$$

We have the two simultaneous equations

$$ALHS = k_{i+1}' \sin \varphi_{i+1}' \cosh \varphi_{i+1}' - k_{i+1}'' \cos \varphi_{i+1}' \sinh \varphi_{i+1}'' \equiv ARHS$$

$$BLHS = k_{i+1}' \cos \varphi_{i+1}' \sinh \varphi_{i+1}'' + k_{i+1}'' \sin \varphi_{i+1}' \cosh \varphi_{i+1}'' \equiv BRHS$$

3.139, 3.140

and initial guesses

$$\varphi_{i+1}' = (\varphi_{i+1}, 0) \quad \text{real Snell solution} \qquad 3.141$$

$$\varphi_{i+1}'' = p(\varphi_{i+1}' \text{ real}) \qquad 3.142$$

where care has been taken to eliminate the spurious root (The error is determined for each root. If both roots are > 0 the smallest error producer is chosen. In practice one solution is always on the order of -1 the other is $\epsilon \sim O(10^{-7})$.

Defining

$$f(\varphi_{i+1}', \varphi_{i+1}'') \equiv ARHS - ALHS \qquad 3.143$$

$$g(\varphi_{i+1}', \varphi_{i+1}'') \equiv BRHS - BLHS \qquad 3.144$$

so that

$$f_{\varphi_{i+1}'} \equiv \frac{\partial f}{\partial \varphi_{i+1}'} = k_{i+1}' \cosh \varphi_{i+1}'' \cos \varphi_{i+1}' + k_{i+1}'' \sinh \varphi_{i+1}'' \sin \varphi_{i+1}'$$

3.145

$$f_{\varphi_{i+1}''} \equiv \frac{\partial f}{\partial \varphi_{i+1}''} = k_{i+1}' \sin \varphi_{i+1}' \sinh \varphi_{i+1}'' - k_{i+1}'' \cos \varphi_{i+1}' \cosh \varphi_{i+1}''$$

3.146

$$g_{\varphi'_{i+1}} \equiv \frac{\partial g}{\partial \varphi'_{i+1}} = -k'_{i+1} \sinh \varphi''_{i+1} \sin \varphi'_{i+1} + k''_{i+1} \cosh \varphi''_{i+1} \cos \varphi'_{i+1} \qquad 3.147$$

$$g_{\varphi''_{i+1}} \equiv \frac{\partial g}{\partial \varphi''_{i+1}} = k'_{i+1} \cos \varphi'_{i+1} \cosh \varphi''_{i+1} + k''_{i+1} \sin \varphi'_{i+1} \sinh \varphi''_{i+1} \qquad 3.148$$

Newtons method is used to generate new estimates of φ'_{i+1} , φ''_{i+1}

$$\varphi'_{i+1_{new}} = \varphi'_{i+1_{old}} - \left(\frac{f \cdot g''_{i+1} - g \cdot f_{\varphi''_{i+1}}}{J(f,g)} \right) \qquad 3.149$$

$$\varphi''_{i+1_{new}} = \varphi''_{i+1_{old}} - \left(\frac{g \cdot f_{\varphi'_{i+1}} - f \cdot g_{\varphi'_{i+1}}}{J(f,g)} \right) \qquad 3.150$$

where

$$J(f,g) = f_{\varphi'_{i+1}} \cdot g_{\varphi''_{i+1}} - g_{\varphi'_{i+1}} \cdot f_{\varphi''_{i+1}} \qquad 3.151$$

Iteration proceeds until convergence is achieved to within permissible error.

3.6.3. Regarding Riemann sheets

The characteristic equation 3.106 has multiple isolated roots. Branch cuts involved in evaluating field equation Brekhovskikh 27.21 (equation 2.68) and discussed in section 2.4.b. are made by Brekhovskikh along lines in the $\tilde{\varphi}_1$ plane for which $\mathrm{Im}\sqrt{n_1^2 - \sin^2\varphi_1} = 0$ and $\mathrm{Im}\sqrt{n_2^2 - \sin^2\varphi_1} = 0$. The functions $R_1(\varphi)$ and $R_2(\varphi)$ are not single valued, since they contain square roots. Brekhovskikh's paths of integration lie on the sheet for which $\mathrm{Im}\sqrt{n_1^2 - \sin^2\varphi} > 0$, and $\mathrm{Im}\sqrt{n_2^2 - \sin^2\varphi} > 0$. He notes that in the lower med-

ium the field of the refracted wave will contain the factor $\exp\left[-\imath k \sqrt{n_1^2 - \sin^2\varphi'} \cdot y\right]$ so as $y \to -\infty$ the field will remain bounded. In our formulation with the $+y$ axis pointed down we will have

$$k_y' = k' \cos\varphi' \cosh\varphi'' + k'' \sin\varphi' \sinh\varphi'' \qquad 3.152$$

$$k_y'' = k' \sin\varphi' \sinh\varphi'' - k'' \cos\varphi' \cosh\varphi'' \qquad 3.153$$

In order to avoid having the field go to ∞ as $y \to \infty$ we require $k_y'' < 0$ in the lower halfspace, given the representation $\exp\left[(\imath k_y' + k_y'') \cdot y\right]$. If the refracted angle were at $\varphi_2' = \frac{\pi}{2}$, $\varphi_2'' = \pm\varphi''$ we would require $\varphi'' < 0$ in order for $k_y'' < 0$. This would be equivalent to $\mathrm{Im}\sqrt{n_1^2 - \sin^2\varphi'} > 0$ and would place any function $f(k_y'')$ on the + Riemann sheet. (We have only (+), or (-) sheets since a free surface exists above the waveguide). For finite dissipation $k_2'' \neq 0$ and $\varphi_2' \neq \frac{\pi}{2}$, so the boundary (branch line) $\mathrm{Im}\sqrt{n_1^2 - \sin^2\varphi'} = 0$ does not correspond exactly to $\varphi_2'' = 0$, but instead to $k_y'' = 0$

i.e. to

$$k_2' \sin\varphi_2' \sinh\varphi_2'' - k_2'' \cos\varphi_2' \cosh\varphi_2'' = 0$$

So

$$\frac{k_2'}{k_2''} \tan\varphi_2' = \operatorname{cotanh}\varphi_2'' \qquad 3.154$$

is the branch line definition in the $\tilde{\varphi}_2$ plane. In chapter 5 we shall use a relation similar to equation 3.154 to characterize a "speculative angle" of incidence, $\varphi_{1\,spec}$, at which the reflection

coefficient for fixed phase velocity shows a discontinuity in the locked mode region. The existence of the discontinuity will be shown to arise when crossing from the (+) sheet to the (-) sheet in order that propagated angle φ_2' remain $< \frac{\pi}{2}$ during the iterative search for eigenangle. This corresponds to choosing a different root to the refraction law equation because of imposition of a physical constraint.

Appendix 3.1

N^2-linear layers with dissipation:

Layers of this type are characterized by the so called "pseudo-linear" sound speed gradient $N^2(z) \equiv \left(\frac{c_0}{c(z)}\right)^2 = \rho \pm g z$. To examine the effect of attenuation on wavefunctions we again allow sound speed to become complex and write it as

3A.1

$$\tilde{c}(z) = \frac{\omega\, c'(z)}{\omega + i\, k''\, c'(z)} \qquad 3A.2$$

with dissipation number $k'' = a$ constant. The index of refraction becomes

$$\tilde{N}(z) = \frac{c_0}{\tilde{c}(z)} = \frac{c_0\,(\omega + i k''(z)\, c'(z))}{\omega\, c'(z)}$$

$$= \frac{c_0}{c'(z)} + \frac{i\, k''(z)\, c_0}{\omega} = \frac{c_0}{c'(z)} + i\,\frac{k''(z)}{k'(0)} \equiv N'(z) + i N''(z) \qquad 3A.3$$

and the Helmholtz equation becomes complex

$$\frac{d^2\Phi(z)}{dz^2} + k_0^2\left[\tilde{N}^2(z) - \sin^2\tilde{\varphi}_0\right]\Phi(z) = 0 \qquad 3A.4$$

here

$$k_0^2 \sin^2\tilde{\varphi}_0 = (k_x')^2 - (k_x'')^2 + 2 i k_x' k_x''$$

$$k_0^2 \tilde{N}^2(z) = \frac{\omega^2}{c_0^2}\left[\left(\frac{c_0}{c'(z)}\right)^2 - \frac{k''^2 c_0^2}{\omega^2} + \frac{2 i k'' c_0^2}{c'(z)\,\omega}\right]$$

$$= \frac{\omega^2}{c'(z)^2} - k''(z)^2 + \frac{2 i k'' \omega}{c'(z)}$$

AD-A079 562 WOODS HOLE OCEANOGRAPHIC INSTITUTION MASS F/G 17/1
ATTENUATION OF LOW ORDER MODES IN LOSSY ACOUSTIC WAVE GUIDES.(U)
DEC 79 H D LESLIE N00014-75-C-0852
UNCLASSIFIED WHOI-79-91 NL

2 OF 3
ADA 079 562

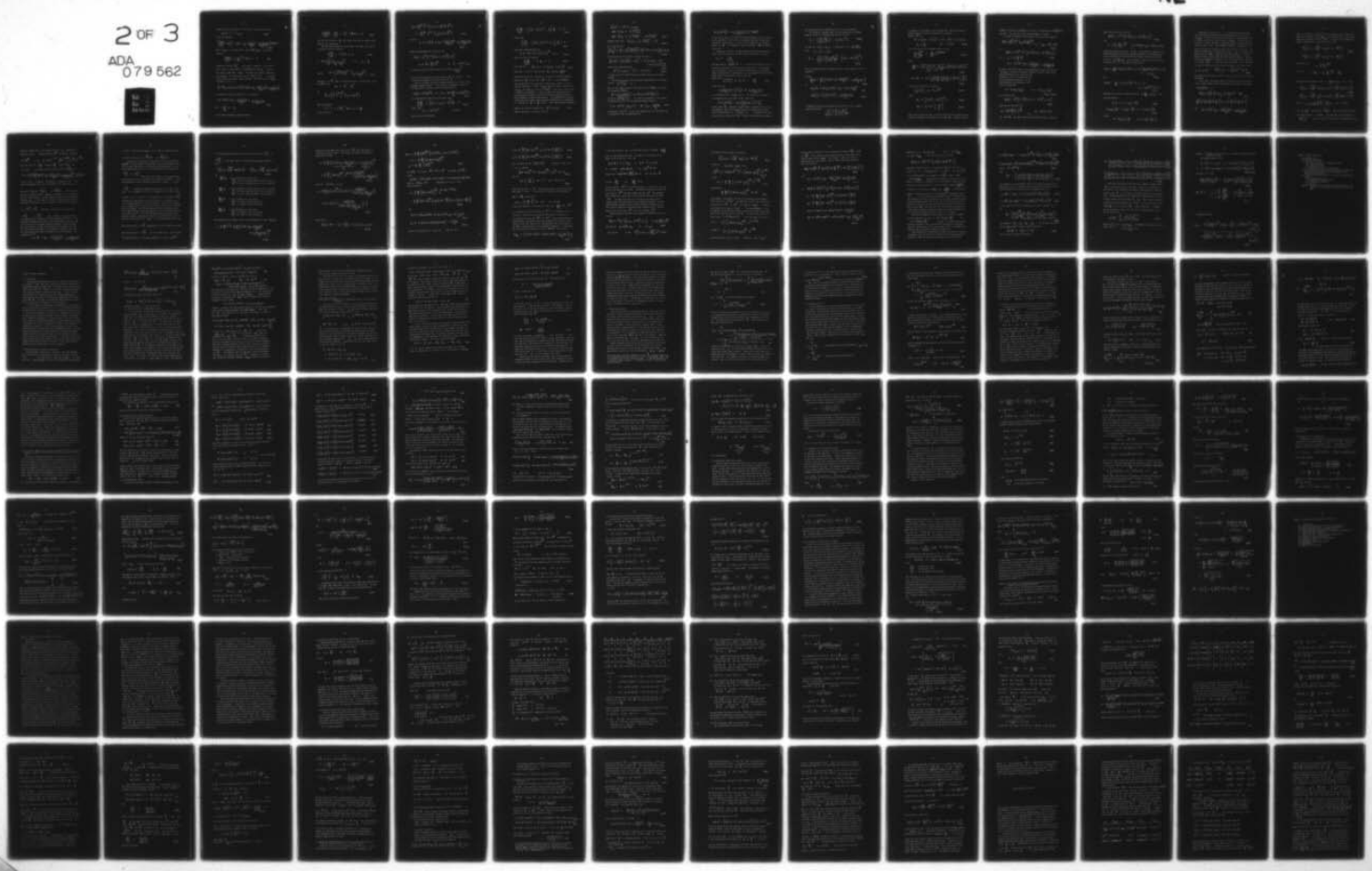

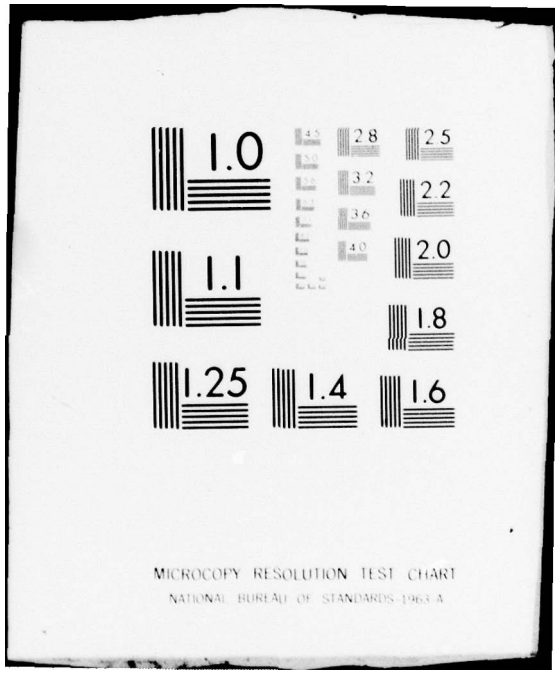
1.0
1.1
1.25
1.4
1.6
2.0
2.2
2.5
2.8
3.2
3.6
4.0
MICROCOPY RESOLUTION TEST CHART
NATIONAL BUREAU OF STANDARDS-1963-A

Assuming that the real part of the index of refraction varies as

$$(N')^2 = 1 \pm g\zeta \qquad 3A.5$$

we get the equation

$$\frac{d^2\phi(\zeta)}{d\zeta^2} + k_0^2\left[1 - \sin^2\varphi_0 \pm g\zeta - \frac{k''(\zeta)^2 c_0^2}{\omega^2} + \frac{2i k''(\zeta) c_0^2}{c(\zeta)\,\omega}\right]\phi(\zeta) = 0 \qquad 3A.6$$

When $k'' \to 0$ the substitution $\zeta = \cos^2\varphi_0 \pm g\zeta$ gives the equation

$$\frac{d^2\phi(\zeta)}{d\zeta^2} + \left(\frac{k_0}{g}\right)^2 \zeta\,\phi(\zeta) = 0 \qquad 3A.7$$

whose solutions are $H^{1,2}_{1/3}$ as we saw in chapter 2. To solve equation 3A.6 we must specify the dependence of $k''(\zeta)$ Hamilton has recently shown that $k''(\zeta)$ decreases with depth in ocean bottom sediments. For the present we let $k''(\zeta) = k''_i$ a constant within an N^2-linear layer. When $k'' \neq 0$ the coefficient of $\phi(\zeta)$ in equation 3A.6 is

$$\tilde{k}_0^2\,\tilde{N}^2(\zeta) - k_0^2\sin^2\varphi_0 = \tilde{k}_0^2\left\{\cos^2\varphi_0 \pm g\zeta - \frac{k''(\zeta)^2 c'(0)^2}{\omega^2} + \frac{2i k''(\zeta) c'(0)}{\omega}\right\}$$

For constant dissipation number k'' we can define

$$\zeta \equiv \cos^2\varphi_0 \pm g\zeta - \frac{k''(\zeta)^2 c'(0)}{\omega^2} + \frac{2i k''(\zeta) c'(0)}{\omega} \qquad 3A.8$$

and $$\frac{d\zeta}{d\zeta} = \pm g$$

so the complex Helmholtz equation becomes

$$\frac{d^2\tilde{\Phi}(\tilde{\zeta})}{d\zeta^2} \cdot \frac{d\zeta^2}{d\zeta^2} + \tilde{k}_o^2 \zeta \tilde{\Phi}(\zeta) = 0 \qquad 3A.9$$

and solutions are again $\frac{1}{3}$ order Hankel functions of complex argument $\tilde{\omega}$ as shown below.

We refer as Brekhovskikh did to Watson (ref. 29) and identify solutions of the Airy equation

$$\frac{d^2V}{d\zeta^2} - c^2 \zeta V = 0 \qquad 3A.10$$

as $V = \left(\frac{\zeta^q}{q}\right) \mathcal{C}_{\frac{1}{2q}}\left(c i \frac{\zeta^q}{q}\right)$ with $q = \frac{3}{2}$

so that $$V = \left[\zeta^{3/2}/\left(\frac{3}{2}\right)\right]^{1/3} \mathcal{C}_{\frac{1}{3}}\left(\frac{c i \zeta^{3/2}}{3/2}\right) \qquad 3A.11$$

Here $\mathcal{C}_\nu$ is a ν^{th} order cylindrical function. In particular it can be taken to be

$$\mathcal{C}_\nu = H_\nu^{(1)}, H_\nu^{(2)}$$

so

$$V = \left[\frac{2}{3} \zeta^{3/2}\right]^{1/3} \mathcal{C}_{\frac{1}{3}}\left(c i \frac{2}{3} \zeta^{3/2}\right)$$

When we associate

$$-c^2 = +\left(\frac{k_o}{a}\right)^2 \Rightarrow ic = \frac{k_o}{a}$$

we get solutions

$$V = \left(\frac{2}{3}\right)^{1/3} \zeta^{1/2} \mathcal{C}_{1/3}\left(\alpha\left(-\alpha\frac{k_0}{a}\right)^{\frac{2}{3}} \zeta^{3/2}\right)$$

$$= \left(\frac{2}{3}\right)^{1/3} \zeta^{1/2} \mathcal{C}_{1/3}\left(\frac{2}{3} k_0 \zeta^{3/2}\right) \qquad 3A.12$$

and now

$$\mathcal{J} \equiv \cos^2\tilde{\varphi}_0 \pm g\zeta - \frac{k''(\zeta)^2 c'(0)^2}{\omega^2} + \frac{2 i k''(\zeta) c'(0)}{\omega} \qquad 3A.13$$

Recall that Brekhovskikh's solution was

$$Z(\zeta) = u^{1/3}\left[A H^{(1)}_{1/3}(u) + B H^{(2)}_{1/3}(u)\right]$$

$$u \equiv \frac{2}{3}\left(\frac{k_0}{g}\right)\zeta^{3/2} \qquad \text{and} \qquad \mathcal{J} = \cos^2\varphi_0 - g\zeta$$

so that our solution differs from his by a factor $\left(\frac{k_0}{g}\right)^{1/3}$

which can be incorporated into the coefficients A and B. There is also the difference in the definitions of $\tilde{\mathcal{J}}$.

Morris (ref. 22) has also included attenuation within an inhomogeneous waveguide layer. If one corrects the apparent misprints in her equations (4) and (5) so that the substitution of

$$\eta(\zeta) = \left(k_1^2 \beta_1\right)^{1/3}\zeta \equiv \eta_1\zeta_1 \Rightarrow \frac{d\eta}{d\zeta} = \left(k_1^2\beta_1\right)^{1/3} = \eta_1 \qquad 3A.14$$

into the Helmholtz equation for N^2-linear layers

$$\frac{d^2\Phi_1}{d\zeta_1^2} + \left[k_1^2(1+\beta_1\zeta_1) - k^2\right]\Phi_1 = 0 \qquad 3A.15$$

rather than

$$\eta_1 = \left(k_1^2\beta_1\right)^{1/3} \qquad \text{a constant}$$

one arrives at the equation

$$\frac{d^2 \Phi_1}{d \eta^2} + \left[\left(k_1^2 - k^2 \right) \eta_1^{-2} + \eta \right] \Phi_1 = 0 \qquad 3A.16$$

rather than

$$\frac{d^2 \Phi_1}{d \eta_1^2} + \left[\left(k_1^2 - k^2 \right) \eta_1^{-2} + \eta_1 \beta_1 \right] \Phi_1 = 0 \qquad 3A.17$$

which upon transformation with

$$\xi_1 \equiv \left(k^2 - k_1^2 \right) \left(k_1^2 \beta_1 \right)^{-2/3} - \eta_1 \beta_1 \qquad 3A.18$$

does yield the Airy equation

$$\frac{d^2 \Phi_1}{d \xi_1^2} - \xi_1 \Phi = 0 \qquad 3A.19$$

with solutions $\Phi_1(\beta_1) = A_1 A_i(\xi_1) + B_1 A_i(\hat{\xi}_1)$ 3A.20

where A_i is the Airy function and $\hat{\xi}_1 = \xi_1 \exp\left(\frac{i 2\pi}{3}\right)$.

Unfortunately, Morris' next step of introducing a sound attenuation coefficient k_1'' so that $\tilde{k}_1 = \frac{\omega}{c_1} + i k_1''$ (with $8.686\, k_1''$ the attenuation of the sound wave in dB per unit length) is a non-physical extension. It does correctly describe layers in which both $k_1'(\beta_1)$ and $k_1''(\beta_1)$ vary as $\sqrt{1 + \beta_1 \beta_1}$, but this is not a likely layering to encounter. It does not precisely describe the constant attenuation layer which Morris claims to analyze and which we have attempted to analyze approximately. Two parameters are required to describe layers where sound speed and attenuation vary independently. Introducing $\tilde{k}_1 = \frac{\omega}{c_1} + i k_1''$ after manipulations have been made on the original equation with $k_1^2 (1 + \beta_1 \beta_1)$, is the same as asserting the original form was

$$\tilde{k}_i(z)^2 = \tilde{k}_i^2 (1+\beta_i z)$$

$$\Rightarrow \tilde{k}_i(z) = \tilde{k}_i \sqrt{1+\beta_i z}$$

$$\Rightarrow \tilde{k}_i(z) = k_i' \sqrt{1+\beta_i z} + i k_i'' \sqrt{1+\beta_i z} \qquad 3A.21$$

when she stated that $\tilde{k}_i(z) = k_i' \sqrt{1+\beta_i z} + i k_i''$ 3A.22

This also says that

$$\left[\tilde{k}_i(z)\right]^2 = \left[k_i' + i k_i''\right]^2 \left[\sqrt{1+\beta_i z}\right]^2 = \left[k_i'^2 - k_i''^2 + 2 i k_i'' k_i'\right](1 \pm \beta_i z) \qquad 3A.23$$

The desired form (for constant dissipation layer) is

$$\left[\tilde{k}_i(z)\right]^2 = \left[k_i' \sqrt{1+\beta_i z} + i k_i''\right]^2 = k_i'^2 (1 \pm \beta_i z) - k_i''^2 + 2 i k_i'' k_i' \sqrt{1 \pm \beta_i z} \qquad 3A.24$$

which we have approximated as

$$k_i'^2 (1 \pm \beta_i z) - k_i''^2 + 2 i k_i'' k_i' \qquad 3A.25$$

in order to get 1/3 order solutions as Hankel functions of complex argument.

The validity of our solution equation 3A.12 depends on the approximation $\sqrt{1 \pm gz} \approx 1$

That is, the imaginary part of the coefficient of $\phi(z)$ in the Helmholtz equation 3A.6 was

$$\tilde{k}_0^2 \, \mathrm{Im}\left[\cos^2 \varphi_0^{\nu}\right] + 2 i k''(z) c'(\omega) \sqrt{1 \pm gz} / \omega$$

and we set $\sqrt{1 \pm gz} \approx 1$. For realistic gradients in the absence of absorption we will find turning point depths given by

$$\xi = \cos^2 \varphi_0 - g z_m = 0 \quad \Rightarrow \quad z_m = \frac{\cos^2 \varphi_0}{g} \qquad 3A.26$$

and typically $g = 10^{-3}$ so that the imaginary part of the coefficient is bounded for real incidence angle by

$$\mathrm{Im}\left[\cos^2 \tilde{\varphi}_0\right] + \frac{2i\, k''(3)\, c'(0)}{\omega} \sqrt{1 - \cos^2 \varphi_0}$$

at the turning point. Although N^2-linear halfspaces return all energy to the isovelocity layer overlying we expect that when dissipation is introduced, "grazing rays" will be further propagated, so we expect angles $\approx \frac{\pi}{2}$ to propagate to longer distances, $\Rightarrow \sin \varphi_0 \approx 1$ as desired.

To see the limitation our approximation places on phase velocity recall that phase velocity for the incident plane wave is given by

$$c_p = \frac{c_0}{\sin \varphi_0}$$

The approximation $\sqrt{1 \pm gz} \approx 1$ for the region above and including the turning point is worst at the turning point. To the extent that dissipation is small, so that the "Turning Point" in the presence of dissipation is approximately at the same depth as the turning point without dissipation we can say that the coefficient

$$\sqrt{1 \pm gz} \approx \sin \varphi_0 = \frac{c_0}{c_p} \qquad 3A.27$$

So for the term

$$\frac{2i\, k''(3)\, c'(0)}{\omega} \sqrt{1 \pm gz} \cong \frac{2i\, k''(3)\, c'(0)}{\omega}$$

it is necessary that $c_0/c_p \approx 1$. The total error, however, in the imaginary part of argument of H comes from

$$\mathrm{Im}\left[\cos^2 \tilde{\varphi}_0\right] + \frac{2i\, k''(3)\, c'(0)}{\omega} \sqrt{1 \pm gz}$$

and as angle $\tilde{\varphi}_0$ decreases towards normal incidence the first term is expected to grow at the same time that the second term is more poorly approximated with $\sqrt{1 \pm gz} \approx 1$. The approximation may be justified by determining $\tilde{\varphi}_0$ through the characteristic equation

and noting the order of magnitude of error in our assumption.

To see how our complex Hankel function approximation argument compares to Morris' treatment note that Morris uses

$$\zeta_i = \left(\frac{K^2 - k_i^2}{(k_i^2 \beta_i)^{2/3}} \right) - \left(k_i^2 \beta_i \right)^{1/3} \zeta \qquad 3A.28$$

and the term $k_i^2 (1 + \beta_i \zeta)$ is equivalent to our $k_0^2 \tilde{N}^2(\zeta)$ with

$$k_i = k_i' + i k_i''$$

$$\tilde{\zeta}_i = \frac{K^2 - (k_i' + i k_i'')^2}{\left[(k_i' + i k_i'')^2 \beta_i \right]^{2/3}} - \left[(k_i' + i k_i'')^2 \beta_i \right]^{1/3} \zeta \qquad 3A.29$$

We will compare the real and imaginary parts, versus depth, of the two arguments.

We have

$$\frac{k_0^2}{g^2} \zeta = \frac{k_0^2}{g^2} \left\{ \cos^2 \tilde{\varphi}_0 \pm g\zeta - \frac{k''(\zeta)\, c'(0)^2}{\omega^2} + \frac{2 i k''(\zeta)\, c'(0)}{\omega} \right\} \qquad 3A.30$$

So

$$Re[\zeta] = Re\left[\cos^2 \tilde{\varphi}_0 \right] \pm g\zeta - k''(\zeta) \frac{c'(0)^2}{\omega^2} \qquad 3A.31$$

$$Im[\zeta] = Im\left[\cos^2 \tilde{\varphi}_0 \right] + \frac{2\, k''(\zeta)\, c'(0)}{\omega} \qquad 3A.32$$

To determine the real and imaginary parts of Morris' Airy argument note that the term

$$\frac{K^2 - (k_i' + i k_i'')^2}{\left[(k_i' + i k_i'')^2 \beta_i \right]^{2/3}}$$

is constant re z although we would assume K^2 itself would have to become complex to satisfy a characteristic equation.

Denoting K^2 as

$$K^2 = \left[K_x' + i K_x'' \right]^2 = K_x'^2 - K_x''^2 + 2i K_x' K_x''$$

$$k_1' = \frac{\omega}{c_1} \qquad k_1'' = \text{constant} \qquad \text{3A.33}$$

The first term of Morris argument may be written

$$\frac{M_N e^{i\Theta_N}}{M_D e^{i\Theta_D}} = \frac{M_N}{M_D} e^{i(\Theta_N - \Theta_D)} \qquad \text{3A.34}$$

where

$$\frac{M_N}{M_D} = \frac{\left\{ K_x'^2 - K_x''^2 - k_1'^2 + k_1''^2 \right\}^2 + \left\{ 2 K_x' K_x'' - 2 k_1' k_1'' \right\}^2}{\left[k_1'^2 + k_1''^2 \right]^{2/3}} \qquad \text{3A.35}$$

$$\Theta_N - \Theta_D = \tan^{-1}\left(\frac{2 K_x' K_x'' - 2 k_1' k_1''}{K_x'^2 - K_x''^2 - k_1'^2 + k_1''^2} \right) - \frac{2}{3} \tan^{-1}\left(\frac{k_1''}{k_1'} \right) \qquad \text{3A.36}$$

The second term of Morris argument is

$$\left(k_1^2 B_1 \right)^{1/3} J \equiv M_2 e^{i\Theta_2} \qquad \text{3A.37}$$

where

$$M_2 = \left[(k_1')^2 + (k_1'')^2 \right]^{1/3} J \qquad \text{3A.38}$$

$$\Theta_2 = \frac{1}{3} \tan^{-1}\left[\frac{k_1''}{k_1'} \right] \qquad \text{3A.39}$$

Then since z multiplies M_2 we see that both real and imaginary parts of Morris argument are functions of z through M_2. Recall that our

argument Im part was independent of z after the approximation $\sqrt{1 \pm gJ} \approx 1$ was made. The real part of ζ had dependence $1 \pm gJ$.

In order to implement the Helmholtz solution given by equation

$$\Phi(J) = \left(\frac{2}{3}\right)^{1/3} \zeta^{1/2} C_{1/3}\left(\frac{2}{3}\frac{k_0}{g}\zeta^{3/2}\right) \quad \text{with} \quad C_\nu = H_\nu^{(1)}, H_\nu^{(2)}$$

3A.40

i.e.

$$\Phi(J) = \left(\frac{2}{3}\right)^{1/3} \zeta^{1/2} \left[A H_{1/3}^{(1)}(u) + B H_{1/3}^{(2)}(u)\right]$$

with $$u = \frac{2}{3}\frac{k_0}{g}\zeta^{3/2} \qquad 3A.41$$

$$\zeta = \cos^2\varphi_0 \pm gJ - \frac{k''(J)^2 c'(0)^2}{\omega^2} + \frac{2i k''(J) c'(0)}{\omega}$$

We need to match solutions in the neighborhood of the turning point $J = J_m$ so that at the upper interface of the N^2-linear region being considered we will have only two unknowns V, and A to determine from the two boundary conditions. In the nondissipative case Brekhovskikh did this and showed that

$$A = B \exp\left(\frac{i\pi}{3}\right) \qquad C = i B \exp\left(\frac{i\pi}{3}\right)$$

3A.42, 3A.43

His solutions were

$$\Phi(\zeta) = u^{1/3}\left[C H_{1/3}^{(1)}(i u_1) + D H_{1/3}^{(2)}(i u_1)\right]$$

3A.44

below the turning point with

$$u_1 = \frac{2}{3}\left(\frac{k_0}{g}\right)(-\zeta)^{3/2} \qquad \zeta = \cos^2\varphi_0 \pm gJ$$

and

ζ was <0 , but real, below the turning point and u was real.

Above the turning point he used

$$\phi(\zeta) = u^{1/3}\left[A\, H^{(1)}_{1/3}(u) + B\, H^{(2)}_{1/3}(u)\right] \qquad 3A.45$$

with

$$u = \frac{2}{3}\left(\frac{k_0}{g}\right)\zeta^{3/2} \qquad \zeta = \cos^2\theta_0 \pm gz = N^2(z) - \sin^2\theta_0$$

and since at the turning point $\zeta = 0$ he was able to linearize the Helmholtz equation, make small argument expansions of the Hankel functions, and match solutions through the boundary conditions at $\zeta = 0$. The term $D\, H^{(2)}_{1/3}(iu_1)$ was eliminated in order for the field to go to zero at infinity. The expansion expressions

$$\phi(z) = \frac{-2i}{\sqrt{3}} A\left\{\exp\left(-i\frac{\pi}{3}\right) C_1 u + C_2\right\} + \frac{2i}{\sqrt{3}} B\left\{\exp\left(i\frac{\pi}{3}\right) C_1 u + C_2\right\}$$

for $z < z_m$

3A.46

and

$$\phi(z) = \frac{2}{\sqrt{3}} C \exp\left(i\frac{\pi}{3}\right)\left(C_1 u - C_2\right)$$

$$u = \left(g k_0^2\right)^{1/3}\left(z - z_m\right)$$

3A.47

combined with continuity conditions on ϕ and $\frac{d\phi}{dz}$ at $z = z_m$ gave the two equations

$$B - A = i\, C \exp\left(i\frac{\pi}{3}\right) \qquad 3A.48$$

$$B \exp\left(i\frac{\pi}{3}\right) - A \exp\left(-i\frac{\pi}{3}\right) = -i\, C \exp\left(i\frac{\pi}{3}\right) \qquad 3A.49$$

So that

$$A = B \exp\left(i\frac{\pi}{3}\right) \qquad C = i \exp\left(i\frac{\pi}{3}\right) B$$

Brekhovskikh remarks (ref. 1) that continuation relations could have been used to obtain the field above the turning point $\zeta < \zeta_m$ once the form below the turning point had been established rather than joining the solutions at $\zeta = \zeta_m$ and that when absorption is present (N complex) these continuation relations are particularly useful, since $\xi = N^2(\zeta) - \sin^2\varphi_0$ becomes zero nowhere, and there is no special plane in which to join solutions. We note that Brekhovskikh's expansions of $J_{1/3}$, $J_{-1/3}$, inorder to get Hankel function $H^{1,2}_{1/3}$ approximations around $\xi = 0$, involved Bessel functions of pure real and pure imaginary argument. The solutions of the Helmholtz equation in the two regions has the same form (i.e. $H^{(1)}_{1/3}$, $H^{(2)}_{1/3}$). The fact that the argument is pure imaginary in region 2 (below the turning point) resulted in the large z form

(as $\mu_1 \to +\infty$) $$H^{(2)}_{1/3}(i\mu_1) \sim \sqrt{\frac{2}{\pi\mu_1}}\, e^{\mu_1} \to \infty \qquad 3A.50$$

and coefficient D was set to zero in order for the field to be finite everywhere.

In our case with complex index of refraction we write the solution on either side of the newly defined "turning point" (arbitrary).

$\mathrm{Re}[\tilde{\zeta}] = 0$, as

$$\Phi(\zeta) = \left(\tfrac{2}{3}\right)^{1/3} \xi^{1/2} C_{1/3}\left(\tfrac{2}{3}\,\tfrac{k_0}{g}\,\xi^{3/2}\right) \Rightarrow \qquad 3A.51$$

$$\left(\tfrac{2}{3}\right)^{1/3} \xi^{1/2}\left[A\, H^{(1)}_{1/3}\left(\tfrac{2}{3}\,\tfrac{k_0}{g}\,\xi^{3/2}\right) + B\, H^{(2)}_{1/3}\left(\tfrac{2}{3}\,\tfrac{k_0}{g}\,\xi^{3/2}\right)\right]$$

and $$\xi = \cos^2\tilde{\varphi}_0 \pm g\zeta - \frac{k''(\zeta)^2\, c'(0)^2}{\omega^2} + \frac{2\, k''(\zeta)\, c'(0)}{\omega}$$

That is, we preserve the solution form throughout the N^2-linear half-space, but introduce a depth $\zeta_{m_{new}}$ at which matching will be done and where solution coefficients may change. Since the large argument asymptotic expansions for the Hankel functions are

$$H^{(1)}_{1/3}(x) \sim \sqrt{\frac{2}{\pi x}}\ \exp\left[i\left(x - \frac{5\pi}{12}\right)\right]$$

$$H^{(2)}_{1/3}(x) \sim \sqrt{\frac{2}{\pi x}}\ \exp\left[-i\left(x - \frac{5\pi}{12}\right)\right] \qquad 3A.52$$

we see that with

$$x = \frac{2}{3}\frac{k_0}{g}\zeta^{3/2}$$

if we let

$$x - \frac{5\pi}{12} = \frac{2}{3}\frac{k_0}{g}\zeta^{3/2} - \frac{5\pi}{12}$$

be defined as the complex number $x - \frac{5\pi}{12} \equiv a + ib$ we will have

$$H^{(1)}_{1/3}(x) \sim \sqrt{\frac{2}{\pi x}}\ \exp\left[i(a+ib)\right] = \sqrt{\frac{2}{\pi x}}\ \exp\left[ia - b\right]$$

$$H^{(2)}_{1/3}(x) \sim \sqrt{\frac{2}{\pi x}}\ \exp\left[-i(a+ib)\right] = \sqrt{\frac{2}{\pi x}}\ \exp\left[-ia + b\right] \qquad 3A.53$$

Then if $b = \mathrm{Im}\left[\frac{2}{3}\frac{k_0}{g}\zeta^{3/2} - \frac{5\pi}{12}\right] > 0$ and $\to \infty$

as $\zeta \to \infty$ the function $H^{(2)}_{1/3}(x)$ blows up and must be rejected in the solution. If $b < 0$ and $\to -\infty$ then the function $H^{(1)}_{1/3}(x)$ must be rejected. Recall that in the nondissipative

case ζ becomes <0 for $\zeta > \zeta_m$ the term μ becomes pure imaginary $= \mu_1$. Brekhovskikh has $\zeta^{3/2}$ for $\zeta < 0$ becoming

$$i(-\zeta)^{3/2} \quad \text{i.e. for} \quad \zeta = A e^{\pm i\pi}, \quad \left[A e^{-i\pi}\right]^{3/2} = A^{3/2} e^{-i 3\pi/2}$$

Note the choice of $-i\frac{3\pi}{2}$ instead $+i\frac{3\pi}{2}$ to get $b > 0$ and $\omega_1 > 0$. In our case we will have to eliminate $H^{(2)}_{1/3}(x)$ if

$$b = \mathrm{Im}\left\{ \frac{2}{3} \frac{k_0}{g} \left[\cos^2 \varphi_0^{\nu} \pm g\zeta - \frac{k''(\zeta)^2 c'(0)^2}{\omega^2} + \frac{2i k''(\zeta) c'(0)}{\omega} \right]^{3/2} - \frac{5\pi}{12} \right\} > 0$$

In the limit of $\zeta \to \infty$ the quantity in brackets $= \zeta$ lies along the negative real axis in the complex ζ plane and we will have to eliminate the $H^{(1)}_{1/3}(x)$ or $H^{(2)}_{1/3}(x)$ term in the region which includes $\zeta \to \infty$, depending on whether b is taken along the $\pm$ imaginary axis. We have some latitude in setting the upper boundary, ζ_m , of that region. We have no special plane as Brekhovskikh did in which to limit the region in which we will take solution $H^{(1)}_{1/3} + H^{(2)}_{1/3}$ from that in which we will take solution $H^{(1)}_{1/3}$ or $H^{(2)}_{1/3}$ only. However, we can arbitrarily pick that point as a function of complex argument and thus z. Since the complex argument never goes to zero we may have to use more than the first terms in the Hankel function expansion to make the match. But once the match is made, and coefficients calculated, the field will be correctly described at its boundaries (z=zmnew, and z= ∞) and thus determined correctly throughout the lower halfspace. The imaginary part of

$$\cos^2 \varphi_0^{\nu} \pm g\zeta - \frac{k''(\zeta)^2 c'(0)^2}{\omega^2} + \frac{2i k''(\zeta) c'(0)}{\omega}$$

is fixed. Then we know as $\zeta \to \infty$ we will need to express the solution as a function only of $H^{(1)}_{1/3}(x)$ or $H^{(2)}_{1/3}(x)$.

In addition to the physical consideration of a finite field at $\zeta \to \infty$ we also consider the asymptotic nature of the Hankel function forms as representing incident and reflected energy, i.e. traveling waves* going in the + or - direction, and then eliminate the

$H^{(1)}_{1/3}$ or $H^{(2)}_{1/3}$

form below a turning point on the grounds that energy can not be arriving as a traveling wave from $\zeta = \infty$. From the expressions (large arg) above we see that if $a > 0$, $b > 0$

$H^{(1)}_{1/3}$ represents a damped traveling wave in the $+\zeta$ direction. (if a increases with z, and b increases with z), and a traveling wave in the -z direction if a decreased with z increasing. $H^{(2)}_{1/3}$ represents a growing wave in the +z direction if b increases with z. It is a traveling wave in the -z direction if $a > 0$ and increases as z increases, and a traveling wave in the +z direction if a decreases as z increases. For the case a=0 both waves are standing waves with either growing or decaying behaviour in the +z direction depending on the sign of b. This was the nondissipative case which Brekhovskikh treated. Brekhovskikh shows that in the N^2-linear layer above the turning point (for $z < \zeta_m$), in the nondissipative case, the term containing A i.e. $H^{(1)}_{1/3}$ degenerates into the reflected wave and that containing B i.e. $H^{(2)}_{1/3}$ into the incident wave. We can estab-

*A traveling wave will have phase dependent on z as well as $e^{-i\omega t}$.

lish the following conditions for eliminating solutions $H^{(1)}_{1/3}$ or $H^{(2)}_{1/3}$ in the lower region. Using the large argument asymptotic forms

$$H^{(1)}_{1/3}(x) \sim \sqrt{\frac{2}{\pi x}}\exp[ix-b] \qquad H^{(2)}_{1/3}(x) \sim \sqrt{\frac{2}{\pi x}}\exp[-ix+b] \qquad \text{3A.54}$$

for

$\frac{da}{dz} > 0$ a will decrease as z gets large
- $H^{(1)}$ will be a traveling wave in the +z direction
- $H^{(2)}$ will be a traveling wave in the -z direction

$\frac{da}{dz} < 0$ a will decrease (or go more negative) as z increases
- $H^{(1)}$ will be a traveling wave in the -z direction
- $H^{(2)}$ will be a traveling wave in the +z direction

$\frac{db}{dz} > 0$ b will increase as z gets large
- $H^{(2)}$ will grow in the +z direction
- $H^{(1)}$ will decay in the +z direction

$\frac{db}{dz} < 0$ b will decrease as z gets large
- $H^{(2)}$ will decay in the +z direction
- $H^{(1)}$ will grow in the +z direction

Now looking at the argument (which is also Brekhovskikh's when $b''(z) = 0$

$$x = \frac{2}{3}\frac{k_0}{g}\zeta^{3/2} = \frac{2}{3}\frac{k_0}{g}\left[\cos^2\tilde{\varphi}_0 \pm gz - \frac{b''(z)\,c'(0)^2}{\omega^2} + \frac{2ib''(z)\,c'(0)}{\omega}\right]^{3/2} \qquad \text{3A.55}$$

Assuming for the moment the usual case of $\tilde{\psi}_0$ real sound speed increasing with depth ($\Rightarrow$ - sign above), the Hankel function argument may be written

$$x = \frac{2}{3}\frac{k_0}{g}\left[\underbrace{\left(\cos^2\psi_0 - gz - \frac{k''(z)^2 c'(0)^2}{\omega^2}\right)}_{AR} + i\underbrace{\left(\frac{2k'' c'(0)}{\omega}\right)}_{AI}\right]^{3/2}$$

$$= \frac{2}{3}\frac{k_0}{g}\left[AR^2 + AI^2\right]^{3/4} e^{i\frac{3}{2}\tan^{-1}\left(\frac{\left(\frac{2k'' c'(0)}{\omega}\right)}{\left(\cos^2\psi_0 \pm gz - \frac{k''(z)^2 c'(0)^2}{\omega^2}\right)}\right)}$$

3A.56

and with $x \equiv a + ib$ we have

$$x = \frac{2}{3}\frac{k_0}{g}\left[AR^2 + AI^2\right]^{3/4}\left\{\cos\left(\frac{3}{2}\tan^{-1}\left(\frac{\frac{2k''(z)c'(0)}{\omega}}{\cos^2\psi_0 \pm gz - \frac{k''(z)c'(0)^2}{\omega^2}}\right)\right)\right.$$

$$\left. + i\sin\left(\frac{3}{2}\tan^{-1}\left(\frac{\frac{2k''(z)c'(0)}{\omega}}{\cos^2\psi_0 \pm gz - \frac{k''(z)^2 c'(0)^2}{\omega^2}}\right)\right)\right\}$$

3A.57

Note that as

$$k''(z) \to 0 \qquad \tan^{-1}\left(\frac{AI}{AR}\right) \to \tan^{-1}(0) = 0, \pm\pi$$

3A.58

$$\Rightarrow x = \frac{2}{3}\frac{k_0}{g}\left[AR^2\right]^{3/4}\left\{\cos\left(\pm\frac{3\pi}{2}\right) + i\sin\left(\pm\frac{3\pi}{2}\right)\right\}$$

$$= \pm i\,\frac{2}{3}\frac{k_0}{g}\left(\left[\cos^2\varphi_0 \pm gJ\right]^2\right)^{3/4}$$

$$\text{or} = \frac{2}{3}\frac{k_0}{g}\left[AR^2\right]^{3/4} \qquad 3A.59$$

For $k''(3)$ finite and $\tilde{\varphi}_0 = \varphi_0' + i\varphi_0''$ we expand $\cos^2\tilde{\varphi}_0$ to get

$$\cos^2\tilde{\varphi}_0 = \cos^2\varphi'\cosh^2\varphi'' - \sin^2\varphi'\sinh^2\varphi'' + 2i\cos\varphi'\sin\varphi'\cosh\varphi''\sinh\varphi''$$

and with $k_1''(3) = K_1''$ independent of z we will have Hankel argument x:

$$x = \frac{2}{3}\frac{k_0}{g}\left[\left[AR^2 + AI^2\right]^{1/2}\right]^{3/2} e^{3/2\,\tan^{-1}\left(AI/AR\right)}$$

$$= \frac{2}{3}\frac{k_0}{g}\left[AR^2 + AI^2\right]^{3/4}\left\{\cos\left(\frac{3}{2}\tan^{-1}\left(\frac{AI}{AR}\right)\right) + i\sin\left(\frac{3}{2}\tan^{-1}\left(\frac{AI}{AR}\right)\right)\right\}$$

$$3A.60$$

with

$$AR \equiv \cos^2\varphi_0'\cosh^2\varphi_0'' - \sin^2\varphi_0'\sinh^2\varphi_0'' - gJ - \frac{k_1''^2\cdot c'(0)^2}{\omega^2} \qquad 3A.61$$

$$AI \equiv 2\cos\varphi_0'\sin\varphi_0'\cosh\varphi_0''\sinh\varphi_0'' + \frac{k''c'(0)}{\omega} \qquad 3A.62$$

only Ar is a function of z. But since $x \equiv a + ib$

$$a \equiv \frac{2}{3}\frac{k_0}{g}\left[A_R^2 + A_I^2\right]^{3/4} \cos\left(\frac{3}{2}\tan^{-1}\left[\frac{A_I}{A_R}\right]\right) \qquad 3A.63$$

$$b \equiv \frac{2}{3}\frac{k_0}{g}\left[A_R^2 + A_I^2\right]^{3/4} \sin\left(\frac{3}{2}\tan^{-1}\left[\frac{A_I}{A_R}\right]\right) \qquad 3A.64$$

As z increases the term $\left[A_R^2 + A_I^2\right]$ increases in both a and b. As $\zeta \to \infty$

$$\left[A_R^2 + A_I^2\right]^{3/4} \to \left((-g\zeta)^2\right)^{3/4} = g\zeta^{3/2} \to +\infty \qquad 3A.65$$

The term

$$\tan^{-1}\left[\frac{A_I}{A_R}\right] \to +\pi \quad \text{not } -\pi \text{ or } 0 \qquad 3A.66$$

Since the real part is <0 (and actually goes to $-az$) and the imaginary part is >0. Thus we see that the angle of the argument goes to $+\frac{3\pi}{2}$ and we have

$$b \to -1 \cdot \frac{2}{3}\frac{k_0}{g}\zeta^{3/2} \to -\infty \qquad \text{as } z \to \infty$$

b gets very negative. This would say that since $\frac{db}{d\zeta} < 0$ $H^{(2)}$ will decrease in the +z direction and $H^{(1)}$ will increase in the +z direction. Therefore to avoid having the field go to infinity in this formalism we must use $H^{(2)}$ not $H^{(1)}$ in the solution below the turning point. Notice also that since $a \neq 0$ but is itself a function of z (but not linear with z) the wave below the turning point is no longer a standing wave (in the asymptotic expansion). If we define the turning point as the point at which $A_R \to 0$ we will have

$$\zeta_{m_{new}} = \left[\cos^2\varphi_0 \cosh^2\varphi_0'' - \sin^2\varphi_0' \sinh^2\varphi_0'' - \frac{k_z''^2 c'(0)^2}{\omega}\right]/g \qquad 3A.67$$

In the nondissipative, real incidence angle case this becomes $\frac{\cos^2\varphi_c}{g}$

which is what Brekhovskikh uses. The angle of the argument of the Hankel function then will vary from

$\frac{3}{2}\left(+\frac{\pi}{2}\right)$ at $J = J_{new}^{m}$ to $\frac{3}{2}\pi$ at $J = \infty$

As $J \to \infty$ $a \to (-0)(+\infty)$. Since $g J^{3/2} \to \infty$

faster than $\cos\left(\frac{3}{2}\tan^{-1}\left(\frac{\Delta z}{\Delta R}\right)\right) \to -0$ and $a \to -\infty$

so both $\frac{da}{dJ}$ and $\frac{db}{dJ} < 0$

Then we require $H^{(2)}$ as a traveling wave in -z direction, and also so the field does not go to ∞ . Brekhovskikh showed that above the turning point $H^{(2)}$ was the incident wave and $H^{(1)}$ the reflected wave. Below the turning point he had standing waves and eliminated $H^{(2)}$. We have shown that with dissipation the waves are not standing below the turning point (pure imaginary argument), but have complex Hankel arguments whose large arg asymptotic expansion gives both traveling behaviour and growth decay characteristics. We have however had to eliminate $H^{(1)}$ while he eliminated $H^{(2)}$.

Looking again at Brekhovskikh's argument of the Hankel function, he uses

$$\Phi(J) = u_1^{1/3}\left[C\,H^{(1)}_{1/3}(iu_1) + \Delta\,H^{(2)}_{1/3}(iu_1)\right] \qquad u_1 \equiv \frac{2}{3}\left(\frac{k_0}{g}\right)(-\zeta)^{3/2}$$

and then has $\zeta = \cos^2\varphi_0 - gJ$ for $J > J_m$ 3A.68

$u_1 \to +\infty$ so that $H^{(2)}_{1/3}(iu_1) \sim \sqrt{\frac{2}{\pi u_1}}\,e^{u_1} \to \infty$

which came from the asymptotic expansion

$$H^{(2)}_{1/3}(i\mu_1) \sim \sqrt{\frac{2}{\pi x}}\, \exp\left[-i\left(x - \frac{5\pi}{12}\right)\right] \qquad 3A.69$$

so that for $(\cos^2\varphi_0 - g\zeta) < 0$

$$(\zeta)^{3/2} = \left(|\cos^2\varphi_0|\, e^{\pm i\pi}\right)^{3/2} = \left[|\cos^2\varphi_0 - g\zeta|\right]^{3/2} \underbrace{e^{\pm i\frac{3\pi}{2}}}_{\pm i}$$

so that

$$\mu_1 = \frac{2}{3}\frac{k_0}{g}\left[|\cos^2\varphi_0 - g\zeta|\right]^{3/2} e^{\pm i\frac{3\pi}{2}} \qquad 3A.70$$

and denoting

$$\frac{2}{3}\frac{k_0}{g}\left[|\cos^2\varphi_0 - g\zeta|\right]^{3/2} \equiv \mu_1'' \qquad 3A.71$$

the argument of the Hankel function in the nondissipative example is really seen to be $\pm i\mu_1''$. So depending on which sign we choose we can have either $H^{(1)}$ or $H^{(2)}$ go to ∞ as $z \to \infty$. Brekhovskikh chose to use $\mu_1 = +i\mu''$. The case $b''(\zeta) = 0$ which he treated, is the only one in which ambiguity can exist in the μ_1 definition, when the definition of μ_1 is restricted to the principal value $-\pi \le \theta_{\mu_1} \le +\pi$. If he had chosen to use the + sign in

$$\zeta = \left[|\cos^2\varphi_0 - g\zeta|\right]^{3/2} e^{\pm i\,3\pi/2}$$

instead of

$$\zeta = \left[|\cos^2\varphi_0 - g\zeta|\right]^{3/2} e^{-3\pi/2}$$

he would have had $\mu_1 = -i\mu_1''$ instead of $\mu_1 = +i\mu_1''$

Since we have no ambiguity, we will choose to eliminate $H^{(1)}_{1/3}$ instead of $H^{(2)}_{1/3}$. As a result we have a wave below the turning point which not only goes to 0 as $z \to \infty$, but travels in the + z direction. Matching at the turning point: We will have fields above and below the "turning point"

$$\phi(\zeta) \equiv \left(\frac{2}{3}\right)^{1/3} \zeta^{1/2} \left[A H^{(1)}_{1/3}\left(\frac{2}{3}\frac{k_0}{g}\zeta^{3/2}\right) + B H^{(2)}_{1/3}\left(\frac{2}{3}\frac{k_0}{g}\zeta^{3/2}\right)\right] \qquad 3A.72$$

with

$$\zeta = \cos^2\tilde{\varphi}_0 \pm g\zeta - \frac{k''(3)^2 c'(0)^2}{\omega^2} + \frac{2i\,k''(3)\,c'(0)}{\omega} \qquad 3A.73$$

or $$\phi(\zeta) \equiv \left(\frac{2}{3}\right)^{1/3} \zeta^{1/2} \left[A H^{(1)}_{1/3}(a+ib) + B H^{(2)}_{1/3}(a+ib)\right]$$

$$a = \frac{2}{3}\frac{k_0}{g}\left[A_R^2 + A_I^2\right]^{3/4} \cos\left(\frac{3}{2}\tan^{-1}\left(\frac{A_I}{A_R}\right)\right)$$

$$b = \frac{2}{3}\frac{k_0}{g}\left[A_R^2 + A_I^2\right]^{3/4} \sin\left(\frac{3}{2}\tan^{-1}\left(\frac{A_I}{A_R}\right)\right)$$

$$A_I \equiv 2\cos\varphi'\sin\varphi'\cosh\varphi''\sinh\varphi'' + \frac{k''\,c'(0)}{\omega}$$

$$A_R \equiv \cos^2\varphi_0'\cosh^2\varphi'' - \sin^2\varphi'\sinh^2\varphi'' \pm g\zeta - \frac{k''(3)^2 c'(0)^2}{\omega^2}$$

3A.74

These definitions a, b, A_1, A_2 hold for $\zeta \gtrless \zeta_{m_{new}}$

For $\zeta > \zeta_{m_{new}}$ below the turning point we have

$$\phi(\zeta) = \left(\frac{2}{3}\right)^{1/3} \zeta^{1/2} \left[D H_{1/3}^{(2)} \left(\frac{2}{3} \frac{k_0}{g} \zeta^{3/2} \right) \right]$$

and again no ambiguity exist in the determination of the root of complex ζ with $-\pi \leq \Theta_\zeta \leq +\pi$ (i.e. $\zeta^{1/2}$). The factor $\zeta^{1/2}$ will be incorporated in the expansion of $H_{1/3}^{1,2}$ around $a=0$, $b = b(\zeta_{m_{new}})$. Now expanding the Hankel functions in terms of Bessel functions as in appendix 2.2.b. and expanding the Bessel functions as an infinite series, in terms of complex argument $\left(\frac{k_0}{g}\right)^{2/3} \zeta$, we obtain infinite series for $\phi(\zeta)$ and $\frac{d\phi(\zeta)}{d\zeta}$ in the two depth regions. These series differ from Brekhovskikh's expression 16.60 (ref. , p. 211) in the multiplying coefficients, in the fact that the expansion variable is complex and in our use of the entire series. Using the boundary conditions of continuity of pressure and normal velocity we are able to solve for coefficients A and D in terms of B and find A=0, D=B. This says that with this method, or appealing to "continuation", we may eliminate the growing solution throughout the entire constant parameter region in which it is defined.

When the same approach using Cramers rule is taken to Brekhovskikh's expansions his result of $A = B \exp\left(i \frac{\pi}{3}\right)$ and $C = i B \exp\left(i \frac{\pi}{3}\right)$ follows. His coefficients do not match ours because he has used different expansions of the Hankel functions above and below the turning point, where his arguments are taken as pure real and pure imaginary respectively.

When Brekhovskikh's coefficients A and C are used as in the non-dissipative case, the reflection coefficient at the ocean bottom interface for model 2a comes from the boundary conditions at z=0

$$(1+\tilde{R})(-i\omega\rho_1) = (-i\omega\rho_2)\left[e^{i\pi/3}\omega^{1/3}H^{(1)}_{1/3}(\omega) + \omega^{1/3}H^{(2)}_{1/3}(\omega)\right]\tilde{B}_0 \qquad 3A.75$$

$$(ik_0\cos\varphi_0)(1-\tilde{R}) = (-k_0\cos\varphi_0)\left[e^{i\pi/3}\omega^{1/3}H^{(1)}_{-\frac{2}{3}}(\omega) + \omega^{1/3}H^{(2)}_{-\frac{2}{3}}(\omega)\right]\tilde{B}_0$$

$$\text{and} \quad \tilde{A} = e^{i\pi/3}\tilde{B} \qquad 3A.76$$

Then

$$\tilde{R} = -\left\{\frac{\rho_1(J_{-\frac{2}{3}} - J_{\frac{2}{3}}) + i\rho_2(J_{\frac{1}{3}} + J_{-\frac{1}{3}})}{\rho_1(J_{-\frac{2}{3}} - J_{\frac{2}{3}}) - i\rho_2(J_{\frac{1}{3}} + J_{-\frac{1}{3}})}\right\} \qquad 3A.77$$

as in chapter 2, and the Bessel function (of complex argument now) is evaluated at z=0. On the other hand, using A=0 we will derive the reflection coefficient starting with the boundary conditions

$$(1+\tilde{R})(-i\omega\rho_1) = (-i\omega\rho_2)\left[\omega^{1/3}H^{(2)}_{1/3}(\omega)\right]\tilde{B} \qquad 3A.78$$

$$(1-\tilde{R})(k_0\cos\varphi_0) = (-k_0\cos\varphi_0)\left[\omega^{1/3}H^{(2)}_{-\frac{2}{3}}(\omega)\right]\tilde{B} \qquad 3A.79$$

In this case the reflection coefficient is shown in appendix 3.2 to be

$$\tilde{R} = -\left\{\frac{\rho_1(e^{-i\frac{2\pi}{3}}J_{-\frac{2}{3}} - J_{\frac{2}{3}}) + i\rho_2(e^{i\frac{\pi}{3}}J_{\frac{1}{3}} - J_{-\frac{1}{3}})}{\rho_1(e^{-i\frac{2\pi}{3}}J_{-\frac{2}{3}} - J_{\frac{2}{3}}) - i\rho_2(e^{i\pi/3}J_{\frac{1}{3}} - J_{-\frac{1}{3}})}\right\} \qquad 3A.80$$

The argument of $J_{\frac{1}{3}}$, $J_{-\frac{1}{3}}$, $J_{\frac{2}{3}}$, $J_{-\frac{2}{3}}$, is as we have seen x=a+ib. With a complex Bessel function routine returning

$$\tilde{J}_\nu(\chi) \equiv RJV + i\,SJV \qquad 3A.81$$

we will have a reflection coefficient

$$\tilde{R} = \frac{\left\{-\rho_1\left[\cos\frac{\pi}{3}\,RJ_{-\frac{1}{3}} + RJ_{\frac{1}{3}} - \sin\frac{\pi}{3}\,SJ_{-\frac{1}{3}}\right] - \rho_2\left[\sin\frac{\pi}{3}\,RJ_{\frac{1}{3}} + \cos\frac{\pi}{3}\,SJ_{\frac{1}{3}} - SJ_{-\frac{1}{3}}\right]\right\} + i\left\{-\rho_1\left[\cos\frac{\pi}{3}\,SJ_{-\frac{1}{3}} + SJ_{\frac{1}{3}} + \sin\frac{\pi}{3}\,RJ_{-\frac{1}{3}}\right] - \rho_2\left[\sin\frac{\pi}{3}\,SJ_{\frac{1}{3}} - \cos\frac{\pi}{3}\,RJ_{\frac{1}{3}} + RJ_{-\frac{1}{3}}\right]\right\}}{\left\{-\rho_1\left[\cos\frac{\pi}{3}\,RJ_{-\frac{1}{3}} + RJ_{\frac{1}{3}} - \sin\frac{\pi}{3}\,SJ_{-\frac{1}{3}}\right] + \rho_2\left[\sin\frac{\pi}{3}\,RJ_{\frac{1}{3}} + \cos\frac{\pi}{3}\,SJ_{\frac{1}{3}} - SJ_{-\frac{1}{3}}\right]\right\} + i\left\{-\rho_1\left[\cos\frac{\pi}{3}\,SJ_{-\frac{1}{3}} + SJ_{\frac{1}{3}} + \sin\frac{\pi}{3}\,RJ_{-\frac{1}{3}}\right] + \rho_2\left[\sin\frac{\pi}{3}\,SJ_{\frac{1}{3}} - \cos\frac{\pi}{3}\,RJ_{\frac{1}{3}} + RJ_{-\frac{1}{3}}\right]\right\}}$$

3A.82

Both these coefficients are functions of complex incidence angle $\tilde{\varphi}_0$ at the top of the N^2-linear layer. When $\tilde{R}$ is determined it can be used in the characteristic equation algorithmns as in the iso-velocity case. $\tilde{\varphi}_0$ is the angle in the water column and will be complex. The complex Bessel routine need only calculate at z=0. To determine complex Bessel functions $J_{1/3}$, $J_{-1/3}$, $J_{2/3}$, $J_{-2/3}$ of complex argument we note from Watson that $J_{\tilde{\nu}}(\tilde{\zeta})$ is an analytic function of $\tilde{\zeta} \equiv a\tilde{r}g$ for all values of $a\tilde{r}g$ ($a\tilde{r}g$ =0 possibly excluded) and its an analytic function of $\tilde{\nu}$ for all complex values of $\tilde{\nu}$. We use the formula

$$J_{\tilde{\nu}}(\tilde{\zeta}) = \sum_{m=0}^{\infty} \frac{(-1)^m \left(\frac{1}{2}\zeta\right)^{\nu+2m}}{m!\,\Gamma(\nu+m+1)} \qquad 3A.83$$

defining ζ^{ν} to be $\exp(\nu \log \zeta)$ with phase of z given by its principal value so

$$-\pi < \arg\zeta < \pi$$

Appendix 3.2 Reflection coefficient for case when only downgoing Hankel waveform is used:

The boundary equations are

$$1.\quad (1+\tilde{R})(-i\omega\rho_1) = (-i\omega\rho_2)\left[\omega^{1/3} H^{(2)}_{1/3}(\omega)\right]\tilde{B}$$

$$2.\quad (1-\tilde{R})(k_0\cos\varphi_0) = (-k_0\cos\varphi_0)\left[\omega^{1/3} H^{(2)}_{-\frac{4}{3}}(\omega)\right]\tilde{B}$$

3A.84, 3A.85

Dividing 2 by 1 gives

$$\frac{i k_0\cos\varphi_0\,(1-\tilde{R})}{\omega\rho_1\,(1+\tilde{R})} = \frac{-k_0\cos\varphi_0}{-\omega\rho_2}\,\frac{\left[\omega^{1/3} H^{(2)}_{-\frac{2}{3}}(w)\right]\tilde{B}}{\left[w^{1/3} H^{(2)}_{1/3}(w)\right]\tilde{B}}$$

3A.86

$$\Rightarrow \tilde{R} = \frac{1 - i\frac{\rho_1}{\rho_2}\frac{H^{(2)}_{-2/3}}{H^{(2)}_{1/3}}}{1 + i\frac{\rho_1}{\rho_2}\frac{H^{(2)}_{-2/3}}{H^{(2)}_{1/3}}} = \frac{\rho_2 H^{(2)}_{1/3} - i\rho_1 H^{(2)}_{-4/3}}{\rho_2 H^{(2)}_{1/3} + i\rho_1 H^{(2)}_{-2/3}}$$

3A.87

Manipulation gives

$$\tilde{R} = \frac{\rho_2\left[\frac{-i}{\sin\frac{\pi}{3}}\left(e^{i\frac{\pi}{3}} J_{\frac{1}{3}}(\tilde{w}) - J_{-\frac{1}{3}}\right)\right] - i\rho_1\left[\frac{-1}{\sin\frac{\pi}{3}}\left(e^{-i\frac{2\pi}{3}} J_{-\frac{2}{3}}(\tilde{w}) - J_{\frac{2}{3}}(w)\right]\right.}{\rho_2\left[\frac{-i}{\sin\frac{\pi}{3}}\left(e^{i\frac{\pi}{3}} J_{\frac{1}{3}}(\tilde{w}) - J_{-\frac{1}{3}}\right)\right] + i\rho_1\left[\frac{-i}{\sin\frac{\pi}{3}}\left(e^{-i\frac{2\pi}{3}} J_{-\frac{2}{3}} - J_{\frac{2}{3}}(w)\right]\right.}$$

3A.88

Chapter 4- Modal Attenuation

4.1 Introduction
4.2 Rigorous formulation
4.3 Intuitive formulation
  4.3.1 Physical basis of inhomogeneous waves
  4.3.2 Ray mode analogy
  4.3.3 Reflection loss
  4.3.4 Summary of dispersion constraints
4.4 The relation between the intuitive attenuation coefficient and the attenuation coefficient calculated with the accepted period equation
4.5 Literature attenuation coefficient summary, implementation details
  4.5.1 Ingenito and Wolfe
  4.5.2 Brekhovskikh approximations
  4.5.3 Kornhauser and Raney
  4.5.4 Bucker
Appendix: Equivalence of accepted period equation and period equation from Kornhauser and Raney for the two layer case

Chapter 4- Modal attenuation

4.1 Introduction

The preceeding development allows us to solve for complex angles of incidence in each layer and to calculate reflection coefficient magnitude and phase for each layer. For mode n we use the reflection coefficient phase with $\varphi_1'' = 0$, to solve the intuitive characteristic equation 3.107 for eigenvalues $\omega(n, c_p)$. We then use magnitude and phase to iteratively solve the rigorous characteristic equations 3.107 and 3.108, for eigenvalues $\omega'(n, c_p)$ and normal mode poles $\tilde{\varphi}(n, c_p)$. Our goal is to determine modal attenuation coefficients as functions of frequency w and mode number n.

In this chapter the attenuation of normal modes is developed from both a rigorous and physical point of view. The rigorous formulation follows directly from the field equations developed in chapters 2 and 3. The intuitive attenuation coefficient is developed as an integral of vertical and horizontal wavenumber along ray paths. Reflection loss is added for waveguides with bounding layers, and modal attenuation arises when rays are associated with waves comprising the modes. In developing this intuitive approach we examine the mathematical representation of waves in terms of complex angles and discover the physical meaning of complex angle and inhomogeneous waves. Intuitive dispersion constraints are then summarized, the source wavenumber boundary condition reviewed, and the intuitive attenuation coefficient related to the rigorous coefficient. In the latter part of the chapter several attenuation coefficients from the literature are developed to the extent needed for inclusion in our acoustic models. Comparison of the coefficients is left to chapter 5.

4.2 Modal attenuation- Rigorous formulation

Rigorous modal attenuation is included in the range dependent term of the acoustic field equation Brek. 26.7 (eq.2.67) or Brek. 27.42 . The mode decays as $H_0^{(1)}(\tilde{k} \cdot r \sin\tilde{\varphi})$. For ranges such that $|kr\sin\varphi| \gg 1$ we may use the asymptotic approximation

$$H_0^{(1)}(kr\sin\varphi) \sim \frac{\sqrt{2}}{\sqrt{\pi kr\sin\varphi}} \exp\left[i\left(kr\sin\varphi - \frac{\pi}{4}\right)\right] \qquad 4.1$$

and for $k' >> k''$

$$H_0^{(1)}(kr\sin\varphi) \sim \frac{\sqrt{2}}{\sqrt{\pi \cdot r \cdot Re\left[\tilde{k}\cdot\sin\tilde{\varphi}\right]}} \exp\left[i\left(\tilde{k}\cdot r\cdot\sin\tilde{\varphi} - \frac{\pi}{4}\right)\right] \qquad 4.2$$

We identify the modal attenuation coefficient

$$\alpha_n(\omega) = Re\left[i\left(\tilde{k}_n \sin\tilde{\varphi}\right)\right] = \tilde{k}_x(\omega,n) \qquad 4.3$$

4.3 Modal attenuation- Intuitive formulation

4.3.1 Physical basis of inhomogeneous waves

It is intuitively puzzling that the imaginary part of the horizontal component $\tilde{k}_x$ of wavenumber will be zero in a nonabsorbing ocean for real incidence angles (equation 3.42, with $k_1'' = 0$, $\varphi_1'' = 0$), but the desired mode attenuation coefficient has been set equal to k_n'' in the past (ref. 19). The fact that this confusion still exists is demonstrated by a recent journal article (ref. 31) where real incidence angle is still used. Since the horizontal wavenumber in all layers is a constant for a wave at any particular frequency by Snells law, transitivity of Snells law suggests that the imaginary part is also equal in all layers (i.e. LHS of eq. 3.56 =0 $\Rightarrow$ RHS of eq. 3.56 =0 for arbitrary i). We are using independent variables k_i', k_i'', φ_i', φ_i'' with $k_i = k_i' + i\,k_i''$ related to frequency, sound speed, and attenuation in the medium. But how do we choose φ_i' and φ_i''? The rigorous formulation provides $\tilde{\varphi}_i$ as solution to the characteristic equations. The intuitive formulation uses real incidence angle in the source layer per a spherical wave decomposition (excluding those inhomogeneous waves in the expansion for which $C_p < C$ ocean). The effect of horizontal propagation of a plane wave is expressed as $\exp(i\,\tilde{k}_x \cdot x)$ where $\tilde{k}_x = \tilde{k}\sin\tilde{\varphi}$.

$$i\tilde{k}\sin\tilde{\varphi} = i(k\sin\varphi'\cosh\varphi'' - k''\cos\varphi'\sinh\varphi'') - (k'\cos\varphi'\sinh\varphi'' + k''\sin\varphi'\cosh\varphi'') \qquad 4.4$$

The effect of upward, vertical propagation is given by

$$\exp(-i\tilde{k}_z\cdot z) \qquad \tilde{k}_z = \tilde{k}\cos\tilde{\varphi} \qquad 4.5$$

$$-ik_z = -i(k'\cos\varphi'\cosh\varphi'' + k''\sin\varphi'\sinh\varphi'') + (k''\cos\varphi'\cosh\varphi'' - k'\sin\varphi'\sinh\varphi'')$$

Using the notation of equations 3.41-3.44, horizontal propagation in the +x direction is expressed by $\exp(i k_x' + k_x'')x$ and vertical propagation in the -z direction by $\exp(-z(ik_z' + k_z''))$. Note that when the medium is nondissipative $k''=0$ and the exponential horizontal propagation factor becomes

$$-k'\cos\varphi'\sinh\varphi'' + ik'\sin\varphi'\cosh\varphi''$$

$\varphi''=0$ is required for unattenuated propagation. The vertical propagation factor becomes $-k\sin\varphi'\sinh\varphi'' - ik'\cos\varphi'\cosh\varphi''$. When φ'' and k'' are both set = 0 in the layer of incidence i the Snell's law equation become

$$k_i'\sin\varphi_i' = k_{i+1}'\sin\varphi_{i+1}'\cosh\varphi_{i+1}'' - k_{i+1}''\cos\varphi_{i+1}'\sinh\varphi_{i+1}'' \qquad 4.6$$

$$0 = k_{i+1}'\cos\varphi_{i+1}'\sinh\varphi_{i+1}'' + k_{i+1}''\sin\varphi_{i+1}'\cosh\varphi_{i+1}'' \qquad 4.7$$

If layer i+1 is nondissipative and $k_{i+1}''=0$, necessarily $\varphi_{i+1}''=0$. If layer i+1 is dissipative $k_{i+1}''\neq 0$ and a solution for $\varphi_{i+1}''\neq 0$ is obtained. Note also, that eq 4.4 is eq 4.6- eq 4.7 of Snell's law, so that Snell guarantees that both the imaginary and real parts of the horizontal propagation factor are separately constant for all layers. Thus we can specify the real part of horizontal phase velocity alone as the independent parameter in the generation of dispersion curves with eigenvalues $\omega, \tilde{\varphi}$. The imaginary part of wavenumber, constant throughout the layers, will change as the angle $\tilde{\varphi}$, is changed, for constant real horizontal wavenumber component $K(c_\phi)$. Neither the phase nor

amplitude parts of the vertical exponential propagation factor remain constant, however from layer to layer.

The condition Im(kx)=0 in all layers including those where dissipation occurs is a result of the plane waveform of the source (its decomposition into plane waves), the stratified layering model, and the assumption of real initial incidence angle in the source layer. For complex source angles the Im(kx)=constant≠0 in all layers. Intuitively this becomes clear by observing the ray paths followed by a wavefront traveling from a nondissipative ocean halfspace into a dissipative isovelocity sediment halfspace.

Referring to figures 4.1.a. and 4.1.b.(Refraction of homogeneous waves into a dissipative halfspace)

The wave at raytip A in figure 4.1 will have the same amplitude (different phase) as that at raytip B because both have traveled the same total distance in layer 2. Yet they are at different horizontal positions and the same vertical position. Thus

$$e^{+(k''_{2y}\cdot y_a - k''_{2x}\cdot x_a)} = e^{+(k''_{2y}\cdot y_b - k''_{2x}\cdot x_b)} \qquad 4.8$$

$$\Rightarrow k''_{x_2} = 0 \qquad \text{since} \quad x_a \neq x_b \quad \text{and} \quad y_a = y_b$$

k'' = constant within a homogeneous isovelocity layer. Raytips B and C are at different vertical positions and the same horizontal position. Their amplitudes will be different because they have traveled different total distances in medium 2. Recall the property of real wavenumber components k'_x , k'_y , for real incidence angle φ , that the phase change ζ in going from points A to C (see figure 4.1.b) on a raypath is the sum

$$\begin{aligned}\zeta &= k'_x\cdot\Delta x + k'_y\cdot\Delta y \\ &= (k\sin\theta)'\cdot\Delta x + (k\cos\theta)'\cdot\Delta y \\ &= k'(\sin\theta\cdot\Delta x + \cos\theta\cdot\Delta y) = k'\cdot\ell\end{aligned} \qquad 4.9$$

The amplitude decrement from A to C over length ℓ is

$$k'' \cdot \ell = k'' \left(\sin\varphi \cdot \Delta x + \cos\varphi \cdot \Delta z \right) = k_x'' \cdot \Delta x + k_z'' \cdot \Delta z \qquad 4.10$$

for the case $\varphi'' = 0$ where $k_x'' = k'' \sin\varphi$. $\vec{k''} \cdot \vec{x_1}$ and $\vec{k''} \cdot \vec{x_2}$ could be used to relate amplitudes of points $\vec{x_1}$ and $\vec{x_2}$ on a raypath. They cannot, however, be used for amplitude comparisons of points off a ray, simply, without introducing φ'' because these points have different histories involving boundaries and previous layering encountered. For example in figure 4.2. the phase at time t, at wavefront points A and B' which do not lie along a raypath should be related by $k' \cdot \ell$, where ℓ = the distance AA' normal to wavefronts passing through the two.

$$k \cdot \ell = k \cdot \Delta x \sin\varphi = k_x \cdot \Delta x \qquad 4.11$$

The log amplitude decrement will be $k_x'' \cdot \Delta x = k'' \sin\varphi \cdot x = k'' \cdot \ell$ when the point B is in medium 2. But the point B and A have different amplitudes although on the same phase front, so that to correctly relate amplitudes at A and B', using the coordinates of the two points, k_x'' must be modified. In fact, the correct modification is to introduce an imaginary part of angle φ'' such that the amplitude decrement is 0 from A to B'.

In this intuitive formulation of attenuation we may determine the complex angles required for wave representation in underlying layers by imposing the "correct" attenuation along a raypath, when k_x'' =0. That is, we require of a wave of real incidence angle refracted from a nondissipative halfspace into a dissipative halfspace that amplitude be independent of x but dependent on z and equal to that calculated by following the raypath. Then in the dissipative medium

$$k'' \cdot \ell = k_x'' \cdot \Delta x + k_z'' \cdot \Delta z = k_z'' \cdot \Delta z \qquad 4.12$$

with ℓ the arc length along a ray from the point of incidence (0,0) to same point (x,z) see fig. 4.1.b., with A=(0,0), c=$(\Delta x, \Delta z)$.

$$k_z'' = k' \cos\theta' \cosh\theta' - k'' \sin\theta' \sinh\theta'' \qquad 4.13$$

$$k_x'' = k' \cos\theta' \sinh\theta'' + k'' \sin\theta' \cosh\theta'' \qquad 4.14$$

Using equation 4.14 we can eliminate k' from equation 4.13

$$k' = - \frac{k'' \sin\theta' \cosh\theta''}{\cos\theta' \sinh\theta''}$$

so that in equation 4.12

$$k''.\ell = k''.\cosh\theta'' \qquad 4.15$$

is required. Now z and ℓ are real and related to the real incidence angle ξ connecting points A and C $\ell = z/\cos\xi$. Substituting for ℓ on the LHS of equation 4.15 we can equate the actual attenuation along the raypath at real angle ξ to that using the *required complex angle* $\tilde{\theta}$.

$$\frac{k''.z}{\cos\xi} = \frac{k''\cosh\theta''}{\cos\theta}.z$$

$$\Rightarrow \cos\xi = \frac{\cos\theta'}{\cosh\theta''} \qquad 4.16$$

For small dissipation $\cosh\theta'' \approx 1$ and $\xi \approx \theta'$. This says that the wave function at depth z within a dissipating medium has local amplitude dependent on complex angle $\tilde{\theta}$ satisfying the boundary conditions. That amplitude is equivalent to the amplitude of a plane wave propagating along a ray direction at real angle ξ between the origin and the point (x,z). In the limit of zero dissipation the ray angle ξ is identified with the real part of the complex angle θ. For finite dissipation they differ.

Thus we see that complex wavenumber within a layer describes propagation effects along a wavefront only when combined with actual initial amplitudes and phases along the wavefront. Boundaries may

destroy equiamplitude of a plane wavefront when not normal to the ray direction. In fact, defining a plane wavefront as a line of equiphase (phase $\equiv Re\left[\vec{k}\cdot\vec{x}-\omega t\right]$) we find that plane wavefronts will generally be nonequiamplitude fronts. Plane wave refraction in multilayered attenuating media requires a constant horizontal attenuation coefficient equal to that $Im\left[\text{horizontal wavenumber}\right]$ for the layer within which the source is located. When source is decomposed into plane waves whose phase fronts are also equiamplitude fronts (homogeneous plane waves) refraction into absorbing layers will produce inhomogeneous plane waves whose amplitude decays away from the boundary along the phase front. Inhomogeneous incident waves will be similarly transformed. The nature of inhomogeneous waves in the water column is examined further in section 4.4.

4.3.2 Ray-mode analogy

Ray attenuation could be determined now by integrating the horizontal and vertical attenuation factors as the ray travels over a cycle through upper and lower turning points z_u , z_ℓ . Strictly speaking the discussion of section 4.3.1 holds only for isovelocity layers where upper and lower turning points will correspond to reflective interfaces. We are saying here, however, that if sound speed and density change gradually so that reflections can be ignored attenuation may be calculated as a line integral over local complex wavenumber. This is equivalent to WKB approximation with complex vertical wavenumber $\gamma(z)$ used only in the exponent. Upper and lower turning points z_u and z_ℓ are then refractive turning points where the real part of vertical wavenumber goes through zero.

Modal attenuation coefficients could be determined by dividing the total ray cycle attenuation by the horizontal cycle length L and associating ray with traveling waves comprising the modes. With generalized horizontal and vertical wavenumbers $\xi_x''(z)$, $\xi_z''(z)$ *

*By generalized wavenumber components we mean $\vec{\xi}$ such that the wave may be represented by the exponential function $\exp\left[i\vec{\xi}\cdot\vec{x}-i\omega t\right]$. $\vec{\xi}$ is a complex vector function of coordinates. In the WKB approximation it would be a phase integral. In isovelocity layers it would be the usual wavenumber.

and ray cycle length $L(\Theta)$ for real source incidence angle Θ. The mode would attenuate by a factor $A(x,\Theta)$ over distance x.

$$A(x,\Theta) = e^{\left[\left(2\int_{3\ell}^{3u} \xi''_3 \cdot d_3 / L(\Theta)\right) + 2\int_{3\ell}^{3u} \frac{\xi''_x \cdot \sin\Theta \, d_3}{(N^2(3)-\sin^2\Theta)^{1/2}} / L(\Theta)\right]\cdot x}$$

$$\equiv e^{\delta_s \cdot x} \qquad 4.17$$

Here $L(\Theta_0)$ is the ray horizontal cycle length

$$L = 2\int_{3\ell}^{3u} \frac{\sin(\Theta_0)}{(N^2(3) - \sin^2(\Theta_0))^{1/2}} d_3 \qquad 4.18$$

The first integral in the exponent is over the imaginary part of vertical wavenumber normalized by horizontal cycle length. The second integral gives the horizontal contribution to attenuation along the ray. The modal attenuation coefficient δ_s due to absorption in the source layer would be

$$\delta_s = \frac{2\int_{3\ell}^{3u} \left(k'' \cos\varphi' \cosh\varphi'' - k' \sin\varphi' \sinh\varphi''\right) d_3 + 2\int_{3\ell}^{3u} \frac{\left(k' \cos\varphi' \sinh\varphi'' + k'' \sin\varphi' \cosh\varphi''\right) \sin\Theta_0 \, d_3}{(N^2(3) - \sin^2\varphi_0)^{1/2}}}{2\int_{3\ell}^{3u} (\sin\varphi_0)/(N^2(3) - \sin^2\varphi_0)^{1/2} \, d_3} \qquad 4.19$$

Complex incidence angle at the source, $\varphi_0 = \varphi_0' + i\varphi_0''$, will be a function of ω, m for normal modes through the characteristic equation and an additional constraint. Note that for real source exit angles equation 4.19 becomes an integral over only vertical attenuation since both k'' and $\varphi_0'' = 0$ in the water column and thus k_x'' =constant=0. Note also that the attenuation for a ray passing through

$(x,z)=(0,0)$ to (x',z') is not the same as the modal attenuation from point $(0,0)$ to (x',z') unless $z'=0$. That is the ray that will have amplitude $A(0,0)\, e^{-\alpha(k_x'' \cdot x' + k_z'' \cdot z')}$. The mode will have amplitude $A(0,0)\, e^{-(\delta_s \cdot x')}$.

The intuitive ray-mode attenuation coefficient then ascribes to the mode the same attenuation as the constructively interfering traveling waves which compose it. In infinite, continuously stratified media all points on a traveling wavefront will suffer identical attenuation as the simplified drawing figure 4.3 illustrates for the component which starts out downward and ends up upward in an inhomogeneous halfspace.

4.3.3 Reflection loss

In multilayered media the actual emergent energy at any point B will result from multiple reflections and refractions in the underlying media. The reflection coefficient gives the complex ratio of the reflected wave function (say plane wave) description of that energy to the wave function description of the incident energy. Energy contributions are received from segments of the original source plane wave fronts extending back infinitely in the x direction. The steady state emergent amplitude is used at every interface to establish coefficients for the traveling wave components within the waveguide. The decay of these waves within the source layer is traced by the I_z'' and ζ_x'' integral. Thus we are led to adjust the integration limits in the intuitive formulation from "turning point" depths z_ℓ and z_a

z_u

i.e $\int_{z_\ell} dz$, to waveguide source layer boundaries z_{is+1}, z_{is}

z_{is}

i.e $\int_{z_{is+1}} dz$, and to adjust the wave amplitude

by the combined upper and lower interface reflection coefficients. Then for multilayered media the intuitive modal attenuation coefficient becomes

$$\delta = \frac{\left[2 \int_{z_{ls}}^{z_{ls+1}} \left(\xi_z'' \, dz + \xi_x'' \, dx(z) \right) + 1 - |R\uparrow| \cdot |R\downarrow| \right]}{2 \int_{z_{ls}}^{z_{ls+1}} \frac{\sin \varphi_0}{\left(N^2(z) - \sin^2 \varphi_0 \right)^{1/2}} \, dz} \qquad 4.20$$

So that the attenuation factor after a distance x will be

$$A(x, \varphi_0) = e^{\left\{ 2 \int_{z_{ls}}^{z_{ls+1}} \frac{\xi_z'' \cdot dz + \xi_x'' \, dx(z)}{L(\varphi_0)} \right\} x} \cdot e^{-\delta_b \cdot x} \qquad 4.21$$

In these formulae z_{ls} and z_{ls+1} are interface depths for top and bottom of the source layer. The exponential attenuation factor due to boundary reflection loss arises from noting that the complex reflection coefficients from above are

$$R\uparrow \equiv \rho\uparrow \cdot e^{i\phi\uparrow} \qquad R\downarrow \equiv \rho\downarrow e^{i\phi\downarrow} \qquad 4.22$$

Then the effect of both imperfect reflections over a reflected cycle is

$$R\uparrow \cdot R\downarrow = \rho\uparrow \cdot \rho\downarrow \cdot e^{i(\phi\uparrow + \phi\downarrow)} \qquad 4.23$$

and the decrement of amplitude per horizontal distance due boundary interaction is

$$\Delta A = \frac{-\epsilon}{L_{ls}(\varphi_0)} \cdot A \qquad 4.24$$

where $\epsilon = 1 - \rho\uparrow \cdot \rho\downarrow$ and A is the incident amplitude. Then

$$A = A_0 \, e^{-\delta_b \cdot x} \qquad \text{with} \qquad \delta_b \equiv \frac{1 - \rho\uparrow \cdot \rho\downarrow}{L(\varphi_0)} \qquad 4.25$$

Equation 4.19 is appropriate for calculating loss in an absorptive duct (muddy SOFAR channel) within which phase integral approximations are valid. That is, within a channel where characteristic impedance varies continuously and within which partial reflections are ignored. Equation 4.20 would be used when discrete characteristic impedance changes occured and phase integral approximations were invalid. Equation 4.20 would describe an arbitrary number of layers which could be dissipative or not and of arbitrary velocity variation, provided appropriate formulae for $R\downarrow$ and $R\uparrow$ are available. In chapter 5 we will examine results for the intuitive attenuation coefficient with $k_1'' = 0$, $\varphi_1'' = 0$. Attenuation is then due only to δb .

4.3.4 Summary of Dispersion Constraints for Intuitive Propagation:

In a physical formulation of the problem we use a characteristic equation $|R\downarrow| \cdot |R\uparrow| = 1$ for nondissipative media, or

$\chi\uparrow + \chi\downarrow = 2m\pi$, for both dissipative and nondissipative waveguides. The propagation variables are ω' , ω'' , k' , k'' , φ' φ'' . c and $\delta(\omega)$ are specified for each layer so that for real frequency $\omega'' = 0$ the layer wavenumbers are given by

$$k = k' + i k'' = \frac{\omega}{c} + \delta(\omega)$$

The source emits waves at angle φ with wavenumber k_s we have four independent variables given k' , k'' . These are ω' , ω'' , k_x' , k_x'' or ω' , ω'' , φ' , φ'' . In the steady state there is no temporal decay so that dispersion constraint number one is $\mathrm{Im}(w) \equiv w'' = 0$. Then when another variable, say k_x' is chosen as the independent variable, the characteristic equation 3.112 will fix one more, say w'. k_x'' is left as a free variable. A requirement that imaginary part of group velocity $\mathrm{Im}(U) = 0$, could determine complex k_x , as it did for Phinneys (ref. 41) transients. However, our analysis has preserved $\mathrm{Re}(k_x)$ and $\mathrm{Im}(k_x)$ throughout the waveguide, consistent with complex Snell's Law, and the second requirement we will impose on in our physical formulation is that $\mathrm{Im}(kx) = kx''$ of the spherical wave expansion, corresponding to the first section of contour Γ_1 in

figure 2.5, along the real $\tilde{\gamma}_1$ axis. However we should now consider how fundamental that contour really is.

The contour relation for k_x' and k_x'' is discussed by Aki (ref. 32) and Brekhovskikh amoung others and leads to equation Brek. 18.15 given on page 33 and to the source layer incidence angle contour shown in Brek. figure 90., and in our figure 2.5. In the expansion of the spherical wave into plane waves, equation Brek. 18.15 was continued into space by adding the term $\pm i k_z \cdot z$ to arrive at Brek. 18.17. This can be shown (see Aki) to result also by starting with a 3-D wavenumber representation of the spherical wave

$$\frac{1}{R} \exp\left[i\omega\left(t - \frac{R}{c}\right)\right] = \frac{e^{i\omega t}}{(2\pi)^2} \int_{-\infty}^{\infty}\int\int \frac{e^{-ik_x \cdot x - ik_y \cdot y - ik_z \cdot z}}{\left(k_x^2 + k_y^2 + k_z^2 - \frac{\omega^2}{c^2}\right)^{1/2}} dk_x\, dk_y\, dk_z \qquad 4.26$$

and carrying out the integration with respect to kz by extending kz to complex values and applying Cauchy's theorem. Then two poles are at

$$k_z = +\sqrt{\frac{\omega^2}{c^2} - k_x^2 - k_y^2} \qquad k_z = -\sqrt{\frac{\omega^2}{c^2} - k_x^2 - k_y^2} \qquad 4.27$$

Introducing small attenuation makes c complex and shifts the pole position

$$\frac{1}{c} = \frac{1}{c_0}(1 - i\epsilon) \qquad \epsilon > 0 \quad \text{for} \quad \omega > 0 \qquad 4.28$$

Pole positions are indicated in figure 4.5. Integrating over kz by contour integration in the upper or lower kz plane depending on the sign of z yields

$$\frac{e^{-i\frac{\omega}{c}R}}{R} = \frac{1}{2\pi} \int_{-\infty}^{\infty}\int \frac{e^{-ik_x \cdot x - ik_y \cdot y - \nu|z|}}{\nu} dk_x\, dk_y \qquad 4.29$$

$$\nu \equiv ik_z$$

For $\frac{\omega^2}{c^2} < k_x^2 + k_y^2$ becomes real and the plane waves

represent inhomogeneous waves propagating parallel to the x-y plane and changing amplitude most rapidly in the z direction. Implicit in the above is that the attenuation introduced to move the poles off the real axis does not alter the Fourier decription. That is, the integration paths are still over real values of kx, ky, kz. These integration paths are fundamental. For the Sommerfeld integral in terms of complex angles the integration variable is change first to

(k_r, ϕ) where $k_x = k_r \cos\phi$

$k_y = k_r \sin\phi$

$$\frac{e^{-\imath \frac{\omega}{c} R}}{R} = \int_{-\infty}^{\infty} \frac{k_r J_0(k_r \cdot r)\, e^{-\nu|z|}}{\nu}\, dk_r \qquad 4.30$$

$\nu = \imath\sqrt{\frac{\omega^2}{c^2} - k_r^2}$ and sign determined by $\mathrm{Re}\,\nu > 0$

The integral is further transformed using incidence angle φ with

$$k_r = \frac{\omega}{c}\sin\varphi \qquad dk_r = \frac{\omega}{c}\cos\varphi\, d\varphi \qquad 4.31$$

$$\nu = \imath \frac{\omega}{c}\cos\varphi \qquad 4.32$$

The integration limits are now $0 < k_r < \infty \Rightarrow 0 < \sin\varphi < \infty$

and $0 < \sin\varphi < 1 \Rightarrow \varphi'' = 0 \quad 0 < \varphi' \leq \frac{\pi}{2}$

$1 < \sin\varphi < \infty \Rightarrow \varphi' = \frac{\pi}{2} \quad 0 < \varphi'' \leq \infty$

or $\varphi' = \frac{\pi}{2} \quad -\infty < \varphi'' < 0$

$$\nu = i\frac{\omega}{c}\cos\varphi \qquad k_r = i\frac{\omega}{c}\sin\varphi \qquad Re\,\nu = \frac{\omega}{c}\sin\varphi'\sinh\varphi''$$

$$\text{so} \quad \frac{e^{-i\frac{\omega}{c}R}}{R} = -i\frac{\omega}{c}\int_0^{\frac{\pi}{2}+i\infty} J_0\left(\frac{\omega}{c}r\sin\varphi\right)\sin\varphi\, e^{-\nu|z|}\, d\varphi \qquad 4.33$$

Our expressions for kx' and kx'' as functions of complex sound speed and incidence angle are given in equations page 72 where φ' and φ'' will vary so as to satisfy the boundary condition. The "boundary condition at the source" is that $\tilde{\varphi}$ lie on the contour shown in figure 4.6. Along this contour in interval (1)

$$k_r' = k'\sin\varphi'\cdot 1$$
$$k_r'' = -k''\sin\varphi''\cdot 1 \qquad \text{since} \quad \sinh\varphi'' = 0 \qquad 4.34$$

Along contour interval (2)

$$k_r' = k'\cosh\varphi''\cdot 1$$
$$k_r'' = -k''\cosh\varphi''\cdot 1 \qquad 4.35$$

since $\cos\frac{\pi}{2} = 0$ along (2) . Along the entire contour

$$k_r'' = -\frac{k''}{k'}k_r' \qquad 4.36$$

But the contour is valid for infinitesimal Im(c) $\Rightarrow$ K'' $\to$ 0 and $k_r'' \to 0$. For finite K'' we must modify the solution to the inhomogeneous wave equation, since the transform pair expressed by Brek 18.11 or by equation 4.26 above holds for real kx, ky, kz only when k(c) is real. For the present we note that for sources in the ocean $k'' \approx 0$ so we could follow the contour

$0 < \varphi < \frac{\pi}{2} + i\infty$ or k''=0. We really have no constraint how-

ever if the decomposition is nonunique in the complex $\vec{k}$ space. The Fourier transform may be unique. The transformation to angular coordinates ϕ and ψ certainly is not, since we could have chosen inhomogeneous waves propagating parallel to any plane through the source. But for sources in the ocean we can impose physical constraint (2), $kx''=0$ and the contour definition $\tilde{\psi}_i = \psi_i(\Gamma_i)$.
We consider the contour above to be the source boundary condition in the physical formulation. It says the source is emitting waves at these real wavenumbers. It has no meaning in the rigorous treatment since the spherical wave representation is nonunique in terms of incidence angle. It does however retain the physical quality of real angles of incidence along contour segment (1) of Γ_i in the nondissipative source layer. The contour integral solution determined by the rigorous characteristic equation says the greatest contribution to the field integral comes from certain inhomogeneous waves of complex incidence angle and wavenumber. The physical formulation says we start with homogeneous waves and select out those which interfere constructively. The physical formulation has the computational advantage of reducing the number of degrees of freedom in the angle solution to the characteristic equation from 2 to 1, significantly reducing the number of steps required for iterative solution.

4.4 The relation between the intuitive attenuation coefficient and the attenuation coefficient calculated with the accepted period equation:

We have outlined above the physical considerations leading to the intuitive modal attenuation coefficient represented by equation 4.19. They were expansion of the source in a nondissipative layer into plane waves whose angles of incidence were real in the ocean, reflection loss at the boundaries, constructive interference of modal component waves, and modal attenuation equivalent to that of the superimposing waves. Modal attenuation was appended as a coefficient not as an imaginary part of angle. The characteristic equation was

$$\phi'\uparrow + \phi'\downarrow + 2kh\cos(\tilde{\psi}) = n2\pi \qquad 4.37$$

Only the phase of the reflection coefficient was used. The eigenvalues

$\varphi'(\omega)$ then lay along the contour Γ . We did not worry that the eigenangles were on the contour, because we were not calculating the field with a complex integral.

The accepted period equation, used by Brekhovskikh requires that

$$\tilde{\Phi}\uparrow + \tilde{\Phi}\downarrow + 2kh\cos(\tilde{\varphi}) = n\angle\pi \qquad 4.38$$

We examine below the implications of these choices.

The accepted period- locating the poles:

We can write the period equation explicitly in terms of complex angle of incidence $\tilde{\varphi} = \varphi' + i\varphi''$ and complex reflection coefficient phase $\tilde{\Phi} = \Phi' + i\Phi''$.

$$2kh\cos(\tilde{\varphi}) + \tilde{\Phi}\uparrow + \tilde{\Phi}\downarrow = 2\pi l \qquad 4.39$$

or $$2kh\left[\cos\varphi'\cosh\varphi'' - i\sin\varphi'\sinh\varphi''\right] + \Phi'\uparrow + i\Phi''\uparrow + \Phi'\downarrow + i\Phi''\downarrow = 2\pi l$$

leading to the two simultaneous equations

$$2kh\cos\varphi'\cosh\varphi'' + \Phi'\uparrow + \Phi'\downarrow = 2\pi l \qquad 4.40$$

$$-2kh\sin\varphi'\sinh\varphi'' + \Phi''\uparrow + \Phi''\downarrow = 0 \qquad 4.41$$

Note that 4.40 insures that there is constructive interference of waves at angle $\tilde{\varphi} = \varphi' + i\varphi''$ 4.41 relates the dissipation in the boundaries to the apparent dissipation in the layer. In fact it requires that the vertical propagation loss (acutally a gain) in the laver expressed as $e^{-(\sin\varphi'\sinh\varphi'' 2kh}$

exactly balance the reflection loss. Then the only net loss from propagation at angle with reflection will be contained in the horizontal propagation factor. The angle for which vertical propagation gain and reflection loss are balanced will induce a horizontal decrement given by the usual $e^{k_x''\cdot x}$ where $k_x'' = k\cos\varphi'\sinh\varphi''$ in a dissipationless layer.

To see this more clearly examine the phase and attenuation terms

kx', kx'', kz', kz'' for a nonattenuating isovelocity source layer (k''=0). Then using

$$\cos\tilde{\varphi} = \cos(\varphi' + i\varphi'') = \cos\varphi' \cosh\varphi'' - i \sin\varphi' \sinh\varphi''$$

and

$$\sin\tilde{\varphi} = \sin(\varphi' + i\varphi'') = \sin\varphi' \cosh\varphi'' + i \cos\varphi' \sinh\varphi''$$

and with propagation represented by $e^{i\tilde{k}(\cos\tilde{\varphi}\cdot z + \sin\tilde{\varphi}\cdot x)}$

we have

$$k_x = i\,k \sin\tilde{\varphi} \qquad k_z = i\,k \cos\tilde{\varphi}$$

$$k_x' = \mathrm{Im}\left[i k' \sin\tilde{\varphi}\right] = i k' \sin\varphi' \cosh\varphi'' \qquad 4.42$$

$$k_x'' = \mathrm{Re}\left[i k' \sin\tilde{\varphi}\right] = -k' \cos\varphi' \sinh\varphi'' \qquad 4.43$$

$$k_z' = \mathrm{Im}\left[i k' \cos\tilde{\varphi}\right] = i k' \cos\varphi' \cosh\varphi'' \qquad 4.44$$

$$k_z'' = \mathrm{Re}\left[i k' \cos\tilde{\varphi}\right] = k' \sin\varphi' \sinh\varphi'' \qquad 4.45$$

Note that propagation in the +x, +z direction gives amplitude decay for +x but amplitude increase for +z if $\varphi'' > 0$

i.e.

$$k' \sin\varphi' \sinh\varphi'' > 0 \qquad \text{for} \qquad \varphi'' > 0$$

$$\text{and} \quad 0 < \varphi' < \frac{\pi}{2}$$

$$-k' \cos\varphi' \sinh\varphi'' < 0 \qquad \text{for} \qquad \varphi'' > 0$$

Phase changes are both > 0 as would be expected. For a layer in which dissipation occurs ($k'' \neq 0$) we examine the full expansion of kx', kx'', kz', kz''

$$k_x' = i\left(k' \sin\varphi' \cosh\varphi'' - k'' \cos\varphi' \sinh\varphi''\right) \qquad 4.46$$

$$k_x'' = -k' \cos\varphi' \sinh\varphi'' - k'' \sin\varphi' \cosh\varphi'' \qquad 4.47$$

$$k_3' = i\left(k' \cos\varphi' \cosh\varphi'' + k'' \sin\varphi' \sinh\varphi''\right) \qquad 4.48$$

$$k_3'' = + k' \sin\varphi' \sinh\varphi'' - k'' \cos\varphi' \cosh\varphi'' \qquad 4.49$$

The behaviour of the terms for increasing x, z at angle $\breve{\varphi}$ is as shown below with $P[\ ] \equiv$ phase associated with, $A[\ ] \equiv$ amplitude associated with.

$$P\left[k_x'(k')\right] = P\left[k' \sin\varphi' \cosh\varphi''\right] \quad \text{increases} \qquad 4.50$$

$$P\left[k_x'(k'')\right] = P\left[-k'' \cos\varphi' \sinh\varphi''\right] \quad \underline{\text{decreases}} \qquad 4.51$$

$$P\left[k_3'(k')\right] = P\left[k' \cos\varphi' \cosh\varphi''\right] \quad \text{increases} \qquad 4.52$$

$$P\left[k_3'(k'')\right] = P\left[k'' \sin\varphi' \sinh\varphi''\right] \quad \text{increases} \qquad 4.53$$

$$A\left[k_x''(k')\right] = A\left[-k' \cos\varphi' \sinh\varphi''\right] \quad \text{decreases} \qquad 4.54$$

$$A\left[k_x''(k'')\right] = A\left[-k'' \sin\varphi' \cosh\varphi''\right] \quad \text{decreases} \qquad 4.55$$

$$A\left[k_3''(k')\right] = A\left[k' \sin\varphi' \sinh\varphi''\right] \quad \underline{\text{increases}} \qquad 4.56$$

$$A\left[k_3''(k'')\right] = A\left[-k'' \cos\varphi' \cosh\varphi''\right] \quad \text{decreases} \qquad 4.57$$

We see that the terms kz''(k') and kx'(k''0 vary in directions contrary to what we physically expect for a progressing wave. The contrary terms both contain $\sinh\varphi''$ which is expected to be small.

$$k_x'(k'') < k_x'(k') \quad \text{if} \quad -k'' \cos\varphi' \sinh\varphi'' < k' \sin\varphi' \cosh\varphi'' \qquad 4.58$$

$$k_3''(k') < k_3''(k'') \quad \text{if} \quad +k' \sin\varphi' \sinh\varphi'' < -k' \cos\varphi' \cosh\varphi'' \qquad 4.59$$

As far as the dissipationless source layer goes we are left with an amplitude relation in the characteristic equation

$$1 - R\uparrow \cdot R\downarrow \exp(i 2k_3 h) = 0 \qquad 4.60$$

of

$$i(-i\,2kh\,[\sin\varphi' \sinh\varphi''] + i\phi''\uparrow + i\phi''\downarrow) = 0 \qquad 4.61$$

i.e. $2kh\,[\sin\varphi' \sinh\varphi'']$ represents a growth for $\varphi'' > 0$, $\varphi' > 0$; $-\phi''\uparrow - \phi''\downarrow$ represents a decay. With no leakage $\phi'' = 0$ the characteristic equation requires $\varphi'' = 0$. With leakage $+2kh \sin\varphi' \sinh\varphi''$ balances leakage and horizontal decay is $(-k' \cos\varphi' \sinh\varphi'')\,x = k_x'' \cdot x$

Eliminating $\sinh\varphi''$ gives rigorously a horizontal attenuation factor of

$$-k'\cos\varphi' \left[\frac{\phi''\uparrow + \phi''\downarrow}{2k'h \sin\varphi'}\right] \cdot x = \left[\frac{\phi''\uparrow + \phi''\downarrow}{2h \tan\varphi'}\right] x = k_x'' \cdot x \qquad 4.62$$

This is just reflection loss divided by horizontal cycle length, using only the real part of angle to calculate cycle length, but complex angle to determine reflection coefficient magnitude. This attenuation form is the one we have programmed as the rigorous attenuation coefficient and for which results are given in chapter 5. It corresponds to $\int$ in equation 4.3.

Calculation of phase change requires both real and imaginary parts of angle.

$$k_x' = k' \sin\varphi' \cosh\varphi'' \approx k' \sin\varphi' \qquad 4.63$$

$$k_3' = k' \cos\varphi' \cosh\varphi'' \approx k' \cos\varphi' \qquad 4.64$$

Since the real part of the characteristic equation is

$$2kh \cos\varphi' \cosh\varphi'' = 2\pi l - \phi'\uparrow - \phi'\downarrow$$

we can eliminate $\cosh\varphi''$ to get vertical and horizontal phase change of the modal propagating waves.

$$k_x' = k' \sin\varphi' \left[\frac{2\pi l - \phi'\uparrow - \phi'\downarrow}{2k'h \cos\varphi'}\right] = \frac{\tan\varphi'}{2h}\left[2\pi l - \phi'\uparrow - \phi'\downarrow\right]$$

$$4.65$$

$$k_z' = k' \cos\varphi' \left[\frac{2\pi\ell - \phi'\uparrow - \phi'\downarrow}{2k'h \cos\varphi'} \right] = \frac{2\pi\ell - \phi'\uparrow - \phi'\downarrow}{2h} \qquad 4.66$$

kz'= modal full cycle vertical phase integral-phase change outside the layer (dependent on complex angle)/twice the layer thickness.

kx'= the vertical phase length in the layer x tan of the real angle of propagation.

Then the modal component wave represented by a pole in the accepted period equation can be viewed as propagating at real angel φ' within the source layer for cycle length calculations and geometric relation of horizontal and vertical phase change. The phase and amplitude changes $\phi'(\varphi', \varphi'')$ and $\phi''(\varphi', \varphi'')$ due to reflection depend on the full complex $\tilde{\varphi}$ however.

The intuitive modal attenuation coefficient in a dissipationless isovelocity source layer with real incidence angel φ_1 is

$$\frac{k'' \Delta z + k_x'' \Delta x}{L} + \frac{1 - |R\uparrow| \cdot |R\downarrow|}{L} \Delta x = \delta_{INT} \qquad 4.67$$

This will not be equivalent to being emitted at any complex angle $\tilde{\varphi}_1 = \varphi_1' + i\varphi_1''$ unless

$$k' \sin\varphi_1' \sinh\varphi_1'' \frac{h}{L} - k' \cos\varphi_1' \sinh\varphi_1'' + \left(\frac{1 - |R(\varphi_1', \varphi_1'')\downarrow| \cdot |R(\varphi_1', \varphi_1'')\uparrow|}{L} \right) =$$

$$k' \sin\varphi_0' \sinh\varphi_0'' \frac{h}{L} - k' \cos\varphi_0' \sinh\varphi_0'' + \left(1 - |R(\varphi_0', \varphi_0'')\downarrow| \cdot |R(\varphi_0', \varphi_0'')\uparrow| \right)$$

$$4.68$$

with $\varphi_0'' = 0$ and h = layer thickness

The additional loss due to $k' \sin\varphi_1' \sinh\varphi_1'' \frac{h}{L} - k' \cos\varphi_1' \sinh\varphi_1''$ would have to be balanced by an additional gain represented by

$\left[1 - |R(\varphi_1', \varphi_1'')|\right]/L$ in order for the two angles $\tilde{\varphi}_0$ and $\tilde{\varphi}_1$ to be attenuatively equivalent

i.e.

$$k' \sin\varphi_0' \sinh\varphi_0'' \frac{h}{L} - k' \sin\varphi_1' \sinh\varphi_1'' - k' \cos\varphi_0' \sinh\varphi_0'' + k' \cos\varphi_1' \sinh\varphi_1''$$

$$= \left[1 - |R(\varphi_1', \varphi_1'')|\right] - \left[1 - |R(\varphi_0', \varphi_0'')|\right] \qquad 4.69$$

In particular, to show that the modal attenuation coefficient $\int$ arising from the assumption of real source angle φ_0 with reflection loss $R(\varphi_0', 0)$ is equivalent to that arising from propagation in source layer at complex angle $\tilde{\varphi}_0 = \varphi_0' + i\varphi_0''$ we would have to show that

$$-k' \sin\varphi_0' \sinh\varphi_0'' \frac{h}{L} + k' \cos\varphi_0' \sinh\varphi_0'' = |R(\varphi_0', 0)| - |R(\varphi_0', \varphi_0'')|$$

We have represented intuitive loss by $e^{-\epsilon x}$ with $\dfrac{1 - e^{-\phi''\uparrow - \phi''\downarrow}}{L} \equiv \epsilon$ 4.70

We can compare the loss in the intuitive (A) and accepted (B) formulations. Amplitude of eigenfunction $\underline{\Phi}$ after propagation to a distance x becomes

$$\text{(A)} \quad \underline{\Phi}_A = \underline{\Phi}_0 \, e^{-(1 - e^{-\phi''\downarrow - \phi''\uparrow})} \qquad 4.71$$

or intuitively

$$\text{(B)} \quad \underline{\Phi}_B = \underline{\Phi} \, e^{+(-\phi''\downarrow - \phi''\uparrow) x/L} \qquad 4.72$$

by the accepted period equation where in the case (A) $\phi''(\phi''(\varphi', 0))$ while in case (B) $\phi'' = \phi''(\varphi', \varphi'')$ and angles φ' differ slightly. In case (A) for example after propagation to distance $x = 2L$ we have

$$\underline{\Phi}_A = \underline{\Phi} \, e^{(1 - |R|)\cdot 2} = \underline{\Phi}_0 \, e^{-2\epsilon} \qquad 4.73$$

in (B)

$$\underline{\Phi}_B = \underline{\Phi} \, e^{-\phi''\cdot 2} = \underline{\Phi} \cdot |R|^2 \qquad 4.74$$

Taking $\ln$ of amplitudes for arbitrary x gives

$$\ln \Phi_A = [\delta_A] \frac{x}{L} = \frac{x}{L}\left(-\left(1-e^{-\phi''}\right)\right) =$$

$$= \frac{x}{L}\left(-\left[1-\left(1-\phi'' + \frac{\phi''^2}{2} - \frac{\phi''^3}{3!} + \dots\right)\right]\right) = \left(-\phi'' + \frac{\phi''}{2} - \dots\right)\frac{x}{L}$$

4.75

$$\ln \Phi_B = [\delta_B] \frac{x}{L} = -\phi'' \frac{x}{L}$$

4.76

To first order the attenuation coefficients are the same provided

$$\phi''(\varphi_B', \varphi_B'') \approx \phi''(\varphi_A', 0)$$

4.77

In chapter 5 we will compare reflection coefficient magnitude for waves which satisfy the intuitive characteristic equation with those which satisfy the rigorous equation. Table 5.4 gives example values of

$$\varphi_1' \equiv \varphi_B' \qquad \varphi_1'' \equiv \varphi_B'' \qquad \varphi_{1_0}' \equiv \varphi_A'$$

and $\underbrace{\left|R|_{\tilde{\varphi}=\tilde{\varphi}_B}\right|}_{|R|}$ versus $\underbrace{\left|R|_{\tilde{\varphi}=\tilde{\varphi}_A}\right|}_{|R_0|}$

for locked modes.

4.5 Attenuation coefficient summary:

We will compare attenuation coefficient results using equation 4.62 with those arising form the current theory of Ingenito and Wolf . We also offer below expressions from Brekhovskikh, and from Kornhauser and Raney. In the computer algorithmn for our rigorous (Brek.) formula and Ingenitos the same unperturbed normal mode eigenvalues are used. Since the same Snell routine and the same characteristic equation is used, the values of χ_0 , k_0 will be the same and the differences in the attenuation coefficients will depend on the analytic form, as well as slight differences between the initial

unperturbed reflection coefficient used in the Ingenito formula and final reflection coefficients (as dissipation and complex angle are included in our iterative characteristic equation solution).

We use the rigorous attenuation coefficient

$$\delta = -\left[\frac{\phi''\uparrow + \phi''\downarrow}{2h\tan\psi_1'}\right] \qquad 4.78$$

This is log reflection magnitude divided by horizontal cycle length, using only the real part of angle to calculate cycle length, but complex angle to determine reflection coefficient magnitude. The quantities are determined as eigenangle and reflection coefficient magnitude while solving for poles of the complex characteristic equation.

We have also shown an intuitive form

$$\delta_{INT} = -\frac{1-e^{-\phi''}}{L} = -\frac{\left[1-e^{-\phi''}\right]}{2h\tan\psi_1'} \qquad 4.79$$

This is in fact reflection loss divided by horizontal cycle length.

4.5.1 Comparison with Ingenito and Wolfe:

Ingenito (20) essentially follows the approach Freehafer used for EM modes in the atmosphere. Initially the propagation constant in the bottom is assumed complex. Separate wave equations are written for both ocean and the bottom. Complex conjugate equations are written as well and cross multiplied by conjugate eigenfunctions. The pairs of equations are subtracted for both layers and integrated over the depth of the layer. The boundary conditions are used to write a single integral equation involving the complex horizontal propagation number and the eigenfunction integral

$$(\bar{k}_n^2 - k_n^2)\left[\rho_1\int_0^1 |V_n^{(1)}|^2 d\xi + \rho_2\int_1^\infty |V_n^{(2)}|^2 d\xi + (\beta_2^2-\beta_1^2)\rho_2\int_1^\infty |V_n^{(\omega)}|^2 d\xi = 0\right] \qquad 4.80$$

where

$$\beta_1 = \frac{\omega}{c_1(\xi)} \qquad \beta_2 = \frac{\omega}{c_2(\xi)} + i\epsilon$$

When K_n is written as $K_n = k_n + i\delta_n$ the modal attenuation coefficient δ is solved for

$$\delta_n = \epsilon \frac{\omega}{c_2 k_n} \left| \frac{\rho_2 \int_1^\infty |V_n^{(2)}|^2 \, d\xi}{\rho_1 \int_0^1 |V_n^{(1)}|^2 \, d\xi + \rho_2 \int_1^\infty |V_n^{(2)}|^2 \, d\xi} \right| \qquad 4.81$$

For $\frac{\omega}{c_2} >> \epsilon$, to a good degree of approximation

$$\delta_n \approx \epsilon \left(\frac{\omega \rho_2}{c_2 k_n} \right) \int_1^\infty \left[U_n^{(2)}(\xi)^2 \right] d\xi \qquad 4.82$$

Physically this solution is appealing. Loss occurs in the bottom leading to a net power flow from water to bottom. Per unit horizontal distance, the total power loss for a mode must equal the power lost in the bottom by that mode. The ratio of attenuation coefficients (modal and bottom) is inversely proportional to the ratio of respective powers. Freehafer using similar equation manipulation derives an expression whose denominator is the horizontal cycle length.

In Ingenito and Wolfe (21) a perturbation solution is derived in terms of the reflection coefficient at a fluid-solid boundary. The boundary condition is first expressed in terms of the reflection coefficient. An equation connecting the imaginary part of the eigenvalue (their mode attenuation coefficient) with boundary values of the eigenfunction and its derivative is then derived as in Ingenito (20). This equation is expressed in terms of the reflection coefficient and a perturbation analysis yields the attenuation coefficient in terms of the unperturbed quantities. This is the attenuation coefficient we will use for comparison, substituting the reflection coefficient at a dissipative liquid boundary where they treat the case of an elastic nondissipative boundary.

Ingenito's basis equation is

$$\delta = \rho_1 \frac{u_0^2(H)}{8 k_0} \chi_0 \left[1 + \left(\frac{\rho_1 \gamma_0}{\rho_2 \chi_0} \right)^2 \left[1 - |R(k_0)|^2 \right] \right] \qquad 4.83$$

and normalization

$$\rho_1 \int_0^H u_0^2(z)\, dz + \rho_2 \int_H^\infty V_0^2(z)\, dz = 1 \qquad 4.84$$

is made, where he gives the following quantities with sound speed constant through the water column and the bottom.

$$u_0(z) = N \sin(\chi_0 z) \qquad 4.85$$

$$V_0(z) = C e^{-\gamma_0 z} \qquad 4.86$$

$$\chi_0 = \left(\frac{\omega^2}{c_1^2} - k_0^2 \right)^{1/2} \qquad 4.87$$

$$\gamma_0 = \left(k_0^2 - \frac{\omega^2}{c_2^2} \right)^{1/2} \qquad 4.88$$

with reflection coefficient

$$R_0 = -e^{+2i\Psi_0} \qquad 4.89$$

$$\tan \Psi_0 = \frac{\rho_2 \chi_0}{\rho_1 \gamma_0} \qquad 4.90$$

Here

$u_0^2(H)$ is the mode shape squared at the bottom

χ_0 is vertical wavenumber in the ocean

γ_0 is vertical wavenumber in the bottom

k_0 is horizontal wavenumber

ρ_+ and ρ_- are densities in the ocean and bottom respectively

$\epsilon = \left[1 - |R(k_0)|^2\right]$ represents an energy loss per reflection

All the quantities above are calculated using unperturbed solution values for ω , φ_1' , i.e. eigenvalues for the nondissipative problem. The reflection coefficient (we use in our implementation of his fomula) is obtained as the reflection coefficient in our first dissipative iteration when the bottom is absorbing, but the imaginary part of angle is 0 in the water column, (corresponding to the eigenvalues for the phase equation with real angles).

For the mode shape in $u(H)$ we use the mode shape from chapter 2 for the isovelocity layer

$$S(z) = |\Phi(z)| \qquad 4.91$$

i.e. for the Pekeris model when the reflection coefficient is $R = e^{i2\Theta}$

we get $S(z) = 2A\cos(k_{0z}\cos\varphi - \Theta)$ in our notation 4.92

or $S(z) = 2A\cos\left(\frac{\omega}{c_1} z\cos\varphi - \psi_0 + \pi\right)$ in his .

The critical step in applying Ingenito's result is the normalization to obtain A. Since our mode shape was derived for model 1 (see figure 1.1) with one layer and the surface at z=-H, the correct normaligation is

$$\rho_1 \int_{-H}^{0} S_1^2(z)\, dz + \rho_2 \int_{0}^{\infty} S_2^2(z)\, dz = 1 \qquad 4.93$$

We note right here difficulty in extending the Ingenito expression to leaky modes since the normalization integral will diverge. In the halfspace 2 the mode shape is $S(z) = |\tilde{T} A \exp(-\gamma z)|$

with $\tilde{T} \equiv$ complex transmission coefficient. 4.94

$$\gamma = k_1 \sqrt{\sin^2 \varphi_1 - N^2} = \frac{\omega}{c_1} \sqrt{\sin^2 \varphi_1 - N^2} \qquad 4.95$$

The transmission coefficient is given by

$$T = \frac{\rho_2}{\rho_1} \cdot \frac{2 Z_2}{Z_1 + Z_2} = \frac{2 \rho_1 \cdot c_2 \cdot \cos \varphi_1}{\rho_2 c_2 \cos \varphi_1 + \rho_1 c_1 \cos \varphi_2} \qquad 4.96$$

so that beyond the critical angle where

$$\tilde{\varphi}_2 = \frac{\pi}{2} + i \varphi_2'' \qquad \text{and} \qquad \varphi_2'' < 0$$

we have

$$\tilde{T} = \frac{2 \rho_1}{\rho_2} \frac{c_2 \cos \varphi_1}{\rho_2 c_2 \cos \varphi_1 - i \rho_1 c_1 \sinh \varphi_2''} \qquad 4.97$$

Using the refraction law we get

$$|T| = \frac{2 \rho_1 c_2 \cos \varphi_1}{\left[(\rho_2 c_2 \cos \varphi_1)^2 + \left(\rho_1 c_2 \sqrt{\sin^2 \varphi_1 - N^2} \right) \right]^{1/2}} \qquad 4.98$$

At the critical angle this becomes

$$|T| = \frac{2 \rho_1}{\rho_2}$$

Performing the integrals we find

$$\rho_2 \left[A |T| \right]^2 \int_0^\infty e^{-\gamma_{23} z} dz = \frac{\rho_2 A^2 |T|^2}{2 \frac{\omega}{c_1} \sqrt{\sin^2 \varphi_1 - N^2}} \qquad 4.99$$

and the contribution from the layer itself

$$\rho_1 \int_{-H}^{0} S_1^2(z)\, dz = \rho_1 A^2 \int_{-H}^{0} (2\cos(k_1 z \cos\varphi - \Theta))^2\, dz$$

$$= 4\rho_1 A^2 \left\{ -2\cos\Theta \sin\Theta \left[\frac{\sin^2 k_1 \cos\varphi_1 H}{2 k_1 \cos\varphi_1} \right] + \right.$$

$$\left. \cos^2(\Theta) \left[\frac{H}{2} + \frac{\sin 2k_1 \cos\varphi_1 H}{4 k_1 \cos\varphi_1} \right] + \sin^2\Theta \left[\frac{H}{2} - \frac{\sin 2k_1 \cos\varphi_1 H}{4 k_1 \cos\varphi_1} \right] \right\}$$

4.100

4.99 and 4.100 are solved for A^2 which is used in $S^2(z)$ in Ingenito's coefficient.

4.5.2 Comparison with Brekhovskikh

Brekhovskikh provides asymptotic approximations for attenuation coefficients, for low order modes i.e. small ℓ or kh large, solutions will have small grazing angle α_ℓ . Then Brekhovskikh expands the reflection coefficient exponent in terms of angle α

i.e. $R_1(\varphi) = -\exp\left[i\Phi_1(\varphi)\right]$ $\quad R_2(\varphi) = -\exp\left[i\Phi_2(\varphi)\right]$

at the lower boundary

$$R_1(\varphi) = \frac{m_1 \sin\alpha - \sqrt{N_1^2 - \cos^2\alpha}}{m_1 \sin\alpha + \sqrt{N_1^2 - \cos^2\alpha}} \qquad 4.101$$

$$N_1 = \frac{k_2}{k_1} = \frac{c_1}{c_2} \qquad m_1 = \frac{\rho_2}{\rho_1}$$

expansion of $R_1(\alpha)$ in a power series in α neglecting terms of order α^3 has the form

$$R_1(\alpha) = -\left[1 - 2\rho_1\alpha + 2\rho_1^2\alpha^2 + \dots\right] \qquad 4.102$$

with $\rho_1 = \frac{m_1}{\sqrt{N_1^2 - 1}}$. To second order $R_1(\alpha) = -e^{-2\rho_1 \alpha}$

so that $\Phi_1 = 2i\rho_1\alpha$. The characteristic equation to first order is

$$2k_1 h \sin\alpha + 2i(\rho_1 + \rho_2)\alpha = 2\pi l \qquad 4.103$$

and for small α

$$\alpha_l = \frac{\pi l}{k_1 h + i(\rho_1 + \rho_2)} \qquad 4.104$$

or with $k_1 h$ large

$$\alpha_l \approx \frac{\pi l}{k_1 h} - i\frac{\pi l}{(k_1 h)^2}(\rho_1 + \rho_2) \qquad 4.105$$

Then the quantity Δl which determines the attenuation will be

$$\Delta_l = \frac{\pi l}{(k_1 h)^2} Re(\rho_1 + \rho_2) \qquad 4.106$$

To see how this quantity actually determines the attenuation Brekhovskikh takes expression Brek. 27.21 for the field of normal modes

$$\varphi = \int \Phi(\varphi) H_0^{(1)}(k_1 r \sin\varphi) \sin\varphi \, d\varphi = 2\pi i \sum Res[\Phi(\varphi)] \cdot H_0^{(1)}(kr\sin\varphi)\cdot\sin\varphi\, d\varphi + \int_{i\infty}^{A_1+} + \int_{i\infty}^{A_2+} \qquad 4.107$$

The first term is the sum of residues of the integrand at poles encompassed during deformation of the path. The last two integrals are over borders of cuts beginning at the points $\varphi = \sin^{-1}N_1$ $\varphi = \sin^{-1}N_2$ and going along lines $Im\sqrt{N_1^2 - \sin^2\varphi} = 0$ and $Im\sqrt{N_2^2 - \sin^2\varphi} = 0$. Brekhovskikh assumes no accumultion points of poles in the finite region of the φ plane. He states that it can be shown that poles in

the remote regions are equidistantly situated on a line asymptotically approaching the imaginary axis. (See our figure 5.5 for pole locations) The residues are determined by replacing the denominator by multiplying the result by $2\pi i$ and summing over ℓ. From the characteristic equation Brekhovskikh can show that

$$\left(\frac{df}{d\varphi}\right)_{\varphi_\ell} = -\left(\frac{1}{R_1}\frac{dR_1}{d\varphi} + \frac{1}{R_2}\frac{dR_2}{d\varphi} - 2ikh\sin\varphi\right)_{\varphi_\ell} \qquad 4.108$$

Then assuming $k_1 h$ large and with the asymptotic form of the Hankel function he gets

$$\psi = \frac{1}{h}\sqrt{\left(\frac{\pi}{2k_1 r}\right)}\exp\left(i\frac{\pi}{4}\right)\sum_{\ell=1}^{\infty}\left[\exp(-b_\ell z) + R(\varphi_\ell)\exp(b_\ell z)\right]\times$$

$$\left[\exp(-b_\ell z_0) + R_1(\varphi_\ell)\exp(b_\ell z_0)\right]\frac{\exp(ik_1 r\sin\varphi_\ell)}{R_1(\varphi)\sin^{1/2}\varphi_\ell} \qquad 4.109$$

Then if $\Delta_\ell h$ is small 27.42 can be simplified

$$\cos\varphi_\ell \approx \frac{\pi\ell}{k_1 h} \qquad b_\ell \approx i\frac{\pi\ell}{h} \qquad 4.110$$

everywhere in 27.42 except in the exponent $\exp(ikr\sin\varphi)$ where the imaginary part of φ must be taken into account. So with

$$\varphi_\ell \approx \arccos\frac{\pi\ell}{kh} + i\Delta\ell \qquad 4.111$$

and

$$\sin\varphi_\ell = \sqrt{1-\left(\frac{\pi\ell}{k_1 h}\right)^2} + i\frac{\pi\ell}{k_1 h}\Delta\ell \qquad 4.112$$

Brekhovskikh gets

$$\psi = \frac{1}{h}\sqrt{\frac{\pi}{2k_1 r}}\exp\left[i\frac{\pi}{4}\right]\sum_{l=1}^{\infty}\left[\exp\left(-i\frac{\pi l z}{h}\right) + R_1(\varphi_l)\exp\left(i\frac{\pi l z}{h}\right)\right]$$

$$\exp\left[\left(-i\frac{\pi l z_0}{h}\right) + R_1(\varphi^0)\exp\left(i\frac{\pi l z_0}{h}\right)\right] \propto \frac{\exp\left(ik_1 r \sin\varphi_l^0\right)}{R_1(\varphi_l)\sin^{1/2}\varphi_l^0}\exp\left(-\frac{\pi l}{h}\right)\Delta$$

4.113

So the amplitude of the normal wave decreases as

$$\frac{1}{\sqrt{r}}\exp\left[-\left(\frac{\pi l}{h}\right)\Delta_l r\right]$$

The assumptions made in getting to this point were

1. Expansion of $R_1(\varphi)$ to α^2 to get 27.33
2. $\sin\alpha \approx \alpha$ to get 27.38
3. kh large to get 27.39 and 27.42
4. Asymptotic form of Hankel function
5. $\Delta_l h$ small

Combining 27.40 and 27.43 we see that modal attenuation as we have defined it (i.e. $\exp(k_x'' \cdot x)$) will be

$$k_x'' = \frac{\pi l}{h}\cdot\Delta l = \frac{\pi l}{h}\cdot\frac{\pi l}{(k_1 h)^2}\cdot R_e(\rho_1 + \rho_2)$$

4.114

$$\rho_1 = \frac{m_1}{\sqrt{N_1^2 - 1}} \qquad \rho_2 = \frac{m_2}{\sqrt{N_2^2 - 1}}$$

In our model $m_2 = 0 \implies \rho_2 = 0$

The index of refraction is complex

$$N_1 = \frac{c_1^{\sim}}{c_2^{\sim}} = \frac{c_1}{c_2}\left[1 + i\frac{k_2''}{\omega}\cdot c_1\right] \qquad \text{since } k_1'' = 0$$

so

$$N_1^2 = \left(\frac{c_1}{c_2}\right)^2 \left[1 - \left(\frac{k_L''}{\omega} c_L\right)^2 + \frac{2i k_L''}{\omega} \cdot c_L\right] \qquad 4.115$$

and

$$p_1 = \frac{m_1}{\sqrt{\frac{c_1^2 - c_2^2}{c_L^2} - \left(\frac{k_L'' c_1}{\omega}\right)^2 + \frac{2i k_L'' \cdot c_1^2}{\omega \cdot c_L}}} \qquad 4.116$$

We get

$$Re[p_1] = \frac{m_1}{\left(p_r^2 + p_i^2\right)^{1/4}} \cdot \cos\left(\frac{\tan^{-1}\left(\frac{p_i}{p_r}\right) + \frac{\pi}{2}}{2}\right) \qquad 4.117$$

with

$$p_i = \frac{2 k_L'' \cdot c_1^2}{\omega c_L} \qquad p_r = \frac{c_1^2 - c_L^2}{c_L^2} - \left(\frac{k_L'' c_1}{\omega}\right)^2$$

So the attenuation coefficient is

$$\left(\frac{\pi \ell}{k_1}\right)^2 \cdot \frac{1}{h^3} \cdot Re[p_1] \equiv \delta_{BR} \qquad 4.118$$

Brekhovskikh also offers an attenuation coefficient approximation for higher order modes where $\ell >> 1$ With $|\phi| \leq 2\pi$ he neglects ϕ to get a first approximation to the grazing angle of

$$\alpha_\ell^{(1)} = \sin^{-1}\left(\frac{\pi \ell}{k_1 h}\right) \qquad 4.119$$

Substitution then gives the second approximation

$$\alpha_\ell = \sin^{-1}\left[\frac{\pi\ell}{k.h} - \frac{\phi(\alpha_\ell^{(1)})}{2kh}\right] \qquad 4.120$$

$$\alpha_\ell \cong \sin^{-1}\frac{\pi\ell}{k.h} - \frac{\phi(\alpha_\ell^{(1)})}{2\sqrt{(k.h)^2-(\pi\ell)^2}}$$

and since $\phi_{.1}(\ell) = -i\ln(-R_{.1}) \qquad \phi = -\ln R_{.1}R_2$

4.121

$$\alpha_\ell \approx \sin^{-1}\frac{\pi\ell}{kh} \qquad 4.122$$

The attenuation of his normal modes is given by $\Delta\ell = \mathrm{Im}\,\alpha_\ell$

so $$\Delta\ell = \frac{-\ln|R_{.1}(\alpha_\ell^{(1)})\,R_2(\alpha_\ell^{(1)})|}{2\sqrt{(k.h)^2-(\pi\ell)^2}} \qquad 4.123$$

We are puzzled however by his assumption that $|\phi| \leq 2\pi$

since we have found reflection coefficient phases in the hundreds of radians for modal 2a and Brekhovskikh himself gives the asymptotic formula (for large Bessel argument (i.e. for angles not to near grazing at the top of the N^2-linear layer))

$$\phi = \frac{4k_0}{3g}\cos^3\varphi - \frac{\pi}{2} \qquad 4.124$$

The modulo 2π operation should be accounted for in the mode number.

Brekhovskikh also states that his formulas are applicable for ℓ=1, 2, 3.... We, however, calculate modal dispersion and attenuation values for modes ℓ=0, 1, 2, 3... with ℓ=0 corresponding to the fundamental mode. The difference arises as follows. Since

$$R = \frac{m_1 \sin\alpha - \sqrt{N_1^2 - \cos^2\alpha}}{m_1 \sin\alpha + \sqrt{N_1^2 - \cos^2\alpha}} \qquad 4.125$$

it can be expanded to first order in α as

$$R = -\left[1 - 2\rho_1\alpha + 2\rho_1^2\alpha^2 - \dots\right] \qquad 4.126$$

Now we have a choice of using either $R = -e^{i\phi_1}$ as Brekhovskikh and others have done, or $R = +e^{i\phi_1}$ as we have done. Writing R to first order as $R = -e^{-2\rho_1\alpha}$ lets us identify in these two cases either

$$\phi_1 = i\,2\rho_1\alpha \qquad \text{or} \qquad \phi_1 = \pm\pi + 2i\rho_1\alpha$$

Now since at a free surface the phase change is a retardation of $-\pi$ we know from limiting arguments that at the upper surface we will have

$$R_1 = -1 = e^{-i\pi} \quad \text{and} \quad \rho_1 \to 0 \quad \text{since} \quad \rho_1 \to 0$$

Then in case (1) $\phi_1 = 0$ in case (2) $\phi_1 = -\pi$

The characteristic equation in case (1) will be as Brekhovskikh has it

$$2kh\sin\alpha + 2i\rho\alpha + 0 = 2\pi l \qquad 4.127$$

In case two it's

$$2kh\sin\alpha + (2i\rho\alpha - \pi) + (-\pi + 0) = 2\pi l$$

$$\Rightarrow \quad 2kh\sin\alpha + 2i\rho_1\alpha = 2\pi(l+1) \qquad 4.128$$

and here l can start at 0. The two forms will then be equivalent.

4.5.3 Attenuation coefficient from Kornhauser and Raney

We also have formulae from Kornhauser and Raney for direct comparison in the two layer case. K & R assume z dependent solutions of the form

$$\phi_1 = \sin \gamma_1 z \qquad \phi_2 = A e^{-\gamma_2 z} \qquad 4.129$$

in layer and halfspace respectively with

$$k_1^2 = \gamma_1^2 + h^2 \qquad k_2^2 = -\gamma_2^2 + h^2$$

h is the horizontal propagation factor. For real k_1, and k_2 and guided waves both γ_1 and γ_2 are real and γ_2 positive. Invoking the boundary conditions

$$\frac{\partial \phi_1}{\partial z} = \frac{\partial \phi_2}{\partial z} \; ; \quad \rho_1 \phi_1 = \rho_2 \phi_2 \quad \text{at} \quad z = H$$

K & R eliminate A and γ_2 to get equation

$$\gamma_1^2 \left[1 + \left(\frac{\rho_2}{\rho_1} \right)^2 \cot \gamma_1 H \right] = k_1^2 - k_2^2 \qquad 4.130$$

When the lower medium becomes dissipative k_2 becomes complex

$k_2 = \frac{\omega}{c_2} + i\alpha$ The vertical wavenumber in layer two must become complex as indicated in (K & R- 4). Then with $\gamma_2 = a + ib$ and assuming $b << a$ cot is expanded in a Taylor series to first order. The real and imaginary parts of equation (K & R- 4) are separately satisfied and a solution is obtained for b
i.e. from

$$a(a+i2b)\left[1 + \left(\frac{\rho_2}{\rho_1} \right)^2 \cot^2 (aH + ibH) \right] = \left(\frac{\omega}{c_1} \right)^2 - \left(\frac{\omega}{c_2} \right)^2 - \frac{i 2\omega\alpha}{c_2} \qquad 4.131$$

expanding cot and neglecting terms in b^2 they get two equations The real part gives an equation identical with 4. The imaginary part gives

an equation for b.

$$b\left\{\left(\frac{1}{a}\right)\left(\frac{\omega^2}{c_1^2}-\frac{\omega^2}{c_2^2}\right)+aH\left(\frac{\rho_2}{\rho_1}\right)\left(\frac{\omega^2}{c_1^2}-\frac{\omega^2}{c_2^2}-a^2\right)^{1/2}\cdot\left[1+\left(\frac{\rho_1}{\rho_2 a}\right)^2\cdot\left(\frac{\omega^2}{c_1^2}-\frac{\omega^2}{c_2^2}-a^2\right)\right]\right\}=-\frac{\omega\alpha}{c_2} \qquad 4.132$$

The modal attenuation coefficient is taken as the imaginary part of h.

$$Im(h)\cong -ab\left(\frac{\omega^2}{c_1^2}-a^2\right)^{-1/2} \qquad 4.133$$

K & R note that b is directly proportional to α and equals α. (a function of a and ω). The value of a is determined by ω and mode number, so only ω and n need be specified. Defining $X_n = a_n H$

$\beta = \frac{\omega H}{c_1}$ K & R derive the function $F(\eta, \beta)$ such that $Im(h)=\alpha$. $F(\eta, \beta)$ n is mode number. The asymptotic (large β) proportionality for F is

$$F \sim \frac{n^2}{\omega^3 H^3} \quad \text{or} \quad \frac{n^2 \lambda^3}{H^3} \qquad 4.134$$

They provide the formula

$$F(\eta,\beta)=\left(\frac{c_1}{c_2}\right)\left(\frac{\beta}{X_n}\right)\left[\left(\frac{\beta}{X_n}\right)^2-1\right]^{-1/2}\cdot\left\{\left(\frac{\beta}{X_n}\right)^2\left[1-\left(\frac{c_1}{c_2}\right)^2\right]+\left(\frac{\rho_2}{\rho_1}\right)X_n\left[\left(\frac{\beta}{X_n}\right)^2\left(1-\frac{c_1^2}{c_2^2}\right)-1\right]^{1/2}\cdot\left[1+\left(\frac{\rho_1}{\rho_2}\right)^2\cdot\left\{\left(\frac{\beta}{X_n}\right)^2\left(1-\frac{c_1^2}{c_2^2}\right)-1\right\}\right]\right\}^{-1} \qquad 4.135$$

χ_n is the nth solution of

$$\chi_n^2 \left[1 + \left(\frac{\rho_2}{\rho_1} \right)^2 \cot^2 \chi_n \right] = \beta^2 \left(1 - \frac{c_1^2}{c_2^2} \right) \qquad 4.136$$

At cutoff modal attenuation is equal to bottom attenuation. Then $\gamma_2 = 0$ and the wave is a plane wave propagating in the bottom. As β increases above cutoff $F(\eta, \beta)$ decreases rapidly as the fraction of energy carried by the bottom decreases.

4.5.4 Attenuation Coefficient from Bucker

Finally we note that Bucker (1964) has investigated the effect of bottom absorption on the shape of dispersion curves for a variable velocity water layer over an absorbing bottom halfspace. He develops the form of the dispersion equation given by equation (2.41) and comments that for partial reflection the characteristic equation $R\uparrow \cdot R\downarrow = 1$ can not be satisfied. By associating sound energy at a particular frequency and group velocity (and thus mode number) with a ray path he calculates an approximate bottom loss equal to the magnitude of bottom reflection coefficient raised to a power equal to the number of bottom reflections. This reflection coefficient is that for a fluid-solid interface with absorption represented by complex Lame constants $\tilde{\lambda}$ and $\tilde{\mu}$. To facilate calculation of phase shift in bottom reflection he assumes plane wave fronts at the bottom and real propagation number k. This is equivalent to using a real angle of incidence and no dissipation in the water column. Satisfaction of the boundary condition leads to a complex vertical propagation number and a complex reflection coefficient. Reflection coefficient phase when substituted in the dispersion equation connects bottom absorption with group velocity and dramatically effects the shape of the dispersion curves.

In Bucker (1970) sound propagation is more rigorously treated for a channel with lossy boundaries. The surface and bottom halfspace reflection coefficients are not made explicit and the normal mode solution is developed very generally in terms of the Helmholtz solution functions $U(z)$ and $V(z)$ satisfying surface and bottom

boundary conditions respectively. Bucker indicates forms of intermediate layer solution f and g (e.g. for constant velocity profile, N^2-linear, parabolic, Potter Murphy and Epstein profiles) and requires solution of 2m-2 interface boundary condition equations to determine the f and g coefficients which will comprise solution U(z) and V(z). He mentions that iteration techniques must be used to determine eigenvalues k_n and suggests use of the ray-mode analogy to determine starting values for Re(kn) and Im(kn). His ray-mode analogy is to associate the mode and ray having the same horizontal phase velocity.

$$c_n'(\text{ray}) = \frac{\omega}{Re(k_n)}(\text{mode}) \cong Re(c_n)(\text{mode}) \qquad 4.137$$

An estimate of the imaginary part of the kn is made by noting that the mode attenuation is due to boundary loss so that

$$Im(k_n) \approx (SL_n + BL_n) / 8.686\, H_n \qquad 4.138$$

with

SL_n surface loss in dB

BL_n bottom loss in dB

H_n ray horizontal cycle distance.

The conditions for ray constructive interference is again equation 2.41. He presents calculations for a particular shallow water channel whose velocity profile includes both surface duct and modes reflecting at bottom surface and bottom. Plots are presented of Im(cn) versus Re(cn) for ray mode analogy solutions and exact solutions. Exact solutions are solutions to a dispersion equation he develops in terms of generalized solutions to U and V.

i.e. $w(kn)=0$ where $w=U(z_o)\,V'(z_o) - U'(z_o)\,V(z_o)$

and

$$\phi = \frac{-i2\pi \sum_n V_n(z_o) U_n(z) k_n H_0^{(1)}(kr)}{\left[\frac{2\omega(k)}{dk}\right]_{k=k_n}} \qquad 4.139$$

is the sum of residues solution. The point source is a depth z . The thrust of the paper is that of the modal field may be expressed as

$$\psi = \left(\frac{2\pi}{r}\right)^{1/2} \sum \Phi_n(z_0)\,\Phi_n(z)\,\exp(i k_n r)/k_n^{1/2}\,N_n \qquad 4.140$$

where

$$N_n = \int_0^{z_b} \Phi_n^2(z)\,dz + \Gamma_n$$

and

$$\Gamma_n = \left[u_n^2(0)\left(\frac{d\rho}{dk}\right)_{0,k_n} - u_n^2(z_b)\left(\frac{dz}{dk}\right)_{z_b,k_n}\right]/2k_n$$

for a surface duct with zb the lower turning point and

$$\frac{dv}{dz} \equiv \rho v \quad \text{and} \quad \frac{dV}{dz} \equiv \eta V \qquad 4.141$$

The advantage of this formulation is that modal excitation is given by a function defined between channel boundaries rather than for $0 < z < \infty$ Implicit in the development is the ability to include complex propagation constant kx in the layer boundary equations and to determine a halfspace reflection coefficient for lossy halfspaces. Elaboration on these points (of the type presented in our thesis) is required for implementation, and Bucker has presumably done this at least for the shallow water example given.

Appendix: Equivalence of the accepted period equation and the period equation from Kornhauser and Raney.

Eigenvalues used in the Kornhauser and Raney attenuation coefficient given on page 4.28 are solutions to equation K & R- 4. Eigenvalues used in the computer implementation are solutions to the phase characteristic equation

$$2 k_{1,3} \cdot H + \Phi'\uparrow + \Phi'\downarrow = n 2\pi \qquad n=0,1,2$$

4A.1

The reflection coefficient for a two layer system

$$R = \frac{Z_2 - Z_1}{Z_2 + Z_1} \qquad \text{with} \qquad Z = \frac{\rho c}{\cos \varphi} \qquad 4A.2$$

gives

$$R = \frac{m \cos \varphi_1 - \sqrt{N^2 - \sin^2 \varphi_1}}{m \cos \varphi_1 + \sqrt{N^2 - \sin^2 \varphi_1}} \qquad m \equiv \frac{\rho_2}{\rho_1} \qquad N \equiv \frac{c_1}{c_2} \qquad 4A.3$$

Now with refraction law

$$\frac{c_1}{\sin \varphi_1} = \frac{c_2}{\sin \varphi_2} \qquad \text{we have} \qquad \sin \varphi_1 = \frac{c_1}{c_2} \sin \varphi_2$$

Beyond the critical angle where $\sin \varphi_1 > \frac{c_1}{c_2}$

$$R = \frac{m \cos \varphi_1 - i \sqrt{\sin^2 \varphi_1 - N^2}}{m \cos \varphi_1 + i \sqrt{\sin^2 \varphi_1 - N^2}} \qquad 4A.4$$

and $$\phi' \downarrow = -2 \tan^{-1} \left[\frac{\sin^2 \varphi_1 - N^2}{m \cos \varphi_1} \right], \quad \phi' \uparrow = -\pi$$

4A.5

The characteristic equation is then

$$2 k_{1,3} \cdot H - 2 \tan^{-1} \frac{\sqrt{\sin^2 \varphi_1 - N^2}}{m \cos \varphi_1} - \pi = 2m\pi$$

$$\Rightarrow 2 k_{1,3} \cdot H - (2m+1)\pi = 2 \tan^{-1} \left[\frac{\sqrt{\sin^2 \varphi_1 - N^2}}{m \cos \varphi_1} \right]$$

4A.6

now with

$$\tan\left[k_{1,j}\cdot H-(2m+1)\frac{\pi}{2}\right]=\frac{\tan k_{1,j}\cdot H-\tan\frac{\pi}{2}}{1+\tan k_{1,j}\cdot H\cdot\tan\frac{\pi}{2}}$$

$$=-\cot k_{1,j}\cdot H \qquad 4A.7$$

and

$$\tan\left[k_{1,j}\cdot H-(2m+1)\frac{\pi}{2}\right]=\frac{\sqrt{\sin^2\varphi_1-N^2}}{m\cos\varphi_1} \qquad 4A.8$$

we have

$$-\frac{\rho_2}{\rho_1}\cot k_{1,j}\cdot H=\frac{\sqrt{\sin^2\varphi_1-N^2}}{\cos\varphi_1}=\frac{\frac{c_1}{c_2}\sqrt{\frac{c_2^2}{c_1^2}\sin^2\varphi_1-1}}{\cos\varphi_1}$$

$$=\frac{\frac{\omega}{c_2}\sqrt{\frac{c_2^2}{c_1^2}\sin^2\varphi_1-1}}{\frac{\omega}{c_1}\cos\varphi_1}=\frac{\sqrt{k_1^2\sin^2\varphi_1-k_2^2}}{k_{1,j}}$$

$$=\frac{\sqrt{k_1^2-k_{1,j}^2-k_2^2}}{k_{1,j}^2} \qquad 4A.9$$

$$\Rightarrow\quad k_{1,j}^2\left[1+\left(\frac{\rho_2}{\rho_1}\right)^2\cot^2\left(k_{1,j}\cdot H\right)\right]=k_1^2-k_2^2$$

Chapter 5 Observations and Computational Results:

5.1 Introduction
5.2 Reflection coefficient for real incidence angle
5.3 Reflection coefficient for complex incidence angle
5.4 Snell equations: Details and observations
5.5 Summary of observed behaviour of the reflection coefficient and of the Snell algorithm
5.6 Analysis of R , refracted angle discontinuity
5.7 Comments of angle trajectories
5.8 Reflection coefficient phase behaviour
5.9 Dispersion results
5.10 Attenuation coefficient results
5.11 Sensitivity
5.12 Numerical difficulties

Chapter 5- Observations and computational results

5.1 Introduction

The algorithm outlined in chapter 3 has been implemented in Fortran 4 on an HP2100 minicomputer with 32K core memory and disc storage. A segmented computer code was required because of program length and so that several operations could be performed for the same input model parameters and modal solutions. Central to the determination of modal dispersion and attenuation characteristics is calculation of the reflection coefficient at the ocean bottom. We discuss below issues involved in choosing propagated angles, and determining the reflection coefficient and eigenangles for the Pekeris guide. The algorithm developed here, and for which a computer listing is provided in the appendix, handles multilayer complex waveguides as well, but results are insufficient at thus point to comment on its behaviour for those waveguides.

In developing wave representation in terms of complex angle and complex wavenumber it was noted that the mapping from incidence angle domain to wavenumber domain is nonunique and that multiple angle roots exist for the phase velocity equation 3.59. Additionally we have seen that Riemann sheets exist in the complex wavenumber space, corresponding to values of $\mathrm{Im}\left[k_3\right]$ greater or less than zero. Solution of the equation sets 3.143 to 3.151 involved in our dispersion algorithm, required that restrictions be placed on the incidence angle domain in order to preserve continuity in reflection coefficient and characteristic equation functionals. We begin this chapter by examining the form of the reflection coefficient for the dissipative Pekeris guide when incidence angle in the source layer is real. Then when incidence angle in the source layer is allowed to become complex we examine separately situations in which the underlying medium is nondissipative ($k_L''=0$) and when it is dissipative ($k_L''\neq 0$). In the first case we find that allowing the transmitted angle to go to real values $> \frac{\pi}{2}$ may give reflection coefficients of magnitude >1. In order to get reflection coefficients of magnitude <1 we find that the real transmitted angles may be $< \frac{\pi}{2}$, but that the imaginary transmitted angle could then be >0 with the implication of growing

wave in the bottom halfspace. Both circumstances present us with non physical solutions, which is the apparent dilemma of the complex angle representation. For the situations in which the bottom is absorbing and $k_2'' \neq 0$ we examine all possible combinations of complex angles in both layers, and note the effect on the magnitude of the reflection coefficient. A necessary condition for solution of the characteristic equation is found to be $|R| < 1$ when the imaginary part of incidence (φ_1'') angle is > 0 , or $|R| > 1$ when the imaginary part of incidence angle is < 0 . Since the integration contour indicated in chapter 2 is in the upper half complex incidence angle plane we seek combinations of incident and propagated angles such that $|R| < 1$.

Consideration is next given to solution of the refraction law equations and the particular algorithm we have implemented to solve them. We first look for conditions on the transmitted angle $\tilde{\varphi}_2$, such that an initial approximation for $\tilde{\varphi}_2$ may be calculated at any layer, in order to start the iterative procedure. We find that the sign of the transmitted imaginary angle cannot be delimited on this basis. Similarly, we find that the domain of $\tilde{\varphi}_2$ cannot be determined by simply requiring each side of the refraction law equation to be > 0 , as they are for the source layer, where $\varphi_1' < \frac{\pi}{2}$ and $\varphi_1'' > 0$. We must examine more closely the refraction laws. When the incident angle $\tilde{\varphi}_1$ is real we find that $\varphi_2' < \frac{\pi}{2}$, $\varphi_2'' < 0$ is a compatible solution. When the incident angle is complex with $\varphi_1'' > 0$ we seek conditions which might allow φ_2' to go to "critical refraction" at $\frac{\pi}{2}$, and also conditions which would allow φ_2'' to become > 0 . We show two limiting cases for which φ_2'' could be > 0 and < 0 . Conditions are then determined for the "speculative angle $\varphi_{1_{spec}}$" at which transition occurs from growing to decaying waves in layer 2.

With this preliminary viewing of the refraction laws and reflection coefficients we are better prepared to understand the results of our computational algorithm. When the physical constraint of transmitted angle $\varphi_2' < \pi/2$ is imposed, discontinuities arise in both the sign of the imaginary part of transmitted angle and the reflection coefficient magnitude and phase, as incidence angle

is varied for a fixed phase velocity C_ρ . These discontinuities were great hindrances in getting our iterative equation solvers to converge. The behaviour of the solutions is discussed for several cases of dissipation number. Limiting arguments are then used to show that these discontinuities should in fact exist given the refraction law constraints, and are not artifacts of the program. We summarize the discussion above by discussing the solution trajections for propagated angles as the incident angle is varied along a C_ρ locus. A comparison is made with a complex wavenumber formulation of the problem and position of angle solutions on the Riemann sheets are established corresponding to positive and negative value of kz. This is done in both the locked and leaky region of incidence angles where we encounter respectively "speculative angles" and branch lines. Finally reflection coefficient phase is discussed for "critical reflection" off of dissipative media. It is shown that phase delay is produced by the process.

In the second part of chapter 5 the major results of the thesis are presented. Dispersion curves are drawn for the Pekeris guide and attenuation coefficients determined. We find that as dissipation number is increased in the halfspace poles move into the first quadrant of incidence angle. For any given number k_2'' or incidence angle $\tilde{\varphi}_1$ poles move toward the real φ_1' axis as mode number is increased, but attenuation coefficient increases as mode number increases.

Both eigenangles and eigenfrequencies are slightly perturbed with dissipation, but the major effect is to introduce a finite imaginary part of wavenumber. In addition to the rigorous attenuation coefficient represented by the imaginary part of wavenumber we calculate approximations to modal attenuation coefficients proposed in the literature by various authors. These were developed in chapter 4 and are compared here with the rigorous coefficient. Their shortcomings or suitability are determined. Finally, sensitivity of the modal characteristics to model parameters is discussed along with numerical difficulties involved in their determination.

5.2 Reflection coefficient for real incidence angle

Brekhovskikh has examined the reflection coefficient at a water packed sea sand interface. We need to verify his results for real incidence angle as a check on program perfromance.

With $m \equiv \frac{\rho_2}{\rho_1}$ and $N \equiv \frac{c_1}{c_2}$

he gets

$$R = \frac{m \cos\varphi - \sqrt{N^2 - \sin^2\varphi}}{m \cos\varphi + \sqrt{N^2 - \sin^2\varphi}} \qquad 5.1$$

when $N<1$ and $\sin\varphi > N$ he gets total reflection

$$R = \frac{m \cos\varphi - i\sqrt{\sin^2\varphi - N^2}}{m \cos\varphi + i\sqrt{\sin^2\varphi - N^2}} \qquad 5.2$$

He notes that at total reflection the interface presents a reactive impedance. His graph of $|R|$ versus φ is found in Waves in Layered Media (ref. 1) p. 20. We have programmed magnitude and phase versus complex angle using the formulae in chapter 3 and present it in figure 5.1 for the two layer case with $\varphi_1'' = 0$. There is very close agreement in the form of the curves. We have expanded the scale of phase for angles less than the critical to show the effect of dissipation parameter kz'' not indicated in Brekhovskikh's small figure.

5.3 Reflection coefficient for complex incidence angle

From the reflection coefficient formulae in chapter 3 (section 3.4.5) we can make the following observations, accounting now for non-zero imaginary part of source layer incidence angle φ_1'' . For a non-dissipative layer where k''=0, A and B in equation 3.93 for the reflection coefficient are given by

$$A = \omega \cos\varphi' \cosh\varphi'' \quad ; \quad B = -\omega \sin\varphi' \sinh\varphi''$$

At critical angle of incidence such that propagated angle

$\varphi_2' = \frac{\pi}{2}$, γ_2 defined in equation 3.102 equals zero. Then

$$|R|^2 = \left[(-\gamma_1)^2 + (\delta_2 - \delta_1)^2\right] \Big/ \left[(\gamma_1)^2 + (\delta_2 + \delta_1)^2\right] \qquad 5.3$$

if also the incident angle were real, $\varphi_1'' = 0$, then $\beta_1 = 0$ and $\delta_1 = 0$

and

$$|R|^2 = \left[(-\gamma_1)^2 + (\delta_2)^2\right] \Big/ \left[(\gamma_1)^2 + (\delta_2)^2\right] = 1 \qquad 5.4$$

However for nontotal reflection we will later see that the characteristic equation imposes the requirement of an imaginary part of angle in layer one. If $\varphi_1'' \neq 0$ the reflection coefficient magnitude given in equation 5.2 is not equal to 1. δ_1 and δ_2 will contribute even though, for example, the wave traveled at the "critically refracted angle $\varphi_2' = \frac{\pi}{2}$

Consider now the situation where the propagated angle is permitted to assume values $\varphi_2' > \frac{\pi}{2}$. For $\varphi_2' > \frac{\pi}{2}$, $\cos\varphi_2' < 0$ and

$\gamma_2 > 0$. From equation 3.93 we had

$$|R|^2 = \frac{(\gamma_n - \gamma_m)^2 + (\delta_n - \delta_m)^2}{(\gamma_n + \gamma_m)^2 + (\delta_n + \delta_m)^2} \qquad 5.5$$

If the incident layer 1 $\varphi_1'' > 0$ then $\delta_1 > 0$ since $\beta_1 < 0$. If also in layer 2 $\varphi_2'' < 0$, $\beta_2 > 0 \Rightarrow \delta_2 < 0$, and

$$\frac{(\delta_n - \delta_m)^2}{(\delta_n + \delta_m)^2} > 1$$

The implication is that for γ_1 , $\delta_1 > 0$ (when $0 < \varphi_1' < \frac{\pi}{2}$, and $0 < \varphi_2'' < \infty$) we need γ_2 , $\delta_2 > 0$ in order to get reflection coefficients < 1 .

(This actually is sufficient but not necessary). In order to get $A_2 > 0$, $B_2 > 0$ so $\gamma_2 > 0$, $\delta_2 > 0$ when $k_2'' = 0$ we require

$$\omega \cos\varphi_2' \cosh\varphi_2'' > 0 \Rightarrow \varphi_2' < \frac{\pi}{2} \qquad 5.6$$

$$-\omega \sin\varphi_2' \sinh\varphi_2'' < 0 \Rightarrow \varphi_2'' > 0 \qquad 5.7$$

Then $|R| < 1$. But for $\varphi_1'' > 0$ and $\varphi_2'' > 0$ these waves will grow in both layer and halfspace. We see then that for certain complex incidence angles and combinations of ρ , c , ω we may be faced with two nonphysical criteria for choosing refraction law solutions. We may either constrain propagated angle to be $\varphi' < \frac{\pi}{2}$ and the transmitted wave downgoing, or require $\varphi_2'' < 0$ and the wave decaying, but not both. We will later find, however, that actual locked mode eigenangle solutions to the characteristic equation will have both $\varphi_2' < \frac{\pi}{2}$ and $\varphi_2'' < 0$

When the bounding halfspace is dissipative, $k_2'' \neq 0$, a systematic examination of the reflection coefficient formulae allows us to distinguish regimes of R for possible combinations of

$$\varphi_1'' \gtrless 0 \quad , \quad \varphi_2'' \gtrless 0$$

as shown in the table below.

δ_1 (ocean) < 0 if $\varphi_1'' < 0$

δ_1 (ocean) > 0 if $\varphi_1'' > 0$ since $k''=0$

γ_1 will always be > 0 regardless of the sign of φ_1''

$$\gamma_i = \rho_i \omega c_i \frac{A}{A^2 + B^2} \; ; \quad \delta_i = -\rho_i \omega c \frac{B}{A^2 + B^2}$$

5.8 , 5.9

φ_1''	φ_2''	γ_1	δ_1	A_2	B_2	γ_2	δ_2	$\lvert R\rvert$	Conditions
>0	>0	>0	>0	>0	$C_3<0$	>0	$C_3>0$	<1	C_3
					$C_4>0$		$C_4<0$	$>1, <1$	C_8
>0	<0	>0	>0	$C_1<0$	>0	<0	<0	>1	C_1
				$C_2>0$		>0		$>1, <1$	C_5
<0	>0	>0	<0	>0	$C_3<0$	>0	$C_3>0$	$>1, <1$	C_6
					$C_4>0$		$C_4<0$	<1	
<0	<0	>0	<0	$C_1<0$	>0	<0	<0	$<1, >1$	C_7
				$C_2>0$		>0		<1	

Conditions

C_1 : $\omega \cos\varphi_2' \cosh\varphi_2'' + k_2'' c_2 \sin\varphi_2' \sinh\varphi_2'' < 0$

$\varphi_2'' < 0$

C_2 : $\omega \cos\varphi_2' \cosh\varphi_2'' + k_2'' c_2 \sin\varphi_2' \sinh\varphi_2'' > 0$

C_3 : $k'' c \cos\varphi_2' \cosh\varphi_2'' - \omega \sin\varphi_2' \sinh\varphi_2'' < 0$

$\varphi_2'' > 0$

C_4 : $k'' c \cos\varphi_2' \cosh\varphi_2'' - \omega \sin\varphi_2' \sinh\varphi_2'' > 0$

From the imaginary part of the characteristic equation 3.113 we immediately see that φ_1'' and Φ'' must have the same sign for

$$0 < \varphi_1' < \frac{\pi}{2}$$

Necessary conditions for solution of the characteristic equation in the case $k_1'' = 0$ may then be summarized as follows.

For $\varphi_1'' > 0$ we need $|R| < 1$. This happens when either

C3: δ_1 and δ_2 have the same sign with $\delta_1 > 0$
Also γ_1 and γ_2 have the same sign with $\gamma_1 > 0$
Here $\varphi_1'' > 0$, $\varphi_2'' > 0$. This is the normal condition for leaky modes.

C8: This is the condition C4 plus the requirement that

$$(\gamma_1 - \gamma_2)^2 + (\delta_1 - \delta_2)^2 < (\gamma_1 + \gamma_2)^2 + (\delta_1 + \delta_2)^2$$

C4 states that δ_1 and δ_2 are opposite signs with $\delta_1 > 0$

Also we have here γ_1 and γ_2 the same sign, $\gamma_1 > 0$

$\varphi_1'' > 0$, $\varphi_2'' > 0$

C5: This is condition C2 plus the requirement that

$$(\gamma_1 - \gamma_2)^2 + (\delta_1 - \delta_2)^2 < (\gamma_1 + \gamma_2)^2 + (\delta_1 + \delta_2)^2$$

C2 states that γ_1 and γ_2 are the same sign with $\gamma_1 > 0$

Also here δ_1 and δ_2 are of opposite sign $\delta_1 > 0$

Note $\varphi_2'' > 0$ here, but $\varphi_2'' < 0$. This is the condition of dissipative "locked modes".

For $\varphi_2'' < 0$ we need $|R| > 1$. This happens when

C6: This is condition C3 plus the requirement that

$$(\gamma_1 - \gamma_2)^2 + (\delta_1 - \delta_2)^2 > (\gamma_1 + \gamma_2)^2 + (\delta_1 + \delta_2)^2$$

C3 states that δ_2 and δ_1 are opposite sign with $\delta_1 < 0$

Also, here γ_1 and γ_2 are of the same sign $\gamma_1 > 0$

$\varphi_1'' < 0$, $\varphi_2'' > 0$

C7: This is condition C1 plus the requirement that

$$(\gamma_1 - \gamma_2)^2 + (\delta_1 - \delta_2)^2 > (\gamma_1 + \gamma_2)^2 + (\delta_1 + \delta_2)^2$$

with C1 stating that γ_1 and γ_2 are opposite sign with $\gamma_1 > 0$. Also here δ_1 and δ_2 are the same sign $\delta_1 < 0$ with $\varphi_1'' < 0$, $\varphi_2'' < 0$.

We note however that poles for which $\varphi_1'' < 0$ do not contribute to the solution as expressed by Brekhovskikh's contour integral, and our solution set is limited to conditions C3, C8, C5.

5.4 Snell equations, details and observations.

For a nondissipative halfspace and layer, critical angle

may be solved for as

$$\varphi_{1c} = \tan^{-1}\left[\frac{c_1/c_2}{\sqrt{1-(c_1/c_2)^2}}\right] \qquad 5.10$$

The propagated wave travels at $\tilde{\varphi}_2 = \left(\frac{\pi}{2}, 0\right)$. Beyond the critical angle where $\tilde{\varphi}_2 = \varphi_2' + i\varphi_2'' = \frac{\pi}{2} + i\varphi_2''$ the refraction law requires

$$\sin\tilde{\varphi}_1 \frac{c_2}{c_1} = \sin\tilde{\varphi}_2 = \cosh\varphi_2'' \qquad 5.11$$

$$\cos\tilde{\varphi}_2 = -i\sinh\varphi_2''$$

The vertical wavenumber component is imaginary and waves are inhomogeneous in the halfspace.

Slow inhomogeneous incident waves may also be defined at incidence angle $\varphi_1' = \frac{\pi}{2}$. There with

$$c_p = \frac{c_1}{\sin\varphi_1' \cosh\varphi_1''}$$

and for $c_p < c_1$

$$\cosh\varphi_1'' = \frac{c_1}{c_p}$$

The waves will lie along the locus

$$\varphi_1' = \frac{\pi}{2}, \quad \varphi_1'' = \ln\left[\frac{c_1}{c_p} \pm \sqrt{\left(\frac{c_1}{c_p}\right)^2 - 1}\right] \qquad 5.12$$

They form the part of the spherical wave expansion into plane waves which we do not include in a physical formulation of the problem.

In general for $C_p > C_1$, φ_1'' is one of the two roots of

$$\exp(2\varphi_1'') - \frac{2\,C_1}{\sin\varphi_1' \cdot C_p}\exp(\varphi_1'') + 1 = 0 \qquad 5.13$$

i.e.

$$\varphi_1'' = \ln\left[\frac{C_1}{\sin\varphi_1' \cdot C_p} \pm \sqrt{\frac{\left(\frac{C_1}{C_p}\right)^2 - 1}{\sin^2\varphi_1}}\right]$$

$$= \ln\left[\cosh\varphi_1'' \pm \sinh\varphi_1''\right] \equiv \ln\left[X_1\right] \qquad 5.14$$

In the layer 1 C_p formula both signs of φ_1'' are solutions to equation 5.11. The phase velocity expression is insensitive to sign of φ_1'' . Both growing and decaying waves at the same phase velocity travel at the same real incidence angle. Using

$$\cosh = \frac{\left(e^{+\varphi_1''} + e^{-\varphi_1''}\right)}{2} \quad \text{and} \quad \sinh = \frac{\left(e^{+\varphi_1''} - e^{-\varphi_1''}\right)}{2}$$

We see that

$$\varphi_1'' = \ln\left[X_+ \text{ or } X_-\right] \quad \text{with} \quad X_+ \equiv \cosh + \sinh \qquad 5.15$$

$$X_- \equiv \cosh - \sinh$$

X_+ gives $\varphi_1'' > 0$. X_- gives $\varphi_1'' < 0$.

We need a criterion for choosing the sign of angle φ_1'' with which to start the Snell iteration for $\tilde{\varphi}_\ell$. $\ell = 1, 2, 3 \ldots$ given C_p . That criterion will be satisfaction of the characteristic equation in the angle domain of interest for the Brekhovskikh contour, namely $\varphi_1'' > 0$. Then we will seek angles for which $|R| < 1$.

Details of the refraction law calculations were presented in section 3.6.2. We can briefly survey the possibilities of solution for

the angle algorithm we have implemented. Iteration starts with an initial guess at angle $\tilde{\varphi}_2$ calculated as in equation 3.135+. We need to see in what domain of $\tilde{\varphi}_2$ values of $X_2 > 0$ will be possible, since

$$\varphi_2''_{initial} = \ln[X_2] \qquad 5.16$$

and

$$X_2 = \frac{-B \pm \sqrt{B^2 - 4AC}}{2A} \qquad 5.17$$

Here

$$B = -\frac{BLHS}{B4} \qquad A = \frac{B3}{B4} \qquad C = 1$$

$$BLHS \equiv k_1' \cdot \cos\varphi_1' \sin\varphi_1'' + k_1'' \cdot \sin\varphi_1' \cosh\varphi_1''$$

$$B1 \equiv k_2' \cdot \cos\varphi_2' \qquad B2 \equiv k_2'' \cdot \sin\varphi_2'$$

$$B3 \equiv (B1 + B2)/2 \qquad B4 \equiv (B2 - B1)/2$$

Setting k_1'' =0 we look for conditions on φ_2'' . Note that $B1 > 0$, $B2 > 0$, and generally $B1 > B2$ when $0 < \varphi_2' < \frac{\pi}{2}$. So for the case $B1 > B2$, $A < 0$ (since $B3 > 0$ and $B4 < 0$) and $\sqrt{B^2 - 4AC} > B$.

If $BLHS < 0$ a solution is possible since

$$\left(\frac{-B - \sqrt{\quad}}{2A}\right) > 0$$

If $BLHS > 0$ a solution is possible since

$$\left(\frac{-B - \sqrt{\quad}}{2A}\right) > 0$$

For the case $B1 < B2$ and $B1 > 0$, $B2 > 0$ we get $B4 > 0$,

$B3 > 0$, so we have $A > 0$ $C > 0$ $\Rightarrow |B| > \sqrt{B^2 - 4AC}$

If $BLHS < 0$ a solution is not possible, but if $BLHS > 0$ a solution is possible since

$$\frac{-B + \sqrt{B^2 - 4AC}}{2A}$$

Only the situation $B1 < B2$ and $BLHS < 0$ leads to an impossible first guess as we have programmed it, and BLHS will be only for certain values of $\varphi_1'' < 0$, a case we do not treat here.

Secondly with $0 < \varphi_1' < \frac{\pi}{2}$, and setting $\varphi_1'' > 0$

on the basis of the characteristic equation, we need to see in what domain of φ_2 angles might lie so that ARHS (3.110) and BRHS (3.111) will be > 0 (required since ALHS (3.110), BLHS (3.111) in this $\tilde{\varphi}_1$ domain). With dissipation in layer 2 the Snell equation are

(A) $\underbrace{k_1' \sin\varphi_1' \cosh\varphi_1''}_{\equiv ALHS} = k_2' \sin\varphi_2' \cosh\varphi_2'' - k_2'' \cos\varphi_2' \sinh\varphi_2'' \equiv ARHS$ 5.18

(B) $\underbrace{k_1' \cos\varphi_1' \sinh\varphi_1''}_{\equiv BLHS} = k_2' \cos\varphi_2' \sinh\varphi_2'' + k_2'' \sin\varphi_2' \cosh\varphi_2'' \equiv BRHS$ 5.19

ALHS and BLHS are > 0 for $0 < \varphi_1' < \frac{\pi}{2}$, $\varphi_1'' > 0$

Chart of angle domains and resultant ARHS, BRHS of the Snell equation:

φ_2'	φ_2''	A	D	α	B	γ_2	δ_2	ARHS	BRHS
$0 < \varphi_2' < \frac{\pi}{2}$	$0 < \varphi_2'' < \infty$	>0	<0 probably	>0	<0 pr.	>0	>0 pr.	either	>0
$0 < \varphi_2' < \frac{\pi}{2}$	$-\infty < \varphi_2'' < 0$	<0 pr.	>0	<0 pr.	>0	<0 pr.	<0	>0	either
$\frac{\pi}{2} < \varphi_2' < \pi$	$0 < \varphi_2'' < \infty$	<0 pr.	<0	<0 pr	<0	<0 pr	>0	>0	either
$\frac{\pi}{2} < \varphi_2' < \pi$	$-\infty < \varphi_2'' < 0$	<0	<0 pr.	<0	<0 pr.	<0	>0 pr.	either	>0

So we can not eliminate any section within $0 < \varphi_2 < \pi$ on Snell considerations alone. Everything depends on k_2', k_2''. We must examine more closely the refraction law in order to establish criteria for selecting the transmitted angle.

We saw that in the nondissipative case the imaginary part of angle for critical reflection and beyond will be

(with $\varphi_1'' = 0$) $$\varphi_2'' = \ln\left(\left(\frac{c_2}{c_p} \pm \left(\left(\frac{c_2}{c_1} \right)^2 - 1 \right)^{1/2} \right) \right)$$

With dissipation in layer 2 $k_2'' \neq 0$, and if $\varphi_1'' = 0$ solution will be

$$\varphi_2' < \frac{\pi}{2} \quad , \quad \varphi_2'' < 0$$

so that $$k_2' \cos\varphi_2' \sinh\varphi_2'' + k_2'' \sin\varphi_1' \cosh\varphi_2'' = 0 \qquad 5.20$$

In the first Snell equation we require

$$A_{LHS} = A_{RHS} = k_2' \sin\varphi_2' \cosh\varphi_2'' - k_2'' \cos\varphi_2' \sinh\varphi_2'' > 0 \qquad 5.24$$

$\varphi_2' < \frac{\pi}{2}$, $\varphi_2'' < 0$ is a compatible solution.

For the case in which $\varphi_2'' > 0$ $\quad BLHS = k_1 \cos\varphi_1' \sinh\varphi_1'' > 0$

We first consider conditions which might allow φ_2' to stay at $\frac{\pi}{2}$ now that $\varphi_1'' > 0$

From $$k_1' \sin\varphi_1' \cosh\varphi_1'' = k_2' \sin\varphi_2' \cosh\varphi_2'' - k_2'' \cos\varphi_2' \sinh\varphi_2'' \qquad 5.22$$

and $$k_1' \cos\varphi_1' \sinh\varphi_1'' = k_2' \cos\varphi_2' \sinh\varphi_2'' + k_2'' \sin\varphi_2' \cosh\varphi_2'' \qquad 5.23$$

we get

$$\frac{k_2'}{k_2''} = \frac{\sin\varphi_1' \cosh\varphi_1''}{\cos\varphi_1' \sinh\varphi_1''} = \frac{\tan\varphi_1'}{\tanh\varphi_1''} \qquad 5.24$$

φ_2'' and k_1' drop out k_1'' is assumed =0.
Further, for that model and incidence angle combination

$$\cosh\varphi_2'' = \frac{k_1'}{k_2'} \sin\varphi_1' \cosh\varphi_1'' \qquad 5.25$$

or

$$\cosh\varphi_2'' = \frac{k_1'}{k_2''} \cos\varphi_1' \sinh\varphi_1''$$

So if conditions $\check{\varphi}_1$, $\tilde{k}_2$ allow $\varphi_2' = \frac{\pi}{2}$, then k_2', k_2'' being arbitrary, k_1' determines φ_2'' . Examining the terms in this equation we expect

$\frac{\tan\varphi_1'}{\tanh\varphi_1''}$ to be large and $\frac{k_2'}{k_2''} = \frac{\omega}{c_2 k_2''}$ so for

dissipating locked (where $\varphi_1'' \neq 0$) modes $\varphi_2' \rightarrow \frac{\pi}{2}$ as either

$\omega \rightarrow \infty$ or $k_2'' \rightarrow 0$

The equation says that for $\varphi_2' = \frac{\pi}{2}$ if $\varphi_1'' = 0$.

RHS(5.21) blows up and requires either $\omega \rightarrow \infty$ or $k_2'' = 0$.
That is, for $\varphi_2' = \frac{\pi}{2}$, if modes are either nonattenuating

($\varphi_1'' = 0$) or if $\varphi_1' = \frac{\pi}{2}$, then either $\omega \rightarrow \infty$ or $k_2'' = 0$
If modes are attenuating ($\varphi_1'' \neq 0$) then if also $\varphi_1' \neq \frac{\pi}{2}$ neces-

sarily $k_2'' \neq 0$, if the mode is attenuating and if also $\varphi_1' = \frac{\pi}{2}$

then $k_2'' \rightarrow 0$. These issues are raised to clarify behaviour of the Snell algorithm where it was found that for a specified convergence accuracy a range of incidence angles $\tilde{\varphi}_1$ with $\varphi_1'' = 0$ leads to propagated angle $\tilde{\varphi}_2$ with real part $\varphi_2' = \frac{\pi}{2}$.

Equation 5.21 says the relation is unique and the result $\varphi_2' = \frac{\pi}{2}$

for a range of $\tilde{\varphi}_1$ arises either from insufficient accuracy being specified in the Snell algorithm (we use generally convergence to 10^{-5}) or angle solutions $\tilde{\varphi}_2$ being infinitesimally less than $\frac{\pi}{2}$.

We would also like to determine when φ_2'' will be > 0. For $\varphi_2' < \frac{\pi}{2}$ and with $k_1'' = 0$ we look at the limiting cases. We

have equations 5.18 and 5.19 on page 171 . For $\varphi_1'' \rightarrow \infty$ then LHS 5.18 $\rightarrow \infty$, LHS(5.19) $\rightarrow \infty$ and for

$$k_2' \cos \varphi_2' > k_2'' \sin \varphi_2'$$

it is necessary that $\varphi_2'' > 0$ in equation 5.19. Equation 5.18 could also be satisfied because the terms $k_2' \sin \varphi_2' \cosh \varphi_2''$ dominate. For the extreme of k_2'' very large it would be necessary that $\varphi_2'' < 0$. As a result we see that when $\varphi_1'' = 0$ dissipation in layer 2 requires attenuating waves in layer 2 at

$\varphi_2' < \frac{\pi}{2}$ When $\varphi_1'' > 0$ dissipation may lead to $\varphi_2'' > 0$ or $\varphi_2'' < 0$ depending on the relative magnitudes of φ_1'' and k_2''

$$\varphi_1'' >> 0 \Rightarrow \varphi_2'' > 0$$

$$k_2'' >> 0 \Rightarrow \varphi_2'' < 0$$

We can seek the point for $\varphi_1'' > 0$ at which φ_2'' =0 giving the transition from growing to decaying waves. Going to equations 5.18 and 5.19 and setting φ_2'' =0 gives

$$k_1' \sin \varphi_1' \cosh \varphi_1'' = k_2' \sin \varphi_2' \cosh \varphi_2'' \qquad 5.26$$

$$k_1' \cos \varphi_1' \sinh \varphi_1'' = k_2'' \sin \varphi_2' \cosh \varphi_2'' \qquad 5.27$$

and

$$\frac{k_2'}{k_2''} = \frac{\tan \varphi_1'}{\tanh \varphi_1''} \qquad 5.28$$

which is exactly the same equation as for $\varphi_2' = \frac{\pi}{2}$. k_1' and φ_2' fall out above. So at this combination of $\tilde{\varphi}_1$ and $\tilde{k}_2$ φ_2' and φ_2'' can have several values. In particular they can be $\varphi_2' = \frac{\pi}{2}$ and φ_2'' a function of k_1 (as we saw above) or $\varphi_2'' = 0$ and φ_2' a function of k_1 , but not both. To determine the actual value of φ_1' at which $\varphi_2'' \to 0$ we use

$$\frac{k_2'}{k_2''} = \frac{\tan \varphi_1'}{\tanh \varphi_1''} \qquad 5.29$$

and the Cp relation

$$c_p = \frac{c_1}{\sin \varphi_1' \cosh \varphi_1''}$$

and get

$$\tan \varphi_1' = \left[1 - \sin^2 \varphi_1' \left(\frac{c_p}{c_1}\right)^2\right]^{1/2} \cdot \frac{k_2'}{k_2''} \qquad 5.30$$

For k_2'' =0, the nondissipative case, it says $\varphi_1' = \frac{\pi}{2}$ in order for φ_2'' =0. For $k_2'' > 0$ we require

$$1 - \sin^2 \varphi_1' \left(\frac{c_p}{c_1}\right)^2 > 0$$

$$\Rightarrow \quad \sin \varphi_1 \frac{c_p}{c_1} < 1 \qquad 5.31$$

Case 1: choose $c_p = c_2$ (critical angle case) then in order for

$$\sin^2 \varphi_1 \cdot \left(\frac{c_p}{c_1}\right)^2 = \sin^2 \varphi_1 \cdot \left(\frac{c_2}{c_1}\right)^2 = \frac{\sin^2 \varphi_1}{\sin^2 \varphi_{1\,\text{critical}}} < 1$$

it is necessary that $\varphi_1' < \varphi_{1\,\text{critical}}'$

The transition angle is less than the critical angle.

Case 2. $c_p < c_2$ Solutions must be at larger values of φ_1' as Cp decreases, but the domain of φ_1' defined by

$$1 - \sin^2 \varphi_1 \left(\frac{c_p}{c_1}\right)^2 > 0$$

gets bigger too..

Solving for $\varphi_{1\,\text{spec}}'$ itself we get a quartic in $\sin \varphi_1$

$$\sin^4\varphi_1 \cdot Q \cdot P + \sin^2\varphi_1 \left(-P\cdot Q - P - 1\right) + P = 0 \qquad 5.32$$

$$P = \left(\frac{k_2'}{k_2''}\right)^2 \qquad Q = \left(\frac{C_p}{C_1}\right)^2$$

or a quadratic in $X = \sin^2\varphi_1$

$$X = \frac{1 + P + QP}{2QP} \pm \sqrt{\frac{(1+P+QP)^2}{4Q^2P^2} - \frac{4QP^2}{4Q^2P^2}} \qquad 5.33$$

$$\varphi_{1\,spec}' = \tan^{-1}\left(\left(\frac{X}{1-X}\right)^{1/2}\right)$$

We have called this angle the speculative angle. Conditions (model values) do not permit its existance along the phase velocity locus we have defined for $C_p < C_2$, the locked mode region, when the constraint $\varphi_2' < \frac{\pi}{2}$ is imposed. There is instead a discontinuity with $\varphi_1'' < 0$ on one side and $\varphi_1'' > 0$ on the other. $\tilde{\varphi}_{1\,spec}$ does exist in the leaky mode region of incidence angle, $C_p > C_2$. We will choose to eliminate $\varphi_2' > \frac{\pi}{2}$ on physical grounds. In the computer program both domains $0 < \varphi_2'' < \infty$ and $-\infty < \varphi_2'' < 0$ are searched for a solution with $0 < \varphi_2' < \frac{\pi}{2}$. The first solution found is taken. The domain searched first is determined by whether the nondissipative case critical angle has been exceeded, since propagated waves in the underlying medium are expected to have negative imaginary part of angle.

5.5 Summary of observed behaviour of the reflection coefficient and of the Snell algorithm for Cp < C2: (locked modes)

Along any particular locus Cp=constant, for $\varphi_1'' > 0$, we examine cases of low and high attenuation. For low attenuation, say

$k_2'' \leq .001$ nepers/m:

As φ_1' increases*, $|R|$ increases from a value < 1.

φ_2' increases and φ_2'' decreases from a value > 0.

When φ_2' goes to $\frac{\pi}{2}$, φ_2'' flips negative. It will start becoming less negative. $|R|$ goes to > 1 and starts getting closer to 1.

For high attenuation:
After the flip $|R|$ will decrease but be > 1 with $\varphi_2' = \frac{\pi}{2}$ and φ_2'' becoming less negative. φ_2' can come off of $\frac{\pi}{2}$ and $|R|$ still > 1. Eventually $|R|$ may drop to less than 1.

So as attenuation goes up the point of flip to $\varphi_2'' < 0$, $\varphi_2' = \frac{\pi}{2}$ comes at steeper and steeper (smaller) values of φ_1'.

For $\varphi_1'' < 0$ (not included in domain of Brek. contour deformation) we examine cases of low and high attenuation.

For low attenuation say $k_2'' \leq .001$:
As φ_1' increases φ_2' increases, φ_2'' gets more negative, and $|R|$ increases from < 1.

For higher attenuation:
As φ_1' increases there may be a point where φ_2' will drop back a little then continue increasing. φ_2'' will fall to a smaller negative value and then begin to get more negative, where as before the jump it was getting less negative.

* As φ_1' decreases along a $\tilde{\varphi}_1$ locus of constant Cp φ_1'' will increase from its 0 value at the locus limit $\tilde{\varphi}_1 = (\varphi_{1_{lim}}', 0)$.

As attenuation goes up the point of jump occurs at greater and greater values of φ_1' . $|R|$ will jump back but continue to increase although < 1 .

This behaviour is illustrated in figures 5.2 and 5.3.*

5.6 Analysis of magnitude of R discontinuity-refracted angle discontinuity:

We have seen the behaviour of the propagated angle $\tilde{\varphi}_2$ for the case k_2'' finite and φ_1'' =0 (Many authors have used φ_1'' =0, it does not satisfy the complex characteristic equation, however). We saw that solution (of the Snell equations) was at $\varphi_2' < \frac{\pi}{2}$, $\varphi_2'' < 0$. Now as φ_1' and φ_1'' are changed along the locus defined by

$$c_p = \frac{c_1}{\sin \varphi_1' \cosh \varphi_1''}$$

what can we expect of φ_2' , φ_2'' . Should we get the observed discontinuity in φ_2' or φ_2'' or both? Recall the Snell equations we are dealing with for the nondissipative ocean

$$k_1' \sin \varphi_1' \cosh \varphi_1'' = k_2' \sin \varphi_2' \cosh \varphi_2'' - k_2'' \cos \varphi_2' \sinh \varphi_2'' \quad 5.34$$

$$k_1' \cos \varphi_1' \sinh \varphi_1'' = k_2' \cos \varphi_2' \sinh \varphi_2'' + k_2'' \sin \varphi_2' \cosh \varphi_2'' \quad 5.35$$

LHS (5.34) is fixed by the Cp relation. In fact LHS= $\frac{\omega}{c_p} \equiv k(c_p)$ for fixed ω. In 5.35 as φ_1' decreases φ_1'' increases $\Rightarrow$ LHS (5.35) increases.

i.e. $$\frac{d\,(\text{LHS}(5.29))}{d\,\varphi_1'} < 0$$

* In the computation to generate figure 5.2 and table 5.2 frequency was fixed. In the iterative solution ω varies also as $\tilde{\varphi}_1$ is shifted along a contour in search of the eigenvalues $\omega, \tilde{\varphi}_1$. However, $\tilde{\varphi}_{1,\text{spec}}$ is a weak function of ω , and for k_2'' proportional to ω^1 it is independent of ω .

Thus we see that as $\tilde{\varphi}_1$ is brought away from $(\varphi_{1\,lim}', 0)$** along the Cp locus the waves at angle $\tilde{\varphi}_1$ have increasing growth by the same phase velocity. We find that as φ_1' gets less grazing (with Cp held constant) φ_2' will go to $\frac{\pi}{2}$ * with $\varphi_2'' < 0$, and we have shown the angle at which this could occur, namely when in equation 5.34

$$k(C_p) = k_2' \cosh \varphi_2'' \qquad 5.36$$

and in equation 5.35

$$k_1' \cos \varphi_1' \sinh \varphi_1'' = k_2'' \cosh \varphi_2'' \qquad 5.37$$

Now as φ_1', φ_1'' vary, φ_2', φ_2'' will vary so as to increase RHS (5.35) while keeping RHS (5.34) constant. We need to relate the change in φ_2' to change in φ_2'' and then find the point, if any, at which

$$\left.\frac{d(\text{RHS (5.29)})}{d\varphi_2'}\right|_{\varphi_2'' < 0} = 0$$

This should be the point at which a change from $\varphi_2'' < 0$ to $\varphi_2'' > 0$ would be required in order that RHS (5.35) continue to increase as φ_1' decreases. From equation 5.34 we have

$$\cosh \varphi_2'' = \frac{K_p(C_p) + k_2'' \cos \varphi_2' \sinh \varphi_2''}{k_2' \sin \varphi_2'} \qquad 5.38$$

Then in equation 5.35: LHS (5.35) $=$

$$\cos \varphi_2' \sinh \varphi_2'' \left(k_2' + \left(\frac{k_2''}{k_2'} \right)^2 \right) + \frac{k_2''}{k_2'} K_p(C_p) \qquad 5.39$$

The first term on the right in equation 5.35 is negative and gets less negative as φ_1' decreases (φ_2' increases toward $\frac{\pi}{2}$, and the behaviour of φ_2'' is undetermined now). If φ_2' were to get to $\frac{\pi}{2}$

* For fixed φ_1'', say =0, increasing φ_1' will also cause φ_2' to go towards $\frac{\pi}{2}$.

** $\varphi_{1\,lim}'$ is defined as φ_1' (Cp) such that $\varphi_1'' = 0$.

and be constrained there it is clear that φ_2'' must become >0 in order for RHS (5.35) to grow. In the special case when parameter values permit we would reach $\varphi_2' = \frac{\pi}{2}$ so that in equation 5.34

$$K_p(C_p) = k_2' \cosh \varphi_2'' \qquad 5.40$$

and in equation 5.35

$$K_1' \cos \varphi_1' \sinh \varphi_1'' = k_2'' \cosh \varphi_2'' = \frac{k_2'' K_p(C_p)}{k_2'} \qquad 5.41$$

If φ_2' grows toward $\frac{\pi}{2}$ but a maximum is reached in the function RHS (5.35) (under the $\varphi_1', \varphi_1''(Cp)$ constraint and with $\varphi_2'' < 0$) it will be necessary for φ_2'' to become >0 . RHS (5.35) could become less negative by making φ_2'' less negative or by increasing φ_2' . In fact we observe from the computer results that φ_2' increases, but φ_2'' becomes more negative as $\varphi_2' \to \frac{\pi}{2}$, with $\cos \varphi_2' \sinh \varphi_2''$ going to zero. This behaviour is seen to hold in the limiting case of $\varphi_2' \to \frac{\pi}{2}$ where from equation 5.34 the phase velocity constraint, we have

$$\cosh \varphi_2'' = \left[K_p(C_p) + k_2'' \cos \varphi_2' \sinh \varphi_2'' \right] \Big/ \left[k_2' \sin \varphi_2' \right] \qquad 5.42$$

Since the second term in the numerator must be getting less negative (going to zero) in order for RHS (5.35) to grow, the numerator is growing. In the limit of $\varphi_2' \simeq \frac{\pi}{2} - \epsilon$ the denominator is constant, to first order $= k_2'$, so that $\cosh \varphi_2''$ must be growing. Thus φ_2'' is seen to be getting more negative as $\varphi_2' \to \frac{\pi}{2}$. So we see that the discontinuity in solution to the Snell equations arises from the constraint that $0 < \varphi_2' < \frac{\pi}{2}$ and by the locus we have chosen to

follow in setting angles φ_1', φ_1''. The first constraint is based on the radiation condition. For $\varphi_2' > \frac{\pi}{2}$ waves are traveling upward from $z = \infty$ toward the interface. If we relax this constraint we find multiple roots of the Snell equation ($\varphi_2' > \frac{\pi}{2}$, $\varphi_2'' > 0$) and ($\varphi_2' < \frac{\pi}{2}$, $\varphi_2'' < 0$) for values of $\varphi_1' > \varphi_{1\,spec}'$ or ($\varphi_2' < \frac{\pi}{2}$, $\varphi_2'' > 0$) and ($\varphi_2' > \frac{\pi}{2}$, $\varphi_2'' < 0$) for values of $\varphi_1' < \varphi_{1\,spec}'$. These roots lie in the complex $\tilde{\varphi}_2$ plane.

5.7 Comments on angle trajectories

In table 5.2b and figure 5.2c we present the $\tilde{\varphi}_2$ locus of refracted angle as $\tilde{\varphi}_1$ is varied along the locus Cp=1750 m/sec. The speculative angle is seen to occur at $\varphi_1' \approx 1.02965$ radians. For angles $\varphi_1' > \varphi_{1\,spec}'$, $\varphi_2' > \frac{\pi}{2}$ along the locus for which $\varphi_2'' < 0$ When Cp is also taken as a variable these loci form two sheets in $\tilde{\varphi}_2$ space. In figure 5.2.b we illustrate the multiple $|R|$ values corresponding to the $\tilde{\varphi}_2$ loci above, as $\tilde{\varphi}_1$ is varied along $\tilde{\varphi}_1$ ($c_p = 1750$ m/sec). $|R|$ is seen to vary smoothly along either curve and to have values both >1 and <1 as complex incidence angle is varied. If we had an apriori criterion for setting the sign of φ_2'' the iteration routine could be constrained to one sheet ($\varphi_2'' > 0$ or $\varphi_2'' < 0$) and difficulties of convergence through a discontinuity avoided altogether. In implementing the Snell algorithm we felt that the choice $\varphi_2' < \frac{\pi}{2}$ was as reasonable, valid and arbitrary as $\varphi_2'' > 0$ or $\varphi_2'' < 0$ on physical grounds. For the multilayer guide and in the leaky mode region we will find solutions for which $\varphi_2' < \frac{\pi}{2}$ and $\varphi_2'' > 0$, although angles in layer two for which $\varphi_2' > \frac{\pi}{2}$ and $\varphi_2'' < 0$ could just as well have been chosen to satisfy the layer 1, 2 boundary condition.

In a complex wavenumber formulation of this problem leaky modes are defined as modes for which $k_{z_j}'' \geq 0$. That is, if $k_{z_j}'' < 0$ and the wave is expressed as $\exp\left((\imath k_{z_j}' + k_{z_j}'')z - \imath\omega t\right)$, motion is confined to the vicinity of the waveguide. There is exponential decay in the bottom halfspace. Authors such as Watson (ref. 33) using a complex wavenumber formalism have depicted branch lines in the integral expression for the field along $Re\,\nu = 0$ and amplitude decay of the field is $e^{-\nu z}$ where $\nu = \pm\left(k^2 - \frac{\omega^2}{c_2^2}\right)^{1/2}$. Presumably his waves are described by $\exp(\imath k_z^{\nu} z - \imath\omega t)$ with $k_z = \left(\frac{\omega^2}{c_2^2} - k^2\right)^{1/2}$ In the region for which $k > \frac{\omega}{c_2}$ (i.e. locked modes with phase velocity real and $< c_2$) this leads to

$$k_z = \imath\left(\frac{\omega^2}{c_p^2} - \frac{\omega^2}{c_2^2}\right)^{1/2} = \imath\left(k^2 - \frac{\omega}{c_2^2}\right)^{1/2} \qquad 5.43$$

and the field in layer two is

$$\exp\left(\imath\cdot\imath\left(k^2 - \frac{\omega^2}{c_2^2}\right)^{1/2} z - \imath\omega t\right) = \exp\left(-\nu z - \imath\omega t\right) \qquad 5.44$$

In the region for which $c_p > c_2$ energy leaks and Cp becomes complex. If $Re(\nu) > 0$ the wave will behave as $\imath(\pm\imath\nu) = \mp\nu z$ Characteristic equation roots for $Re(k) < \frac{\omega}{c_2}$ i.e. $c_p > c_2$ (steep rays) are found displaced into the first quadrant of the $\tilde{k}$ plane when $Re\,\nu < 0$ is taken (growing waves). The branch line lies along the real axis and then goes to ∞ along the imaginary axis. $Re\,\nu = 0$ is along that path. The first quadrant of k space then corresponds to either $\nu \lesseqgtr 0$ depending on which ν sheet is chosen. Along the real k axis ahead of the branch

points γ may be chosen as $\gtrless 0$ depending on the sheet chosen. Behind the branch point on the real K axis $\gamma = 0$. Satisfaction of the characteristic equation puts poles on the real axis in the locked region and off the real axis in the leaky region. Watsons figures 1 and 2 sketched in figures 5.4a and 5.4b

(Intentionally left blank)

show a contour deformation to minimize the branch line contribution at the expense of including leaky mode poles on (-,-) sheet and (+,-) sheet. No poles are depicted for $R_e(K) < K_\beta$ on the (+,+) sheet. Of interest here also is the observation that the branch line exists for $Re(K) < K_\beta$ or $Re(K) < K_\alpha$. In an incidence angle formulation this would correspond to rays at angles steeper than the critical angle (small incidence angle) for which $c_\rho > c_2$ (Although the branch line contribution is commonly associated with the critically refracted wave, and the major contribution to the integral will in fact occur near $c_\rho = c_2$.)

We have plotted our incidence angle and reflection coefficient discontinuity occuring for incidence angles $\tilde{\varphi}_1 >$ critical angle. What we are encountering then is not a branch line crossing but a Riemann sheet switching, away from the branch line $K_{2\zeta}'' = 0$, along the locus $\varphi_2' = \frac{\pi}{2}$. Brekhovskikh's figure 122 shows the branch line in the $\tilde{\varphi}_1$ plane occuring for angles $\varphi_1' < \varphi_{1cr}$ and going toward $\varphi_1' \approx 0$, $\varphi_1'' = \infty$. Our global exploration of the

transmitted angle and reflection coefficient values along any $\tilde{\varphi}_1(c_p)$ loci has shown the discontinuity beyond $\varphi_1' = \varphi_{1cr}$ and no discontinuity but a maximum in $|R|$, for $\varphi_1' < \varphi_{1cr}$. That is, we observe in Table 5.3 for values of $c_p > c_2$ smooth variation in φ_2', φ_2'', $|R|$ and $\measuredangle R$ as φ_1' increases (with φ_1'' decreasing) towards $\varphi_{1\,lim}'$. The real part of refracted angle reaches a maximum $< \frac{\pi}{2}$ the imaginary part decreases through zero towards negative values, the reflection coefficient magnitude reaches a maximum and the reflection coefficient phase decreases through zero to negative values.

We have computed $k_{2z}'' = k_2' \sin\varphi_2' \sinh\varphi_2'' - k_2'' \cos\varphi_2' \cosh\varphi_2''$ along these Cp loci as well and find that for $c_p < c_2$, $\varphi_2'' < 0$ corresponds to the $+\nu$ sheet (decaying waves). Angle solutions with $\varphi_2'' > 0$ lie on the $-\nu$ sheet. In the region $c_p > c_2$ angle solutions for which $\varphi_2'' > 0$ may be on either sheet. For bottom halfspaces with slight dissipation φ_2'' starts < 0 at $\tilde{\varphi}_1 = \varphi_{1\,lim}$ As φ_1' is brought away from $\varphi_{1\,lim}$ (growing waves) φ_2'' becomes > 0 at the speculative angle, but the angle $\tilde{\varphi}_2$ is still on the $+\nu$ sheet. At the branch line $\varphi_2'' > 0$ and k_{2z}'' becomes > 0 so that $\tilde{\varphi}_2$ is on the $-\nu$ sheet. These regions are depicted in figure 5.5b. The following values were obtained for Model 1a

c_p	$\varphi_{1\,spec}'$	$\varphi_{1\,spec}''$	$\varphi_{1\,BL}'$	$\varphi_{1\,BL}''$
$10^4 \frac{m}{sec}$	$> 7.507 \times 10^{-2}$ radians	$< 3.86 \times 10^{-4}$	$\approx 7.504 \times 10^{-2}$	$\approx 2.4 \times 10^{-2}$
5×10^3	3.0469×10^{-1}	1×10^{-3}	$\approx 3.0468 \times 10^{-1}$	$\approx 6.2 \times 10^{-3}$
2.45×10^3	6.588946×10^{-1}	2.3×10^{-3}	6.588912×10^{-1}	$\approx 3.8 \times 10^{-3}$

We also note at φ_1' spec and φ_{1BL}' the following values of $\tilde{\varphi}_2$:

C_p	$\varphi_{1\,spec}'$	$\varphi_{2\,spec}'$	$\varphi_{2\,spec}''$	$\varphi_{1\,BL}'$	$\varphi_{2\,BL}'$	$\varphi_{2\,BL}''$
2450	6.58894×10^{-1}	.95502	0	.658891	.95502565	2.4×10^{-3}
5000	3.04692×10^{-1}	.411517	0	.304686	.4115284	7.2×10^{-3}
10000	< .07507			.075042	.10021	3.36×10^{-2}

So the branch line ν =0 does not correspond to $\varphi_2' = \frac{\pi}{2}$. The line $\varphi_2' = \frac{\pi}{2}$ is the line of discontinuity in φ_2'' , $|R|$ in the region $C_p < C_2$.

In the region $C_p > C_2$ (steep rays) we pass through φ_2'' =0 but never get to $\varphi_2' = \frac{\pi}{2}$ as φ_1' increases along a C_p locus to $\varphi_{1\,lim}'$. The leaky mode region is best delimited by $k_{z_3}'' = 0$ rather than either $\varphi_2' = \frac{\pi}{2}$ or φ_2'' =0. To see how multiple value of k_{z_3} (i.e. $\lesseqgtr 0$) for the same Kx arises in the angle formalism recall that we have used

$$K_x' = i\left(k' \sin\varphi' \cosh\varphi'' - k'' \cos\varphi' \sinh\varphi''\right)$$

$$K_x'' = -\left(k' \cos\varphi' \sinh\varphi'' + k'' \sin\varphi' \cosh\varphi''\right)$$

$$k_3' = i\left(k' \cos\varphi' \cosh\varphi'' + k'' \sin\varphi' \sinh\varphi''\right)$$

$$k_3'' = +\left(k' \sin\varphi' \sinh\varphi'' - k'' \cos\varphi' \cosh\varphi''\right)$$

Now the characteristic equation requires $\varphi_1'' > 0$ if $|R| < 1$ and the contour integration is over Brekhovskikh's final contour Γ shown in figure 2.5b . Then given a value of K we have a unique value of $\tilde{\varphi}_1$ namely one confined to the sector $0 < \varphi_1' < \frac{\pi}{2}$, $0 < \varphi_1''$.

However there will be two complex angles $\tilde{\varphi}_2$ satisfying the refraction law and thus preserving k_x', k_x''. One will have $\varphi_2' > \frac{\pi}{2}$ and the other have $\varphi_2' < \frac{\pi}{2}$. In the region $c_p > c_2$ our Snell algorithm returns a value $\varphi_2' < \frac{\pi}{2}$ reaching a maximum at the speculative angle where φ_2'' goes through zero. The trajectory of $\tilde{\varphi}_2$ is shown in figure 5.13. In the locked region $c_p < c_2$ it was seen to be that shown in figure 5.3. This corresponds to picking up the root $\varphi_2' < \frac{\pi}{2}$ for which $k_{z_3}'' < 0$ and $\varphi_2'' < 0$. So we see that when we start with $\varphi_1' < \frac{\pi}{2}$ and $c_p > c_2$ and φ_1'' close to zero so that we are in region (a) of figure 5.5b we are on the $+\nu$ sheet. As we move up along $\tilde{\varphi}_1$ locus φ_2' goes towards $\frac{\pi}{2}$ and reaches a maximum as φ_2'' goes through zero at the speculative angle of φ_1'. k_{z_3}'' is still < 0. As φ_1' increases further φ_2' decreases and φ_2'' increases until the branch point is reached at which $k_{z_3}'' \geq 0$. The relation between k_x', k_x'', φ_1', φ_1'', φ_2', φ_2'' is nonunique, but the additional root in $\tilde{\varphi}_2$ has $\varphi_2' > \frac{\pi}{2}$ which we exclude in the convergence routine, and the additional root of K in $\tilde{\varphi}_1$ has $\varphi_1'' < 0$ which is excluded as being outside the contour of interest.

In the region $c_p < c_2$ (region (c) of figure 5.5b) we start out with $\varphi_2' < \frac{\pi}{2}$, $\varphi_2'' < 0$. $\tilde{\varphi}_2$ follows a trajectory which is interrupted by the artifical boundary $\varphi_2' = \frac{\pi}{2}$ beyond which it continues into the region $\varphi_2' > \frac{\pi}{2}$. This solution starts on the $k_{z_3}'' < 0$ sheet and remains on it. The other angle solution starts on $k_{z_3}'' > 0$ and stays on it. From the work of Watson, Rosenbaum (ref.) etc. we expect that for $c_p > c_2$ field calculation will require poles on the $k_{z_3}'' > 0$ sheet. Characteristics for "leaky modes" are given in table 5.5 and 5.8 for poles which satisfy $k_{z_3}'' > 0$. Since the reflected wave in either layer is given by $\varphi_{refl} = \pi - \varphi_{inc}$ we see that permissible Snell solutions

AD-A079 562 WOODS HOLE OCEANOGRAPHIC INSTITUTION MASS F/G 17/1
ATTENUATION OF LOW ORDER MODES IN LOSSY ACOUSTIC WAVE GUIDES.(U)
DEC 79 H D LESLIE N00014-75-C-0852
UNCLASSIFIED WHOI-79-91 NL

3 OF 3
ADA 079 562

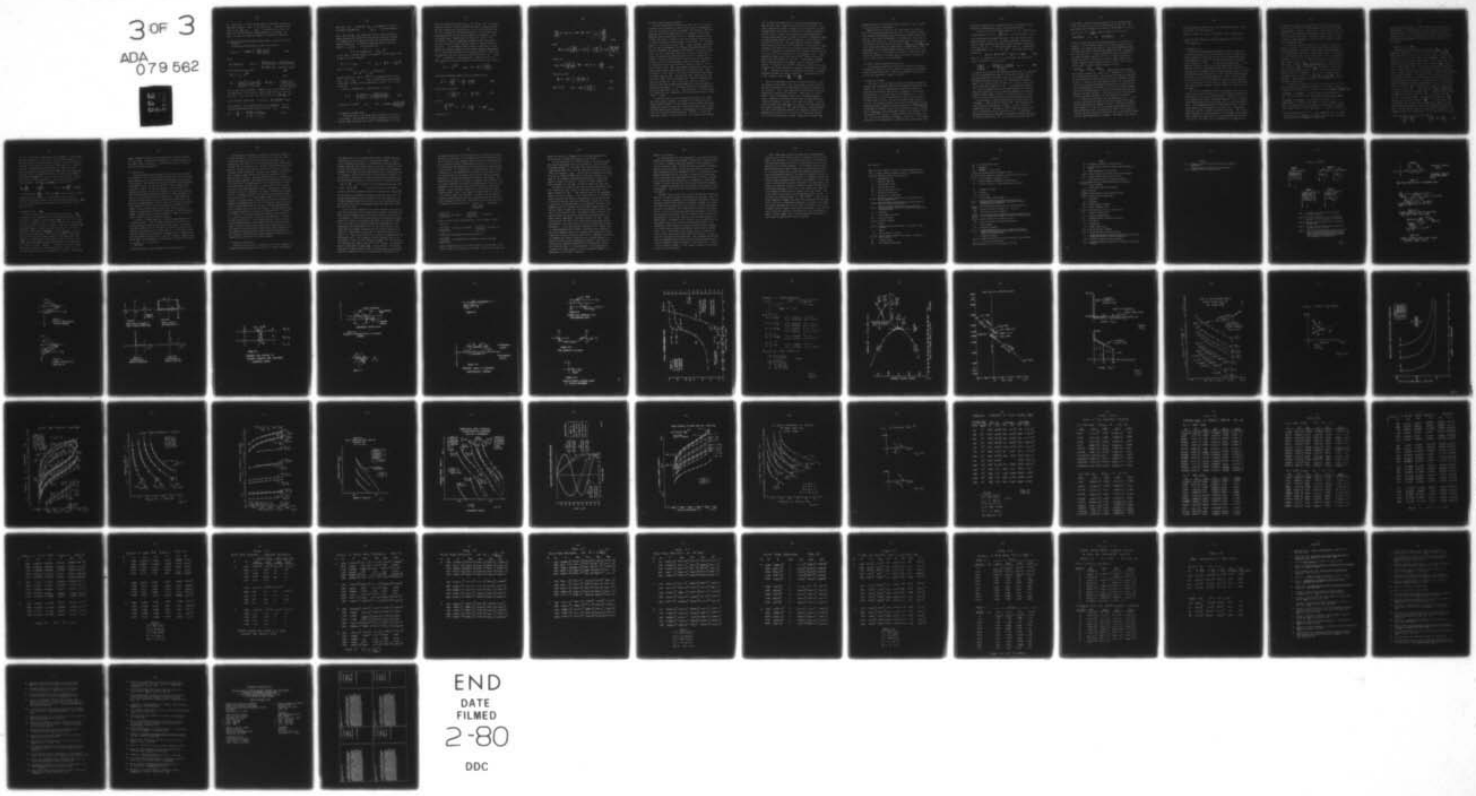

END
DATE FILMED
2-80
DDC

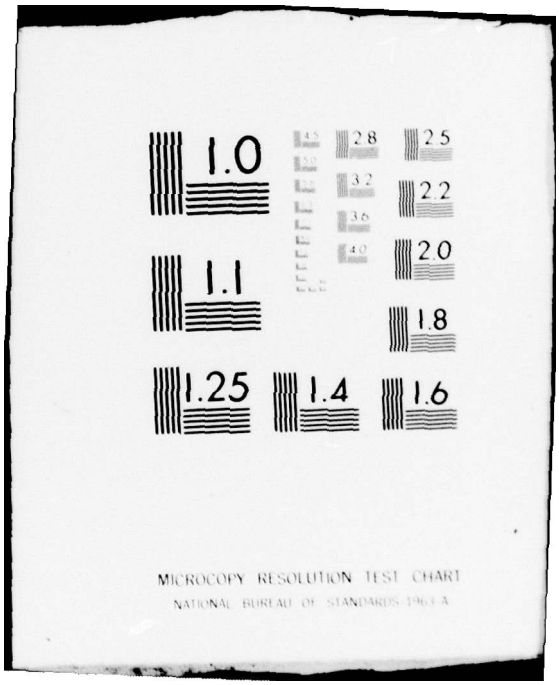
1.0
1.1
1.25
1.4
1.6
2.8
3.2
3.6
4.0
2.5
2.2
2.0
1.8
MICROCOPY RESOLUTION TEST CHART
NATIONAL BUREAU OF STANDARDS 1963-A

for $C_p > C_2$ in the multilayer guide lie along the trajectories depicted in regions I and II of figure 5.13 . Both waves should start on the $k_{zj} > 0$ sheet. In the region $C_p < C_2$ one wave is on the plus sheet and changes downgoing to upcoming. The other is on the minus sheet and changes from upcoming to downgoing.

5.8 Reflection Coefficient Phase- Phase advance or retard at the turning point?

We have written the reflection coefficient phase as

$$\chi_{n,n+1} = \arctan\left[\frac{-\gamma_{n+1}\,\rho_n}{\gamma_n\,\rho_{n+1}}\right] \qquad 5.45$$

where

$$R = \exp(2i\chi) \qquad R_{n,n+1} = \frac{\gamma_n(H)\,\rho_{n+1}(H) - \rho_n(H)\,\gamma_{n+1}(H)}{\gamma_n(H)\,\rho_{n+1}(H) + \rho_n(H)\,r_{n+1}(H)} \qquad 5.46$$

With dissipation we have used

$$R_{12} = \rho_{12}\, e^{i\phi_{12}} \qquad 5.47$$

$$\rho_{12} = \frac{(\gamma_2-\gamma_1)^2 + (\delta_2-\delta_1)^2}{(\gamma_2+\gamma_1)^2 + (\delta_2+\delta_1)^2} \qquad \tan\phi_{12} = \frac{2(\delta_2\gamma_1 - \gamma_2\delta_1)}{\gamma_2^2 - \gamma_1^2 + \delta_2^2 - \delta_1^2}$$

for the layer over a halfspace. Computer results are discussed below for these forms. First, however, consider phase shift upon total reflection. If C_1 and C_2 are real, $C_1 < C_2$ and $\sin\Psi_1 > \frac{C_1}{C_2}$, then total reflection takes place. In this case $k_{zj} = \frac{\omega}{C_2}\cos\psi_2$ becomes pure imaginary. The transmitted waves are inhomogeneous. The reflection coefficient can be written in terms of k_{1j} and k_{2j} as

$$\frac{B}{A} = \frac{\rho_2 k_{1j} - \rho_1 k_{2j}}{\rho_2 k_{1j} + \rho_1 k_{2j}} \qquad 5.48$$

Then since k_{1j} is real and k_{2j} pure imaginary A and B are complex conjugate and $\frac{B}{A} = 1$ in the nondissipative case. Aki (ref. 32) has stated that there is always a phase advance associated with total reflection and the fact that it should be in advance and not an additional delay can be proved from the radiation condition. The radiation condition requires vanishing waves as $3 \to \infty$. Aki uses wave forms

$$P = P_0 \exp\left[i\omega t - i k_j \cdot 3\right]$$

In this case it requires $\mathrm{Im}(k_{2j})$ to be negative. Using equation 5.39 we have at critical reflection

$$\gamma_2 = \pm i g_2 \qquad \text{with} \qquad g_2 = \frac{\omega}{c}\left(1 - \frac{c^2}{\alpha^2}\right)^{1/2}$$

Then if in layer 2,

$$\psi = e^{-i\gamma_2 \cdot 3} = e^{i\left(\pm i g_2 \cdot 3\right)}$$

and we require the - sign in $e^{\pm i g_2 3}$ for nongrowing field, we must have $\gamma = +i g_2$. The R formula above was derived for z axis down, so there will be a phase delay $\phi < 0$ for critical reflection.

Similarly, Brekhovskikh in equation Brek. 3.19 gives

$$R = \frac{m\cos\varphi - i\sqrt{\sin^2\varphi - N^2}}{m\cos\varphi + i\sqrt{\sin^2\varphi - N^2}} \qquad 5.49$$

and he has $R = \rho e^{i\Phi}$ with $\Phi = -2\arctan\dfrac{\sqrt{\sin^2\varphi - N^2}}{m\cos\varphi}$

corresponding to phase delay.

Phase behaviour in the complex angle formulation is difficult to anticipate. We have seen the following tendencies in our algorithm for phase velocities lower than C2 ("locked modes"). For any

particular phase velocity Cp and k''_2 , as φ_1' and φ_1'' are varied along the Cp locus, reflection coefficient phase is negative corresponding to phase delay, and varies only in the fourth decimal place as φ_1' decreases to the speculative angle. At the discontinuity phase becomes positive and varies monotonically thereafter, in the leaky mode region. Phase advance is smaller for smaller φ_1' . We indicate in table 5.3 magnitude and phase of the reflection coefficient on either side of the spec. angle for selected values of Cp and K''_2 . For the Pekeris model reflection coefficient is independent of frequency (except for second order frequency dependence of K''_2). These values of phase versus incidence angle $\tilde{\varphi}_1$ should not be compared to the usual reflection coefficient versus φ_1' , where φ_1'' is assumed =0. (That comparison is made with figure 5.1).

Note: Tolstoy has given the reflection coefficient for total reflection

$$R = -e^{2i\Theta} \quad \text{and} \quad \Theta = \tan^{-1}\left(\frac{\rho_2 \gamma_1}{\rho_1 g_2}\right)$$

Using normal impedance equality at the interface so that

$$Z = \frac{\rho_1 \phi}{\phi_3} = \frac{\rho_1}{i\gamma_1} \frac{1+R}{1-R} \qquad 5.50$$

and the general relation

$$\int \frac{f'(x)}{f(x)}\, dx = \log f(x) \qquad 5.51$$

so that

$$\frac{d}{dz} \log \phi = i\gamma_1 \frac{1-R}{1+R} \quad \text{in layer 1} \qquad 5.52$$

we solve for R

$$\frac{\Phi_3}{i\Phi\gamma_1}(1+R) = (1-R) \Rightarrow R = \frac{1 + i\frac{\Phi_3}{\Phi\gamma_1}}{1 - i\frac{\Phi_3}{\Phi\gamma_1}} \qquad 5.53$$

where

$$\Phi = \tan^{-1}\left[\frac{\Phi_3}{\Phi\gamma_1}\right] = \tan^{-1}\left[i\,\frac{1-R}{1+R}\right] = \tan^{-1}\left[\frac{\frac{d}{d_3}\log\Phi}{\gamma_1}\right] \qquad 5.54$$

Tolstoy has

$$\Theta = \tan^{-1}\left[\frac{-\gamma}{\frac{d}{d_3}\log\Phi}\right] \Rightarrow \tan\Theta = -\frac{\gamma\Phi}{\Phi_3} \qquad 5.55$$

Similarly we find

$$\Phi = \tan^{-1}\left(\frac{-\rho_1 g_2}{\rho_2 \gamma_1}\right) \qquad 5.56$$

where he has $$\chi = \tan^{-1}\left(\frac{\rho_2\gamma_1}{\rho_1 g_2}\right) \qquad 5.57$$

5.9 Pekeris Model Dispersion Results:

We have implemented the Brekhovskikh theory and run it for several models, most thoroughly for model 1A consisting of a homogeneous ocean over a dissipative acoustic halfspace. Dissipation in the halfspace was varied from .0001 nepers/m to .01 nepers/m. Other model parameters were c1=1500 m/sec, K1''=0. n/m, C2=2000 m/sec, while layer thickness was 1000 m. Dispersion results are plotted in figure 5.6. In figure 5.5 pole positions are shown in the complex $\check{\varphi}_1$ plane for modes 0, 1, 2 at several values of K_2''. As K_2'' increases, poles move out into the first quadrant. As $\varphi_1' \to 0$ there appears to be a tendency for $\varphi_1'' \to \infty$ as suggested by Brekhovskikh. Curiously for any given K_2'', $\check{\varphi}_1$ values move toward the real axis as mode number increases, although the attenuation coefficient will increase as m increases. Figure 5.6 shows frequency versus the real part of phase velocity both for locked and leaky regions of low order modes 0, 1, 2. Dispersion results are presented in tables 5.4 and 5.5. In tables 5.4 and 5.5 ω_0, φ_{10} are frequency and angle solutions to the nondissipative model, phase characterisitic equation 3.112. These are used as initial values in the iterative solution for the dissipative model. ω_R, φ_1', φ_1'' are solutions after convergence for the dissipative model with both characterisitc equations 3.112 and 3.113 requiring satisfaction. Only in the leaky region are there discernable differences between eigenfrequencies for the nondissipative and dissipative models. In the locked region angle and frequency differences between δ_{10} are δ_1' extremely small. The major effect of including $K_2''\neq 0$ is introduction of a finite imaginary part of angle φ_1'' in layer 1.

Dispersion results can be distinguished by whether the independent phase velocity parameter was chosen in the locked ($Cp < C2$) or leaky ($Cp > C2$) regions. For the locked region we observe that eigenfrequencies ω_R are lower than in the nondissipative case. Eigenincidence angles are also smaller, corresponding to slightly steeper rays than in the nondissipative case and $\varphi_1'' > 0$, so that the waves grow slightly in the source layer. The imaginary part of angle

φ_1'' as seen to be proportional to the dissipation parameter K_2''. Departure from ω_ϕ is greater for $K_2''=.01$ than for $K_2''=.001$. Similarly, departure from φ_{10}' is greater for $K_2''=.01$ than for $K_2''=.001$. The magnitude of the reflection coefficient is greater for $K_2''=.001$ than for $K_2''=.01$. Extent of perturbation of these eigensolutions from the nondissipative case is shown in Table 5.6. Frequencies ω_a for mode 0 change by about 5×10^{-4} radians/sec. for the case $K_2''=.01$ and 5×10^{-6} for $K_2''=.001$. For higher modes at $K_2''=.001$, frequency differences were less than 1×10^{-6} radians/sec. The variation in $\Delta\omega$ as shown in this table is due to our specification of an accuracy of only 10^{-4} in solution of the characteristic equations iteratively, and to insensitivity of the equations to slight changes in ω . Angle changes are found to be on the order of 5×10^{-5} radians for $K_2''=.01$, mode 0, and 1×10^{-6} radians for $K_2''=.001$. As mode number increases angle difference become infinitesimal, going to less than 1×10^{-7} radians. The regularity of the φ_1'' values as a function of Cp is due to sensitivity of the characteristic equation functionals to the value of $\tilde{\varphi}_1$. Derivatives, iteration corrections, and errors in a sample convergence sequence are shown in Table 5.11. The great sensitivity to $\tilde{\varphi}_1$ changes is given by $\frac{df}{d\varphi_1'}$ and $\frac{dg}{d\varphi_1'}$.

One of the advantages of the sum of residues formalism is that the locked and leaky regions (the region beyond so called cutoff) of the complex wavenumber (or incidence angle) planes are treated in a unified manner. Thus, "leaky mode poles" may be found for which both characteristic equations are satisfied. These poles will lie on formerly (prior to Rosenbaum, Gilbert etc.) forbidden wavenumber sheets. Departure of rigorous solution from the unperturbed values is much more dramatic for waves in the leaky mode region. Since the reflection coefficient magnitude is < 1 here in the unperturbed case, much larger perturbation of $\tilde{\varphi}_1$ away from $\tilde{\varphi}_{1\,lim}$ is required along a Cp locus in order that both characteristic equations be satisfied. Eigenangles were found to lie in region c of figure 5.5b and this will be on the lower Riemann kz sheet. Angles for the lowest modes

changed by as much as .05 radians along a constant Cp locus; frequencies by as much as .5 radians/sec.

Behaviour of the solutions in the leaky region is counter to that of the locked mode case, and puzz ling. For example, although both frequency and eigenangle are perturbed away towards smaller values, as in the case of locked modes, the perturbation is greater for $K_2''=.001$ than for $K_2''=.01$. Also the imaginary part of angle required is smaller for $K_2''=.01$ than for $K_2''=.001$ and $|R|_{k_2=.01} > |R|_{k_2=.001}$ The Reflection coefficient magnitudes end up being smaller after perturbation in this regime whereas they were slightly larger in the locked mode region. At this point we cannot fully explain the behaviour of the solution in the leaky region and thus will present few results there, and with little confidence.

5.10 Pekeris Model Attenuation Coefficients:

The attenuation coefficients discussed in chapter 4 have been calculated for Model 1A in both locked and leaky regions of the phase velocity domain $C1 < Cp < \infty$. Results are presented in Figure 5.7 and 5.8 and summarized in tables 5.7 and 5.8.

a. Comparison with δKR:

From table 5.7 we can observe spectacular agreement between the residue series attenuation coefficient developed by Brekhovskikh and labelled δ , and the 1955 attenuation coefficient derived by Kornhauser and Raney and labelled δR. Agreement is to the third decimal place, i.e. to better than 1% and frequently to .1%. This agreement holds for both large and small values of K_2'', high and low mode numbers, and over the entire tabulated range of phase velocities. The rigorous values δ have been calculated from perturbed eigenvalues used to determine reflection coefficient $\Phi''(\varphi_1', \varphi_1'')\downarrow$, the Kornhauser and Raney result from the equation $Im(h)=K_2'' \cdot F(\gamma, \beta)$ given in eq 4.135 , using unperturbed values of γ_n and β_n in the full equation for $F(\gamma, \beta)$. We place confidence in the results for δ and the close agreement with δ_{KR} is satisfying. It also demonstrates that the computationally exhaustive search required for exact

solution is unnecessary for the Pekeris guide in the locked regime, where the Kornhauser Raney results are quite satisfactory.

In figure 5.10 we have plotted values of δ (i.e. δ_{KR} also) on a log-log graph of δ vs. $\frac{\omega H}{c_1} = \beta$, for several models including the one used by Kornhauser and Raney. This plot should be compared to Figure 3 in ref. 19. Kornhauser and Raney's own graph of $F(\eta, \beta)$ shows convergent mode number curves plotted on log-log axes of $F(\eta, \beta)$ vs β. If attenuation coefficient δ is proportional to some power of β i.e. $\delta \sim A\beta^r$ then taking log of both sides gives

$$\log \delta = \log (A \cdot \beta^r) = \log A + r \log \beta \qquad 5.58$$

When δ is plotted versus β on log-log paper the slope of the line in linear units will be given by

$$\frac{d \log \delta}{d \log \beta} = \frac{d\left[\log A + r \log \beta\right]}{d \log \beta} = r \qquad 5.59$$

In figure 5.10 we have plotted attenuation coefficient δ versus β for the intermediate depth model 1A at dissipation numbers $K_2''=.01$ and $K_2''=.001$, and for the shallow water sand bottom model used by Kornhauser and Raney with K_2'' set $=.01$. Extrapolated slopes are shown in the figure and given in Table 5.12. Strictly we must plot log of dimensionless quantities. β is dimensionless frequency δ has units nepers/m and is made dimensionless by dividing by dissipation number K_2'' to give a quantity comparable with the Kornhauser and Raney quantity $F(\eta, \beta)$. We note that this will serve simply to raise or lower the curves on the log-log plot by (K_2'').

From the model 1A results we see that at a given value of β (frequency), $\delta(K_2''=.01) = 10 \times \delta(K_2''=.001)$. The figure 5.10 curves are shifted by one decade in $F(\eta, \beta)$, and δ is directly proportional to K_2''. The quantity log A in equation 5.58 will contain all proportionalities in addition to β^r. In particular attenuation coefficient dependence on mode number may be determined by noting differences for δ at any particular value of β for

a given model. Table 5.12b gives values of δ at selected values of β for model 1A with $K_2''=.01$ and model KR with $K_2''=.001$. Our mode numbers are shifted by 1 from those of the KR paper. If K & R's asymptotic law $F \sim \frac{n^2}{\omega^3 H^3}$ holds, we should have the ratio of

$$\delta_{n=1}/\delta_{n=0} = 4 \quad \text{and} \quad \delta_{m=2}/\delta_{m=0} = 9$$

Table 5.12b shows that the mode number dependence is a function of frequency. For the highest values of β we have plotted, the dependence is to a power less than two. From the extrapolated slopes in linear units we also see that the dependence on β is considerably less than β^3. In the intermediated region (below $\beta = 10$), for model 1A slopes ranged from 1.1 to 1.7. Slope is greater for higher mode number. Similarly for the K & R model slopes in the highest frequency range presented were from 1.22 to 1.82. The curves for model 1A shows an inflection point at about

$$\beta = 10\big|_{m=0}, \; 20\big|_{m=1}, \; 30\big|_{m=2}$$

Beyond these points slopes were slightly greater i.e. 1.48 to 1.70. Inflection in K & R figure 3 is also barely discernable. Our curves have perhaps not been pushed to the asymptotic limit required for the K & R asymptotic formula to hold. In light of the close agreement between δ calculated by the K & R rule and the Brekhovskikh method we do not doubt that this limit might eventually be reached. Our results do indicate however that the K & R approximation is invalid in the region where the dispersion curve shows character. This region is also the region where temporal separation of modes at a fixed frequency is possible.

In figure 5.9 we plot both δ and eigenfrequency ω in logarithmic coordinates for model 1A with various power laws of body wave attenuation versus frequency in layer 2. We have not reached the asymptotic limit for any of the curves except perhaps exp=1.0. When attenuation varies to a higher power than f^1 (as it should for liquids) the modal attenuation curves are seen to have smaller slopes and thus weaker dependence on frequency. For example, with exp=1.2

at w=10 radians/sec slope of the curve is approximately .95. Slopes at w=10 for the three curves are

exp=1.0 slope=1.27; exp=1.2 slope=.945; exp=1.4 slope=.729

Indicating modal attenuation frequency dependence of $f^{1.27}$, $f^{.95}$, $f^{.729}$ respectively.

b. Comparison with

Figure 5.7 also demonstrates agreement to within a factor of 2 in dB/m of attenuation, in the worst case for mode 0, between the rigorous attenuation coefficient and the intuitive attenuation coefficient computed on the basis of our physical arguments in chapter 4, using the equation 4.79 and unperturbed eigenvalues. If this degree of accuracy is permissible great computational economy is realized by using this attenuation coefficient rather than the iterative solution. Although we lack results at grazing angles $\alpha < \alpha_{cr}$ (Cp=1510) the curves show asymptotic limits (for small grazing angles as (Cp$\rightarrow$C1) with even greater agreement. Further, since the shape of the curves are similar the δ_{INT} value might be adjusted downward by this known factor of overestimation. Results for many more models and higher modes are necessary, however, before this can be done with confidence.

The intuitive attenuation coefficient depends on $|R|$ and cycle length L only, and can thus be used in a continuously variable ocean provided only that we can calculate $|R(w)|$ or $|R(Cp)|$ and L(w) or L(Cp) (depending on whether independent parameter w or Cp is chosen). The Kornhauser Raney result on the other hand is tied to the Pekeris model. The independence of δ_{INT} from mode number shown in Figure 5.7 arises because of its dependence on only $|R|$ and L. Unperturbed values of w and φ_1' are used to calculate $|R|$ and L. $|R|$ is only weakly dependent on ω when attenuation is introduced into the bottom, and for the Pekeris model shows no interference effects from underlying layers. Thus $|R|$ and L are dependent only on φ_{10}' which is

the same for all modes at a given phase velocity.* When attenuation is plotted as a function of frequency δ_{int} is found also to be mode number dependent as shown in figure 5.7b. Of particular interest in Figure 5.7 is the bounding nature of δ_{int} as the asymptotic limit of δ for higher mode number. Comparison of δ_{int} with δ for $\omega=3$ in table 5.7 shows agreement to closer than 5%, considerably better than the 200% for mode 0.

The asymptotic nature of the intuitive attenuation coefficient arises in two ways. First the reflection coefficient magnitude for the exact solution with complex incidence angle decreases towards its limit at $\tilde{\varphi}_1 = \varphi_{1,lim}$ where the incidence angle is real. In figure 5.6 we note how pole positions shift toward the real axis as mode number increases. This shift in incidence angle gives rise to the convergence of $|R|$ towards $|R_0|$. For any given K_2'', Cp combination, as mode number increases, $\phi''(\varphi_0', \varphi_B'') \rightarrow \varphi''(\varphi_{1,0})$, as shown in Table 5.4. Secondly, as ϕ'' diminishes for high frequency, lower phase velocity, the exponential series $1-e^{-\phi''}$ is better represented by the first term in its expansion. That is, for low grazing angles and phase velocities close to C1, $\delta_{int}(\phi'') \rightarrow \delta_{ray}(\phi'')$ for the same ϕ''. These numerical observations correspond to the last equations in section 4.4.

In figure 5.7b we see that the intuitive attenuation coefficient when plotted versus frequency is dependent on mode number. Rather than being the asymptotic limit of δ_m so that $\epsilon_m \equiv \delta(m, c_0) - \delta(c_1) \rightarrow 0$ as $m \rightarrow \infty$ or $\omega \rightarrow \infty$, it gives instead a good approximation to δ for all m and the error $\epsilon_m \equiv \delta(m,\omega) - \delta_{int}(m,\omega) \rightarrow 0$ as $m \rightarrow \infty$ or $\omega \rightarrow \infty$. The variability of δ_{int} with m is understandable. Figure 5.6 shows that for a given frequency in the Pekeris guide phase velocity increases with mode number, corresponding to steeper rays for higher mode number. In figure 5.5 we see that

* For the case $K_2''(w)=A\cdot f^{1.0}$ R, L are independent of f. For exponent $\neq 1.0$, R is dependent on frequency and the intuitive attenuation coefficient is dependent on mode number.

lines of constant frequency, if drawn through the curves of model 1A with $K_2''=.001$, will have negative slope, so that angle and resultant reflection coefficient will change with mode number. As frequency increases, poles for all modes approach the real axis and the reflection coefficients approach the intuitive reflection coefficient at those angles.

c. Comparison with δ_{BR}

We have calculated asymptotic approximations δ_{BR} to rigorous attenuation coefficient δ from the formula given in eq.4.118. and present them in Figure 5.7b. For $K_2''=.01$ these curves converge towards δ in the limit of grazing angle $\alpha \longrightarrow 0$, however attenuation is smaller for higher mode numbers. For $K_2''=.001$ there is also convergence at small grazing angles. Here, however, δ_{BR} increases with increasing mode number. The formula is an asymptotic approximation. In Table 5.9 we list the magnitude of the quantities assumed small or large in the derivation (see 4.5.2). From the equations 4.117 at the bottom of page 4. we see that if attenuation varies as the first power of frequency, as we have assumed, the quantities pr and pi are independent of frequency. The quantity Re(p) is fixed for all modes and frequencies once the model parameters c1, c2, k2'' are specified. The quantity $\Delta\ell$ is Brekhovskikh's asymptotic approximation to $Im(\alpha)$ for small α. Table 5.9 gives $\Delta_\ell h = \Delta\ell \times 10^3$ in this example, and the eigenangle φ_1'' .* Agreement between $\Delta\ell$ and φ_1'' even at grazing angles as large as .7 radians (Cp=1950) is usually within 25% of φ_1''. The attenuation coefficient δ_{BR} depends on the multiplying factor $\frac{\pi\ell}{h}$. For the case $K_2''=.01$ the imaginary part of angle and its approximation $\Delta\ell$, at a given phase velocity, decrease at a rate slightly greater than (mode number)$^{-1}$, so that the net effect is to have smaller attenuation in the asymptotic formula for higher modes. For the case $K_2''=.001$ the imag-

* The imaginary part of grazing angle $\tilde{\alpha}$ is

$$Im\left[\frac{\pi}{2} - \tilde{\varphi}\right] \quad = \quad Im\left[\frac{\pi}{2} - \varphi' - i\varphi''\right] \quad = \quad -\varphi''$$

ary part of angle and its approximation value $\Delta\ell$, at a given phase velocity, decrease at a rate slightly less than (mode number)$^{-1}$, so that the net effect of the asymptotic formula is to have a larger attenuation in the asymptotic formula for higher modes, as is the actual case. Brekhovskikh's approximations also required kh large. Table 5.9 shows that the approximation $KH >> |P|$ used to get equation Brek. 27.40, is generally valid for this model, since $|P| \approx .5$. The approximation $\Delta_\ell H$ small, which is used to go from Brek. 27.42 to Brek. 27.43, says that attenuation is small over the distance of a layer thickness. Then $b_\ell = ik\cos\varphi_\ell$ may be written as

$$ik \cdot \frac{\pi\ell}{kh} = \frac{i\pi\ell}{h} \qquad \text{since} \quad \sin\left(\frac{\pi\ell}{kh} - i\Delta\ell\right),$$

is approximated as $\frac{\pi\ell}{kh}$. Values of $\Delta_\ell h$ given in table 5.9 would indicate that this assumption is violated for phase velocities 1550 m/sec and greater, and we confirm the low mode approximation δ_{BR} is not in close agreement for the portion of the dispersion curves dealt with here.

d. Comparison with δ_{ING}

Finally in figure 5.7 we show attenuation coefficient δ_{ING} calculated from our implementation of the Ingenito & Wolfe perturbation theory. Agreement is poor between δ_{ING} and δ. The curves for m=0, 1, 2 shown in figure 5.7 hold for both $K_2''=.01$ and $K_2''=.001$ since differences are small as indicated in table 5.7. Equation 4.83 shows that δ_{ING} is insensitive to K_2'' since K_2'' only has direct influence on the quantity $|R(k_0)|$. Column $|R_{12\varphi}|$ given in table 5.4 shows that there is less than a 10% change in $|R|$ going from $K_2''=.01$ to $K_2''=.001$ even for mode 0 at high phase velocities. δ_{ING} is in fact directly proportional and most sensitive to the normal mode shape $u(H)$ at the ocean bottom and to the normalization required to scale $U_0^2(H)$. In figure 5.11 we have plotted mode shapes calculated for the Pekeris model 1A, modes 1, 2, 3, 0 to assure ourselves that our implementation is correct. These shapes

appear reasonable and have the required feature of going to zero at the sea surface. The asymptotic agreement at low grazing angles δ and δ_{sing} shown in figure 5.7 is not meaningful given the insensitivity to dissipation parameter.

5.11 Sensitivity:

From the dispersion and attenuation coefficient results presented in Tables 5.4 and 5.7 we can assess the sensitivity of the various modal characteristics to body wave dissipation number in the underlying halfspace. From Table 5.6 we note a hundredfold greater frequency perturbation for $K_2''=.01$ than for $K_2''=.001$. Even at these high attenuations, however, the total perturbation is on the order 10^{-3} radians/sec at most, and thus well beyond the resolution of spectral analysis even assuming perfect knowledge of all model parameters (so that dispersion curves could be fit versus K_2''). These dispersion curves are highly sensitive on the other hand to water depth. Comparing the eigenfrequencies listed in Table 5.7 for the K & R shallow water model with those for model 1A we see that a factor of 10 increase in depth at phase velocity 1650 m/sec, mode 0, leads to a change in eigenfrequency from 67.651 radians/sec to 7.645 radians/sec. Change in frequency due to changing attenuation number will be completely masked by slight variations in depth.

Similarly, incidence angle has an extremely weak dependence on dissipation number. Table 5.6 shows unresolvable directional differences between dissipative and nondissipative cases. At Cp=1650 an angular resolution of 10^{-7} radians is required to distinguish between the case $K_2''=.001$ and $K_2''=0$ for model 1A. In the shallow water model this phase velocity occurs for the same initial incidence angle and the perturbation at $K_2''=.001$ is now 2×10^{-7} radians. However using conventional array processing a vertical array of length on the order

$$L = \frac{\lambda}{\text{resolution}} \simeq 2\times10^{+9} \text{ m}$$

would be required at these frequencies to achieve resolution.

The most sensitive measure, of course, of dissipation number K_2'', is modal attenuation. The curves of Figure 5.7 for K_2''=.001, .005, .01 show that modal attenuation is directly proportional to K_2''. Increasing K_2'' from .001 n/m to .01 n/m at any particular phase velocity increases δ by a factor of 10. Similarly, when plotted versus frequency as in Figure 5.10 scaling by a factor of 10 gives a 10-fold increase in modal attenuation. We note, also, however, in figure 5.9 that a change in power law can also lead to an upward shifting of modal attenuation curves. When body wave attenuation is measured at some reference frequency, like 100 Hz which we have used in this study, its extrapolation to eigenfrequencies for the model chosen is dependent on the power law chosen and will significantly alter the level and shape of the modal attenuation curves. Although most investigators have relied on f^1 dependence, the several investigations (Knopoff ref. 29), (Ingenito ref. 20) which have shown attenuation exponents as high as f^2 or $f^{1.75}$, would suggest that this variation must be explored in two phase media. Figure 5.9 indicates that changing the exponential dependence from $f^{1.0}$ to $f^{1.4}$ leads to a factor of 10 decrease in modal attenuation for the model 1A whose eigenfrequencies are 1-2 decades below the reference frequency. Additionally, the modal attenuation power law is seen to have changed from $f^{1.27}|_{K_2''\sim f^{1.0}}$ to $f^{.73}|_{K_2''\sim f^{1.4}}$, measured around the frequency w=10 radians/sec. This relation between power laws may be model dependent. Certainly the magnitude scaling is, since increasing layer thickness directly effects eigenfrequencies, moving them further away from a high frequency reference. Results must be obtained for many models, but it is clear that the inverse problem of attenuation number estimation is a two parameter problem and thus requires extensive measurement of over frequency. Results such as those presented by Ingenito at three frequencies are minimal for the inverse problem.

5.12 Numerical difficulties:

The algorithm used here as implementation of theory suggested by Brekhovskikh has been difficult to work with. Some of the problems

have been peculiar to an incidence angle domain treatment and could be avoided by working directly in the wavenumber domain. In particular, programming considerations connected with nonunique mappings between wavenumber and incidence angles discussed in sections 5.2 and 5.7 have been stumbling points along the way leading to convergence problems in the exact solution where Riemann sheet switching occurred. In retrospect, these discontinuities can be avoided by seeking only solutions on a particular ν sheet, by presetting the imaginary part of angle and relaxing physical constraints such as transmitted angle $\varphi_2' \leq \frac{\pi}{2}$. All solutions for the locked mode case were found to have $\varphi_2' \leq \frac{\pi}{2}$. It was only during the convergence scheme itself that intermediate angles were computed with $\varphi_2' > \frac{\pi}{2}$. By constraining intermediate step angles to physical portions of incidence angle sheets we have introduced limits (nonlinearities) into the Newton-Raphson algorithm and thus very likely increased the number of steps required for convergence causing the algorithm to march down the limit line.

For the results presented in this paper iteration limits were usually set at 40 steps for the characteristic equation and 40 steps for each sign of propagated angle in the Snell algorithm. Our algorithm is successful in computing perturbed angles and frequencies for phase velocities in model 1A $Cp \geq 1520$ m/sec ($\alpha \approx .12$ radians) for modes ≤ 3 (low order), and dissipation number $\geq .0005$ nepers/m. Convergence has not been obtained within 40 iterations when all these conditions are violated, although singly the restrictions can be relaxed (i.e. higher modes at $K_2'' > .001$, or lower phase velocity for modes 0, 1). Table 5.6 and figure 5.5 are useful in understanding the convergence limits. For $K_2'' <$ about .001 the imaginary part of incidence angle in layer 1 will be smaller than about 10^{-4}. The real part will have been perturbed by about 10^{-6} to 10^{-7} radians. As incidence angle or mode number increases $\Delta\varphi$, is even smaller. 10^{-7} radians represents the eighth decimal place in incidence angle at lower phase velocities, beyond the limits of single precision accuracy for the

minicomputer used here, but within the limits of accuracy for the double precision algorithm. For the HP2100 with 16 bit words and 3 word (39 bit fraction, 7 bit exponent) double precision floating point format, significant numerical representation to the user is to the 11th or 12th decimal digit depending on the magnitude of the leading digit in the fraction. In our algorithm it is believed that loss of significance occurs in the exponentiation involved in forming cosh, sinh. This problem might be relieved by more judicious choice of sequence operations in forming the characteristic equation functionals. We observe from the results of figure 5.7, however, that an effort is for our purposes needless, and actually counterproductive, since the time expended in iteration about these small perturbations yields small changes in modal attenuation coefficient, for high order or high frequency modes. That is, we suggest for modes higher than m=3 or 4, or for grazing angles less than about .2 radians, that the physical attenuation coefficient be used as a close approximation to the rigorous attenuation coefficient. From Table 5.7 we see that for $K_2''=.01$ at Cp=1530 relative error will be $\frac{5.7\times10^{-7}\ n/m}{3.45\times10^{-6} n/m}$ for mode 0,

$\frac{2.4\times10^{-7}\ n/m}{3.73\times10^{-6} n/m}$ for mode 1, $\frac{1.4\times10^{-7} n/m}{3.83\times10^{-6} n/m}$ for mode 2.

That is, 16.5%, 6.5%, 3.6% respectively. For $K_2''=.005$ relative errors are

$\frac{.17\times10^{-6} n/m}{9.73\times10^{-7} n/m}$ for mode 0 at 1515=Cp, $\frac{1.2\times10^{-7} n/m}{1.6\times10^{-6} n/m}$ for mode 1 at

Cp=1525 where convergence was last achieved, and

$\frac{.14\times10^{-6} n/m}{2.64\times10^{-6} n/m}$ at Cp=1545 where convergence was last achieved.

These correspond to errors of 17.5% for mode 0, 7.5% for mode 1, and 5.3% for mode 2, when plotted versus Re(Cp). Relative error when com-

puted as a function of frequency will be the same as above since neither Cp nor w are perturbed greatly by dissipation.

For low order modes δ should be used in the inverse problem of estimating parameter values from attenuation. Here the slope differences between δ and δ_{INT} can be confused with a variation in attenuation power law. For high order modes, curves for δ and δ_{INT} are congruent. δ_{INT} can be used in attenuation estimation, including at frequencies away from the reference frequency, e.g. for model 1A δ changed by 500-1000% at ω=10 radians in going from exp=1.0 to exp=1.4 for K_2''=.01. The error at that frequency for exp=1.0 between δ and δ_{INT} was 25% for mode 0 the worst case.

We should fairly mention that the alternative and commonly used multi-isovelocity layer reflection coefficient algorithm is the Haskell method (ref. 39). That algorithm works in the wavenumber domain as a matrix operator. Fryer (JASA Vol 63, No. 1, JAN 78) has recently applied this method to the computation of reflection coefficients and describes numerical difficulties inherent in its use. In particular, the method suffers from exponential overflow at high frequencies and for low phase velocities where supercritical reflection leads to exponentially growing and decaying solutions below the critical reflection point. Considerable effort by various authors has gone into analytically avoiding troublesome terms in the Haskell matrix computation. The Dunkin-Thrower (ref. 40) algorithm and Kinds (ref. 65) use of delta matrices have been found to be successful in solving the loss of precision problem and to speed computation. In our algorithm matrix methods are not invoked, rather, a Newton-Raphson search method is employed at each interface to determine propagated angles, and a complex angle formulation of the three layer recursive reflection coefficient is repeatedly calculated to propagate the reflection coefficient to the ocean bottom. We chose the incidence angle implementation because it has a physical interpretation, because Brekhovskikh had indicated the direction which might be taken in its implementation, and because angle of incidence may be used directly in forming arguments of $\phi(z)$ for inhomogeneous (e,g N^2-linear) layerings.

Chapter 6- Conclusions:

It has been shown that the representation of attenuation through complex sound speed and of wavenumber through complex incidence angle is a viable if somewhat cumbersome approach to wave propagation in stratified acoustic media. We have presented algorithms and computed results to show the effect of body wave dissipation on the normal mode representation of the propagating field. In the process we have demonstrated quantitatively the order of magnitude of the perturbation of eigenangles and eigenfrequencies usually, correctly, assumed to be second order when dissipation is introduced in a normal mode problem. We have discovered that the principal effect of attenuation is to introduce an imaginary part of eigenangle and of modal horizontal wavenumber. Both are directly proportional to body wave dissipation number.

The major result of the thesis has been delineation of domains of validity for several asymptotic attenuation laws proposed in the literature. Excellent agreement was found between the complete classical attenuation coefficient proposed by Kornhauser and Raney for the Pekeris model and the coefficient resulting from a rigorous wave theory analysis of the acoustic field based largely on the work of Brekhovskikh. An intuitive attenuation coefficient developed in this thesis was also found to agree well with the rigorous coefficient and to be the asymptotic limit of that coefficient for high mode number or low grazing angle. We suggest use of that the intuitive coefficient for mode numbers $n \geq 4$ by virtue of its computational economy. Fair agreement was found between the rigorous coefficient and the asymptotic coefficients proposed by Kornhauser and Raney and by Brekhovskikh. Use of these coefficients, however, must be limited to regions of small grazing angle where modal phase velocity is within about 5% of the water column sound speed. Poor agreement was obtained with our implementation of the perturbation theory attenuation coefficient proposed by Ingenito and Wolfe. That coefficient is insensitive to dissipation number. It does however converge to the correct result at low grazing angle.

The ultimate goal of acoustical modelling, through whatever formulation, will be either to predict the acoustic field from knowledge of the waveguide, or to estimate properties of the waveguide from measurements made on the field. Normal modes are particularly appropriate to the latter endeavor. For the Pekeris guide we have found that portions of modal dispersion curves whose phase velocity Cp lies midway between water column sound speed and bounding half-space sound speed are generally the regions of greatest character in terms of both variation of phase velocity with frequency, and of variation of modal attenuation coefficient with frequency. This is precisely the region where asymptotic expressions are inapplicable. We suggest that parameter estimation be based on extensive measurements of the amplitude decay of the three or four lowest order modes over wide frequency and phase velocity ranges, within that region. Only in this manner can we hope to estimate parameters α and β in the body wave attenuation power law $k'' = \alpha f^{\beta}$. In the line of future research we suggest that the existing mechanism for the treatment of multilayer inhomogeneous waveguides, contained in the computer program developed here, be exercised so that sensitivity to the parameter values of deeper layers may be ascertained. Given the time costly process of iteration to solution upon which this program is based, we also suggest that a cartesian wavenumber formulation of the problem be coded and efficiencies compared.

Table of Notation:

$\Phi(x,y,z,t)$	velocity potential as a function of spatial coordinates and time
$\phi(z)$	velocity potential z dependence, solution to the Helmholtz equation
$X(x), T(t), Y(y)$	independent components of velocity potential
ω	radian frequency – real
f	frequency in Hertz real
c_j	real sound speed in layer j
c_p	horizontal phase velocity
$\tilde{\varphi}_j$	complex incidence angle in layer j
φ'	real part of incidence angle
φ''	imaginary part of incidence angle
$\varphi'_{im}(c_p)$	real part of complex incidence angle at a given phase velocity for which the imaginary part = 0
$\varphi'_{a1}(c_p)$	real part of complex incidence angle at a given phase velocity at which reflection coefficient magnitude =1.
$\varphi'_{re\ spec}$	real part of complex incidence angle at which a discontinuity is found under certain constraints for propagated angle and reflection coefficient magnitude
α	grazing angle
φ_0	incidence angle at the source
x,y,z	Cartesian coordinates
r,z,ψ	cylindrical coordinates
p	pressure
$p^{(1)}, p^{(2)}$	pressure contributions from incident (1), or reflected (2) waves in a layer
ρ	density
v_z	particle velocity in z direction
$v_z^{(1)}, v_z^{(2)}$	particle velocity contribution from incident(1), or reflected (2) waves in a layer
h_j	thickness of layer j
d_j	layer thickness of Pekeris model

Notation 2.

$\tilde{c}_j$ = complex sound speed in layer j

ζ = displacement

$\tilde{k}_j$ = complex wavenumber in a layer, complex

k_j', k_j'' = real and imaginary parts of wavenumber in layer j

k_x', k_x'' = horizontal component of wavenumber in a layer, real and imaginary parts

k', k'' = vertical component of wavenumber in a layer

$b_.$ = vertical component of wavenumber in source layer (Brek.)

Γ = contour of integration in complex angle plane Brek formulation

k_0 = wavenumber in the ocean

λ = wavelength

T = ray cycle time

X = ray cycle length in Bucker treatment

$R_{j,j+1}$ = reflection coefficient at interface between layers i and i+1, treating layer i as a halfspace, but including partial reflection from underlying layers for layer i+1

$R\uparrow, R\downarrow$ = reflection coefficient looking up or down at any particular level z

$V_{i,i+1}$ = reflection coefficient at interface i,i+1 also $R_{i,i+1}$

$\tilde{\phi}$ = complex phase of reflection coefficient

$\phi'\downarrow, \phi''\downarrow$ real and imaginary parts of downward looking reflection coefficient phase

$\phi'\uparrow, \phi''\uparrow$ real and imaginary parss of upward looking reflection coefficient phase

$\chi\uparrow, \chi\downarrow$ = reflection coefficient phase looking up or down

Θ = reflection coefficient at the ocean bottom phase part

z = normal impedance

z_c = characteristic impedance

$z\downarrow, z\uparrow$ = normal impedance defined as the ratio of pressure to the vertical component of particle velocity for the downward or upward travelling solution to the Helmholtz equation.

T = transmission coefficient

G_b, G_s = reflection coefficient phase at bottom and surface in Bucker formulation

C_ν = ν^{th} order cylindrical function

$H_\nu^{(1)}, H_\nu^{(2)}$ = Hankel function of first and second kind, ν^{th} order

Notation 3

ς = contribution to argument in N^2-linear type layers

g = N^2-linear gradient, derivative of index of refraction squared w.r.t depth z

β = pseudo linear gradient in Morris notation

$N(z)$ = index of refraction with reference to source layer sound speed

u, v = argument of Bessel function or Hankel function

p = index of refraction at top of N^2-linear layer where z=0

$J_{mag}, \theta_N, \theta_M$ = quantities used in reflection coefficient for N^2-linear layer

h = vertical wavenumber

S = vertical phase integral in WKB formulation

$S(z)$ = mode shape

$D(h, f(\omega))$ = difference operator in finite difference evaluation

$f(\tilde{\varphi})$ = arbitrary function of complex angle

n = mode number

ℓ = mode number

Z^* = complex conjugate of impedance

Q = specific attenuation factor

$E, \Delta E$ = elastic energy per unit volumn change in energy

I = intensity of acoustic field

a = reciprocal absorption length

b, τ = parameters pertaining to properties of the liquid

B = bulk modulus

τ = relaxation time

ν = kinematic shear viscosity

γ, δ = real and imag parts of impedance

ρ, ϕ = magnitude and phase of reflection coefficient

δ = rigorous modal attenuation coefficient determined by satisfying complex characteristic equation with complex incidence angle

δ_{INT} = attenuation calculated using physical reasoning

δ_{KR} = attenuation coefficient calculated using full expression from Kornhauser and Raney

Notation 4.

α_{BA} = attenuation coefficient calculated usisng Brekhovskih's asymptotic approximations

α_{IW} = attenuation coefficient calculated with our implementation of perturbation theory from Ingenito and Wolfe.

Layering Models

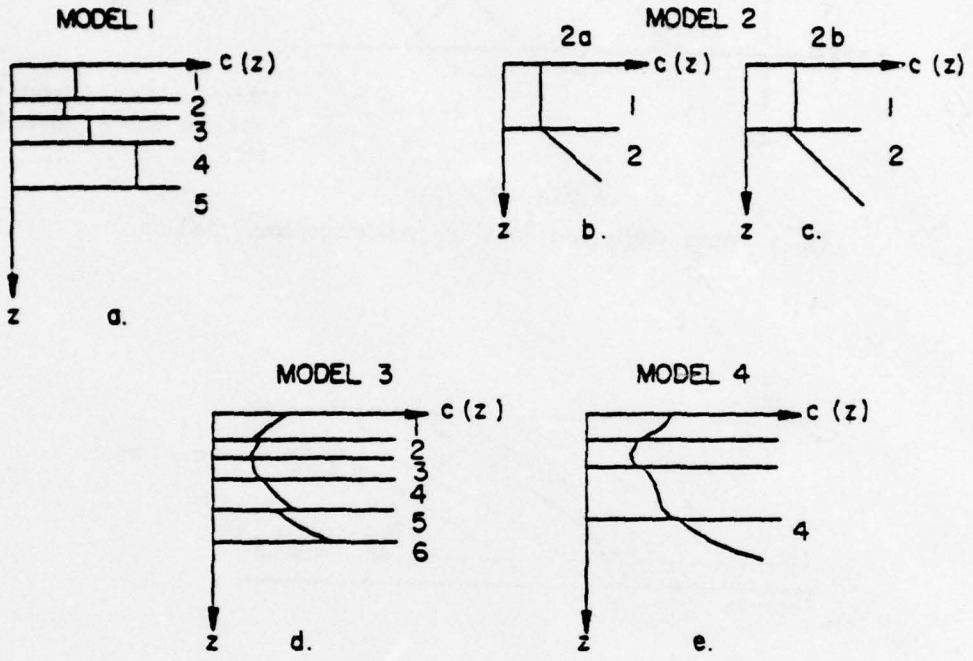

a. Model 1: An isovelocity liquid multilayering with constant densities in each layer

b. Model 2a: An isovelocity ocean overlying a liquid bottom halfspace with an N^2-linear sound speed in the halfspace

c. Model 2b: Model 2a with a sound speed discontinuity permitted at the ocean bottom

d. Model 3: N^2-linear liquid multilayering with sound speed discontinuities permitted at all layers

e. Model 4: Arbitrary continuous sound speed variation permitted within each layer, discontinuities permitted at the interfaces- a piecewise WKB approximation because eigenfunctions are determined by WKB approximation within each layer and matched at the discontinuities

Figure 1.1

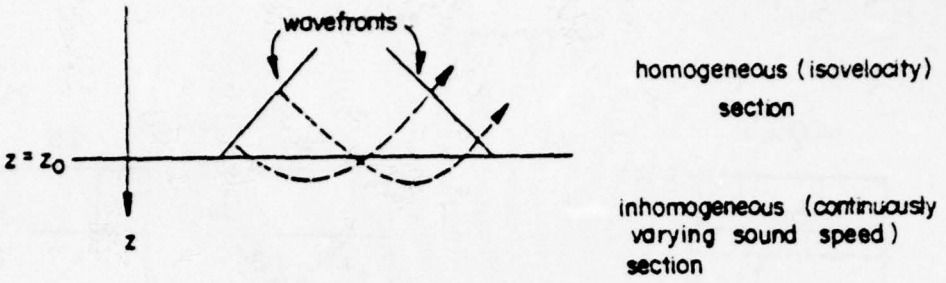

Figure 2.1
Plane Wave reflection from an inhomogeneous medium

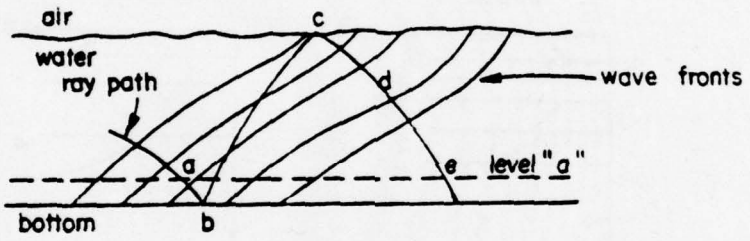

Figure 2.2 a
Downgoing wavefronts for ocean with slowly varying sound speed vs depth (from Bucker)

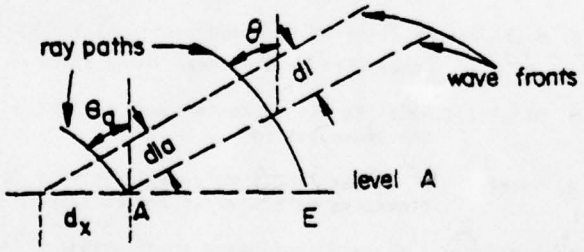

Figure 2.2 b
Wavefront geometrical quantities used in Buckers characteristic equation derivation

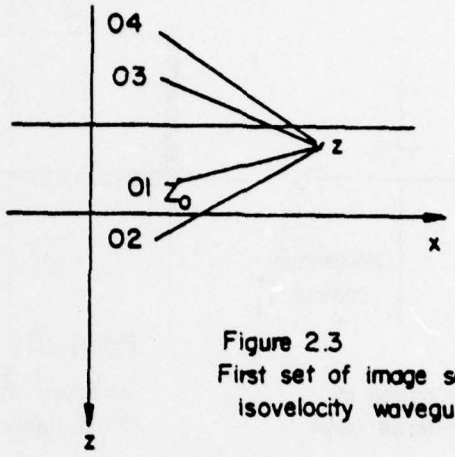

Figure 2.3
First set of image sources for isovelocity waveguide

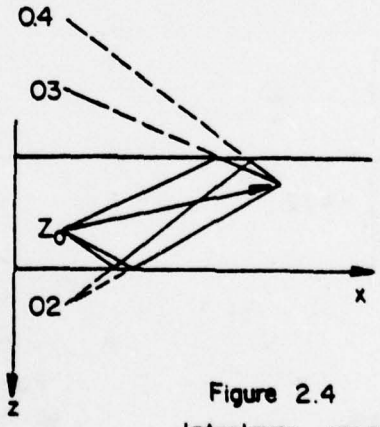

Figure 2.4
Intralayer ray paths for first image source set

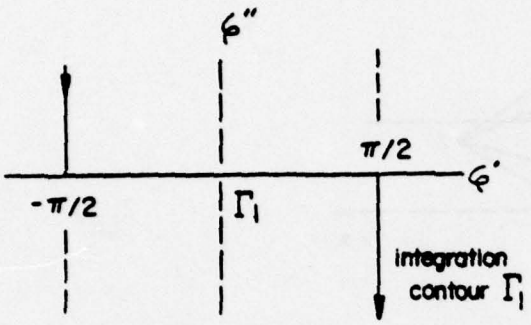

Figure 2.5a

Original contour of integration in plane of complex incidence angle

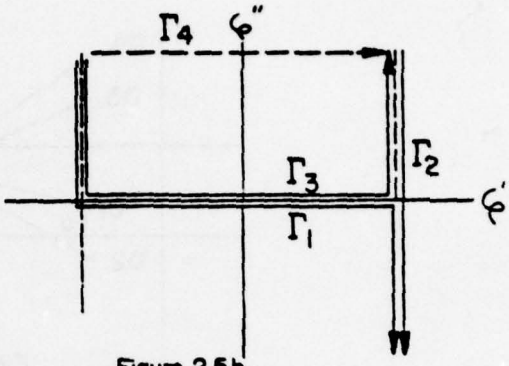

Figure 2.5b

contours involved in field integral Brelt. 27.2

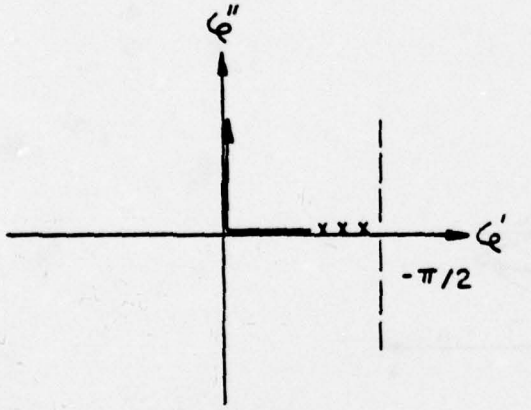

Figure 2.6a
Pole and branch cut positions for lossless case

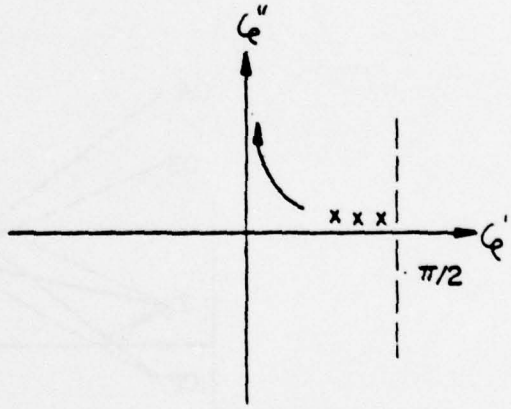

Figure 2.6b
Pole and branch cut positions for lossy case

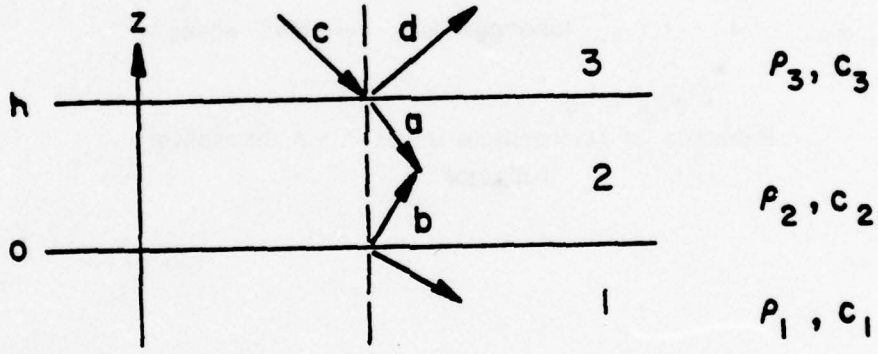

Figure 2.7

Geometry and notation of
recursive reflection coef. derivation
– isovelocity layers

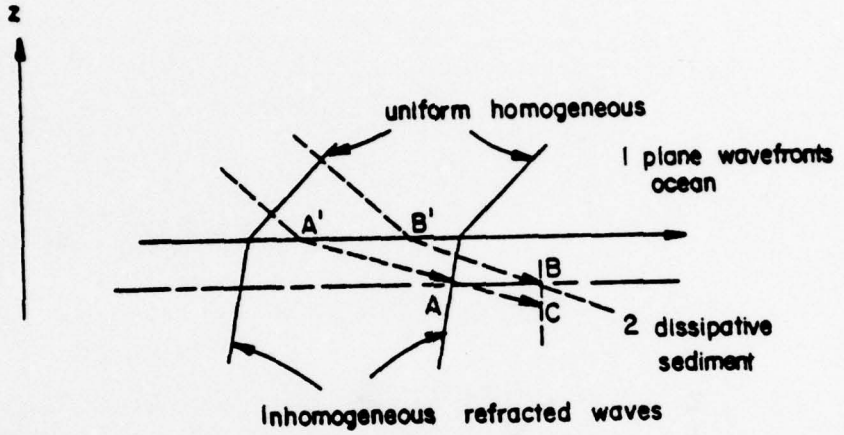

Figure 4.1 a
Refraction of homogeneous waves into a dissipative halfspace

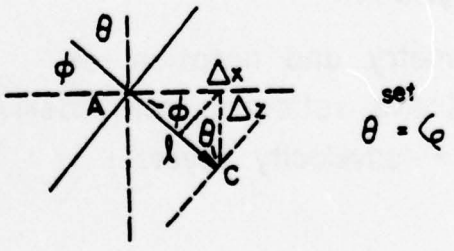

Figure 4.1 b

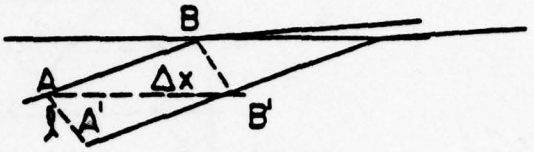

Figure 4.2

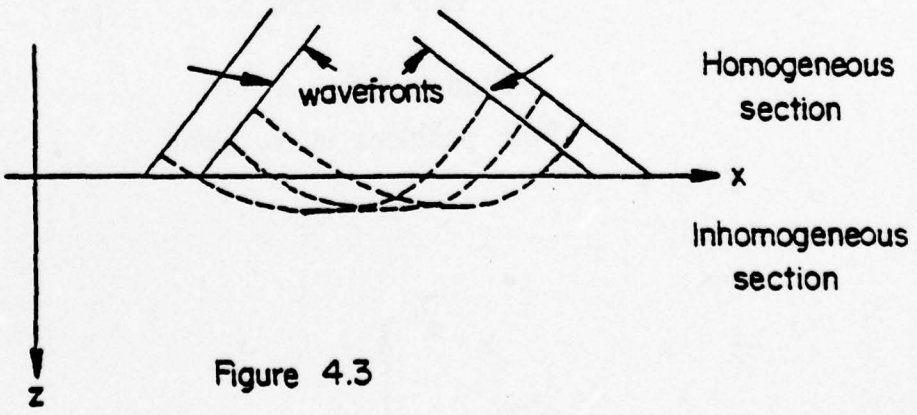

Figure 4.3

Refracted waves in a dissipative Inhomogeneous Halfspace

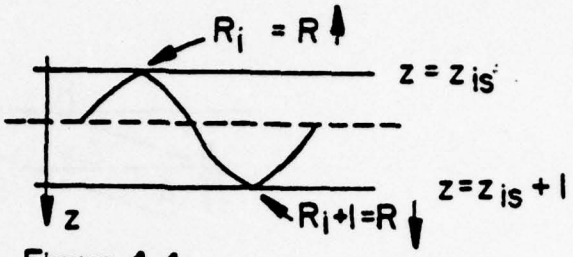

Figure 4.4

Guided wave reflection in an inhomogeneous layer

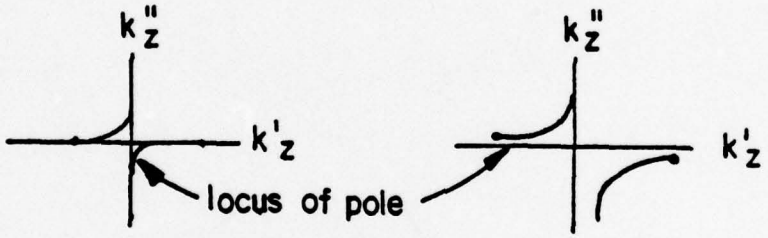

Figure 4.5

Pole positions in R_z plane

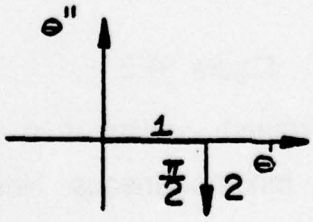

Figure 4.6

Locus of source incidence angle in Intuitive formulation

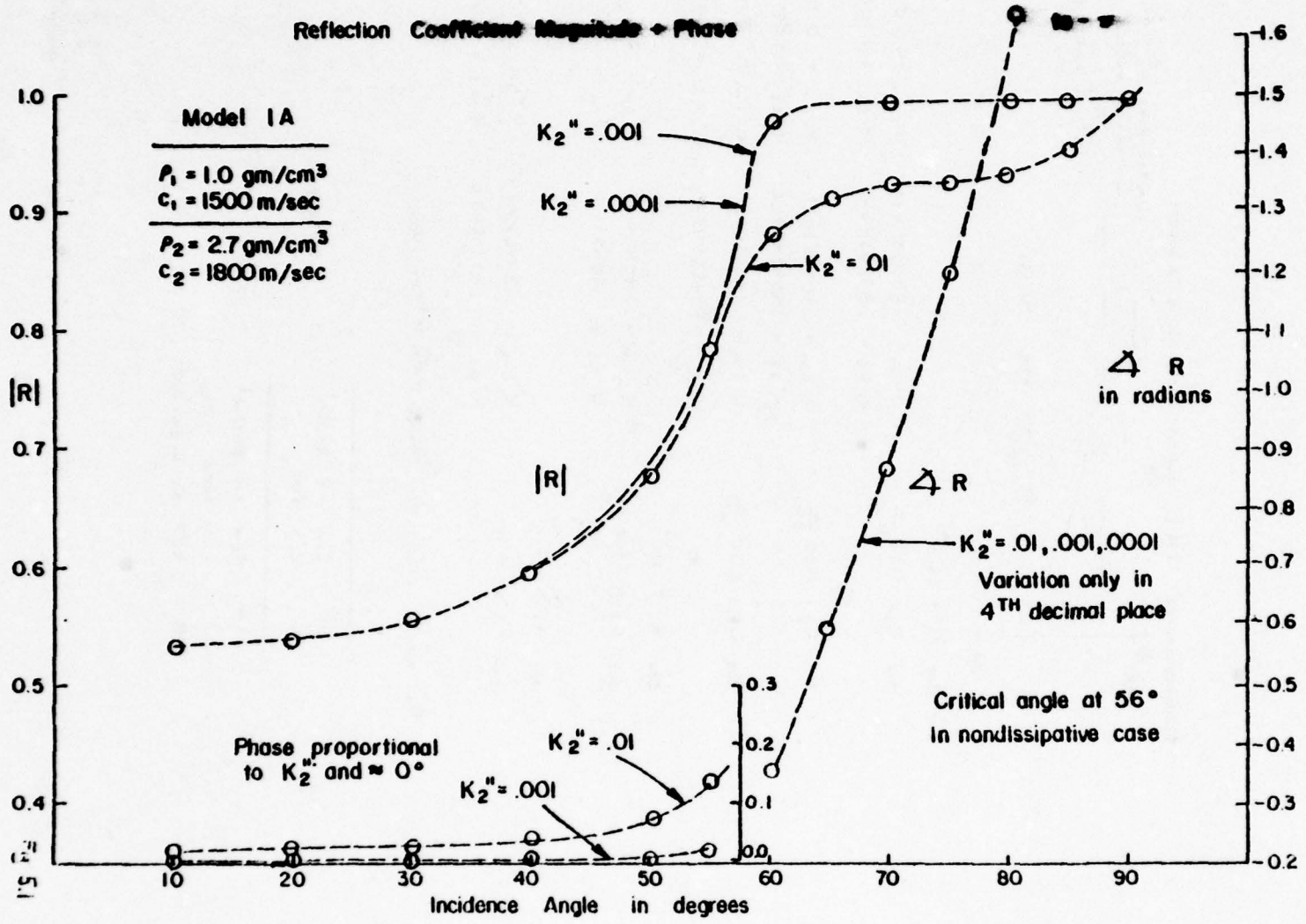
Reflection Coefficient Magnitude & Phase
Model 1A
ρ_1 = 1.0 gm/cm^3
c_1 = 1500 m/sec
ρ_2 = 2.7 gm/cm^3
c_2 = 1800 m/sec
K_2'' = .001
K_2'' = .0001
K_2'' = .01
|R|
Δ R
in radians
Δ R
K_2'' = .01, .001, .0001
Variation only in
4TH decimal place
Critical angle at 56°
In nondissipative case
Phase proportional
to K_2'' and ≈ 0°
K_2'' = .01
K_2'' = .001
|R|
Δ R
Incidence Angle in degrees

Illustration of $|R|$ discontinuity along Cp locus:

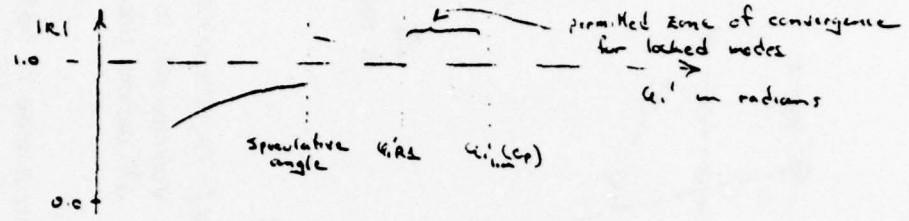

e.g. for $K_L'' = 5_{A10}^{-4}$

for $C_p = 1950 \frac{m}{sec}$

$\psi_{i\,lim}' = .877636419$, $\psi_{i\,lim}'' = 0.0$

$\psi_{iRL}' = .877634645$, $\psi_{iRL}'' = 1.7051 \times 10^{-3}$

for $C_p = 1900 \frac{m}{sec}$

$\psi_{i\,lim}' = .90995103$, $\psi_{i\,lim}'' = 0.0$

$\psi_{iRL}' = .9099949422$, $\psi_{iRL}'' = 1.5773 \times 10^{-3}$

for $C_p = 1850 \frac{m}{sec}$

$\psi_{i\,lim}' = .94553606$, $\psi_{i\,lim}'' = 0.0$

$\psi_{iRL}' = .94553458$, $\psi_{iRL}'' = 1.4716 \times 10^{-3}$

for $K_L'' = 10^{-3}$

for $C_p = 1900 \frac{m}{sec}$

$\psi_{i\,lim}' = .90995103$, $\psi_{i\,lim}'' = 0$

$\psi_{iRL}' = .9099944$, $\psi_{iRL}'' = 3.19441 \times 10^{-3}$

for $K_L'' = 10^{-2}$

for $C_p = 1950$

$\psi_{i\,lim}' = .877636419$, $\psi_{i\,lim}'' = 0$

$\psi_{iRL}' = .87746642$, $\psi_{iRL}'' = 1.6807 \times 10^{-2}$

The model used in these calculations was

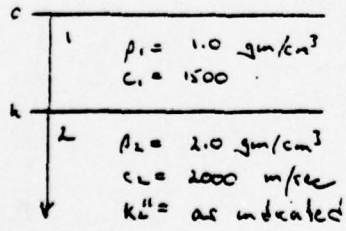

$h = 1000$ m

Fig 5.2
Table 5.2

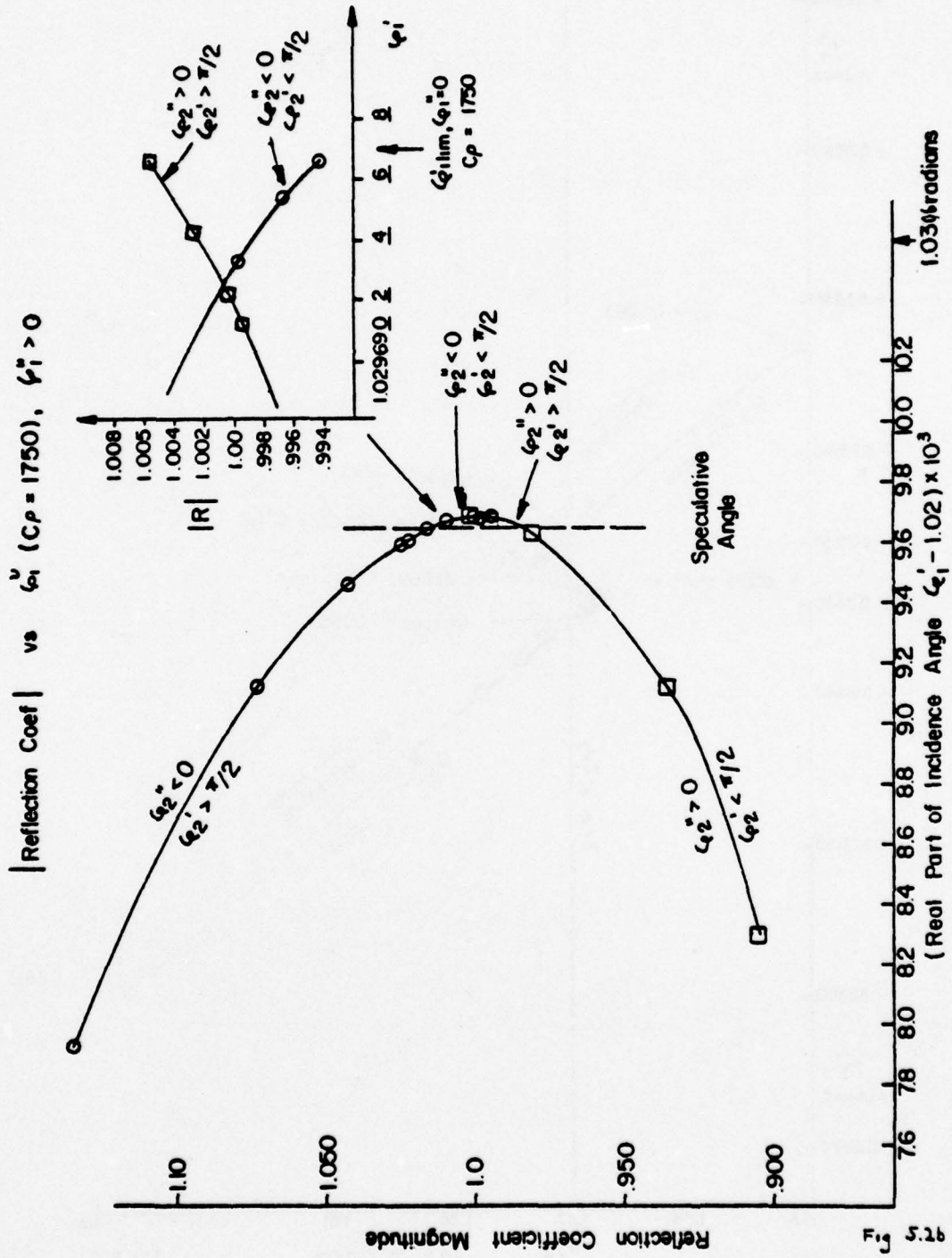
|Reflection Coef| vs φ_i'' (C_ρ = 1750), $\varphi_i'' > 0$
Reflection Coefficient Magnitude
1.10
1.050
1.0
.950
.900
7.6 7.8 8.0 8.2 8.4 8.6 8.8 9.0 9.2 9.4 9.6 9.8 10.0 10.2
(Real Part of Incidence Angle $\varphi_i' - 1.02) \times 10^3$
1.034 radians
Speculative Angle
$\varphi_2'' < 0$ $\varphi_2' > \pi/2$
$\varphi_2'' > 0$ $\varphi_2' < \pi/2$
$\varphi_2'' < 0$ $\varphi_2' < \pi/2$
$\varphi_2'' > 0$ $\varphi_2' > \pi/2$
|R|
1.008
1.005
1.004
1.002
1.00
.998
.996
.994
1.02969
2 4 6 8
φ_i'
$\varphi_i' = \lim \varphi_i'' = 0$
C_ρ = 1750

Fig 5.26

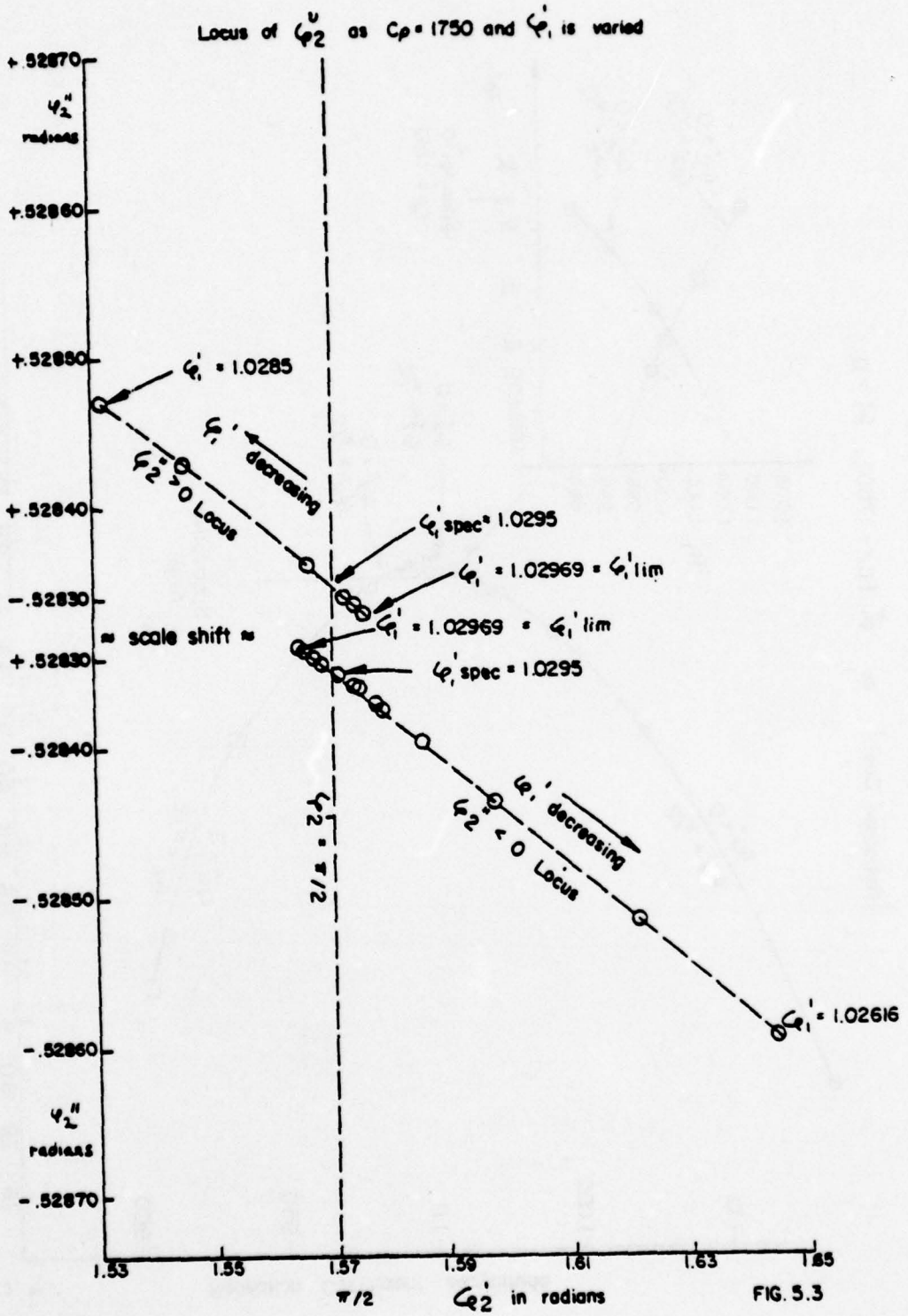
Locus of φ_{2}^{υ} as $C\rho = 1750$ and φ_1' is varied
+.52870
φ_2'' radians
+.52860
+.52850
+.52840
−.52830
≈ scale shift ≈
+.52830
−.52840
−.52850
−.52860
φ_2'' radians
−.52870
$\varphi_1' = 1.0285$
φ_1' decreasing
$\varphi_2'' > 0$ Locus
φ_1' spec = 1.0295
$\varphi_1' = 1.02969 = \varphi_1'$ lim
$\varphi_1' = 1.02969 = \varphi_1'$ lim
φ_1' spec = 1.0295
φ_1' decreasing
$\varphi_2'' < 0$ Locus
$\varphi_2' = \pi/2$
$\varphi_1' = 1.02616$
1.53
1.55
1.57
1.59
1.61
1.63
1.65
$\pi/2$
φ_2' in radians

FIG. 5.3

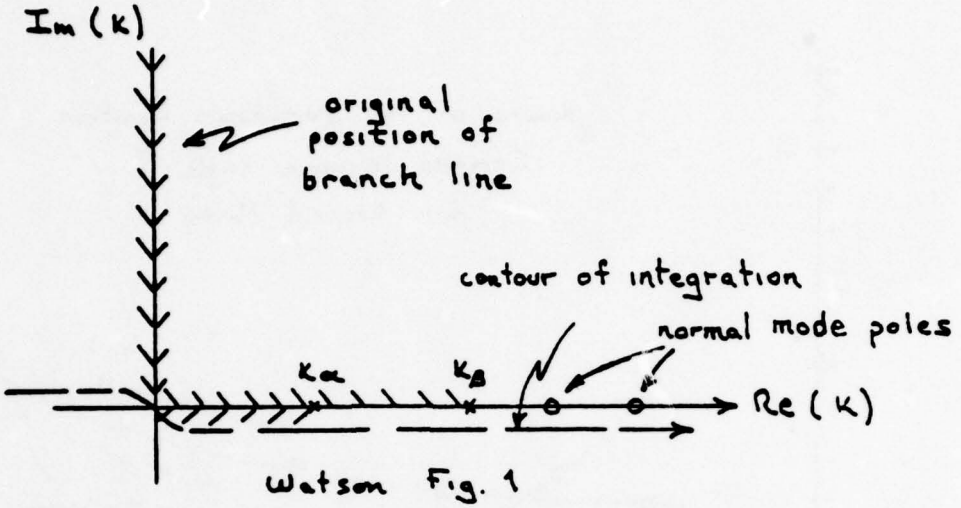

Watson Fig. 1

Figure 5.4 a

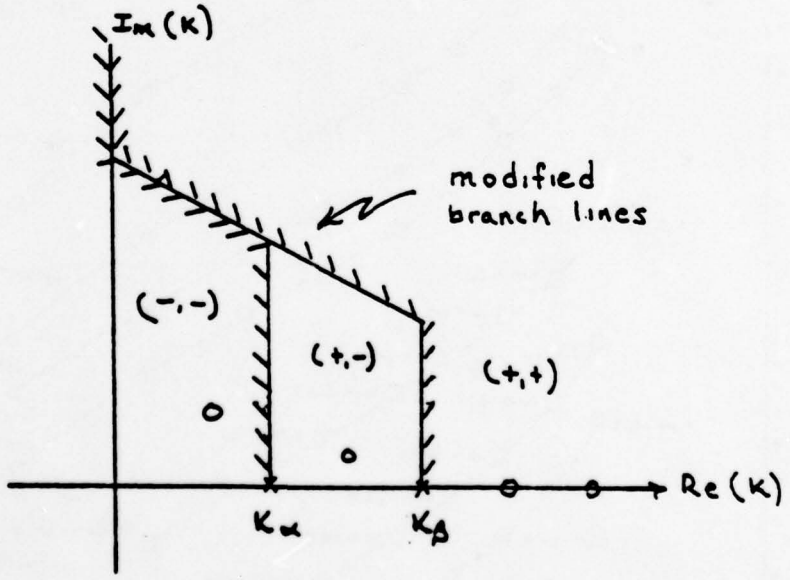

Watson Fig. 2

Figure 5.4 b

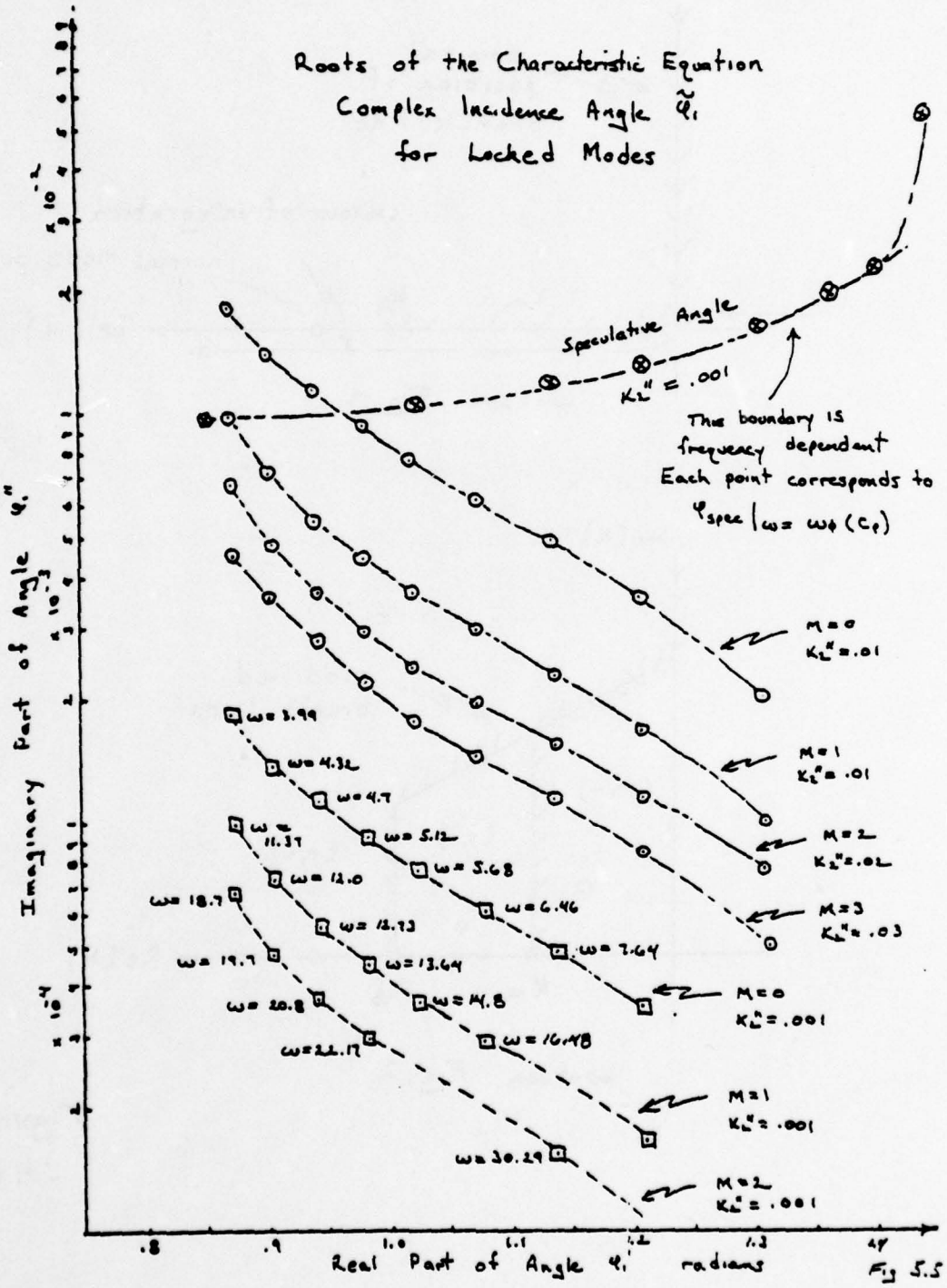
Roots of the Characteristic Equation
Complex Incidence Angle $\tilde{\varphi}_i$
for Locked Modes
Speculative Angle
$K_L'' = .001$
This boundary is frequency dependant
Each point corresponds to
$\varphi_{spec} | \omega = \omega_\phi (C_\phi)$
M=0 $K_L''=.01$
M=1 $K_L''=.01$
M=2 $K_L''=.02$
M=3 $K_L''=.03$
M=0 $K_L''=.001$
M=1 $K_L''=.001$
M=2 $K_L''=.001$
ω = 3.99
ω = 4.32
ω = 4.7
ω = 5.12
ω = 5.68
ω = 6.46
ω = 7.64
ω = 11.37
ω = 12.0
ω = 12.73
ω = 13.64
ω = 14.8
ω = 16.48
ω = 18.7
ω = 19.7
ω = 20.8
ω = 22.17
ω = 30.29
Imaginary Part of Angle φ_i''
Real Part of Angle φ_i' radians
.8
.9
1.0
1.1
1.2
1.3

Fig 5.5

Complex Incidence Angle Domains

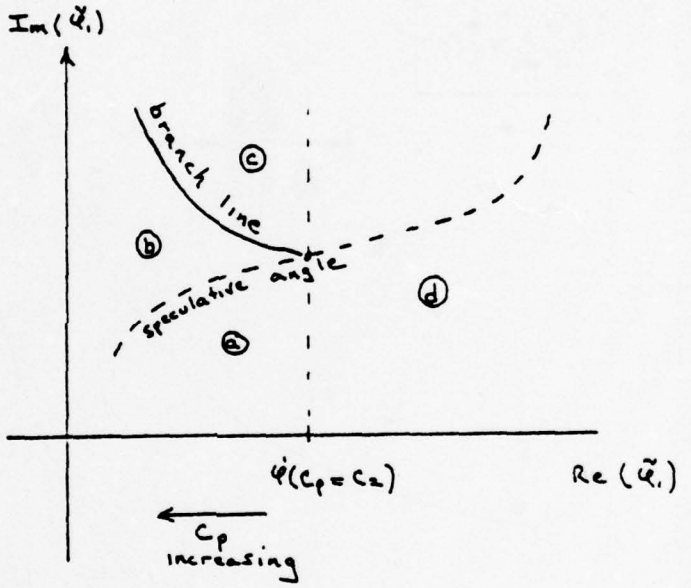

Figure 5.5.b

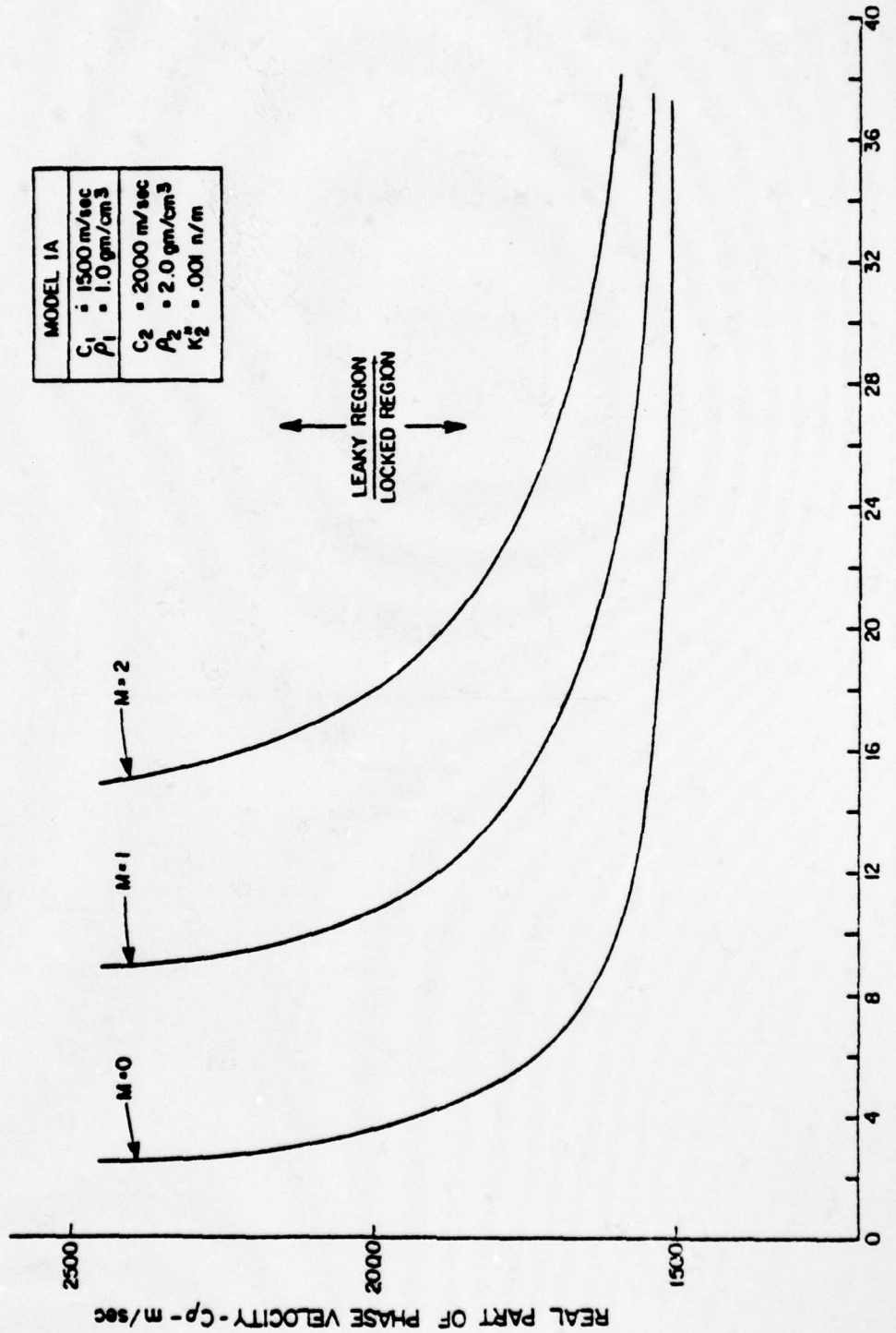
MODAL DISPERSION - LOCKED AND LEAKY REGIONS - PEKERIS GUIDE
MODEL IA
C_1 = 1500 m/sec
ρ_1 = 1.0 gm/cm³
C_2 = 2000 m/sec
ρ_2 = 2.0 gm/cm³
K_2^2 = .001 n/m
LEAKY REGION
LOCKED REGION
M=0
M=1
M=2
REAL PART OF PHASE VELOCITY - Cp - m/sec
2500
2000
1500
0
4
8
12
16
20
24
28
32
36
40
FREQUENCY ω IN RADIANS/SEC

Fig 5.6

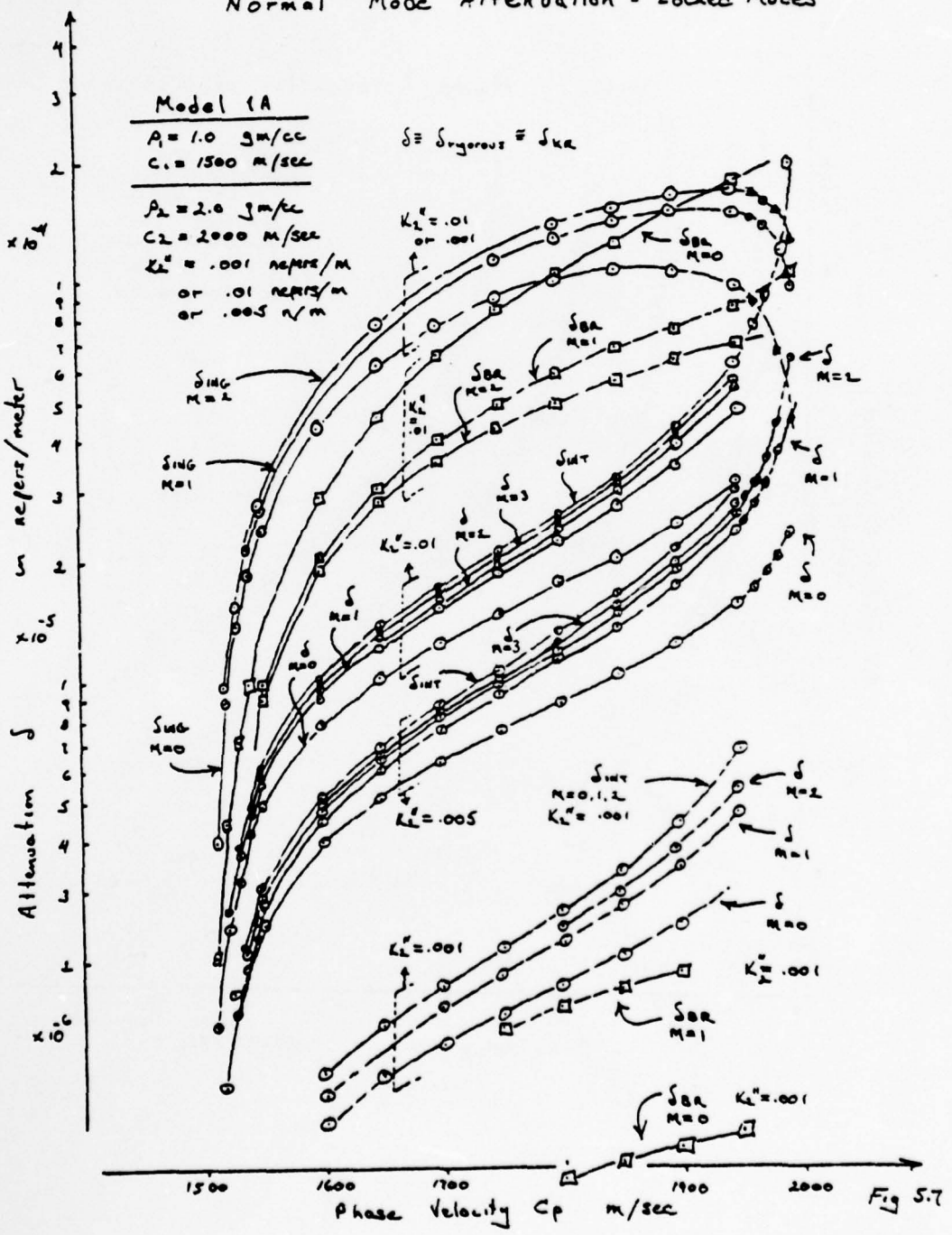
Normal Mode Attenuation - Locked Modes
Model 1A
ρ1 = 1.0 gm/cc
c1 = 1500 m/sec
ρ2 = 2.0 gm/cc
c2 = 2000 m/sec
K2" = .001 nepers/m
or .01 nepers/m
or .005 n/m
δ ≡ δrigorous ≈ δka
Attenuation δ in nepers/meter
Phase Velocity Cp m/sec
1500
1600
1700
1900
2000
δSING M=2
δSING M=1
δSING M=0
δSBR M=0
δSBR M=1
δSBR M=2
δINT
K2" = .01
K2" = .005
K2" = .001

Fig 5.7

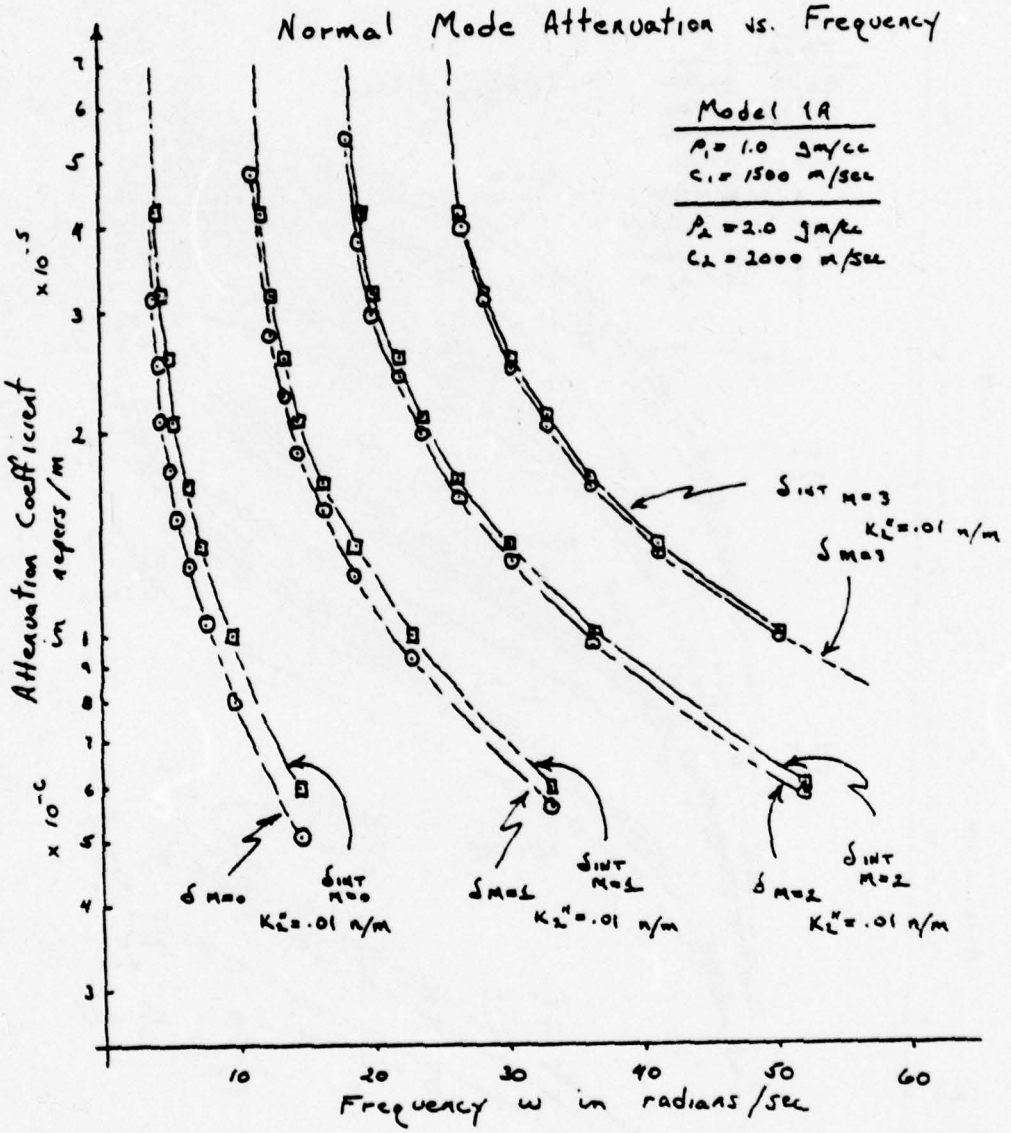
Normal Mode Attenuation vs. Frequency
Model 1A
ρ_1 = 1.0 gm/cc
c_1 = 1500 m/sec
ρ_2 = 2.0 gm/cc
c_2 = 2000 m/sec
Attenuation Coefficient in nepers/m
x 10^-5
x 10^-6
$\delta_{INT\ M=3}$
K_L'' = .01 n/m
$\delta_{M=3}$
$\delta_{M=0}$
$\delta_{INT\ M=0}$
K_L'' = .01 n/m
$\delta_{M=1}$
$\delta_{INT\ M=1}$
K_L'' = .01 n/m
$\delta_{M=2}$
$\delta_{INT\ M=2}$
K_L'' = .01 n/m
10
20
30
40
50
60
Frequency ω in radians/sec

Fig. 5.76

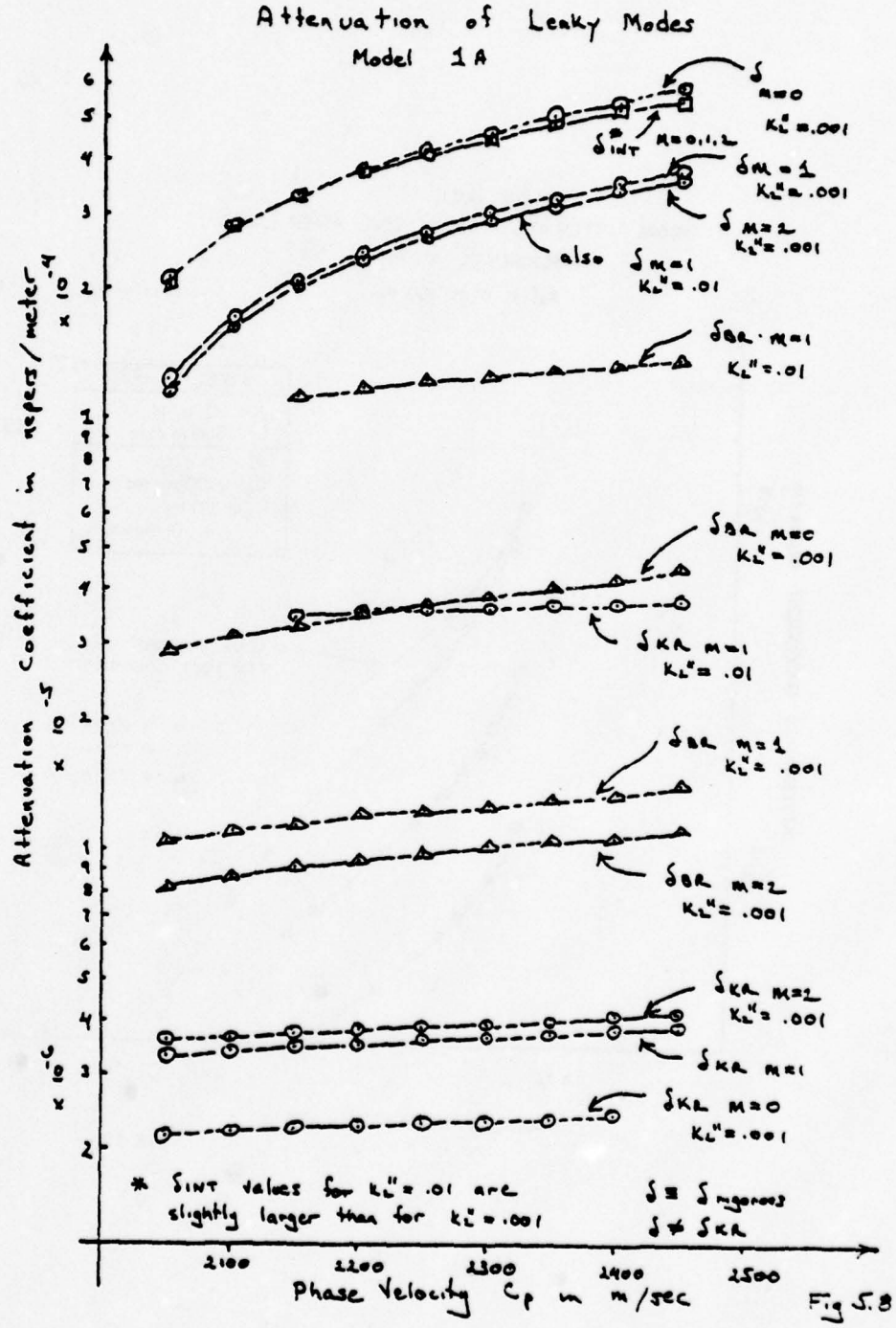
Attenuation of Leaky Modes
Model 1A
Attenuation Coefficient in nepers/meter
x 10^-4
x 10^-5
x 10^-6
δ m=0 KL"=.001
δ INT* m=0,1,2
δ M=1 KL"=.001
δ M=2 KL"=.001
also δ M=1 KL"=.01
δBR m=1 KL"=.01
δBR m=0 KL"=.001
δKR m=0 KL"=.01
δBR m=1 KL"=.001
δBR m=2 KL"=.001
δKR m=2 KL"=.001
δKR m=1
δKL m=0 KL"=.001
* δINT values for KL"=.01 are slightly larger than for KL"=.001
δ ≡ δ nonporous
δ ≠ δKR
2100
2200
2300
2400
2500
Phase Velocity Cp in m/sec

Fig 5.8

PEKERIS GUIDE
MODAL ATTENUATION FOR SEVERAL POWER LAWS
FUNDAMENTAL MODE
$K_2'' = .01$ at 100 Hz

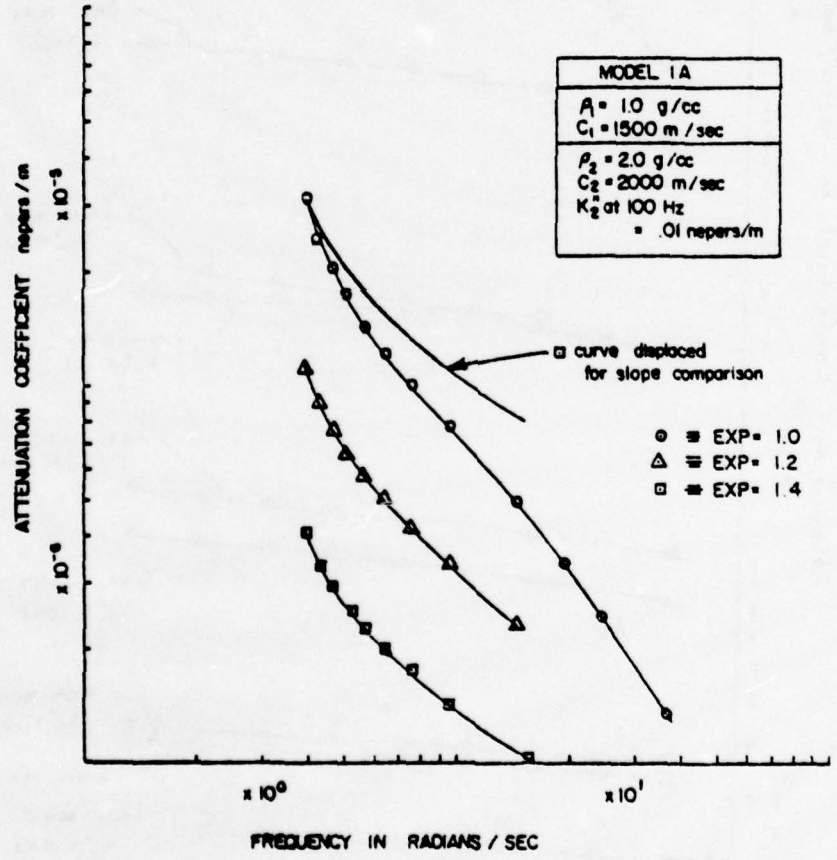

FIG. 5.9

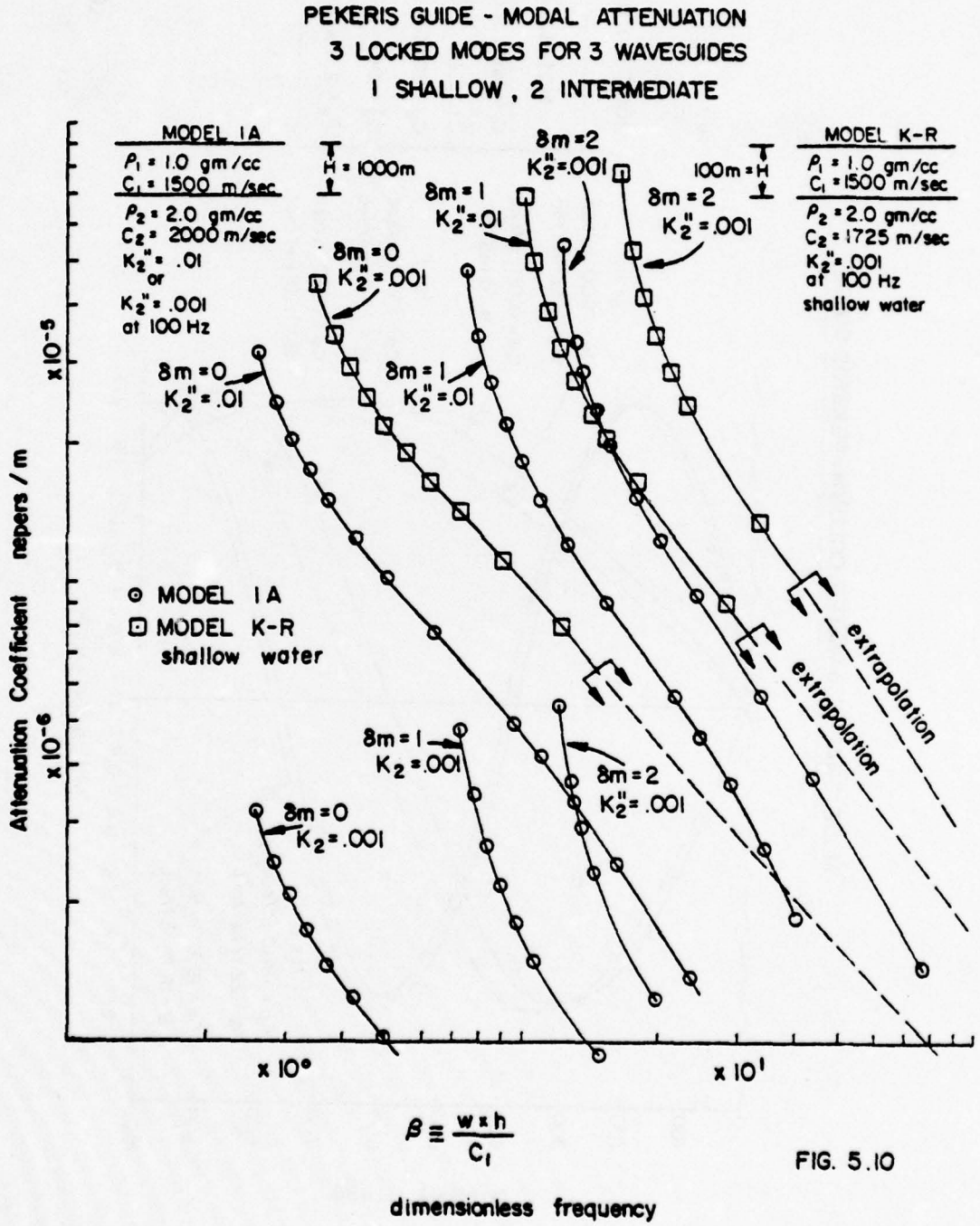
PEKERIS GUIDE - MODAL ATTENUATION
3 LOCKED MODES FOR 3 WAVEGUIDES
1 SHALLOW, 2 INTERMEDIATE
MODEL 1A
ρ_1 = 1.0 gm/cc
C_1 = 1500 m/sec
ρ_2 = 2.0 gm/cc
C_2 = 2000 m/sec
K_2'' = .01 or K_2'' = .001 at 100 Hz
H = 1000m
MODEL K-R
ρ_1 = 1.0 gm/cc
C_1 = 1500 m/sec
ρ_2 = 2.0 gm/cc
C_2 = 1725 m/sec
K_2'' = .001 at 100 Hz
shallow water
100m = H
δm = 0 K_2'' = .01
δm = 1 K_2'' = .01
δm = 2 K_2'' = .001
δm = 0 K_2'' = .001
δm = 1 K_2'' = .001
δm = 2 K_2'' = .001
δm = 0 K_2 = .001
δm = 1 K_2 = .001
δm = 2 K_2'' = .001
extrapolation
extrapolation
extrapolation
⊙ MODEL 1A
⊡ MODEL K-R
shallow water
Attenuation Coefficient nepers / m
x 10⁻⁵
x 10⁻⁶
x 10⁰
x 10¹
$\beta \equiv \frac{w \times h}{C_1}$
dimensionless frequency

FIG. 5.10

MODE SHAPES in WATER COLUMN - PEKERIS GUIDE

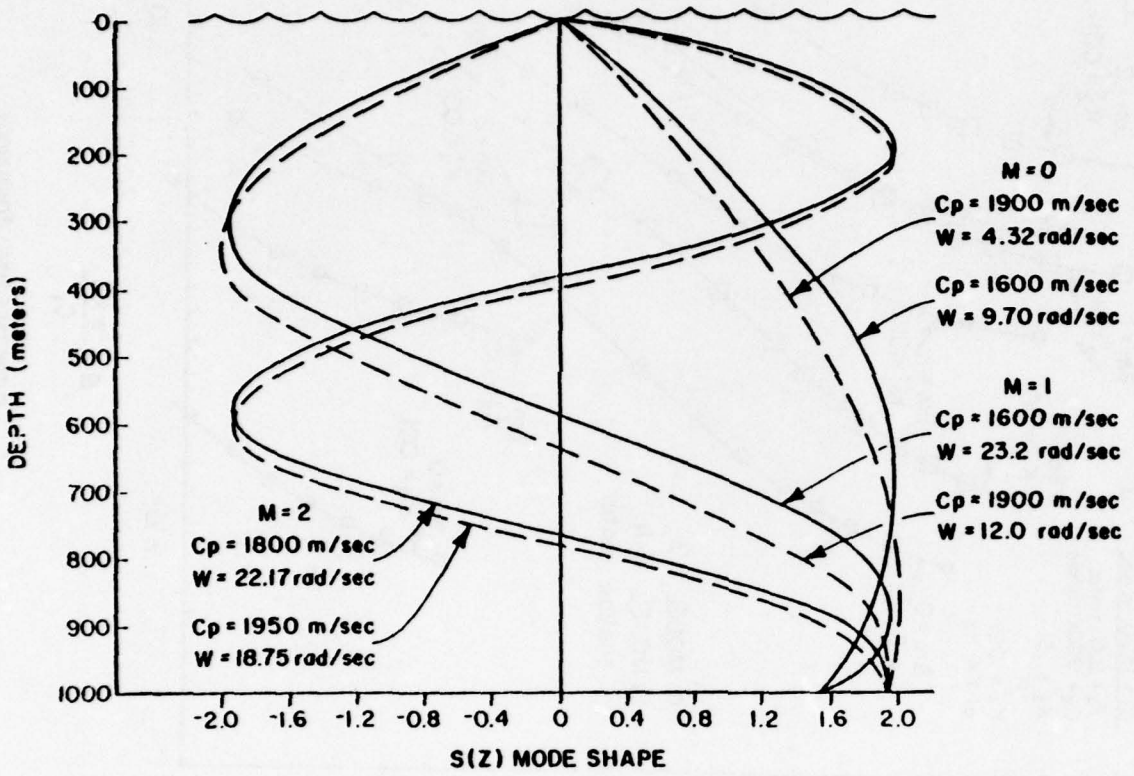

MODE Nº1 & Nº2

MODEL 1A
C_1 = 1500 m/sec K_1'' = 0 ρ_1 = 1.0
C_2 = 2000 m/sec K_2'' = .001 nepers/m ρ_2 = 2.0 g/cm^3

Fig. 5.11

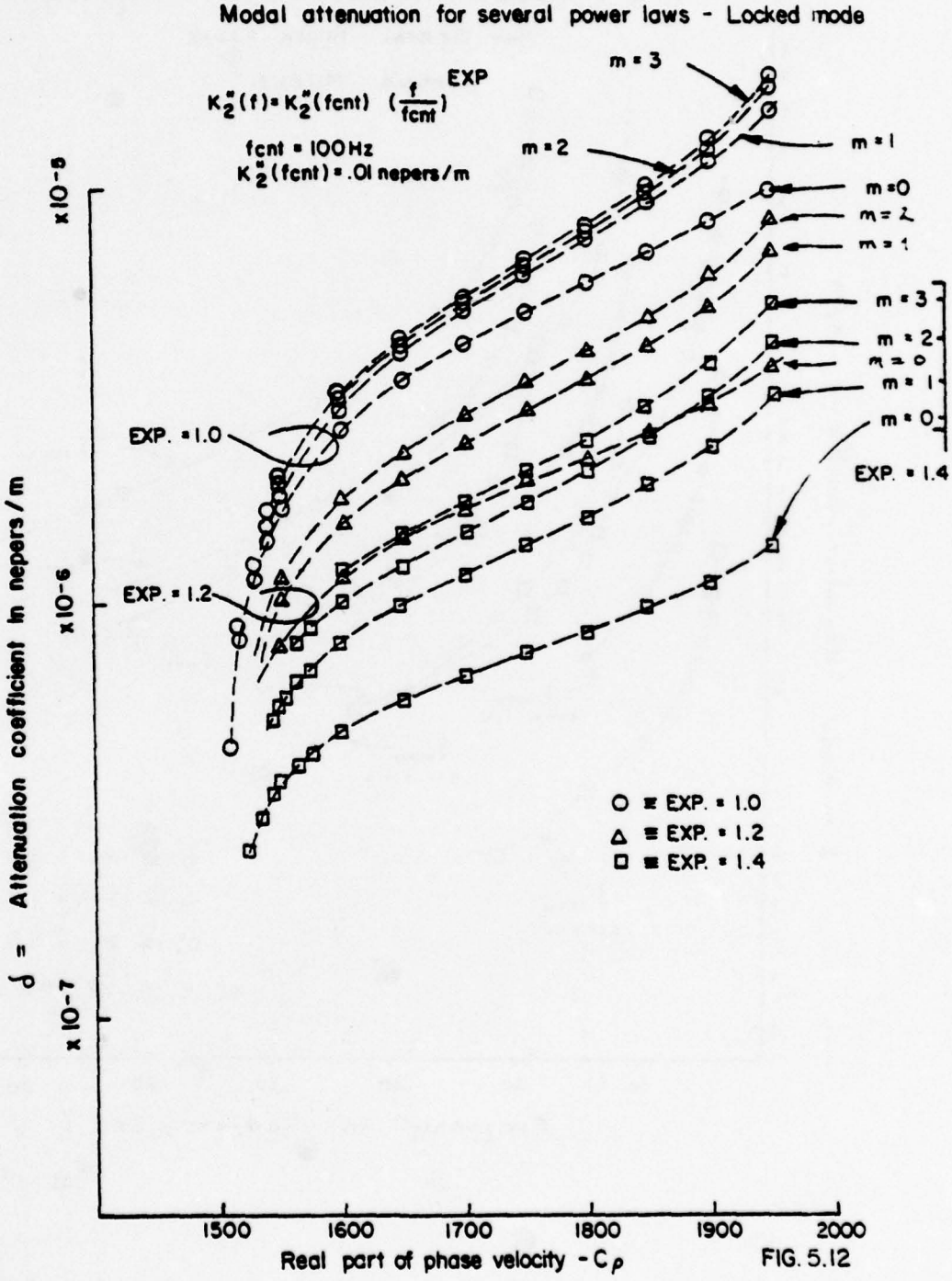
Modal attenuation for several power laws - Locked mode
$K_2''(f) = K_2''(fcnt)\ (\frac{f}{fcnt})^{EXP}$
fcnt = 100 Hz
$K_2''(fcnt)$ = .01 nepers/m
m = 3
m = 2
m = 1
m = 0
m = 2
m = 1
m = 3
m = 2
m = 0
m = 1
m = 0
EXP. = 1.0
EXP. = 1.2
EXP. = 1.4
O ≡ EXP. = 1.0
Δ ≡ EXP. = 1.2
□ ≡ EXP. = 1.4
δ = Attenuation coefficient in nepers/m
x10-5
x10-6
x10-7
1500
1600
1700
1800
1900
2000
Real part of phase velocity - C_p

FIG. 5.12

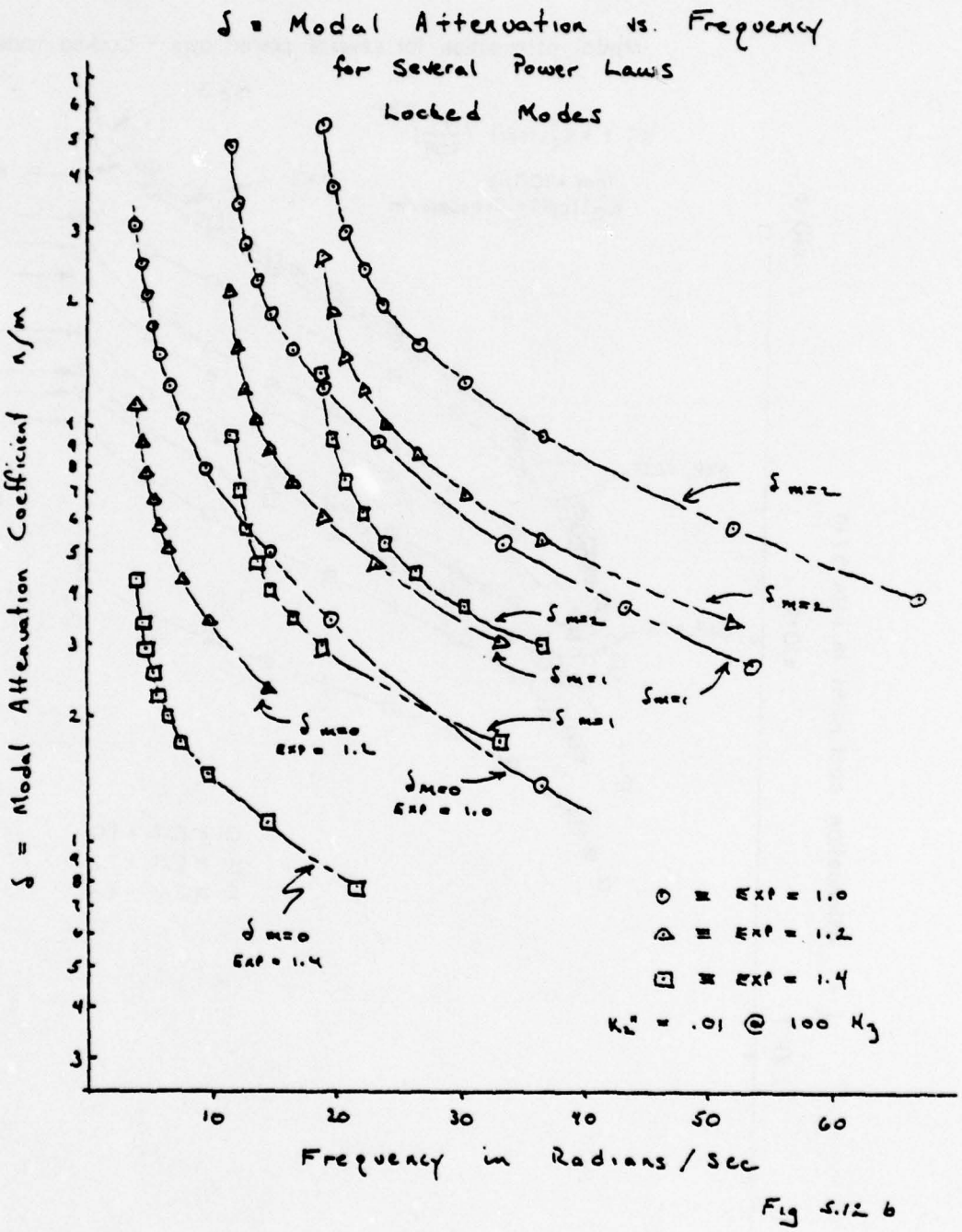
δ = Modal Attenuation vs. Frequency
for Several Power Laws
Locked Modes
δ = Modal Attenuation Coefficient n/m
δ m=2
δ m=2
δ m=2
δ m=1
δ m=1
δ m=1
δ m=0
EXP = 1.2
δ m=0
EXP = 1.0
δ m=0
EXP = 1.4
⊙ ≡ EXP = 1.0
△ ≡ EXP = 1.2
□ ≡ EXP = 1.4
K_L" = .01 @ 100 Kg
10
20
30
40
50
60
Frequency in Radians / Sec

Fig 5.12 b

Loci of Refracted Angle $\tilde{\varphi}_2$

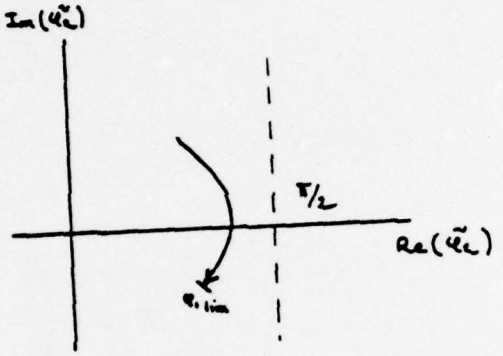

Fig 5.13 a

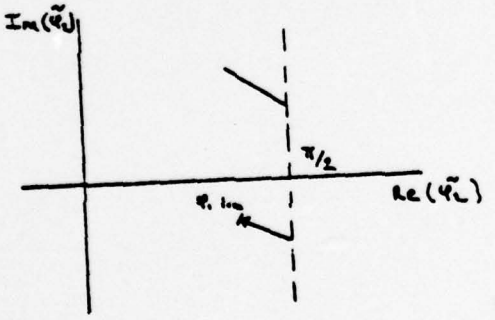

Fig 5.13 b

Reflection Coefficient for Real Incidence Angle

Incidence Angle		$K_2'' = .01$		$K_2'' = .001$		$K_2'' = .0001$	
radians	degrees	$\|R\|$	$\angle R$	$\|R\|$	$\angle R$	$\|R\|$	$\angle R$
.174	10°	.5307	-2.02×10^{-2}	.5307	-2.02×10^{-3}	.530	-2.02×10^{-4}
.348	20°	.5389	-2.26×10^{-2}	.538	-2.26×10^{-3}	.5389	-2.26×10^{-4}
.522	30°	.5560	-2.77×10^{-2}	.556	-2.77×10^{-3}	.556	-2.77×10^{-4}
.696	40°	.5908	-3.87×10^{-2}	.591	-3.86×10^{-3}	.5912	-3.86×10^{-4}
.870	50°	.6764	-7.05×10^{-2}	.6796	-7.14×10^{-3}	.6797	-7.14×10^{-4}
.957	55°	.7828	-1.32×10^{-1}	.811	$-.0159$	.8115	-1.59×10^{-3}
1.044	60°	.8835	-3.35×10^{-1}	.9876	$-.3353$	.9876	-3.35×10^{-1}
1.131	65°	.9142	-5.95×10^{-1}			.99910	-5.95×10^{-1}
1.218	70°	.9218	-8.66×10^{-1}	.9919	$-.8664$	.99919	-8.66×10^{-1}
1.305	75°	.9246	-1.20	.99219	-1.202	.99922	-1.202
1.392	80°	.9303	-1.66	.99279	-1.6568	.99928	-1.6568
1.479	85°	.9509	-2.24	.99497	-2.289	.99950	-2.289
1.566	90°	.9969	-3.09	.9997	-3.094	.99997	-3.094

Table 5.1

Model

$c_1 = 1500$ m/sec
$\rho_1 = 1.0$ gm/cc
$K_1'' = 0$

$c_2 = 1800$ m/sec
$\rho_2 = 2.7$ gm/cc
see table for K_2''

Table 5.2b.

Roots of the Refraction Equation

C_p = 1750 m/sec φ_2' max = π $\varphi_2'' > 0$

φ_1'	φ_1''	φ_2'	φ_2''	$\lvert R \rvert$
1.0246	7.77×10^{-2}	1.479	5.2864×10^{-1}	.804
1.02663	6.343×10^{-2}	1.4981	5.2858×10^{-1}	.8375
1.0285	3.657×10^{-2}	1.53188	5.2847×10^{-1}	.9051
1.0291	2.585×10^{-2}	1.5452	5.2843×10^{-1}	.9338
1.02963	8.960×10^{-3}	1.56624	5.2836×10^{-1}	.9811
1.02968	3.685×10^{-3}	1.57279	5.2834×10^{-1}	.9964
1.029 69106	2.626×10^{-3}	1.574	5.2834×10^{-1}	.9995
1.02969217	2.358×10^{-3}	1.5744	5.2834×10^{-1}	1.0003
1.0296944	1.699×10^{-3}	1.57526	5.2834×10^{-1}	1.0022
1.0296966	4.614×10^{-4}	1.57679	5.2833×10^{-1}	1.0059

C_p = 1750 m/sec φ_2' max = π $\varphi_2'' < 0$

φ_1'	φ_1''	φ_2'	φ_2''	$\lvert R \rvert$
1.0244	8.0068×10^{-2}	1.6629	-5.374×10^{-1}	1.2503
1.02616	6.5248×10^{-2}	1.6438	-5.2859×10^{-1}	1.2003
1.02793	4.6118×10^{-2}	1.6216	-5.2851×10^{-1}	1.1359
1.02946	1.6752×10^{-2}	1.5850	-5.284×10^{-1}	1.0428
1.02959	1.0970×10^{-2}	1.5778	-5.2837×10^{-1}	1.0253
1.02964	8.1823×10^{-3}	1.5744	-5.2836×10^{-1}	1.0164
1.02967	5.189×10^{-3}	1.5706	-5.2835×10^{-1}	1.0080
1.02968	2.869×10^{-3}	1.5677	-5.2834×10^{-1}	1.0012
1.0296895	1.245×10^{-3}	1.5657	-5.28339×10^{-1}	.99645
1.0296946	4.6167×10^{-4}	1.5648	-5.28336×10^{-1}	.99416

Table 5.3

Refracted Angle and Reflection Coefficient $K_2'' = .001$

C_p = 1950 m/sec

φ_1'	φ_1''	φ_2'	φ_2''	$\lvert R \rvert$	$\angle R$
8.77536×10^{-1}	1.288×10^{-2}	1.5369	2.2608×10^{-1}	.45605	2.651×10^{-1}
3.11547	1.215×10^{-2}	1.5396	2.2607×10^{-1}	.95939	2.652×10^{-1}
8.77567	1.073×10^{-2}	1.545	2.2605×10^{-1}	.96587	2.654×10^{-1}
8.77569	1.052×10^{-2}	1.5457	2.2605×10^{-1}	.9668	2.6545×10^{-1}
8.77573	1.022×10^{-2}	1.5468	2.2605×10^{-1}	.96816	2.6549×10^{-1}
8.77577	9.880×10^{-3}	1.5481	2.2604×10^{-1}	.9697	2.655×10^{-1}
8.77579	9.702×10^{-3}	1.5488	2.2604×10^{-1}	.97059	2.6554×10^{-1}
8.77580	9.613×10^{-3}	1.570795	-2.2604×10^{-1}	1.0039	-2.6593×10^{-1}
8.77585	9.23×10^{-3}	1.57079	-2.2603×10^{-1}	1.0038	-2.6593×10^{-1}
8.77614	6.07×10^{-3}	1.57074	-2.2600×10^{-1}	1.0028	-2.6592×10^{-1}
8.77635	1.07×10^{-3}	1.5605	-2.2594×10^{-1}	.98907	-2.6593×10^{-1}
8.77636	6.113×10^{-4}	1.5587	-2.2593×10^{-1}	.98688	-2.6592×10^{-1}
8.776363	4.192×10^{-4}	1.55803	-2.259×10^{-1}	.98598	-2.6592×10^{-1}

C_p = 1550 m/sec

φ_1'	φ_1''	φ_2'	φ_2''	$\lvert R \rvert$	$\angle R$
1.3151083	2.294×10^{-2}	1.5663	7.4468×10^{-1}	.90865	1.7564
1.31533	2.014×10^{-2}	1.5675	7.4468×10^{-1}	.91448	1.7579
1.31555	1.701×10^{-2}	1.5688	7.4468×10^{-1}	.93216	1.7594
1.31558	1.6538×10^{-2}	1.5690	7.4468×10^{-1}	.93413	1.7597
1.31559	1.6287×10^{-2}	1.5691	7.4468×10^{-1}	.93516	1.7598
1.31560	1.6203×10^{-2}	1.570795	-7.4468×10^{-1}	1.0062	-1.7598
1.31562	1.5947×10^{-2}	1.57079	-7.4469×10^{-1}	1.0652	-1.7599
1.315886	1.7076×10^{-2}	1.57019	-7.4467×10^{-1}	1.0437	-1.7617
1.31603	6.367×10^{-3}	1.56838	-7.44667×10^{-1}	1.0236	-1.7627
1.3161	1.721×10^{-3}	1.5664	-7.446608×10^{-1}	1.0029	-1.7632
1.3161607	5.474×10^{-4}	1.5659	-7.44659×10^{-1}	.99772	-1.7633
1.3161608	2.553×10^{-4}	1.5657	-7.44658×10^{-1}	.99531	-1.7633

Table 5.3

C_p = 2050 m/sec $\quad K_2'' = .001$ n/m

q_1'	q_1''	q_2'	q_2''	$\lvert R \rvert$	$\angle R$
.81982	4.319×10^{-2}	1.31064	1.3708×10^{-1}	.74643	1.3417×10^{-1}
.82019	3.4318×10^{-2}	1.3224	1.1281×10^{-1}	.75796	1.117×10^{-1}
.82050	2.4262×10^{-2}	1.3353	8.091×10^{-2}	.77050	8.034×10^{-2}
.82077	9.904×10^{-3}	1.3479	2.668×10^{-2}	.78291	2.565×10^{-2}
.82080	6.425×10^{-3}	1.3491	1.243×10^{-2}	.78414	1.1075×10^{-2}
.820814	4.054×10^{-3}	1.349447	2.6379×10^{-3}	.78443	1.0267×10^{-3}
.820815	3.789×10^{-3}	1.34948	1.5439×10^{-3}	.78447	-9.5506×10^{-5}
.820816	3.5057×10^{-3}	1.34948	3.675×10^{-4}	.78450	-1.302×10^{-3}
.820817	3.1464×10^{-3}	1.3494	-9.130×10^{-4}	.78450	-2.6158×10^{-3}
.820822	1.3876×10^{-3}	1.34929	-8.394×10^{-3}	.78437	-1.029×10^{-2}
.820823	7.700×10^{-4}	1.3491	-1.094×10^{-2}	.78427	-1.290×10^{-2}
.820823	1.5939×10^{-4}	1.3490	-1.346×10^{-2}	.78414	-1.5486×10^{-2}

C_p = 2450 m/sec $\quad K_2'' = .001$ n/m

q_1'	q_1''	q_2'	q_2''	$\lvert R \rvert$	$\angle R$
.65789	5.085×10^{-2}	.94989	8.768×10^{-2}	.56588	4.7718×10^{-2}
.65831	3.868×10^{-2}	.95217	6.584×10^{-2}	.56765	3.528×10^{-2}
.65884	1.1657×10^{-2}	.95487	1.677×10^{-2}	.56979	6.807×10^{-3}
.65884	1.1981×10^{-2}	.95486	1.7366×10^{-2}	.56978	7.153×10^{-3}
.65888	5.3601×10^{-3}	.95501	5.2847×10^{-3}	.56992	8.013×10^{-5}
.658886	5.085×10^{-3}	.95502	4.782×10^{-3}	.56993	-2.1403×10^{-4}
.65889	3.389×10^{-3}	.95502	1.6878×10^{-3}	.56994	2.0271×10^{-3}
.658894	2.3961×10^{-3}	.95502	-1.253×10^{-4}	.56994	-3.0894×10^{-3}
.658896	1.224×10^{-3}	.95501	-2.263×10^{-3}	.56993	-4.3423×10^{-3}
.65889	3.615×10^{-4}	.95499	-3.8386×10^{-3}	.56993	-5.264×10^{-3}

Summary of Normal Mode Dispersion — Table 5.4

M	c_p	ω_2	ω_ϕ	φ_1'	φ_{1_0}'	φ_1''
0	1950	3.99936	3.99936	.8774371	.8776364	1.819×10^{-2}
	1850	4.68455	4.68506	.945447	.945536	1.13×10^{-2}
	1750	5.68890	5.68958	1.029648	1.029697	7.634×10^{-3}
	1650	7.64442	7.64527	1.141071	1.141097	4.84309×10^{-3}
	1550	14.60045	14.6011	1.316100	1.316108	2.9759×10^{-3}
	1530	19.6660	19.66627	1.372437	1.372442	1.31634×10^{-3}
1	1950	11.37408	11.37457	.8775785	.8776364	9.807×10^{-3}
	1850	12.73560	12.73619	.9455152	.9049510	5.4863×10^{-3}
	1750	14.83782	14.83845	1.029686	1.029697	3.6189×10^{-3}
	1650	18.95622	18.95687	1.141091	1.141097	2.31078×10^{-3}
	1550	33.30507	33.30523	1.316106	1.316108	9.90022×10^{-4}
	1530	43.58043	43.58016	1.372441	1.372442	6.5137×10^{-4}
2	1950	18.74888	18.74953	.8776093	.8776364	6.7093×10^{-3}
	1850	20.78667	20.78729	.945527	.9455361	3.0219×10^{-3}
	1750	23.98468	23.98732	1.029692	1.029697	2.3721×10^{-3}
	1650	30.26787	30.26847	1.141094	1.141097	1.5166×10^{-3}
	1550	52.00936	52.00936	1.316107	1.316108	6.5612×10^{-4}
	1530	67.4995	67.49905	1.372441	1.372442	4.3284×10^{-4}
3	1950	26.14282	26.12448	.8776214	.8776364	4.544×10^{-3}
	1850	28.83776	28.83841	.945531	.9455361	2.7034×10^{-3}
	1750	33.13554	33.13618	1.029694	1.029697	1.7643×10^{-3}
	1650	41.57949	41.58006	1.141095	1.141097	1.2864×10^{-3}
	1550	70.71356	70.71350	1.316108	1.316108	4.7096×10^{-4}

Model 1A $K_L'' = .01$ n/m

Summary of Normal Mode Dispersion Table 5.4

M	C_p	ω_a	ω_ϕ	φ_1'	φ_{1_0}'	φ_1''
0	1950	3.999606	3.999609	.8776344	.8776364	1.821×10^{-3}
	1850	4.685057	4.685062	.9455352	.9455361	1.131×10^{-3}
	1750	5.689582	5.689589	1.029696	1.029697	7.639×10^{-4}
	1650	7.645270	7.645278	1.141096	1.141097	4.846×10^{-4}
	1600	9.700959	9.700967	1.215375	1.215375	3.525×10^{-4}
1	1950	11.37456	11.37457	.8776358	.8776364	9.8×10^{-4}
	1850	12.73617	12.73618	.9455359	.9455361	5.49×10^{-4}
	1750	14.83845	14.83846	1.029697	1.029697	3.621×10^{-4}
	1700	16.48290	16.48291	1.080839	1.080839	2.9353×10^{-4}
	1600	23.24288	23.24288	1.215375	1.215375	1.6914×10^{-4}
2	1950	18.74952	18.74953	.8776361	.8776364	6.71×10^{-4}
	1850	20.78729	20.78730	.9455360	.9455361	3.649×10^{-4}
	1800	22.17400	22.17400	.9851107	.9851108	2.914×10^{-4}
	1650	30.26847	30.26847	1.141097	1.141097	1.52×10^{-4}

Model 1A $K_2'' = .001$ n/m

Summary of Leaky Mode Dispersion Table 5.5

M	c_p	ω_a	ω_ϕ	φ_1'	$\varphi_{1,0}'$	φ_1''
0	2450	2.455473	2.9800	.59618	.65889	4.22×10^{-1}
	2350	2.58229	3.06082	.64298	.69228	3.57×10^{-1}
	2250	2.7152	3.16116	.69219	.72972	2.97×10^{-1}
	2150	2.869	3.288	.74624	.7721	2.35×10^{-1}
	2050	3.075	3.456	.8091	.8208	1.48×10^{-1}
1	2450	8.8213	8.940	.6563	.6588	8.07×10^{-2}
	2350	9.067	9.182	.69024	.6922	7.024×10^{-2}
	2250	9.371	9.483	.7282	.7297	5.85×10^{-2}
	2150	9.757	9.866	.7712	.7721	4.49×10^{-2}
	2050	10.246	10.370	.82045	.82082	2.63×10^{-2}
2	2450	14.832	14.900	.6580	.6588	4.69×10^{-2}
	2350	15.238	15.304	.6915	.6922	4.082×10^{-2}
	2250	15.742	15.805	.7292	.7297	3.39×10^{-2}
	2150	16.385	16.444	.7718	.7721	2.59×10^{-2}
	2050	17.229	17.283	.8207	.8208	1.47×10^{-2}

Model

$c_1 = 1500$ m/sec

$\rho_1 = 1.0$ gm/cc

$c_2 = 2000$ m/sec

$\rho_2 = 2.0$ gm/cc

$K_2'' = 1\times10^{-3}$ n/m

Table 5.6

Normal Mode Dispersion Eigenvalue Perturbation

		$k_z'' = .01$ n/m		$k_z'' = .001$ n/m	
M	c_p	$\Delta\omega$ radians/sec	$\Delta\psi_1$ radians	$\Delta\omega$ radians/sec	$\Delta\psi_1$ radians
0	1950	-0.24×10^{-3}	-1.99×10^{-4}	$-.03\times10^{-4}$	$-.20\times10^{-5}$
	1850	-0.51	-0.89	-.05	-.09
	1750	-0.68	-0.49	-.07	-.01
	1650	-0.85	-0.26	-.08	-.01
	1550	-0.65	-0.08	—	—
1	1950	$-.49\times10^{-3}$	$-.58\times10^{-4}$	$-.01\times10^{-4}$	
	1850	-.58	-.21	-.01	$-.06\times10^{-5}$
	1750	-.63	-.11	-.01	-.02
	1650	-.65	-.06	—	-.00
	1550	-.16	-.02	—	—
2	1950	$-.65\times10^{-3}$	$-.27\times10^{-4}$	$-.01\times10^{-4}$	$-.03\times10^{-5}$
	1850	-.62	-.09	-.01	-.01
	1750	-.64	-.05	—	—
	1650	-.60	-.03	—	—
	1550	-.00	-.01	—	—

Computer printout was limited to 6 digits beyond the decimal point.

Summary of Normal Mode Attenuation Table 5.7

M	C_p	δ	δ_{ING}	δ_{INT}	δ_{BR}	δ_{KR}
0	1950	3.10343×10^{-5}	9.49×10^{-5}	6.16×10^{-5}	1.707×10^{-4}	3.10398×10^{-5}
	1850	2.06683	1.049×10^{-4}	3.197×10^{-5}	1.244	2.06801
	1750	1.491684	9.0466×10^{-5}	2.087	8.439×10^{-5}	1.49260
	1650	1.029064	6.355	1.346	4.673	1.02957
	1550	4.95359×10^{-6}	2.362	5.97×10^{-6}	1.281	4.95599×10^{-6}
	1530	3.402942×10^{-6}	1.381×10^{-5}	3.971×10^{-6}	7.062×10^{-6}	3.97135×10^{-6}
1	1950	4.752432×10^{-5}	1.4562×10^{-4}	6.16×10^{-5}	8.44506×10^{-5}	4.75709×10^{-5}
	1850	2.726516	1.3874	3.197×10^{-5}	6.73591	2.7286
	1750	1.845209	1.12278	2.087	4.962	1.8464
	1650	1.216611	7.5557×10^{-5}	1.346×10^{-5}	3.04	1.2174
	1550	5.543×10^{-6}	2.6738	5.97×10^{-6}	9.849×10^{-6}	5.547×10^{-6}
	1530	3.73074×10^{-6}	1.53541×10^{-5}	3.971×10^{-6}	5.7524×10^{-6}	3.73342×10^{-6}
2	1950	5.360956×10^{-5}	1.643×10^{-4}	6.16×10^{-5}	6.993×10^{-5}	5.36681×10^{-5}
	1850	2.937923	1.4961×10^{-4}	3.197×10^{-5}	5.6891×10^{-5}	2.94039
	1750	1.95499	1.19086×10^{-4}	2.087×10^{-5}	4.2724×10^{-5}	1.95639
	1650	1.27544	7.934×10^{-5}	1.346×10^{-5}	2.683×10^{-5}	1.27632
	1550	5.7353×10^{-6}	2.7763×10^{-5}	5.97×10^{-6}	9.08×10^{-6}	5.739×10^{-6}
	1530	3.83846×10^{-6}	1.58652×10^{-5}	3.971×10^{-6}	5.3961×10^{-6}	3.84131×10^{-6}
3	1950	5.065×10^{-5}	1.74×10^{-4}	6.16×10^{-5}	6.384×10^{-5}	5.692×10^{-5}
	1850	3.04083	1.549×10^{-4}	3.197×10^{-5}	5.254	3.0447
	1750	2.00852	1.224	2.087	3.980	2.0100
	1650	1.30419	8.119	1.346×10^{5}	2.527	1.3050
	1550	5.83027×10^{-6}	2.827	5.97×10^{-6}	8.739×10^{-6}	5.834×10^{-6}

Model 1A $K_L'' = .01\left(\frac{f}{100\,Hz}\right)^{1.0}$

Table 5.7

Normal Mode Attenuation with $K_2'' = .01\left(\frac{f}{100\,Hz}\right)^{1.2}$

M	C_p	δ	δ_{ING}	δ_{INT}	δ_{BR}	δ_{KR}
0	1950	1.128990×10^{-5}	9.4764×10^{-5}	2.366×10^{-5}	6.2436×10^{-5}	1.12904×10^{-5}
	1850	7.7641×10^{-6}	1.0445×10^{-4}	1.2369×10^{-5}	4.6964×10^{-5}	7.7642×10^{-6}
	1750	5.82562×10^{-6}	8.9649×10^{-5}	8.337×10^{-6}	3.3104×10^{-5}	5.8259×10^{-6}
	1650	4.2635×10^{-6}	6.2397×10^{-5}	5.6783×10^{-6}	1.9447×10^{-5}	4.2632×10^{-6}
	1550	2.3356×10^{-6}	2.4329×10^{-5}	2.8504×10^{-6}	6.0664×10^{-6}	2.3355×10^{-6}
1	1950	2.13254×10^{-5}	1.4534×10^{-4}	2.7922×10^{-5}	3.8042×10^{-5}	2.13258×10^{-5}
	1850	1.25144×10^{-5}	1.3804×10^{-4}	1.5052×10^{-5}	3.10347×10^{-5}	1.25124×10^{-5}
	1750	8.7288×10^{-6}	1.11220×10^{-4}	1.0066×10^{-5}	2.3571×10^{-5}	8.7293×10^{-6}
	1650	6.0439×10^{-6}	7.492×10^{-5}	6.79219×10^{-6}	1.51649×10^{-5}	6.0449×10^{-6}
	1550	3.08216×10^{-6}	2.5499×10^{-5}	3.35486×10^{-6}	5.4969×10^{-6}	3.0827×10^{-6}
2	1950	2.5878×10^{-5}	1.6403×10^{-4}	3.0519×10^{-5}	3.4769×10^{-5}	2.66×10^{-5}
	1850	1.4868×10^{-5}	1.4888×10^{-4}	1.64759×10^{-5}	2.8902×10^{-5}	1.4870×10^{-5}
	1750	1.0180×10^{-5}	1.18015×10^{-4}	1.10624×10^{-5}	2.2334×10^{-5}	1.01818×10^{-5}
	1650	6.9574×10^{-6}	7.7994×10^{-5}	7.4475×10^{-6}	1.4691×10^{-5}	6.95871×10^{-6}
	1550	3.4809×10^{-6}	2.6589×10^{-5}	3.6576×10^{-6}	5.54199×10^{-6}	3.48710×10^{-6}

Table 5.7

Normal Mode Attenuation with $K_2'' = .01\left(\frac{f}{1000\ Hz}\right)^{1.4}$

M	C_p	δ	δ_{NO}	δ_{INT}	δ_{BR}	δ_{LR}
0	1950	4.106668×10^{-6}	9.4708×10^{-5}	8.7571×10^{-6}	2.2728×10^{-5}	4.1066×10^{-6}
	1850	2.9157×10^{-6}	1.0424×10^{-4}	4.693×10^{-6}	1.764×10^{-5}	2.915×10^{-6}
	1750	2.27387×10^{-6}	8.9316×10^{-5}	3.280×10^{-6}	1.293×10^{-5}	2.2738×10^{-6}
	1650	1.76547×10^{-6}	6.1900×10^{-5}	2.368×10^{-6}	8.0596×10^{-6}	1.765×10^{-6}
	1550	1.10069×10^{-6}	2.1852×10^{-5}	1.3512×10^{-6}	2.8619×10^{-6}	1.1006×10^{-6}
1	1950	9.564×10^{-6}	1.4521×10^{-4}	1.3232×10^{-5}	1.7071×10^{-5}	9.560×10^{-6}
	1850	5.739×10^{-6}	1.3770×10^{-4}	6.9794×10^{-6}	4424×10^{-5}	5.737×10^{-6}
	1750	4.1272×10^{-6}	1.10696×10^{-4}	4.8014×10^{-6}	1.1156×10^{-5}	9.126×10^{-6}
	1650	2.9986×10^{-6}	7.3485×10^{-5}	3.3979×10^{-6}	7.538×10^{-6}	3.0013×10^{-6}
	1550	1.7131×10^{-6}	2.4781×10^{-5}	1.8752×10^{-6}	3.0589×10^{-6}	1.7134×10^{-6}
2	1950	1.3172×10^{-5}	1.638×10^{-4}	1.6106×10^{-5}	1.7262×10^{-5}	1.3172×10^{-5}
	1850	7.5204×10^{-6}	1.4848×10^{-4}	8.472×10^{-6}	1.4634×10^{-5}	7.5208×10^{-6}
	1750	5.2984×10^{-6}	1.1743×10^{-4}	5.8086×10^{-6}	1.1637×10^{-5}	5.2989×10^{-6}
	1650	3.7938×10^{-6}	7.723×10^{-5}	4.0911×10^{-6}	8.0207×10^{-6}	3.7939×10^{-6}
	1600	3.0576×10^{-6}	5.3111×10^{-5}	3.2702×10^{-6}	5.8706×10^{-6}	3.0577×10^{-6}

Table 5.7

Normal Mode Attenuation for K-R Model

M	c_p	δ	δ_{ING}	δ_{INT}	δ_{BR}	δ_{KR}
0	1710	4.4357×10^{-5}	5.9119×10^{-4}	9.9271×10^{-5}	2.7450×10^{-4}	4.4264×10^{-5}
	1670	2.9480×10^{-5}	7.0331×10^{-4}	4.7736×10^{-5}	1.98198×10^{-4}	2.9477×10^{-5}
	1630	2.22679×10^{-5}	6.3407×10^{-4}	3.2373×10^{-5}	1.3872×10^{-4}	2.2267×10^{-5}
	1590	1.6817×10^{-5}	4.9426×10^{-4}	2.2908×10^{-5}	8.6947×10^{-5}	1.6814×10^{-5}
	1550	1.13984×10^{-5}	2.9784×10^{-4}	1.46814×10^{-5}	4.18725×10^{-5}	1.1416×10^{-5}
1	1710	6.9750×10^{-5}	9.3171×10^{-4}	9.8066×10^{-5}	1.3438×10^{-4}	6.9748×10^{-5}
	1670	3.909×10^{-5}	9.33117×10^{-4}	4.7736×10^{-5}	1.0677×10^{-4}	3.9089×10^{-5}
	1630	2.7708×10^{-5}	7.8950×10^{-4}	3.2373×10^{-5}	8.078×10^{-5}	2.77058×10^{-5}
	1590	2.0078×10^{-5}	5.9122×10^{-4}	2.2908×10^{-5}	5.502×10^{-6}	2.00912×10^{-5}
	1530	9.1147×10^{-6}	2.00528×10^{-4}	1.0028×10^{-5}	1.7053×10^{-5}	9.11422×10^{-6}
2	1710	7.893176×10^{-5}	1.06133×10^{-3}	9.86665×10^{-5}	1.11013×10^{-4}	7.94539×10^{-5}
	1670	4.24809×10^{-5}	1.00706×10^{-3}	4.77369×10^{-5}	9.0089×10^{-5}	4.24809×10^{-5}
	1630	2.93998×10^{-5}	8.379×10^{-4}	3.23731×10^{-5}	6.9388×10^{-5}	2.93983×10^{-5}
	1610	2.49874×10^{-5}	7.352×10^{-4}	2.72914×10^{-5}	5.88746×10^{-5}	2.49865×10^{-5}
	1550	1.36984×10^{-5}	3.5825×10^{-4}	1.4181×10^{-5}	2.65638×10^{-5}	1.36979×10^{-5}

Model
$c_1 = 1500$ m/sec
$\rho_1 = 1.0$ gm/cc
$c_2 = 1725$ m/sec
$\rho_2 = 2.0$ gm/cc
$k_L'' = .001$ n/m

Leaky Mode Attenuation Table 5.8

M	C_p	δ	δ_{ING}	δ_{INT}	δ_{BR}	δ_{KR}
0	2450	5.888×10^{-4}	—	2.77×10^{-4}	4.558×10^{-5}	6.8407×10^{-6}
	2350	5.030×10^{-4}	—	2.456×10^{-4}	4.122×10^{-5}	2.387×10^{-6}
	2250	4.206×10^{-4}	—	2.099×10^{-4}	3.728×10^{-5}	2.327×10^{-6}
	2150	3.326×10^{-4}	—	1.654×10^{-4}	3.339×10^{-5}	2.255×10^{-6}
	2050	2.1136×10^{-4}	—	1.005×10^{-4}	2.905×10^{-5}	2.185×10^{-6}
1	2450	3.767×10^{-4}	—	2.77×10	1.412×10^{-5}	3.81×10^{-6}
	2350	3.2767×10^{-4}	—	2.456×10^{-4}	1.3373×10^{-5}	3.692×10^{-6}
	2250	2.733×10^{-4}	—	2.099×10^{-4}	1.2519×10^{-5}	3.576×10^{-6}
	2150	2.046×10^{-4}	—	1.654×10^{-4}	1.1549×10^{-5}	2.461×10^{-6}
	2050	1.23×10^{-4}	—	1.005×10^{-4}	1.043×10^{-5}	3.346×10^{-6}
2	2450	3.6759×10^{-4}	—	2.77×10^{-4}	1.124×10^{-5}	4.098×10^{-6}
	2350	3.19504×10^{-4}	—	2.456×10^{-4}	1.0053×10^{-5}	3.9795×10^{-6}
	2250	2.6595×10^{-4}	—	2.099×10^{-4}	9.982×10^{-5}	3.864×10^{-6}
	2150	2.0284×10^{-4}	—	1.654×10^{-4}	9.2162×10^{-5}	3.7519×10^{-6}
	2050	1158×10^{-4}	—	1.005×10^{-4}	8.333×10^{-6}	3.6438×10^{-6}

Table 5.9

δ, δ_{BR} and Quantities Used in Calculating δ_{BR}

M	c_p	δ	δ_{BR}	ω_R	α	kH	$\Delta_R H$	η''
0	1950	3.10×10^{-5}	1.71×10^{-4}	3.99	6.93×10^{-1}	2.66	19.10	1.81×10^{-2}
	1850	2.06×10^{-5}	1.24×10^{-4}	4.68	6.25×10^{-1}	3.123	14.56	1.13×10^{-2}
	1750	1.49×10^{-5}	8.439×10^{-4}	5.68	5.41×10^{-1}	3.79	10.31	7.63×10^{-3}
	1650	1.03×10^{-5}	4.67×10^{-4}	7.64	4.29×10^{-1}	5.016	6.00	4.84×10^{-3}
	1550	4.95×10^{-6}	1.28×10^{-5}	14.6	2.54×10^{-1}	9.73	1.786	2.017×10^{-3}
1	1950	4.75×10^{-5}	8.44×10^{-5}	11.37	6.93×10^{-1}	7.58	8.152	9.80×10^{-3}
	1850	2.72×10^{-5}	6.73×10^{-5}	12.73	6.25×10^{-1}	8.99	6.562	5.48×10^{-3}
	1750	1.84×10^{-5}	4.96×10^{-5}	14.837	5.41×10^{-1}	9.89	4.884	3.62×10^{-3}
	1650	1.21×10^{-5}	3.04×10^{-5}	18.95	4.29×10^{-1}	12.63	3.029	2.31×10^{-3}
	1550	5.54×10^{-6}	9.84×10^{-6}	33.31	2.54×10^{-1}	22.2	1.00	9.9×10^{-4}
2	1950	5.36×10^{-5}	6.99×10^{-5}	18.74	6.93×10^{-1}	12.49	5.319	6.71×10^{-3}
	1850	2.93×10^{-5}	5.68×10^{-5}	20.78	6.25×10^{-1}	13.85	4.351	3.62×10^{-3}
	1750	1.95×10^{-5}	4.27×10^{-5}	23.98	5.41×10^{-1}	15.99	3.28	2.37×10^{-3}
	1650	1.27×10^{-5}	2.68×10^{-5}	30.267	4.29×10^{-1}	20.17	2.072	1.516×10^{-3}
	1550	5.73×10^{-6}	9.08×10^{-6}	52.00	2.54×10^{-1}	34.67	.708	6.56×10^{-4}

Model 1A

$c_1 = 1500$ m/sec

$\rho_1 = 1.0$ gm/cc

$c_2 = 2000$ m/sec

$\rho_2 = 2.0$ gm/cc

$K_2'' = .01$ n/m

Table 5.10

Summary of Mode Shape S(z) vs Depth z

Mode 0 :	S(z)			
depth c_p:	1900	1800	1700	1600
0	8.42×10^{-6}	3.95×10^{-6}	1.18×10^{-6}	7.3×10^{-7}
100	3.51×10^{-1}	3.75×10^{-1}	4.031×10^{-1}	4.46×10^{-1}
200	6.92×10^{-1}	7.37×10^{-1}	7.896×10^{-1}	8.7×10^{-1}
300	1.012	1.073	1.143	1.25
400	1.300	1.371	1.451	1.567
500	1.547	1.6199	1.6987	1.805
600	1.746	1.811	1.876	1.951
700	1.890	1.938	1.977	1.999
800	1.975	1.996	1.977	1.947
900	1.999	1.983	1.935	1.796
1000	1.960	1.900	1.793	1.555

Mode 1 :	S(z)			
depth c_p:	1900	1800	1700	1600
0	-9.5×10^{-6}	-6.3×10^{-6}	-5.5×10^{-6}	$-6.\times10^{-6}$
100	-.94	-.964	-.988	-1.02
200	-1.66	-1.689	-1.718	-1.762
300	-1.99	-1.996	-1.999	-1.99
400	-1.847	-1.808	-1.757	-1.66
500	-1.26	-1.173	-1.055	-.861
600	-.38	-.2467	-.0778	.187
700	.58	.7405	.9203	1.18
800	1.416	1.544	1.6778	1.84
900	1.914	1.965	1.9966	1.98
1000	1.96	1.900	1.793	1.55

Model 1A with H = 1000 m

Table 5.11

Sample Newton Raphson convergence sequence to solve the characteristic equation

Model 1A $C_p = 1550$ $K_L'' = .001$ n/m

Finite difference derivatives:

iteration	Fω	Gω	$F_{q_1'}$	$G_{q_1'}$
1	-8.5196×10^{-1}	0.	2.301×10^{1}	5.129×10^{3}
2	-8.5197×10^{-1}	-2.3424×10^{-3}	2.2603×10^{1}	5.423×10^{3}
3	-8.5196×10^{-1}	0.	2.0586×10^{1}	6.847×10^{3}
4	-8.5197×10^{-1}	-2.0275×10^{-3}	2.141×10^{1}	6.265×10^{3}
5	-8.5196×10^{-1}	0.	1.8359×10^{1}	8.419×10^{3}
6	-8.5196×10^{-1}	-1.8283×10^{-3}	2.044×10^{1}	6.947×10^{3}
7	-8.5196×10^{-1}	-1.964×10^{-4}	1.636×10^{1}	9.825×10^{3}
8	-8.5196×10^{-1}	-1.5311×10^{-3}	1.807×10^{1}	8.623×10^{3}
9	-8.5196×10^{-1}	-8.0345×10^{-4}	1.366×10^{1}	1.173×10^{4}
10	-8.5197×10^{-1}	-1.0636×10^{-3}	1.1638×10^{1}	1.318×10^{4}
11	convergence achieved to within 10^{-4}			

Convergence error and computed eigenvalue corrections:

iteration	Ferr	GEAR	Δω	Δq_1
1	-9.51×10^{-6}	1.61×10^{-2}	9.60×10^{-5}	3.14×10^{-6}
2	3.02×10^{-5}	-2.13×10^{-2}	-1.4×10^{-4}	-3.93×10^{-6}
3	-4.70×10^{-5}	1.61×10^{-2}	1.12×10^{-4}	2.35×10^{-6}
4	2.31×10^{-5}	-1.63×10^{-2}	-9.26×10^{-5}	-2.60×10^{-6}
5	-3.04×10^{-5}	1.61×10^{-2}	7.69×10^{-5}	1.912×10^{-6}
6	1.86×10^{-5}	-1.31×10^{-2}	-6.72×10^{-5}	-1.89×10^{-6}
7	-1.83×10^{-5}	1.29×10^{-2}	4.68×10^{-5}	1.32×10^{-6}
8	1.18×10^{-5}	-8.38×10^{-3}	-3.45×10^{-5}	-9.72×10^{-7}
9	-4.6×10^{-6}	3.25×10^{-3}	9.86×10^{-6}	2.774×10^{-7}
10	1.27×10^{-6}	-8.99×10^{-4}	-2.43×10^{-6}	-6.84×10^{-8}
11	-3.62×10^{-8}	2.55×10^{-5}		

Table 5.12

Modal Attenuation vs. Mode Number

Model 1A $k_2'' = .01$ n/m

A	$\delta_{\substack{m=0\\l=1}}$	$\delta_{\substack{m=1\\l=2}}$	$\delta_{\substack{m=2\\l=3}}$	ratio $\delta_{m=1}/\delta_{m=0}$	ratio $\delta_{m=2}/\delta_{m=0}$
12.5	3.7×10^{-6}	1.25×10^{-5}	4.1×10^{-5}	3.37	11.08
15	2.78×10^{-6}	9.4×10^{-6}	2.35×10^{-5}	3.38	8.45
20	1.8×10^{-6}	6.4×10^{-6}	1.25×10^{-5}	3.55	6.94
25	1.3×10^{-6}	4.7×10^{-6}	9.0×10^{-6}	3.6	6.92

Model KR $k_2'' = .001$ n/m

17.5	5.4×10^{-6}	1.57×10^{-5}	5.4×10^{-5}	2.90	10
20	4.6×10^{-6}	1.4×10^{-5}	3.3×10^{-5}	3.043	7.17
30	3.0×10^{-6}	8.4×10^{-5}	1.6×10^{-5}	2.8	5.33
40	2.2×10^{-6}	5.8×10^{-6}	1.05×10^{-5}	2.636	4.72

REFERENCES

1. Brekhovskikh,L.M., Waves in Layered Media, Academic Press, New York: 1960

2. Tolstoy and Clay, Ocean Acoustics, Theory and Experiment in Underwater Sound, McGraw Hill, New York: 1966

3. Tolstoy, Wave Propagation, McGraw Hill, New York:1973

4. White,J,E, Seismic Waves: Radiation, Transmission and Attenuation, McGraw Hill,New York: 1965

5. Ewing,Jardetsky and Press, Elastic Waves in Layered Media McGraw Hill, New York:1957

6. Conte,S.D., Elementary Numerical Analysis, McGraw Hill,1965.

7. Dyer,I., Fundamentals of Underwater Sound Applications, MIT Course 13.85 Notes Spring 1975.

8. Officer,C.B., Introduction to the Theory of Sound Transmission, McGraw Hill, New York:1958.

9. Tolstoy,I.,"Note on the Propagation of Normal Modes in Inhomogeneous Media",JASA,Vol 27,NO.2.March 1955,p274.

10. Tolstoy,I.,"Shallow Water Test of the Theory of Layered Wave Guides",JASA,Vol 30,No.4,April 1958.

11. Tolstoy,I.,"Dispersion and Simple Harmonic Point Sources in Wave Ducts",JASA,Vol 27,No.5,Sept.1955,p897.

12. Tolstoy,I.,"Guided Waves in a Fluid With Continuously Variable Velocity Overlying an Elastic Solid:Theory and Experiment", JASA Vol 32, No.1,Jan 1960.

13. Tolstoy,I.,"Resonant Frequencies and High Modes in Layered Waveguides",JASA Vol 28,No.6,Nov.1956

14. Bucker,H.P.,"Normal Mode Sound Propagation in Shallow Water", JASA Vol 36,1964, p251-258.

15. Bucker,H.P.,"Sound Propagation in a Channel with Lossy Boundaries", JASA Vol 48,No 5,pt II, p1187.

16. Bucker,Whitney,Yee and Gardner,"Reflection of Low Frequency Sonar Signals from a Smooth Ocean Bottom",JASA Vol 37,No.6, June 1965,p1037-1051

17. Denham,"Intensity Decay Laws for Sound Propagation in Shallow Water of Variable Depth",JASA Vol 39,No.6,Nov.1965

18. Ferris,"Comparison of Measured and Calculated Normal Mode Amplitude Functions for Acoustic Waves in Shallow Water", JASA Vol 52,No.3,pt 2,p981.,1972

19. Kornhauser and Raney,"Attenuation in Shallow Water Propagation Due to an Absorbing Bottom",JASA Vol 27,No.4,1955

20. Ingenito,"Measurements of Mode Attenuation Coefficients in Shallow Water",JASA Vol 53, p858,1973.

21. Ingenito and Wolf,"Acoustic Propagation in Shallow Water Overlying a Consolidated Bottom",JASA Vol 60,No 3,Sept 1976

22. Morris,H.E.,"Bottom Reflection Loss Model With a Velocity Gradient",JASA Vol 48,No.5,pt 2. 1970.

23. Abeles,F., Ann.Phys 3,p504-520,1948.

24. Pekeris,C.L.,Geol.Soc.Am.,Mem 27,1948.

25. Eby,Williams,Ryan and Tamarkin,"Studies of Acoustic Propagation in a Two-Layered Model",JASA Vol 32,No.1,Jan 1960.

26. Hamilton,"Compressional-Wave Attenuation in Marine Sediments", Geophysics Vol 37,No.4,p620-646,August 1972.

27. Hamilton,E.L.,"Prediction of In-Situ Acoustic and Elastic Properties of Marine Sediments",Geophysics Vol 36, No.2,April 1971.

28. Hamilton,E.L.,"reflection Coefficients and Bottom Losses at Normal Incidence Computed from Pacific Sediment Properties", Geophysics Vol 35, No. 6, p995, Dec. 1970.

29. Watson,G.L., Theory of Bessel Functions, Cambridge University Press, New York, 1956.

30. Banos,Alfredo, Dipole Radiation in the Presence of a Conducting Halfspace, Pergammon Press,Oxford 1966.

31. Fryer,Gerard,"Reflectivity of the Ocean Bottom at Low Frequency", JASA Vol 63,No.1,Jan 1978.

32. Aki,Course Notes for Advanced Seismology-MIT 12.522,1976.

33. Watson,Thomas,"A Real Frequency, Complex Wave-Number Analysis of Leaking Modes .",Bull.Seismol.Soc.of America,Vol 62,No.1,1972.

34. Rosenbaum,"The Long Time Response of a Layered Elastic Medium to Explosive Sound.",JGR Vol 65,No.5,May 1960.

35. Rosenbaum,"A Note on the Propagation of a Sound Pulse in a Two-Layered Medium.",JGR Vol 64,No.1,Jan 1959.

36. Gilbert,"Propagation of Transient Leaking Modes in a Stratified Elastic Waveguide.",Rev Geophysics 2,1964.

37. Gilbert and Dziewonski,"An Application of Normal Mode Theory to the Retrieval of Structural Parameters and Source Mechanisms from Seismic Spectra.",Phil Trans.Roy.Soc.Lond. Ser A 278,p187-269,1975.

38. Gilbert and Laster,"Experimental Investigations of PL Modes in a Single Layer.",Bull.Seism.Soc.Amer.Vol 52,No.1,p59-66 1962.

39. Haskell,"Dispersion of Surface Waves on Multilayered Media.", Bull.Seism.Soc.Amer Vol 43,p17-34,1953.

40. Dunkin,J.W.,"Computation of Modal Solutions in Layered Elastic Media at High Frequencies.",Bull.Seism.Soc.,Amer. Vol 55,No.2,p335-358,1965.

41. Phinney,"Leaking Modes in the Crustal Waveguide-Partl. The Oceanic PL Wave.",JGR Vol 66,No.5,1961.

42. Williams,A.O.,"Acceptable Ignorance About Ocean Bottoms", JASA Vol 59,No.5,p1175,May 1976.

43. Williams,A.O.,"Reflection from a Structured Sea Bottom", JASA Vol 59, No 1, January 1976.

44. Williams,A.O.,"Some Effects of Velocity Structure on Low Frequency Propagation in Shallow Water",JASA Vol 32,No. 3, March 1960.

45. Williams and Eby,"Acoustic Attenuation in a Liquid Layer Over a Slow Viscoelastic Solid",JASA Vol 34,No.6,p836,June 1962.

46. Mintzer and Tannebaum,"Spatial and Temporal Absorption in a Viscous Medium",JASA Vol 32,No.1, p67,Jan.1960.

47. DeBremaecker,Godson,Watkins,"Attenuation Measurements in the Field",Geophysics Vol 31,No.3 p562,June 1966.

48. Busby and Richardson,"The Absorption of Sound in Sediments", Geophysics Vol 22,No.4,p821-828,Oct.1957.

49. O'Brien,P.N.S.,"ADiscussion on the Nature and Magnitude of Elastic Absorption in Seismic Prospecting.",Geophysical Prospecting Vol 9, p261, 1961.

50. Wille,Thiele,Schunk,"Shallow Water Sound Attenuation in a Standard Area.",JASA Vol 54,No.6,p1708,1973.

51. Jensen,"Comparison of Transmission Loss Data for Different Shallow-water Areas with Theoretical Results Provided by a 3-Fluid Normal Mode Propagation Model.",SACLANTCEN Conf. Proc, #14.

52. Laughton,A.S.,"Sound Propagation in Compacted Ocean Sediments.", Geophysics Vol 22,p779-812,1957.

53. Fry and Raitt,"Sound Velocities at the Surface of Deep Sediments." ,JGR Vol 66,No.2,Feb. 1961.

54. Wood and Weston,"The Propagation of Sound in Mud.",Acustica Vol 14,p156,1964.

55. Akal,T.,"The Relationship Between the Physical Properties of Underwater Sediments That Affect Bottom Reflection.", Marine Geology 13,p251-266,1972.

56. Knudsen,"Propagation of a Pressure Transient in a Two-Layered Liquid Model.",JASA Vol 8,p918,Aug.1957.

57. Barakos.P.A.,Review of the Shallow Water Propagation Problem, USL Report No 531 13 June 1962.

58. MacKenzie,K.V.,"Reflection of Sound from Coastal Bottoms.", JASA Vol 32,No. 2, Feb 1960.

59. White,J.E.,"Reflections from Lossy Media.",JASA Vol 38,1965.

60. Cole,B.F.,"Marine Sediment Attenuation and Ocean Bottom Reflected Sound.",JASA Vol 38.,p291,1965.

61. Knopoff,"Q.",Review of Geophysics Vol 2,No. 4, Nov.1964.

62. Strick-White and Walsh,"Discussion on "Proposed Attenuation Dispersion Pair for Seismic Waves",".Geophysics

63. White and Walsh,"Proposed Attenuation Dispersion Pair for Seismic Waves.",Geophysics June 1972.

64. Hermont,A.J.,"Is Seismic Energy of Diagnostic Value?", Geophysics Vol 34,No.2, p196-212,April 1969.

MANDATORY DISTRIBUTION LIST

FOR UNCLASSIFIED TECHNICAL REPORTS, REPRINTS, AND FINAL REPORTS
PUBLISHED BY OCEANOGRAPHIC CONTRACTORS
OF THE OCEAN SCIENCE AND TECHNOLOGY DIVISION
OF THE OFFICE OF NAVAL RESEARCH

(REVISED NOVEMBER 1978)

1 Deputy Under Secretary of Defense
(Research and Advanced Technology)
Military Assistant for Environmental Science
Room 3D129
Washington, D.C. 20301

Office of Naval Research
800 North Quincy Street
Arlington, VA 22217
3 ATTN: Code 483
1 ATTN: Code 460
2 ATTN: 102B

1 CDR J. C. Harlett, (USN)
ONR Representative
Woods Hole Oceanographic Inst.
Woods Hole, MA 02543

Commanding Officer
Naval Research Laboratory
Washington, D.C. 20375
6 ATTN: Library, Code 2627

12 Defense Documentation Center
Cameron Station
Alexandria, VA 22314
ATTN: DCA

Commander
Naval Oceanographic Office
NSTL Station
Bay St. Louis, MS 39522
1 ATTN: Code 8100
1 ATTN: Code 6000
1 ATTN: Code 3300

1 NODC/NOAA
Code D781
Wisconsin Avenue, N.W.
Washington, D.C. 20235

Woods Hole Oceanographic Institution
WHOI-79-91

ATTENUATION OF LOW ORDER MODES IN LOSSY ACOUSTIC WAVE GUIDES by Harold David Leslie. 258 pages. December 1979. Prepared for the Office of Naval Research under Contract N00014-75-C-0852.

Acoustic propagation is treated for sound sources in an ocean bounded from below by stratified layering. The bounding layers of the waveguide may be homogeneous-isovelocity or inhomogeneous with vertical sound speed gradients. The layers may be dissipative or nondissipative. The acoustic field is described with a normal mode expansion and modal attenuation coefficients are calculated for low order modes as a function of mode number and either frequency or phase velocity. The theoretical basis of the calculations is presented for multilayer isovelocity guides and for multilayer guides with index of refraction squared varying linearly with depth. Numerical results are presented for the Pekeris model of a fluid layer over a dissipative fluid halfspace. A comparison is made between various attenuation coefficients proposed in the literature.

1. Acoustic wave guides
2. Low order modes
3. Attenuation coefficients

I. Leslie, Harold David
II. N00014-75-C-0852

This card is UNCLASSIFIED

Woods Hole Oceanographic Institution
WHOI-79-91

ATTENUATION OF LOW ORDER MODES IN LOSSY ACOUSTIC WAVE GUIDES by Harold David Leslie. 258 pages. December 1979. Prepared for the Office of Naval Research under Contract N00014-75-C-0852.

Acoustic propagation is treated for sound sources in an ocean bounded from below by stratified layering. The bounding layers of the waveguide may be homogeneous-isovelocity or inhomogeneous with vertical sound speed gradients. The layers may be dissipative or nondissipative. The acoustic field is described with a normal mode expansion and modal attenuation coefficients are calculated for low order modes as a function of mode number and either frequency or phase velocity. The theoretical basis of the calculations is presented for multilayer isovelocity guides and for multilayer guides with index of refraction squared varying linearly with depth. Numerical results are presented for the Pekeris model of a fluid layer over a dissipative fluid halfspace. A comparison is made between various attenuation coefficients proposed in the literature.

1. Acoustic wave guides
2. Low order modes
3. Attenuation coefficients

I. Leslie, Harold David
II. N00014-75-C-0852

This card is UNCLASSIFIED

Woods Hole Oceanographic Institution
WHOI-79-91

ATTENUATION OF LOW ORDER MODES IN LOSSY ACOUSTIC WAVE GUIDES by Harold David Leslie. 258 pages. December 1979. Prepared for the Office of Naval Research under Contract N00014-75-C-0852.

Acoustic propagation is treated for sound sources in an ocean bounded from below by stratified layering. The bounding layers of the waveguide may be homogeneous-isovelocity or inhomogeneous with vertical sound speed gradients. The layers may be dissipative or nondissipative. The acoustic field is described with a normal mode expansion and modal attenuation coefficients are calculated for low order modes as a function of mode number and either frequency or phase velocity. The theoretical basis of the calculations is presented for multilayer isovelocity guides and for multilayer guides with index of refraction squared varying linearly with depth. Numerical results are presented for the Pekeris model of a fluid layer over a dissipative fluid halfspace. A comparison is made between various attenuation coefficients proposed in the literature.

1. Acoustic wave guides
2. Low order modes
3. Attenuation coefficients

I. Leslie, Harold David
II. N00014-75-C-0852

This card is UNCLASSIFIED

Woods Hole Oceanographic Institution
WHOI-79-91

ATTENUATION OF LOW ORDER MODES IN LOSSY ACOUSTIC WAVE GUIDES by Harold David Leslie. 258 pages. December 1979. Prepared for the Office of Naval Research under Contract N00014-75-C-0852.

Acoustic propagation is treated for sound sources in an ocean bounded from below by stratified layering. The bounding layers of the waveguide may be homogeneous-isovelocity or inhomogeneous with vertical sound speed gradients. The layers may be dissipative or nondissipative. The acoustic field is described with a normal mode expansion and modal attenuation coefficients are calculated for low order modes as a function of mode number and either frequency or phase velocity. The theoretical basis of the calculations is presented for multilayer isovelocity guides and for multilayer guides with index of refraction squared varying linearly with depth. Numerical results are presented for the Pekeris model of a fluid layer over a dissipative fluid halfspace. A comparison is made between various attenuation coefficients proposed in the literature.

1. Acoustic wave guides
2. Low order modes
3. Attenuation coefficients

I. Leslie, Harold David
II. N00014-75-C-0852

This card is UNCLASSIFIED